



3 4456 0023240 6

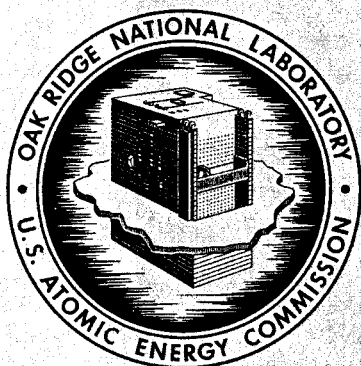
CENTRAL RESEARCH LIBRARY
DOCUMENT COLLECTION

cd

ORNL-4229
UC-4 - Chemistry

REACTOR CHEMISTRY DIVISION
ANNUAL PROGRESS REPORT
FOR PERIOD ENDING DECEMBER 31, 1967

OAK RIDGE NATIONAL LABORATORY
CENTRAL RESEARCH LIBRARY
DOCUMENT COLLECTION
LIBRARY LOAN COPY
DO NOT TRANSFER TO ANOTHER PERSON
If you wish someone else to see this
document, send in name with document
and the library will arrange a loan.
UCN: 7363
13 3-67



OAK RIDGE NATIONAL LABORATORY
operated by
UNION CARBIDE CORPORATION
for the
U.S. ATOMIC ENERGY COMMISSION

Printed in the United States of America. Available from Clearinghouse for Federal
Scientific and Technical Information, National Bureau of Standards,
U.S. Department of Commerce, Springfield, Virginia 22151
Price: Printed Copy \$3.00; Microfiche \$0.65

LEGAL NOTICE

This report was prepared as an account of Government sponsored work. Neither the United States, nor the Commission, nor any person acting on behalf of the Commission:

- A. Makes any warranty or representation, expressed or implied, with respect to the accuracy, completeness, or usefulness of the information contained in this report, or that the use of any information, apparatus, method, or process disclosed in this report may not infringe privately owned rights; or
- B. Assumes any liabilities with respect to the use of, or for damages resulting from the use of any information, apparatus, method, or process disclosed in this report.

As used in the above, "person acting on behalf of the Commission" includes any employee or contractor of the Commission, or employee of such contractor, to the extent that such employee or contractor of the Commission, or employee of such contractor prepares, disseminates, or provides access to, any information pursuant to his employment or contract with the Commission, or his employment with such contractor.

ORNL-4229
UC-4 - Chemistry

Contract No. W-7405-eng-26

REACTOR CHEMISTRY DIVISION ANNUAL PROGRESS REPORT

For Period Ending December 31, 1967

Director

W. R. Grimes

Associate Directors

E. G. Bohlmann

H. F. McDuffie

G. M. Watson

Senior Scientific Advisor

F. F. Blankenship

MARCH 1968

OAK RIDGE NATIONAL LABORATORY
Oak Ridge, Tennessee
operated by
UNION CARBIDE CORPORATION
for the
U. S. ATOMIC ENERGY COMMISSION



3 4456 0023240 6

Reports previously issued in this series are as follows:

ORNL-2931	Period Ending January 31, 1960
ORNL-3127	Period Ending January 31, 1961
ORNL-3262	Period Ending January 31, 1962
ORNL-3417	Period Ending January 31, 1963
ORNL-3591	Period Ending January 31, 1964
ORNL-3789	Period Ending January 31, 1965
ORNL-3913	Period Ending December 31, 1965
ORNL-4076	Period Ending December 31, 1966

Contents

PART I. MOLTEN-SALT REACTORS

1. Direct Support for MSRE Operations

CHEMISTRY OF THE MSRE

R. E. Thoma	3
-------------------	---

The chemical behavior of the fuel in the Molten-Salt Reactor Experiment, from the standpoint of compatibility and stability, has been virtually ideal. Reduction by treatment with metallic beryllium ensured that it remained that way.

FISSION PRODUCT BEHAVIOR IN THE MSRE

F. F. Blankenship and S. S. Kirsliis	5
--	---

The fate of fission products in the MSRE has been revealed in considerable detail. The more noble metals leave the fuel; an appreciable portion of them leave via the off-gas, possibly as smoke consisting of metallic particles rather than as volatile fluorides.

GAS TRANSPORT IN MSRE MODERATOR GRAPHITE

R. B. Evans III, J. L. Rutherford, and A. P. Malinauskas	15
--	----

Gas transport characterization studies of MSRE moderator graphite have been initiated. Work performed to date indicates that Knudsen flow is the predominant transport mechanism and that the flow parameters vary approximately exponentially with penetration distance.

PREPARATION OF FLUORIDE MIXTURES

F. A. Doss, W. K. R. Finnell, W. P. Teichert, and J. H. Shaffer.....	16
--	----

The fuel preparation facility continued to supply high-purity melts for use at ORNL and at other agencies.

PHASE RELATIONS IN FLUOROBORATE SYSTEMS

C. J. Barton, L. O. Gilpatrick, J. A. Bornmann, H. H. Stone, H. Insley, and T. N. McVay.....	16
--	----

Information on phase behavior in fluoroborate systems has been expanded because of the interest in such materials as heat transfer media.

CORROSION OF HASTELLOY N AND ITS CONSTITUENTS IN FLUOROBORATE MELTS

Stanley Cantor and C. E. Roberts.....	18
---------------------------------------	----

Short-term exposures (up to 25 days) of Hastelloy N to melts of NaBF_4 -NaF have yielded negligible corrosion; however, pure chromium was severely attacked.

COMPATIBILITY OF BF_3 WITH GULFSPIN-35 PUMP OIL AT 150°F

F. A. Doss and J. H. Shaffer.....	18
-----------------------------------	----

Helium containing 1000 ppm BF_3 has been bubbled through oil at 150°C in an examination of the long-term compatibility.

COMPATIBILITY AND IMMISCIBILITY OF MOLTEN FLUORIDES AND FLUOROBORATES

C. E. Bamberger, J. P. Young, C. F. Baes, Jr., and C. S. Sherer.....	20
--	----

The behavior of molten $(\text{Na-K})\text{BF}_4$ mixtures with $\text{LiF}-\text{BeF}_2-\text{ThF}_4-\text{UF}_4$ melts was investigated, using fused silica or Pyrex containers for visual examination. The fluoroborates were found to be only partially miscible with the other fluoride mixtures tested.

2. Behavior of Fission Products and Protactinium in Molten Fluorides

MOLTEN-SALT IRRADIATION EXPERIMENTS

E. L. Compere, H. C. Savage, J. M. Baker, and E. G. Bohlmann..... 22

Irradiation of the second fuel salt convection loop in the Oak Ridge Research Reactor was terminated after the development of 8.2×10^{18} fissions/cc. Average fuel power densities up to 150 w per cubic centimeter of salt were attained in the fuel channels of the core of MSRE-grade graphite. Fission product concentrations approximating those anticipated at processing equilibrium in an MSBR were attained.

BEHAVIOR OF MOLYBDENUM FLUORIDES

Potentiometric Study of Molybdenum in LiF-BeF₂ (67-33 Mole %)

N. J. Meyer, C. F. Baes, Jr., and K. A. Romberger..... 32

Measurements on the Mo|MoF₃ electrode in LiF-BeF₂ confirmed that the concentration of MoF₃ in the MSRE should be vanishingly small at equilibrium.

Preparation and Properties of Molybdenum Fluorides

C. F. Weaver, H. A. Friedman, and D. N. Hess 33

MoF₅ and MoF₃ were synthesized and characterized. Lithium fluoromolybdates were studied, and the behavior of MoF₃ in molten LiF-BeF₂ was investigated.

Mass Spectrometric Studies of Molybdenum Fluorides

R. A. Strehlow and J. D. Redman..... 37

Mass spectrometric studies of volatile molybdenum fluoride species have led to the determination of cracking patterns for three fluorides and two oxyfluorides. The equilibria among the molybdenum fluorides were studied with the aid of a newly designed Knudsen cell assembly which permitted direct admission of MoF₆ into the cell.

BEHAVIOR OF RARE-EARTH FLUORIDES IN MOLTEN LiF-BeF₂ MIXTURES

Solubilities of SmF₃ and NdF₃ in Molten LiF-BeF₂ (66-34 Mole %)

F. A. Doss, F. F. Blankenship, and J. H. Shaffer..... 39

Filtrates from saturated solutions were analyzed to give the solubilities of SmF₃ and NdF₃ in LiF-BeF₂ between 550 and 800°C.

Reductive Extraction of Rare Earths from Molten Fluorides into Molten Metals

D. M. Moulton, W. P. Teichert, W. K. R. Finnell, W. R. Grimes, and J. H. Shaffer 39

Additional data on the distribution of rare earths between LiF-BeF₂ melts and bismuth-lithium alloys were obtained. The results were summarized as extraction potentials of fission products from 2LiF-BeF₂ into bismuth.

METALLIC COLLOIDS IN MOLTEN SALTS

H. W. Kohn 42

Conditions under which silver colloids could be formed by photolysis in nitrate melts were explored.

RECOVERY OF PROTACTINIUM FROM MOLTEN LiF-BeF₂-ThF₄ MIXTURES

Reductive Extraction of Protactinium at Tracer Levels from Molten Fluorides into Molten Metals

D. M. Moulton, W. P. Teichert, W. K. R. Finnell, W. R. Grimes, and J. H. Shaffer..... 43

Demonstrations of the removal of protactinium fluoride from breeder-type melts were carried out by reducing the protactinium to metal and transporting it through bismuth alloys. The results were favorable with respect to reprocessing in various breeder reactor concepts.

Protactinium Studies in the High-Alpha Molten-Salt Laboratory

C. J. Barton and H. H. Stone..... 47

Tracer-level studies on the reductive extraction of protactinium from breeder-type melts into bismuth have been supplemented by experiments in which the protactinium concentrations were as high as expected for full-scale reactor operation.

3. Chemical Studies of Molten-Salt Systems

RELATIONS BETWEEN DEVIATIONS FROM IDEALITY AND ASSOCIATION IN BINARY MIXTURES		
Jerry Braunstein.....		50
The representation of deviation from ideality solely in terms of associated species is not adequate in mixtures of charge-unsymmetrical molten salts (e.g., KCl-MgCl ₂ , LiF-BeF ₂).		
THERMODYNAMICS OF LiF-BeF₂ SYSTEM BY EMF MEASUREMENTS		
B. F. Hitch and C. F. Baes, Jr.....		52
Potentials of the Be ²⁺ Be ⁰ electrode vs the HF,H ₂ F ⁻ electrode have been determined, as well as the activity coefficients of BeF ₂ and LiF, over the composition range 30 to 90 mole % BeF ₂ and the temperature range 500 to 900°C.		
VAPOR PRESSURES AND DERIVED THERMODYNAMIC INFORMATION FOR THE SYSTEM NaBF₄-NaF		
Stanley Cantor, C. E. Roberts, and H. F. McDuffie.....		55
From the equilibrium vapor pressure of BF ₃ in the reaction NaBF ₄ (l) ⇌ NaF (l) + BF ₃ (g), the activity coefficients of the components in the melt were derived.		
VISCOSITY AND ITS TEMPERATURE DEPENDENCE IN MOLTEN BeF₂		
C. T. Moynihan and Stanley Cantor.....		57
Abstract of paper in press with the <i>Journal of Chemical Physics</i> .		
ELECTRICAL CONDUCTIVITY OF MOLTEN SALTS		
G. D. Robbins and Jerry Braunstein.....		57
An improved impedance bridge, in conjunction with a dipping cell, has been employed to measure the electrical conductivity of LiF-BeF ₂ (66-34 mole %) between 470 and 500°C.		
CHEMISTRY OF SiO₂ IN MOLTEN FLUORIDES		
C. E. Bamberger, R. B. Allen, and C. F. Baes, Jr.....		60
Fused silica has been found a usable container material for 2LiF-BeF ₂ melts. The partial pressures and the solubility of generated SiF ₄ are low. The partial pressure of SiF ₄ in equilibrium with SiO ₂ + Be ₂ SiO ₄ was measured, giving improved values for the heat and free energies of formation of Be ₂ SiO ₄ .		
SPECTROPHOTOMETRIC MEASUREMENTS OF MOLTEN FLUORIDES IN SILICA		
C. E. Bamberger, J. P. Young, and C. F. Baes, Jr.....		62
Improved molar absorptivities of UF ₄ in 2LiF-BeF ₂ were determined using SiF ₄ as a cover gas. A spectrophotometric study of Cr ³⁺ indicates its solubility to be >0.43 mole %.		
EVALUATION OF SPECTROPHOTOMETRIC CONTAINERS FOR MOLTEN FLUORIDES		
L. M. Toth and G. P. Smith.....		63
The lack of suitable optical systems for containing molten fluorides is a serious difficulty for spectroscopy. Silica or coated silica can be used for short periods at 500°C. Oddly, an overpressure of SiF ₄ shortens the life of silica cells containing LiF-BeF ₂ .		
SPECTROSCOPIC INVESTIGATION OF NIOBIUM FLUORIDES IN MOLTEN SALTS		
L. M. Toth and G. P. Smith.....		64
The chemistry of NbF ₅ and the lower fluorides of Nb is being elucidated.		
CRYSTAL STRUCTURES OF COMPLEX FLUORIDES		
G. D. Brunton and D. R. Sears.....		64
Crystal structures have been determined for KCeF ₄ , β ₁ -K ₂ UF ₆ , and NaKThF ₆ . A computer-operated automatic diffractometer is being installed.		

PART II. AQUEOUS REACTORS AND DESALINATION

4. Corrosion and Chemical Behavior in Reactor and Desalination Environments

HERMETICALLY SEALED PRESSURIZED- AND BOILING-WATER REACTORS

G. H. Jenks and J. C. Griess 71

We briefly reviewed the water chemistry of both pressurized- and boiling-water reactors, particularly as it relates to the necessity of purification systems, and considered means whereby small reactors could operate satisfactorily without water cleanup or special gas handling equipment.

WATER CHEMISTRY IN A SMALL STATE-OF-THE-ART PRESSURIZED-WATER REACTOR

G. H. Jenks and P. D. Neumann 72

Plans and specifications for a low-power pressurized-water reactor based on state-of-the-art information are being prepared by ORNL, and we are providing specifications and recommendations in areas related to water technology in the reactor.

WATER RADIOLYSIS IN THE HFIR

G. H. Jenks 72

Comparison between reported and predicted concentrations of hydrogen in the HFIR moderator led to the tentative conclusion that its radiolytic behavior is near that predicted. Additional analyses of the relative amounts of oxygen and hydrogen peroxide would be required for complete verification.

ANODIC FILM GROWTH ON METALS AT ELEVATED TEMPERATURES

A. L. Bacarella, H. S. Gadiyar, and A. L. Sutton 74

Electrochemical and ac impedance measurements were made on zirconium, titanium, and niobium. The results for zirconium and titanium were interpreted according to a field-dependent anion migration mechanism.

CORROSION SUPPORT FOR THE HIGH-FLUX ISOTOPE REACTOR

P. D. Neumann and J. C. Griess 76

Corrosion studies with potential decontamination solutions showed 10^{-4} M HNO_3 and 10^{-3} M sodium diethylene triamine pentaacetate (pH = 7.2) could be tolerated by HFIR materials for short periods; 10^{-3} M HNO_3 was too aggressive on both aluminum and beryllium. Heat-transfer corrosion tests showed no inhibition of aluminum corrosion by additions of 20 ppm colloidal silica to deionized water.

CORROSION OF TITANIUM IN SALINE WATERS

E. G. Bohlmann, J. C. Griess, F. A. Posey, and J. F. Winesette 77

Titanium crevice corrosion studies have demonstrated the importance of oxygen to initiation of crevice attack and the efficacy of nickel alloy additions for inhibition of such attack.

EFFECT OF SULFIDE ON CORROSION IN SALINE WATERS

E. G. Bohlmann and J. C. Griess 80

The corrosion of a number of alloys used in desalination equipment is being studied in sulfide-containing saline waters at elevated temperatures.

CARBON DIOXIDE SCALE SUPPRESSION STUDIES

S. A. Reed, D. M. Eissenberg, and C. C. Littlefield 81

An investigation is being conducted to determine the feasibility of controlling alkaline scale formation in seawater distillation plants by a self-sustaining feed treatment cycle utilizing only the carbon dioxide which occurs naturally in seawater.

OSW MATERIALS INFORMATION CENTER

J. L. English and S. A. Reed 83

A Materials Information Center is being established at ORNL to disseminate materials information to OSW contractors and other interested parties.

5. Chemistry of High-Temperature Aqueous Solutions

SOLUBILITY OF Fe_3O_4 AT ELEVATED TEMPERATURES

F. H. Sweeton, R. W. Ray, and C. F. Baes, Jr. 84

Measurements have been completed on solutions saturated at room temperature with 1 atm of H_2 , varied from 100 μm KOH to 100 μm HCl, and equilibrated with magnetite at temperatures varied from 50 to 300°C.

THE INDEPENDENCE OF ISOTHERMAL EQUILIBRIA IN ELECTROLYTE SOLUTIONS ON CHANGES IN DIELECTRIC CONSTANT

W. L. Marshall and A. S. Quist 86

When aqueous solvent species were included as reactants in (complete) equilibrium constants, it was shown that the new constants are independent of changes in dielectric constant for aqueous systems from room temperature to 800°C and 4000 bars pressure and for nonaqueous systems for which published data are available.

ELECTRICAL CONDUCTANCES OF AQUEOUS ELECTROLYTE SOLUTIONS FROM 0 TO 800°C AND TO 4000 BARS

A. S. Quist, W. Jennings, Jr., and W. L. Marshall 88

Conductances of aqueous solutions of sodium chloride, sodium bromide, hydrobromic acid, ammonia, and sodium hydroxide were determined for several different and dilute concentrations at temperatures from 0 to 800°C and pressures to 4000 bars. From these and previous studies, a generalized concept of the equilibrium behavior of electrolyte solutions at high temperature is evolving.

EFFECT OF ADDED ELECTROLYTES ON THE CRITICAL TEMPERATURE OF WATER

E. V. Jones and W. L. Marshall 90

The liquid-vapor critical temperatures of aqueous electrolyte solutions have been determined for 18 different electrolytes at molalities up to 1.5–2.5. The results show systematic behavior in that all 1-1 salts produce about the same effect on T_c , but acids show smaller effects.

ACTIVITY COEFFICIENTS, ASSOCIATION BEHAVIOR, AND THERMODYNAMIC FUNCTIONS OF CALCIUM SULFATE IN AN AQUEOUS MIXED ELECTROLYTE TO 350°C

L. B. Yeatts and W. L. Marshall 92

In one of the first extensive studies of the solubility of a salt in an aqueous four-component mixed electrolyte, activity coefficients, association behavior, and thermodynamic functions for calcium sulfate were obtained from 0 to 350°C. From this study it was found that, by allowing for association to form $CaSO_4^0$, the mean activity coefficient (of $CaSO_4$) was invariant with change in composition of mixed electrolyte at constant ionic strength.

THE LANTHANUM FLUORIDE ELECTRODE RESPONSE IN AQUEOUS CHLORIDE MEDIA

R. E. Mesmer 95

The selectivity of this electrode for fluoride over chloride is found to be $>5 \times 10^{+7}$, while Nernstian behavior is exhibited to $<2 \times 10^{-7}$ m fluoride in fluoride buffered solutions. This electrode is uniquely capable of the high-precision direct measurement of fluoride in chloride and other media suitable for metal ion complexing studies.

BERYLLIUM FLUORIDE COMPLEXES IN AQUEOUS CHLORIDE AND PERCHLORATE MEDIA

R. E. Mesmer and C. F. Baes, Jr. 96

The four stepwise formation equilibria for the species BeF^+ , BeF_2 , BeF_3^- , and BeF_4^{2-} have been determined in chloride and perchlorate media at 25°C. Mixed complexes involving OH^- , Cl^- , or H^+ were not detected.

THE HYDROLYSIS OF BERYLLIUM(II) IN 1 m NaCl

R. E. Mesmer and C. F. Baes, Jr. 98

The hydrolysis behavior of beryllium(II) has been defined from 0 to 60°C in 1 m NaCl. The thermodynamic quantities for the formation of the three hydrolysis products are correlated with the data for previously reported polynuclear hydrolysis products of several other metal ions.

APPARATUS FOR HYDROLYTIC EQUILIBRIA STUDIES UP TO ABOUT 300°C	
R. E. Mesmer and C. F. Baes, Jr.	100
A vessel has been designed for conducting hydrolysis measurements using two H ₂ electrodes in a concentration cell with a Teflon liquid junction of controlled leak rate at elevated temperatures and pressures.	
APPARATUS FOR DETERMINING THE DISSOCIATION CONSTANT OF WATER AT ELEVATED TEMPERATURES	
F. H. Sweeton and R. W. Ray	100
A flowing cell has been assembled for bringing an HCl solution in contact with KOH solution, both solutions containing dissolved H ₂ , at temperatures up to 300°C. The emf between Pt electrodes in the flowing solutions on either side of the junction can be used to calculate the dissociation constant of water.	
HIGH-TEMPERATURE ISOPIESTIC STUDIES	
H. F. McDuffie and P. B. Bien	102
The high-temperature isopiestic unit was redesigned and reconstructed to conform to present standards; it now features a new top-loading servo-controlled balance. The "total ion concept" was found applicable to previously obtained results and extended to deduce that aqueous salt solutions can exist in corresponding states among themselves as well as with pure water.	
 6. Interaction of Water with Particulate Solids	
SURFACE CHEMISTRY OF THORIA	
<i>Heats of Immersion and Adsorption</i>	
H. F. Holmes, E. L. Fuller, Jr., and R. B. Gammage	105
Studies of the heat of adsorption of water on thoria have shown that calcination of thoria above 1000°C produces a material of low specific surface area which appears to be a nearly ideal planar homogeneous surface.	
<i>The Effect of Irreversibly Adsorbed Water on the Character of Thoria Surfaces</i>	
R. B. Gammage, H. F. Holmes, and E. L. Fuller, Jr.	106
Aspects of the irreversible adsorption of water on thoria can be explained by a model which is cognizant of the substrate crystal lattice and the hydrogen bonding characteristics of the water molecule.	
<i>Infrared Spectra of Adsorbed Species on Thoria</i>	
E. L. Fuller, Jr., R. B. Gammage, and H. F. Holmes	108
Meaningful spectra of thoria samples having specific surface areas as low as 1.55 m ² /g have been obtained by the use of a modified infrared spectrophotometer operating in the frequency range of 200 to 4000 cm ⁻¹ .	
PROCESSING OF SOL-GEL UO₂ MICROSPHERES	
C. F. Weaver, D. N. Hess, and H. F. McDuffie.....	110
The previously developed sequence of treatments for the calcination and densification of UO ₂ sol-gel microspheres was simplified and shortened by the use of a hydrocarbon analyzer to monitor the removal of carbonaceous material and by the demonstration of densification and reduction at 850°C.	

PART III. GAS-COOLED REACTORS

7. Diffusion Processes

TRANSPORT PROPERTIES OF GASES

Diffusion Studies in Noble Gas Systems

A. P. Malinauskas, M. D. Silverman, and J. Q. Searcy	115
Tests of a proposal to supplement directly measured diffusion coefficients with viscosity-derived data, in order to obtain meaningful inferences regarding molecular interactions, have been continued.	

Thermal Transpiration

- A. P. Malinauskas 116

Current research on the transpiration phenomenon is directed toward an elucidation of the low-pressure anomaly and the use of transpiration data in studies of inelastic collision processes.

RECOIL OF FISSION PRODUCTS IN HETEROGENEOUS CARBON STRUCTURES

- R. B. Evans III, J. L. Rutherford, and R. B. Perez 116

The investigation of the recoil behavior of fission fragments in pyrocarbons has been extended to include five additional structures, varying from high-density material to rather porous structures.

8. Oxidation of Carbonaceous Materials by Water Vapor

L. G. Overholser

REACTION OF BONDED COATED-PARTICLE FUEL COMPACTS WITH STEAM

- C. M. Blood and G. M. Hebert 119

Rates of oxidation of and damage to bonded coated-particle fuel compacts were determined at temperatures of 1000 to 1200°C using helium-steam mixtures having a steam pressure of 20 or 150 torrs.

REACTION OF PYROLYTIC-CARBON-COATED FUEL PARTICLES WITH WATER VAPOR

- J. E. Baker 121

Rates of oxidation and incidence of coating failures were measured for various batches of coated fuel particles at 1100 and 1200°C using a helium-water-vapor mixture containing 1000 ppm of water vapor.

REACTION OF NEEDLE-COKE GRAPHITE WITH STEAM

- C. M. Blood and G. M. Hebert 123

Oxidation rates of virgin and barium-impregnated needle-coke graphite cylinders were determined at temperatures of 1100 to 1400°C by exposure to a helium-steam mixture having a steam pressure of 20 torrs.

9. Irradiation Behavior of High-Temperature Fuel Materials

O. Sisman and J. G. Morgan

IN-PILE TESTS ON PYROLYTIC-CARBON-COATED FUEL PARTICLES

- P. E. Reagan, E. L. Long, Jr., J. G. Morgan, and J. W. Gooch 125

Fission-gas release rates from pyrolytic-carbon-coated uranium oxide particles, coated from propylene at low temperature and high deposition rate and measured during irradiation, showed improved radiation stability over coatings deposited from methane at high temperature and low deposition rate.

IN-PILE TESTS ON SILICON-CARBIDE-COATED FUEL PARTICLES

- P. E. Reagan, E. L. Long, Jr., J. G. Morgan, and T. W. Fulton 126

Irradiation tests at high temperature showed that coated particles with a silicon carbide layer applied between the porous carbon buffer and the dense isotropic layer may be operated to high burnup at 1300°C with low gas release and good coating stability.

FISSION PRODUCT RELEASE BY POSTIRRADIATION ANNEALING OF COATED PARTICLES

- M. T. Morgan and R. L. Towns 128

Postirradiation fission product release from coated fuel particles showed no effect of pyrolytic-carbon-coating variables on fission product release, but definite effects of a silicon carbide barrier layer were found, as well as differences in fission product release between UC_2 and UO_2 .

MECHANISM OF FISSION-GAS RELEASE FROM FUELED PYROCARBON-COATED MICROSPHERES

- C. D. Baumann and P. E. Reagan 130

The mechanism of fission-gas release during irradiation from intact pyrolytic-carbon-coated fuel particles is shown to be solid-state diffusion of fission products originating in the slightly contaminated coatings.

RELEASE OF IODINE FROM BROKEN COATED PARTICLES (IN PILE AND OUT OF PILE)	
M. T. Morgan, P. E. Reagan, O. Sisman, and R. L. Towns	132
The release of fission product iodine from coated fuel particles with fractured coatings was determined by in-pile analyses of the xenon daughter, by postirradiation analyses of separated coatings and cores, and by postirradiation annealing of broken coated particles.	
POSTIRRADIATION STUDIES OF HIGH-BURNUP COATED PARTICLES	
D. R. Cuneo, E. L. Long, Jr., J. A. Conlin, and H. E. Robertson	133
We have demonstrated that OR-HB-23 (triplex) coated particles are capable of operating at 1400°C to about 45% burnup with no indications of potential failures and that GA-320 (biso) coated particles can be operated at the same temperature and burnup levels with only very slight localized inner coating attack.	
RADIATION DAMAGE IN FAST GAS-COOLED REACTOR FUELS	
D. R. Cuneo, E. L. Long, Jr., H. E. Robertson, and J. A. Conlin	135
The results of irradiation of several experimental fuel assemblies have shown some serious problem areas.	
FISSION-GAS RELEASE DURING FISSIONING OF UO₂	
R. M. Carroll, R. B. Perez, G. M. Watson, O. Sisman, and T. W. Fulton	138
Experiments with fine-grain UO ₂ at 1700°C have shown increased gas release caused by grain growth, which was not observed with single-crystal specimens; however, the gas release above 1600°C from the single crystal was by short bursts, presumably from bubbles or microcracks.	
IN-PILE THERMAL CONDUCTIVITY OF URANIUM DIOXIDE	
R. B. Perez, O. Sisman, R. M. Carroll, and J. G. Morgan	138
The theory has been developed for the calculation of in-pile thermal conductivity of fuel material from pulsed experiments, and preliminary results at ~750°C gave $6 \times 10^{-3} \text{ cal cm}^{-1} \text{ sec}^{-1} (\text{°C})^{-1}$ for fine-grain, high-density UO ₂ .	
10. Behavior of Nonfissile Materials Under Irradiation	
EFFECTS OF LARGE DOSES OF FAST NEUTRONS ON THE MONOCARBIDES OF TITANIUM, ZIRCONIUM, TANTALUM, NIOBIUM, AND TUNGSTEN	
G. W. Keilholtz and R. E. Moore	142
At 1000°C there is a substantial in-reactor annealing effect on gross damage and dimensional changes of refractory-metal monocarbides in a fast-neutron flux; none of the carbides were significantly damaged up to a fast (> 1 Mev) neutron dose of 4.8×10^{21} neutrons/cm ² .	
IRRADIATION DAMAGE TO REFRACTORY-METAL NITRIDES EXPOSED TO FAST-NEUTRON DOSES FROM 0.7 TO 4.9×10^{21} neutrons/cm² AT 150°C	
G. W. Keilholtz and R. E. Moore	143
Nitrides of titanium and niobium did not fracture at 150°C until fast (> 1 Mev) neutron doses in excess of 3.8×10^{21} neutrons/cm ² were received, but the nitrides of tantalum and zirconium fractured at doses as low as 0.7×10^{21} neutrons/cm ² ; volume expansion of the nitrides of titanium, niobium, and zirconium was ~2 to 3%.	
IRRADIATION DAMAGE TO REFRACTORY-METAL DISILICIDES EXPOSED TO FAST-NEUTRON DOSES FROM 0.4 TO 2.7×10^{21} neutrons/cm² AT 150°C	
G. W. Keilholtz and R. E. Moore	143
Fracturing of the disilicides of Zr, Ti, and Ta at 150°C occurred at fast (> 1 Mev) neutron doses greater than 1.5 to 2×10^{21} neutrons/cm ² , but specimens of tungsten disilicide fractured at doses as low as 0.4×10^{21} neutrons/cm ² ; the disilicides expanded in volume from 0.3 to 1.0%.	
FAST-NEUTRON EFFECTS ON ELECTRICAL INSULATORS	
G. W. Keilholtz and R. E. Moore	144
High-density Al ₂ O ₃ is more resistant to fast neutrons at 1000°C than at temperatures from 300 to 600°C.	

PART IV. NUCLEAR SAFETY

11. Experiments in Major Facilities

FISSION PRODUCT BEHAVIOR DURING IN-PILE MELTING OF REACTOR FUELS

S. H. Freid, B. F. Roberts, C. E. Miller, Jr., O. W. Thomas, and W. H. Montgomery 149

The results of recent experiments revealed that (1) relatively large amounts of cesium and iodine were released, (2) approximately 3% of the total iodine released was in an organic form, and (3) the nonorganic iodine which reached the aging chamber was desorbed from the hot chamber walls and converted into a more penetrating species.

IN-PILE BEHAVIOR OF HTGR FUEL ELEMENTS IN MIXTURES OF STEAM AND HELIUM

H. J. deNordwall, S. H. Freid, B. F. Roberts, O. Sisman, O. W. Thomas, and W. H. Montgomery 151

The fuel particles of the model HTGR element have been shown to be well protected against oxidation by steam at $\sim 1100^{\circ}\text{C}$ by their binder and surrounding structural carbon.

FISSION PRODUCTS FROM FUELS UNDER REACTOR-TRANSIENT CONDITIONS

G. W. Parker and R. A. Lorenz 152

Studies of fission product release and transport from metal-clad UO_2 fuel transient-melted under water include tests of the effect of pressure and rate of steam release.

BEHAVIOR OF FISSION PRODUCT SIMULANTS IN THE CONTAINMENT RESEARCH INSTALLATION (CRI) TANK

G. W. Parker, W. J. Martin, G. E. Creek, and N. R. Horton 154

Comparison of the behavior of real and simulated fission products has thus far revealed no significant difference.

12. Development of Devices for the Separation and Measurement of Particles and Fission Products

CLASSIFICATION OF SUBMICRON PARTICLES BY A LOW-PRESSURE IMPACTOR

G. W. Parker, H. Buchholtz, and R. J. Davis 156

A low-pressure cascade impactor has been developed. It is a simple device which separates, into seven separate size increments, aerosol particles which are in the size range 0.01 to $2\ \mu$ in diameter.

ATMOSPHERIC PRESSURE SAMPLERS FOR SIZING PARTICULATE AEROSOLS

R. E. Adams and R. J. Davis 157

Both the fibrous filter analyzer and a multistage inertial impactor sampler, of improved design, are being developed concurrently for application as simple field devices for sampling and sizing particulate aerosols at atmospheric pressure.

IODINE CHARACTERIZATION SAMPLERS

R. E. Adams, R. L. Bennett, and W. H. Hinds 158

Conventional May-pack samplers were found to be inadequate for separating elemental iodine from particles or particulate iodine; a new sampler employing a silver-plated honeycomb to accomplish this separation is being developed.

FISSION PRODUCT DEPOSITION CHARACTERISTICS IN THERMAL GRADIENTS

A. P. Malinauskas 160

A thermodynamic argument is presented to describe the deposition characteristics of fission products in thermal gradients.

13. Supporting Laboratory and Theoretical Studies

MECHANISMS OF SORPTION OF MOLECULAR IODINE

- R. J. Davis 162

A detailed study of the pertinent literature suggested six classes of reactions for sorption of iodine in a reactor containment vessel. An equation was developed for each type of reaction showing the iodine concentration in the vessel as a function of time for iodine removal by that particular reaction.

UPTAKE OF METHYL IODIDE FROM WIND TUNNEL GASES BY A SUSPENDED DROP OF WATER

- B. A. Soldano and W. T. Ward 162

The use of additives can markedly improve the rate of mass transfer of methyl iodide from air to liquid sprays.

REMOVAL OF MOLECULAR FORMS OF RADIOIODINE FROM MOIST AIR SYSTEMS

- R. E. Adams, R. D. Ackley, and Zell Combs 163

Additional types of iodized charcoal have been found effective for trapping radioactive methyl iodide from flowing humid air and steam-air. Also, a number of the iodized charcoals have been tested and found adequate for retention of elemental radioiodine at 25°C.

REACTIONS OF IODINE VAPOR IN CONTAINMENT SYSTEMS

- R. E. Adams, R. L. Bennett, and Ruth Slusher 165

Both calculations and experiments have been used to demonstrate that organic iodides are formed by the reaction of iodine with painted surfaces and also by the gas-phase reaction of iodine with trace organic materials.

APPLICATION OF IODIZED CHARCOALS TO AIR CLEANING SYSTEMS

- R. E. Adams, R. D. Ackley, and Zell Combs 166

The effects on iodized charcoal of weathering and of elevated temperature (which may cause loss of impregnant) are under investigation. The results obtained show that these effects are sufficiently deleterious that provision for their mitigation should be included in designing reactor containment systems.

EFFECT OF WATER VAPOR ON THE VOLATILITY OF FISSION PRODUCT OXIDES: TELLURIUM DIOXIDE

- A. P. Malinauskas 167

Experimental measurements at 955°K indicate a slightly weaker dependence of the volatility of TeO₂ on water vapor pressure than that reported by previous workers, but the reported linear dependence has been reaffirmed.

CHEMICAL EQUILIBRIA OF FISSION PRODUCT-FUEL MIXTURES: GAS PHASE COMPOSITION OF THE URANIUM-OXYGEN-STRONTIUM SYSTEM IN THE PRESENCE OF THE CONDENSED PHASE

- M. H. Fontana and R. E. Bailey 170

The results of multicomponent chemical equilibrium calculations for UO₂, UO₃, and UO concentrations in the vapor phase above solid UO₂ were in good agreement with experimental data, and the calculation techniques were extended to include the U-O-Sr system.

CALCULATION OF THE AMOUNT OF VOLATILE RADIOACTIVITY IN FUEL ROD VOID SPACES - THE D' (EMPIRICAL) METHOD

- G. W. Parker and R. A. Lorenz 173

The D' (empirical diffusion) method has been developed to calculate the amounts of stable and radioactive fission gases in fuel rod void spaces that are available for prompt release as a consequence of a loss-of-coolant accident.

PROMPT RELEASE OF FISSION PRODUCTS FROM HIGHLY RATED ZIRCALOY-CLAD UO₂ FUEL	
M. F. Osborne and G. W. Parker	174
Preliminary studies of the prompt release of implanted tracer radioiodine from ruptured Zircaloy fuel capsules show that >50% of the available iodine escaped; further experiments will investigate fission product release from fuel capsules irradiated at high heat ratings.	
DEVELOPMENT OF FILTRATION TECHNOLOGY	
R. E. Adams, R. J. Davis, J. S. Gill, J. Truitt, and W. D. Yuille	175
This program is being conducted to study the effect of reactor accident environments on the behavior of simulated accident aerosols and on the performance of high-efficiency filtration media; preparations are being made to study the coagulation of an aerosol both on a theoretical and an experimental basis.	
IGNITION OF CHARCOAL ADSORBERS	
R. E. Adams, R. P. Shields, and R. J. Davis	178
The ignition of charcoal is being studied in the laboratory and in-pile to determine the influence of fission products and irradiation; an equation has been developed to define ignition temperature analytically.	

PART V. OTHER ORNL PROGRAMS

14. Effects of Radiation on Organic Materials

EFFECT OF RADIATION ON POLYMERS	
W. W. Parkinson and W. K. Kirkland	183
The tensile strength and elongation at break of thin film polyimide irradiated in air were observed to be reduced drastically at a radiation dose of 3×10^9 rads; this value is an order of magnitude lower than for irradiation in vacuum.	
RADIATION-INDUCED REACTIONS OF HYDROCARBONS	
R. M. Keyser and W. K. Kirkland.....	184
Ten alkyl-naphthalenes have been identified as products in gamma-irradiated solutions of naphthalene in hexane, and a mechanism accounting for their formation is proposed.	
ADDITION REACTIONS OF FURAN DERIVATIVES	
C. D. Bopp, J. J. Myron, and W. W. Parkinson	185
Solutions of cyclohexane in tetrahydrofuran have been irradiated and most of the gaseous, low-boiling, and high-boiling products identified. A mechanism is proposed for their formation.	
DEVELOPMENT OF RADIATION-RESISTANT INSULATORS	
M. J. Kelly, W. W. Parkinson, E. J. Kennedy, B. J. Sturm, and C. D. Bopp.....	186
Pre- and postirradiation electrical property measurements on prospective dosimeter insulating materials have severely limited the polymers to be studied in detail during the later stages of the insulation improvement program.	

15. Support for Other ORNL Programs

STUDY OF UNCLAD-METAL-FUELED FAST BREEDER	
J. E. Savolainen and E. L. Compere	188
A sodium-cooled fast breeder reactor with unclad metal fuel shows promise as a power and heat source, especially for desalination. Its feasibility depends on the oxygen content in the sodium, which if uncontrolled could cause excessive corrosion of the fuel.	

CHEMICAL SUPPORT FOR THE CONTROLLED THERMONUCLEAR RESEARCH PROGRAM

D. M. Richardson 189

An apparatus was constructed to sample and analyze continuously gas from a plasma device at a pressure of 10^{-2} torr. It was operated successfully.

PUBLICATIONS 191

PAPERS PRESENTED AT SCIENTIFIC AND TECHNICAL MEETINGS 196

Part I

Molten-Salt Reactors



1. Direct Support for MSRE Operations

CHEMISTRY OF THE MSRE

R. E. Thoma

Fuel Salt Composition

Part of the chemical research and development in support of the Molten-Salt Reactor Program includes continuous surveillance of the composition and purity of the molten salts, cooling air, treated water, and lubricating oils which are circulated within the MSRE. Principal emphasis has been given to examinations of the fuel salt. Chemical analytical results, obtained over extended periods of reactor operation, serve as a sensitive indicator of generalized corrosion and also reflect slight changes in salt composition resulting from uranium burnup and the occasional mixing of the fuel with the residual salt in the drain tank. Another purpose of this program of analysis has been to identify, develop, and evaluate the methods of analysis which will be necessary for operation of larger reactor plants. Such plants will reprocess

the fuel salt on a semicontinuous basis and will, consequently, need precise on-line methods for determination of compositions and oxidation-reduction potentials of the salts returned to the reactor core.

Routine operations with the MSRE alter the composition of the fuel salt by the consumption or addition of ^{235}U and by intermixing fuel and flush salts. Results of current analyses of the fuel salt are compared with earlier values in Table 1.1. These results indicate that estimates of the fuel composition, as computed from operational data, are in satisfactory agreement with analytical results. Final evaluation of operating power levels and residual reactivity depends on such concurrence.

Statistical analysis of the chemically determined values for uranium concentration shows that control limits have not been exceeded. Within these limits, however, a disparity between computed and analytical values appears to be developing; analytical results indicate that the concentration of uranium in the fuel salt is currently lower by

Table 1.1. Composition of the MSRE Fuel Salt

Run No.	Number of Samples	Composition (wt %)			
		Li	Be	Zr	U
Design (initial)		10.95	6.32	10.97	4.73
4-10 (1966)	69	10.79 \pm 0.64	6.57 \pm 0.18	11.20 \pm 0.26	4.63 \pm 0.026
11 (1967)	38	10.82 \pm 0.35	6.47 \pm 0.15	10.97 \pm 0.17	4.571 \pm 0.019
12 (1967)	8	10.93 \pm 0.40	6.52 \pm 0.15	10.78 \pm 0.24	4.555 \pm 0.027
13-14 (1967)	23	10.73 \pm 0.16	6.28 \pm 0.30	11.11 \pm 0.23	4.559 \pm 0.026
Current computer value ^a		10.97	6.33	10.99	4.567

^aNominal average value for runs 13 and 14.

~0.01 wt % than that computed from operational data. The possibility that a real disparity is developing is under continuing examination in relation to its implications concerning fission product chemistry and in respect to computed vs actual operating power levels.

Fuel Circuit Corrosion Chemistry

Corrosion at salt-metal interfaces in the MSRE is reflected by an increase of chromium concentration in salt samples. Currently the chromium concentration of the fuel salt is 72 ± 7 ppm; this concentration represents an increase of only 34 ppm (and removal of about 170 g of chromium from the entire Hastelloy N container) since operation of the MSRE began in 1965. If the total amount of chromium represented by this increase were leached uniformly from the fuel circuit, it would correspond to removal of chromium from a depth of 0.22 mil.

Recent evidence indicates, however, that only one-fourth of the chromium increase observed in the fuel salt may be attributed to corrosion in the fuel circuit. Examination of the average chromium concentration in the fuel salt has shown that occasional stepwise increases (which have appeared when operations of the MSRE were resumed) are proportional to the length of the prior period during which fuel salt resided in the drain tank. Assignment of the appropriate fractions of chromium to the drain tank and to the fuel circuit under this hypothesis suggests that generalized corrosion in the fuel circuit has amounted to no more than 0.075 mil during the initial 50,000 Mwhr of MSRE operation. This inference has been substantiated recently by the results of examinations of metal surveillance specimens removed from the reactor core in June 1967. Results of electron microprobe analysis¹ showed that, to depths of 50 mils, the concentration profile of chromium in these specimens was unchanged after exposure to the fissioning fuel salt for 30,000 Mwhr except possibly within the outermost 2 to 8 μ , the limit of sensitivity of the technique.

Adjustment of the UF_3 Concentration of the Fuel Salt

For reasons described in the preceding report,² a program was initiated early in 1967 to reduce 1 to

1.5% of the uranium inventory of the MSRE to the trivalent state. The U^{3+} concentration has been increased gradually since that time by addition of a total of 84 g of beryllium metal.³ If it is assumed that corrosion of the fuel has produced 3.3 equivalents of UF_3 and that fission has resulted in the oxidation of 0.8 equivalent of UF_3 per gram atom of fissioned uranium,⁴ the additions of beryllium metal to the fuel should have produced the concentrations listed in Table 1.2.

Nuclear reactivity was not affected by the beryllium additions, nor did chemical analyses reveal any changes resulting from the additions until four exposures to beryllium were made at close intervals during run 12, resulting in the addition of 37.8 g of beryllium to the salt. Samples taken shortly after the last of these four exposures showed an unprecedented increase in the concentration of chromium in the salt (from the previous average of 70 ppm to 145 ppm), followed by a similar decrease during the subsequent sampling period. The possibility that surface-active solids were formed as a consequence of the Be^0 additions was tested by drawing samples from the salt-gas interface as well as below the surface. First, specimens were obtained in a vertical three-compartment sample capsule immersed so that the center hole was expected to be at the interface. Next, a beryllium metal rod was exposed to the fuel salt for 8 hr, adding 9.71 g of beryllium metal. Twelve hours later, a second three-compartment capsule was immersed in the pump bowl. Chemical analyses of the fuel salt specimens did not show significant differences in chromium content, although the salt-gas interface in the second salt capsule was blackened. Examination of the metal basket which contained the beryllium rod during its exposure to the fuel disclosed that dendritic crystals of metallic appearance, together with a small amount of salt residue, were retained in the basket. X-ray diffraction examination of a single dendritic spine⁴ identified the phase as metallic chromium. This identification supports

¹Obtained through the courtesy of C. E. Crouthamel and N. H. Stalica, Chemical Engineering Division, Argonne National Laboratory, Argonne, Ill.

²R. E. Thoma, *Reactor Chem. Div. Ann. Progr. Rept.* Dec. 31, 1966, ORNL-4076, p. 46.

³R. E. Thoma and W. R. Grimes, *MSR Program Semiann. Progr. Rept.* Feb. 28, 1967, ORNL-4119, p. 123.

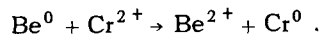
⁴H. Yakel, Metals and Ceramics Division.

Table 1.2. Concentration of UF₃ in the MSRE Fuel Salt^a

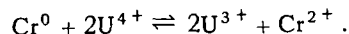
Sample No.	Operation (Mwhr)	U Burned (g)	U Burned (moles)	U ³⁺ Oxidized	Be Added (g)	Be Added (eq)	Net Equivalents Reduced	U ³⁺ /ΣU Calc. (%)	U ³⁺ /ΣU Analysis (%)
9-4	10,978	554	2.34	1.87	0	0	3.13	0.32	0.1
10-25	16,450	829	3.50	2.80	16.28	3.61	5.81	0.60	0.5
11-5	17,743	953	4.02	3.21	16.28	3.61	5.20	0.54	0.37
11-13	20,386	1029	4.34	3.47	27.94	6.20	8.73	0.91	0.42
11-32	25,510	1287	5.43	4.34	27.94	6.20	6.86	0.71	0.34
11-38	27,065	1365	5.76	4.61	27.94	6.20	6.59	0.60	
11-49	30,000	1514	6.39	5.11	36.34	8.06	7.95	0.82	
12-6	32,450	1637	6.91	5.53	36.34	8.06	7.53	0.78	0.37
12-11	33,095	1670	7.05	5.64	54.11	12.01	11.37	1.18	1.2
12-21	35,649	1798	7.59	6.07	74.12	16.45	15.35	1.59	0.5
12-56	39,489	1992	8.41	6.72	83.83	18.60	16.88	1.75	1.4

^aThese numbers are based on assumptions: that the salt originally was 0.16% reduced; that the increase in Cr from 38 to 65 ppm was real, occurred before 11-14-66, and resulted in reduction of U⁴⁺ to U³⁺; that each fission results in oxidation of 0.8 atom of U³⁺; and that there have been no other losses of U³⁺.

the belief that temporary scavenging of chromium from solution results from the localized reduction of chromium by the beryllium metal:



This chromium metal may exist as a nonwetted scum upon the surface of the salt at the gas-liquid interface in the pump bowl. Subsequently, as the mechanical mixing brings the bulk of the fuel salt into contact with the chromium metal, the U⁴⁺ is reduced by the chromium until thermodynamic equilibrium is established, and the chromium is redissolved and dispersed throughout all the salt:



FISSION PRODUCT BEHAVIOR IN THE MSRE

F. F. Blankenship

S. S. Kirslis

Introduction

Previous studies in pile and in the MSRE have been very reassuring regarding most aspects of the chemical compatibility of graphite and Hastel-

loy N with molten fissioning salt. The aspect of chemical behavior currently causing some practical concern is the observed tendency of noble-metal fission products (Mo, Ru, Tc, Te, and Nb) to deposit on graphite surfaces exposed to fissioning fuel in the MSRE. The deposition of these moderate neutron poisons is of minor concern to the operation of the MSRE but might affect significantly the neutron economy of a molten-salt breeder reactor.

It was reported previously that the noble-metal fission products also deposited heavily on Hastelloy N surfaces in the core and were found in appreciable concentrations in the gas phase of the MSRE pump bowl. The fuel phase was therefore considerably depleted in noble metals, while the nuclides with stable fluorides were found in the fuel in expected amounts.

Chemical studies in the past year were directed toward more reliable quantitative determinations of the distributions of the noble metals among the fuel, the cover gas, and the graphite and metal surfaces and toward elucidating the reasons for their observed behavior. Improved techniques for sampling the fuel phase and the cover gas were developed, the effect of reactor operating variables was explored, and special experiments to determine the chemical and physical state of the noble metals in MSRE fuel were carried out.

Analysis of Fuel Samples

ORNL-DWG 67-4784

A large number of fuel salt samples have been taken by the usual lading technique (windlass and well bucket) from the MSRE pump bowl. Analyses for bulk fuel constituents and for fission products with stable fluorides were reproducible and were in fair agreement with calculated values. However, several observations cast doubt upon the validity of the radiochemical analyses for the noble-metal fission products. The results showed wide scatter, often by as much as a factor of 10. Exposures of metal specimens to the pump bowl cover gas showed heavy selective deposition of the noble metals. Finally material balance considerations indicated that all the noble metals produced could be accounted for by the amounts found in the cover gas and deposited on graphite and metal. It was therefore suspected that the metal ladle used for fuel sampling may have been heavily plated with noble metals while it slowly traversed the pump bowl gas phase before and after dipping up a sample of fuel.

Two fuel salt samples were therefore taken in freeze-valve capsules of the design shown in Fig. 1.1. By this technique the contamination of the enclosed salt sample by the activities in the cover gas was avoided. A comparison of the analytical results from the two techniques is shown in Table 1.3. The much lower noble-metal concentrations from the freeze-valve capsule technique indicate that the bulk of the noble metals found in ladle samples did arise from contamination by gas-phase activities. It must be concluded that only 1% or less of the noble-metal nuclides produced remains in the fuel salt phase. This result is of practical importance in planning fuel salt processing procedures for molten-salt reactors.

Qualitative Pump Bowl Tests

The first indications of appreciable noble-metal fission product volatilization came from the analysis of metal specimens exposed to the pump bowl gas phase. The activities deposited included the noble metals and nuclides with rare-gas precursors of appreciable half-life. The remaining fission products possessing stable fluorides were not found on the specimens. A number of different metals (Ag, Ni, Hastelloy N, Au, and stainless steel) were exposed simultaneously in the hope of

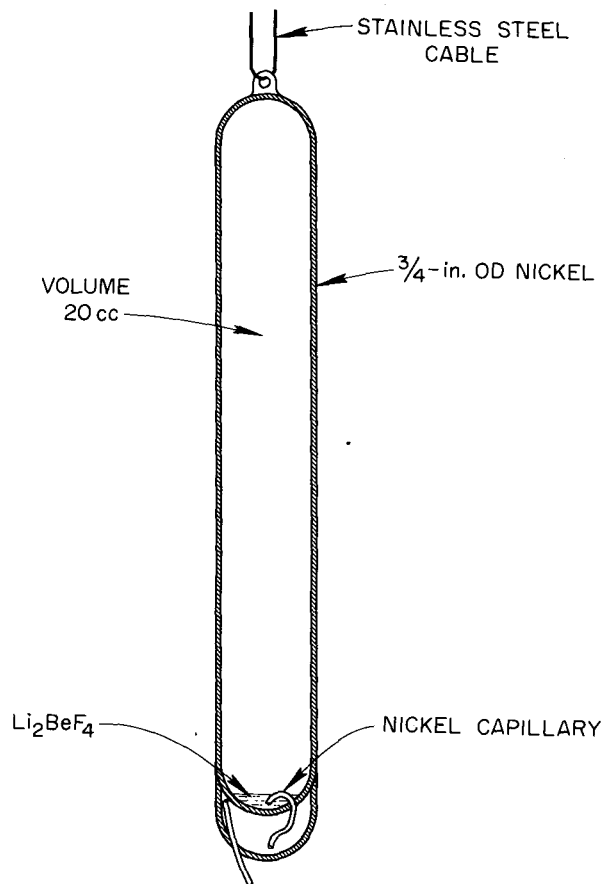


Fig. 1.1. Freeze Valve Capsule.

deriving information on the chemical state of the volatilizing species. Comparative runs were made in which the metal specimens were prefluorinated, prehydrogenated, and left in the normal slightly oxidized condition. Exposure times were varied from 1 to 10 min, and runs were made under a variety of reactor operating conditions.

The reproducibility of the deposition results was poor, with variations between duplicate runs often as high as an order of magnitude. Deposition on the different metals was not significantly different. Prefluorination of the metal specimens approximately halved the deposition of noble metals in most cases compared with the untreated or hydrogenated specimens, but this small difference may not be significant. Exposure time had little effect; samples exposed for 1 min collected as much activity as those exposed for 10 min. Changes in reactor operating conditions also had little effect on deposition. Even samples exposed several

Table 1.3. Fission Products in MSRE Fuel Samples

Sample No.		FP 14-20	FP 14-22	FP 14-30
Sampling date		11-3-67	11-7-67	12-5-67
Sampling method		Freeze-valve capsule	Ladle	Freeze-valve capsule
Isotope	Fission Yield	Activity ^a (dis min ⁻¹ g ⁻¹)		
⁹⁹ Mo	6.06	2.22×10^9	8.15×10^{10}	8.5×10^8
¹³² Te	4.7	8.19×10^8	8.9×10^9	1.26×10^9
¹²⁹ Te	0.35	$<1.07 \times 10^8$	1.86×10^8	
¹⁰³ Ru	3.0	1.40×10^8	3.74×10^9	4.9×10^7
¹⁰⁶ Ru	0.38	2.38×10^7	$\sim 2.7 \times 10^8$	$<6.4 \times 10^6$
⁹⁵ Nb	6.2	4.2×10^7	$<10^8$	7.0×10^5
⁹⁵ Zr	6.2	1.19×10^{11}	1.28×10^{11}	1.29×10^{11}
¹³¹ I	3.1	5.51×10^{10}	6.64×10^{10}	3.40×10^{10}
⁸⁹ Sr	4.79	8.15×10^{10}	9.15×10^{10}	8.46×10^{10}
¹⁴³ Ce	5.7	1.41×10^{11}	1.69×10^{11}	
¹⁴⁷ Nd	2.7	6.75×10^{10}		
¹⁴⁰ Ba	6.35	1.59×10^{11}		1.16×10^{11}
²³⁹ Np		5.96×10^{11}		5.36×10^{11}

^aAll activities calculated back to sampling time.

hours after stopping the fuel pump or two days after draining the fuel out of the reactor showed as much deposition of noble metals as normal samples. The addition of beryllium to reduce the fuel caused no significant change in deposition. The only reactor operating variable which had a definite effect on gas-phase deposition was a long reactor shutdown of two weeks or more. Then definite decreases in noble-metal deposition by an order of magnitude were observed.

As these deposition results accumulated, our suspicions grew that extraneous experimental factors were invalidating the straightforward interpretation of the observations. The last nine tests were carried out partly or wholly to check various features of the experimental technique. The last two identified the basic difficulties. In the first of these, the metal specimens were lowered in the sampling pipe to a position 2 ft above the pump bowl. During the 10-min exposure, a helium flow of 200 cm³/min was passed down the tube as usual. The test assembly was then withdrawn and

analyzed as usual. Approximately the same amounts of noble-metal nuclides were deposited on the test specimens as in normal exposures in the pump bowl. The second test consisted in hanging a standard test assembly on the cable latch, leaving it there for one day as in the customary test procedure but not lowering it at all into the tube leading to the pump bowl, removing it with the sampling cubicle manipulator, and packaging it for shipment for analysis as usual. Again the amounts of noble-metal activities found on the specimens were nearly as great as in normal pump bowl exposures.

These tests of experimental technique explain why roughly similar deposition results were obtained in the many tests carried out under very different experimental conditions. Apparently the test specimens were highly contaminated by repeated contact with the sampling cubicle manipulator and the cubicle floor in the operations involved in placing the test assembly in the cable latch, removing it, and packaging it for shipment. The contamination of the cubicle surfaces is renewed

Table 1.4. Fission Products in MSRE Pump Bowl Gas as Determined from Freeze Valve Capsules

Experiment No.	FP10-11	FP10-22	FP11-42	FP11-46	FP11-53	FP12-7	FP12-26
Sampling date	12-27-66	1-11-67	4-11-67, 02:49	4-18-67, 02:28	5-2-67, 10:43	6-2-67, 06:50	7-17-67, 06:03
Operating time, days ^a	14.5 off, 12.6 on	14.5 off, 27.7 on	65 on, off 1.5 hr	14 off, 72 on	14 off, 86 on	92.3 on, 42.5 off	46 off, 23 on
Nominal power	7.4	7.4	0	7.2 Mw	7.2 Mw	0	7.2 Mw
Be addition	No	After 5.5	After 8.40 g	No	No	No	After 37.8 g
Features	Regular	Regular	Pump off 1.2 hr	Regular	Helium bubbles	Power off 42.5 d	Regular
Accumulated Mwhr	13,600	16,200	27,900	29,100	31,700	32,650	36,500

Isotope	Yield	Disintegrations per minute in total sample ^b					
⁹⁹ Mo	6.06	2.04×10^{11}	1.36×10^{11}	1.05×10^{11}	2.31×10^{11}	1.57×10^{11}	2.74×10^{11}
¹⁰³ Ru	3.0	3.80×10^9	2.63×10^9	2.51×10^9	4.64×10^9	1.12×10^{10}	4×10^9
¹⁰⁶ Ru	0.38	$\sim 6.7 \times 10^7$	7.74×10^7	8.2×10^7	9.49×10^7	4.03×10^8	1.7×10^8
¹³² Te	~ 4.7	5.73×10^{10}	5.08×10^{10}	1.15×10^{11}	3.35×10^{11}	1.88×10^{11}	4.17×10^7
¹²⁹ Te	0.35				7.98×10^8	3.51×10^9	2.17×10^8
⁹⁵ Nb	6.2	$\leq 3.26 \times 10^7$	2.09×10^8	6.45×10^8	1.3×10^9	1.05×10^{10}	2.26×10^9
⁹⁵ Zr	6.2	$< 2.9 \times 10^6$	$\leq 2.2 \times 10^7$	$< 4.4 \times 10^7$	$\sim 2 \times 10^7$	1.8×10^8	8.64×10^7
¹⁴⁰ Ba	6.35	2.75×10^8	3.48×10^8		6.16×10^8		
¹³¹ I	~ 3.1	9.75×10^9	2.03×10^9	5.7×10^9	9.81×10^8	8.63×10^9	1.67×10^{10}
⁸⁹ Sr	4.79			2.13×10^8	4.08×10^9	3.72×10^9	8.35×10^8
¹¹¹ Ag	0.019					5.5×10^8	1.33×10^8
¹⁴¹ Ce	~ 6.0						4.79×10^8
¹⁴⁴ Ce	~ 6.0						4.17×10^7
²³⁵ U		3.86 ^c	0.55 ^c	59 ^c	9.2 ^c	23 ^c	25 ^c

^aDuration of previous shutdown and of continuous operating time just before sample was taken.

^bDisintegrations per minute calculated to the time of sampling or of previous shutdown.

^cMicrograms in sample.

each time a sample is removed from the pump bowl. Alternatively, much of the contamination may have occurred while the test assembly remained for a day on the latch in the highly contaminated cable drive box. This alternative accounts more satisfactorily for the surprisingly uniform "depositions" observed in many of the tests.

These observations make it necessary to discard most of the results of the qualitative deposition tests. They also help to explain the contamination of the salt sampling ladle previously discussed. A sheathed capsule has been designed which will protect metal specimens from contamination except when the test assembly is in the pump bowl.

Quantitative Analysis of Pump Bowl Cover Gas

In order to explore in a more quantitative way the significant qualitative finding that high concentrations of noble-metal activities were present in the pump bowl cover gas, a freeze-valve capsule (Fig. 1.1) was developed for sampling a known volume of cover gas in a way that avoided contamination problems. The technique is described in detail elsewhere.⁵ In brief, a 20-cm³ gas sample is taken into an evacuated capsule sealed by a freeze valve (Fig. 1.1) which opens automatically when the capsule reaches the pump bowl gas space. Since a known volume of gas is sampled, the gaseous concentrations of fission product species may be quantitatively determined from radiochemical analyses of the activities found inside the capsule.

Seven freeze-valve capsule runs have been made — two under normal reactor operating conditions, two after beryllium additions to the fuel, one after a long reactor shutdown, one after stopping the MSRE fuel pump for 1.2 hr, and one after generating helium bubbles in the fuel by suddenly lowering the cover gas pressure from 15 psig to 5 psig. The results, together with the reactor operating conditions and special features of each test, are given in Table 1.4. The results are discussed in detail elsewhere;^{5,6} some of the more important conclusions are summarized below.

Surprisingly high concentrations of noble-metal fission products were found in the helium cover

gas: 2 to 7 ppm by mole for ⁹⁹Mo, 1 to 4 ppm for ¹⁰³Ru, 1 to 10 ppm for ¹³²Te, and 0.07 to 4 ppm for ⁹⁵Nb. If these concentrations are multiplied by the flow of helium through the pump bowl (6000 liters/day), the daily loss to the off-gas of each species is on the average more than half of the daily production of each isotope at 7.2 Mw.

High apparent uranium concentrations (6.5 to 700 ppm ²³⁵U by mole in helium) have not been explained. When the observed concentrations of ⁹⁵Zr were taken as a measure of the fuel salt mist carried into the capsule during sampling, only three of the uranium values could be accounted for.

It is possible that gaseous or suspended species are concentrated in the mist shield region of the pump bowl, from which the gas samples are taken. The observed concentrations of ⁸⁹Sr in the gas samples offer clues in this regard. From comparing the ⁹⁵Zr and ⁸⁹Sr values, it is clear that most of the ⁸⁹Sr in samples taken during power operation arose from the decay of gaseous ⁸⁹Kr rather than from salt mist. However, the so-derived gaseous ⁸⁹Kr concentrations are several times higher than ⁸⁹Kr concentrations calculated on the hypothesis that the stripping of 3.2-min ⁸⁹Kr from the fuel by passage through the spray ring in the pump bowl was 100% efficient. It thus appears that ⁸⁹Kr, and presumably other volatilizable species, may somehow be concentrated several-fold in the mist shield region compared with the rest of the pump bowl gas phase. This correction would bring the noble-metal and uranium losses to the off-gas down to values consistent with other data.

The appreciable concentrations of ⁸⁹Sr found in samples FP11-42 and FP12-7 are puzzling. In each case the reactor had been shut down long enough to permit the complete decay of ⁸⁹Kr before sampling. These data also suggest poor flushing of the mist shield region by the cover gas.

The effect of short shutdown and pump stoppage (FP11-42) on the volatilization of noble metals was minor. This run yielded the highest gaseous uranium concentration. The highest values for ¹⁰³Ru, ¹⁰⁶Ru, and ¹²⁹Te were obtained during the pressure release run (FP11-53). However, the values for ¹³²Te and ⁹⁹Mo were not exceptionally high. The effect of reactor drain and long shutdown (FP12-7) was to lower markedly the volatilization of noble metals. No distinct effect

⁵MSR Program Semiann. Progr. Rept. Feb. 28, 1967, ORNL-4119, p. 138.

⁶MSR Program Semiann. Progr. Rept. Aug. 31, 1967, ORNL-4191, p. 116.

could be ascribed to the addition of beryllium to the fuel before three of the samplings.

For the noble metals, the volatilizing species may be either high-valent fluorides or stable gaseous suspensions of minute metallic particles. The above observations do not decide the issue conclusively. From thermodynamic considerations, the finely divided metallic state is favored. In the case of uranium, it is thermodynamically unlikely that the volatilizing species is metallic uranium. However, if UF_6 is postulated as the volatile species, corresponding pressures of the high-valent noble-metal fluorides should coexist at equilibrium.

From the standpoint of neutron economy, the loss of noble-metal nuclides to the off-gas is advantageous, and it might be desirable to enhance the degree of volatilization. On the other hand, the loss of uranium from the fuel is undesirable, and methods for its recovery might be required.

Examination of Metal and Graphite Samples from the MSRE Core After 24,000 Mwhr Exposure

Another set of long-term surveillance specimens of MSRE graphite and Hastelloy N was examined after exposure to circulating fuel in an axial core position of the MSRE for 24,000 Mwhr of power operation. The results were very much like those previously reported after a 7800-Mwhr exposure.⁷

Results on Graphite Specimens. — Visually, the graphite appeared unchanged by the exposure. Metallographic examination showed no alteration of the structure and no evidence of surface films. X radiography revealed only cracks that were previously known to exist. X-ray diffraction of the surface gave normal graphite lines and a few weak foreign lines that were probably due to traces of adhering fuel. Autoradiography showed a high concentration of activity within a few mils of the surface with diffuse irregular penetration to the center, a distance of $\frac{1}{4}$ in. or more. Bars that were 4.5 in. long gained 0.002 ± 0.002 in. in length and 13 mg (0.03%) in weight.

⁷S. S. Kirsliis and F. F. Blankenship, *Reactor Chem. Div. Ann. Progr. Rept. Dec. 31, 1966*, ORNL-4076, p. 48.

Concentration profiles for fission products in the graphite were determined by milling off layers which were dissolved and analyzed radiochemically. The predominant activities found were molybdenum, tellurium, ruthenium, and niobium. Occasionally some faces of the graphite were permeated to a greater extent than others. The practical concern, in connection with long-term neutron economy, is with ^{95}Mo , ^{97}Mo , ^{99}Te , and ^{101}Ru ; but these particular isotopes are not amenable to direct analysis. Nevertheless, their deposition behavior was indirectly indicated by a radioactive isotope of the same metal or by a radioactive noble-metal precursor with a suitable half-life.

Over 99% of the noble-metal activities were encountered within the first 2 or 3 mils of the graphite surface; the same was true for ^{95}Zr . The profile for ^{132}Te was typical (see Fig. 1.2). The behavior of fission products with rare-gas precursors

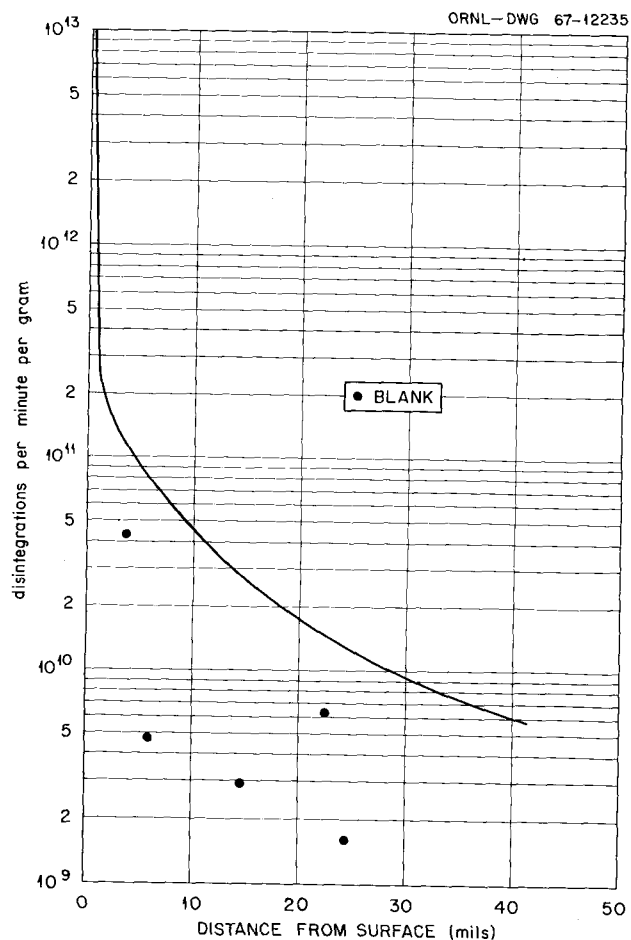


Fig. 1.2. Distribution Profile for ^{132}Te in Graphite from MSRE Core.

Table 1.5. Fission Product Deposition on MSRE Graphite After 7800 and 24,000 Mwhr

Graphite Location	Fission Product Activity (dis min ⁻¹ cm ⁻²) ^a											
	67-hr ⁹⁹ Mo		78-hr ¹³² Te		39.7-day ¹⁰³ Ru		1.02-year ¹⁰⁶ Ru		35-day ⁹⁵ Nb		65-day ⁹⁵ Zr	
	b	c	b	c	b	c	b	c	b	c	b	c
	× 10 ¹⁰	× 10 ¹⁰	× 10 ¹⁰	× 10 ¹⁰	× 10 ¹⁰	× 10 ¹⁰	× 10 ¹⁰	× 10 ¹⁰	× 10 ¹⁰	× 10 ¹⁰	× 10 ¹⁰	× 10 ¹⁰
Top	3.97	3.69	3.22	2.12	0.83	0.91	0.003	0.46	6.2	0.0004	0.001	
Middle	5.14	4.79	3.26	3.82	0.75	1.19	0.006	2.28	1.17	0.003	0.007	
Bottom	3.42	4.39	2.78	2.66	0.48	1.10	0.005	2.40	17.4	0.002	0.02	

^aMean values for all four faces.

^bValue obtained after 7800 Mwhr.

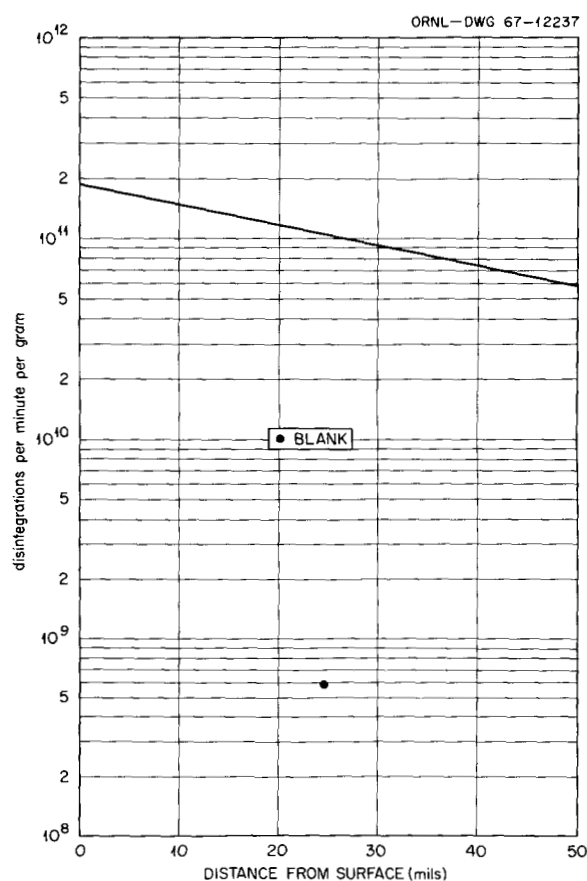
^cValue obtained after 24,000 Mwhr.

Fig. 1.3. Distribution Profile for ⁸⁹Sr in Graphite from MSRE Core.

is like that shown for ⁸⁹Sr in Fig. 1.3. Because of the concentration at the surface, the total amounts of several of the isotopes could be represented by the amount in the first few layers. These amounts, in disintegrations per minute per square centimeter, are compared with the results after 7800 Mwhr in Table 1.5 at the top, middle, and bottom of the core. If the amounts found are the same for all the graphite in the core, the graphite contains only 10 to 30% of the total yield of the noble metals produced by the reactor.

The samples milled from the graphite were analyzed for ²³⁵U by neutron activation. The concentration diminished sharply with depth of milling and represented less than 4 g of ²³⁵U in the entire moderator if the deposition was uniform. The uranium in the fuel was about 30% enriched in ²³⁵U; hence the total uranium deposited would have been 10 to 15 g.

Results on Hastelloy N. — The graphite specimens were assembled and exposed within a cylindrical perforated holder of Hastelloy N. Samples of metal cut from this cylinder gave the results shown in Table 1.6. The noble metals, assuming uniform deposition, are accounted for to the extent of 40 to 80% of their total yield. If these analyses are typical of all the metal, about 1 g of ²³⁵U is accounted for in or on the metal.



Hot-Cell Test of Fission Product Volatilization from Irradiated MSRE Fuel

Two of the freeze-valve capsule gas samples taken after reactor shutdown (FP11-42 and FP12-7) contained appreciable concentrations of noble-metal activities, indicating that fission and a

Table 1.6. Fission Product Deposition on Hastelloy N in MSRE Core After 7800 and 24,000 Mwhr

Isotope	Hastelloy N Location ^a							
	Extreme Top ^b	Top		Middle		Bottom		Extreme Bottom ^b
		c	b	c	b	c	b	
67-hr ⁹⁹ Mo ($\times 10^{-11}$) ^d	2.84	3.12	3.94	2.76	2.86	2.04	4.42	0.74
78-hr ¹³² Te ($\times 10^{-11}$)	6.66	5.08	5.66	3.41	2.06	4.27	4.02	1.94
37.6-day ¹⁰³ Ru ($\times 10^{-10}$)	0.99	3.55	10.6	2.55	1.56	2.32	6.02	
35-day ⁹⁵ Nb ($\times 10^{-11}$)	1.04		2.32		2.32		1.66	0.16
65-day ⁹⁵ Zr ($\times 10^{-8}$)	2.32	18.5	1.56	18.4	8.62	25.8	4.10	0.32
50.5-day ⁸⁹ Sr ($\times 10^{-8}$)	1.69		10.3		46.1		5.93	0.834
8.05-day ¹³¹ I ($\times 10^{-9}$)	1.60	8.24	3.93	3.97	3.18	5.24	7.67	
²³⁵ U ($\mu\text{g}/\text{cm}^2$)	≤ 1.3		1.51		0.92		0.61	0.61

^aAll surveillance specimens in center axis of core.

^bAfter 24,000 Mwhr.

^cAfter 7800 Mwhr.

^dAll values except ²³⁵U in disintegrations per minute per square centimeter of Hastelloy.

neutron flux were not essential to the volatilization process. This suggested the possibility of studying volatilization from a sample of MSRE fuel salt in a hot cell, where control of experimental variables would be much better than in the access tube to the MSRE pump bowl.

The experimental plan was to determine the nature and quantity of activities in the gas phase above the surface of a molten 50-g MSRE fuel salt sample when (1) pure dry helium was passed at a flow rate of 10 to 15 cm³/min over the salt surface, (2) helium containing 5% H₂ was similarly passed over the surface, (3) pure helium was bubbled at 10 to 15 cm³/min through the salt, and (4) 5% H₂-95% He was similarly bubbled through the salt. With the salt contained in a gastight stainless steel reaction vessel, the gas phase was sampled by forcing the helium to exit through a probe tube with its end within 1/4 in. of the molten-salt surface. The nickel probe tube contained successively an empty section, a Feltmetal filter, an NaF trap, and a soda-lime trap. Salt samples were taken with small ladles after steps 2 and 4.

This plan was based on the following assumptions: that only high-valent fluorides would

volatilize in procedure 1, since gentle helium flow would provide no agitation to suspend metallic particles; that volatile fluorides should be reduced by H₂ in procedure 2 to nonvolatile species which should redissolve in the melt, yielding low activities in the probe; and that metallic particles should be suspended in the gas phase by bubbling helium or H₂ in procedures 3 and 4 and should be found on the Feltmetal filters in the probes. Further chemical information would be derived from the relative amounts of activities deposited in the four sections of the probe tubes.

Two hot-cell experiments of this type have been carried out, the first with a sample of MSRE fuel salt 35 days old and the second on the day after salt sampling. The completed analytical results for the first test are given in Table 1.7.

With helium flowing gently over the surface of the molten fuel, substantial amounts of ⁹⁵Nb, ¹⁰³Ru, and ¹⁰⁶Ru were found on the various sections of the probe, particularly on the bottom empty section. According to the analyses for ⁹⁵Zr, ¹⁴¹Ce, and ²³⁵U, about 1 mg of fuel salt was also deposited on the bottom section. The amounts of noble metals, however, exceeded the values for 1 mg of salt (cf. Table 1.3) by at least

Table 1.7. Volatilization of Noble Metals from MSRE Fuel

Flow Conditions	Sample ^a	Disintegrations per Minute per Total Sample ^b								²³⁵ U (μg total)
		¹⁰³ Ru	¹⁰⁶ Ru	⁹⁵ Nb	⁹⁹ Mo	¹³² Te	¹²⁹ Te	⁹⁵ Zr	¹⁴¹ Ce	
10-15 cm ³ /min pure He over surface	B	7.11 × 10 ⁶	4.87 × 10 ⁵	1.80 × 10 ⁹	Low	Low	1.99 × 10 ⁶	1.70 × 10 ⁸	6.72 × 10 ⁷	6.20
	FM	4.30 × 10 ⁶	3.59 × 10 ⁵	1.3 × 10 ⁶	Low	Low	Low	~1.5 × 10 ⁵	1.1 × 10 ⁵	0.064
	NaF	8.14 × 10 ⁴	1.58 × 10 ⁴	≤ 2.3 × 10 ⁵	Low	Low	Low	<6.9 × 10 ⁴	<1.7 × 10 ⁴	0.086
	SL	6.70 × 10 ⁴	1.00 × 10 ⁴	≤ 5.9 × 10 ⁴	Low	Low	Low	≤ 2.2 × 10 ⁴	<8.3 × 10 ³	0.027
10-15 cm ³ /min 5% H ₂ over surface	B	3.77 × 10 ⁷	3.01 × 10 ⁶	9.53 × 10 ⁸	Low	Low	7.45 × 10 ⁶	1.53 × 10 ⁸	1.96 × 10 ⁸	22.7
	FM	4.22 × 10 ⁵	3.50 × 10 ⁴	1.6 × 10 ⁶	Low	Low	Low	1.3 × 10 ⁶	1.43 × 10 ⁶	0.157
	NaF	3.39 × 10 ⁴	5.76 × 10 ³	~3.7 × 10 ⁵	Low	Low	Low	5.3 × 10 ⁵	3.73 × 10 ⁵	0.071
	SL	1.47 × 10 ⁴	3.41 × 10 ³	~9.0 × 10 ⁴	Low	Low	Low	1.6 × 10 ⁵	2.08 × 10 ⁵	0.066
10-15 cm ³ /min 5% H ₂ bubbling through salt	B	3.85 × 10 ⁸	4.7 × 10 ⁷	0	Low	Low	~1.9 × 10 ⁷	5.86 × 10 ¹⁰	5.18 × 10 ¹⁰	7096.00
	FM	2.45 × 10 ⁹	1.7 × 10 ⁸	0	Low	7.8 × 10 ⁹	6.2 × 10 ⁷	2.86 × 10 ¹⁰	2.35 × 10 ¹⁰	3532.00
	NaF	7.5 × 10 ⁷	7.6 × 10 ⁶	7.15 × 10 ⁷	~1.1 × 10 ¹¹	7.8 × 10 ⁹	4.2 × 10 ⁶	~1.2 × 10 ⁶	9.00 × 10 ⁵	0.143
	SL	1.73 × 10 ⁷	~1.5 × 10 ⁶	1.67 × 10 ⁸	~4.2 × 10 ⁹	~3.4 × 10 ⁹	1.9 × 10 ⁶	3.31 × 10 ⁵	4.36 × 10 ⁵	0.149
10-15 cm ³ /min pure He bubbling through salt	B	2.14 × 10 ⁸	1.5 × 10 ⁷	1.72 × 10 ¹⁰	~1.2 × 10 ¹¹	5.9 × 10 ¹⁰	2.2 × 10 ⁷	3.26 × 10 ⁹	2.70 × 10 ⁹	414.00
	FM	1.52 × 10 ⁹	1.65 × 10 ⁸	7.84 × 10 ⁹	~1.9 × 10 ¹²	9.8 × 10 ¹⁰	3.8 × 10 ⁷	1.25 × 10 ⁹	1.17 × 10 ¹⁰	1720.00
	NaF	1.28 × 10 ⁸	9.8 × 10 ⁶	3.53 × 10 ⁷	~2.7 × 10 ¹¹	~1.4 × 10 ¹⁰	6.0 × 10 ⁶	8.8 × 10 ⁵	6.24 × 10 ⁵	0.297
	SL	~6.4 × 10 ⁷	~6.3 × 10 ⁶	7.73 × 10 ⁷	~8.5 × 10 ¹⁰	5.6 × 10 ⁹	3.3 × 10 ⁶	2.09 × 10 ⁶	7.75 × 10 ⁵	0.367

^aB is bottom empty 1 in. of probe, FM is section including the Feltmetal filter, and NaF and SL are the sections packed with NaF and soda lime respectively.

^bActivities calculated back to fuel sampling time: 10-23-67, 0944 AM.

an order of magnitude, particularly for ^{95}Nb . The amounts of ^{95}Nb , ^{95}Zr , ^{141}Ce , and ^{235}U were lower by a factor of 100 to 1000 on the Feltmetal section, but the ruthenium isotopes dropped less than a factor of 2. All these activities penetrated to the NaF and soda-lime sections in measurable amounts.

The results with 5% H_2 -95% He flowing gently over the surface were not significantly different. When helium or 5% H_2 -95% He was bubbled through the fuel melt, much larger quantities of all activities were found in the probes. So much fuel was "volatilized" that the Feltmetal filters partially plugged, requiring higher pressures to maintain a gas flow of 10 to 15 cm^3/min . Even the ^{99}Mo and ^{132}Te , which had largely decayed away in the 35 days since fuel sampling, were detected in most samples. A preferential volatilization of the noble metals was apparently caused by the bubbling procedure, as was observed with the gentle sweep tests.

The bubbling tests rather definitely indicate that both fuel salt and noble metals are carried into the probes as mists or colloids, some of which are so fine that they easily penetrate the 4- μ Feltmetal filters. In the sweep tests the results indicate that fuel salt particles are entrained in the gas phase even at the very slow flows used. This unexpected result suggests that it is at least equally likely that minute colloidal particles of the noble metals are similarly entrained. The test was therefore not as discriminating as was hoped in distinguishing between volatilization as high-valent fluorides and as metallic gaseous suspensions. The minor effect of 5% H_2 in reducing volatilization in the gentle sweep test is evidence that volatile fluorides played a small role in the volatilization of noble metals.

A significant result of this test is that no more ^{235}U was generally found in the probe samples than corresponded to the amounts of salt mist indicated by the analyses for ^{95}Zr , ^{141}Ce , ^{140}Ba , and ^{89}Sr .

Only a few scattered analytical results on ^{99}Mo , ^{132}Te , ^{103}Ru , ^{106}Ru , and ^{95}Nb have been received as yet on the samples from the second volatilization test, which was run on the day after fuel sampling. These results indicate very different behavior from the first test. Bubbling of the gases through the melt caused no greater noble-metal volatilization than the gentle sweep of gas

over the surface. There was also a much smaller decrease in each activity from the bottom section to the soda-lime section of each probe. The second test was carried out with several improvements in experimental technique compared with the first test: the assembly was more nearly leak-tight, the helium contained fewer impurities, and, particularly, the sudden release of reaction vessel pressure, causing rapid bubbling, was avoided at the termination of the bubbling tests. This last experimental difference probably accounts for the difference in results: slow bubbling may cause no more mist or colloid formation than gentle sweeping over the surface. However, slow bubbling of helium through molten Li_2BeF_4 in a laboratory mockup of the hot-cell experiment produced visible droplets of salt on a horizontal metal plate 1 cm above the salt surface. Forthcoming analyses for ^{95}Zr , ^{141}Ce , and ^{235}U will help to clarify these questions.

Fission Product Distribution in the MSRE

From the results reported above for the quantities of fission products found in the fuel salt, in the cover gas, on the metal core specimen, and on the graphite core specimens after 32,000 Mwhr of power operation, an approximate material balance for each species was calculated (Table 1.8). Included is the total inventory of each nuclide just before the reactor shutdown during which the core specimens were removed. These values were obtained from a recently developed computer program for calculating the total amount of each species present in the MSRE at any time.

It is seen that good material balances were obtained for nuclides with stable fluorides which remain in the salt phase; fair balances were obtained for ^{132}Te , ^{95}Nb , and ^{99}Mo ; and ^{103}Ru was poorly accounted for. The cover gas data are given in terms of losses per day. The losses to the cover gas per day are compared with the daily production by fission of each isotope in Table 1.8. As discussed previously, these high percentages indicate that the noble metals and ^{89}Sr are concentrated in the mist shield region, where the gas samples are taken. Efforts will be made in the future to improve the accuracy of all of the figures entering into the fission product material balance.

Table 1.8. Approximate Fission Product Distribution in MSRE After 32,000 Mwhr

Isotope	Inventory in MSRE (dis/min) ^a	Percent in Fuel	Percent on Graphite	Percent on Hastelloy N	Cover Gas ^b (%/day)
	$\times 10^{17}$				
⁹⁹ Mo	7.91	0.94	10.9	40.5	77
¹³² Te	5.86	0.83	10.0	70.0	66
¹⁰³ Ru	3.36	0.13	6.6	14.9	40
⁹⁵ Nb	4.40	0.044	36.4	34.1	5.7
⁹⁵ Zr	6.00	96.1	0.03	0.06	0.14
⁸⁹ Sr	5.02	77.0		0.26	33
¹³¹ I	4.00	64.0		1.0	16

^aThis total inventory was calculated from the power history of the MSRE, assuming no losses to the cover gas stream.

^bThese values represent the percentages of daily production rate lost to the cover gas per day.

GAS TRANSPORT IN MSRE MODERATOR GRAPHITE

R. B. Evans III J. L. Rutherford
A. P. Malinauskas

In the MSRE the liquid fuel is in intimate contact with its graphite moderator. As a result, the moderator has the capability to act also as a fission product trap, and this capacity can likewise influence the reactivity behavior. On the basis of this motivation, an investigation has been initiated for the purpose of characterizing the MSRE graphite from the standpoint of gaseous fission product migration.

The moderator employed in the MSRE was fabricated with the intent of producing a graphite of low penetrability; this appears to have been accomplished by an impregnation technique. Unfortunately, impregnation methods currently in use characteristically yield a material which is non-uniform insofar as gas transport is concerned; that is, the permeability to gases can vary by several orders of magnitude as one proceeds from the surface to the core of the finished material. Accordingly, in order to obtain meaningful data, it is necessary not only to investigate variations in gas transport behavior from specimen to specimen but also as a function of penetration distance within a single specimen.

The experimental program was begun with a series of permeability and diffusion measurements conducted on a single specimen. A significant finding, as a result of the tests, is the observation that Knudsen flow appears to be the dominant transport mechanism.⁸ This provides a most welcome simplification to analyses of gaseous fission product migration.

The experimental portion of a second part of the program has been completed recently. The object of these studies involved the variation of the transport characteristics as a function of penetration distance within a given specimen. Although the data obtained in connection with this activity have not yet been evaluated fully, a superficial examination tends to indicate that the transport parameters vary in an approximate exponential manner with distance from the surface. For example, it appears that the Knudsen flow coefficient D_{iK} of the gaseous fission product i is approximately given by

$$D_{iK} = D_{iK}^S e^{az},$$

where D_{iK}^S is the value of the coefficient at the

⁸A. P. Malinauskas, J. L. Rutherford, and R. B. Evans III, *Gas Transport in MSRE Moderator Graphite. I. Review of Theory and Counterdiffusion Experiments*, ORNL-4148 (September 1967).

surface ($z = 0$) and where a is a numerical constant. In the sense that one can at least describe the variation with penetration distance by a relatively uncomplicated analytic function, this observation, though still tentative, will likewise simplify the analysis of the overall problem.

Any analysis of fission product transport in the MSRE moderator graphite bars will, of course, presuppose some sort of reproducibility in the transport parameters from bar to bar, so that the third portion of the research is fundamentally concerned with obtaining experimental support upon which reproducibility assumptions can be based. This involves the somewhat thankless task of performing permeability experiments on many randomly selected specimens; this facet is currently in progress.

PREPARATION OF FLUORIDE MIXTURES

F. A. Doss W. K. R. Finnell
W. P. Teichert J. H. Shaffer

The Division has continued to maintain a capability for providing fused fluoride mixtures of high chemical purity to the Laboratory's Molten-Salt Reactor Program and, at the request of the AEC, to other agencies. The primary production facility, operated previously to supply fluoride mixtures for the MSRE, consists of a batch process plant with a capacity of about 4 ft³ of fused fluoride mixtures per week. This facility was operated only on demand for projects requiring specific fluoride mixtures in quantities exceeding 50 kg. During this report period, approximately 100 kg of pure LiF was prepared to fulfill an ORNL contract with the NASA Lewis Research Center. An additional 180 kg of the mixture LiF-BeF₂ (66-34 mole %) was supplied to Princeton University at the request of the USAEC. The MSRP has required 208 kg of the simulated MSRE fuel solvent, LiF-BeF₂-ZrF₄ (65-30-5 mole %), for the Fuel Solvent Distillation Experiment.

An intermediate-scale production facility with a batch capacity of about 0.5 ft³ has been operated to maintain supplies of fluoride mixtures needed for experimental projects of the MSRP. Approximately 50 kg of NaBF₄-NaF (92-8 mole %), 50 kg of LiF-BeF₂ (66-34 mole %), 25 kg of LiF-BeF₂-UF₄ (65.5-34-0.5 mole %), and 40 kg of LiF-BeF₂-ThF₄ (73-2-25 mole %) have been dispensed to

various laboratory-scale experimenters. An additional 20-kg batch of LiF-NaF (60-40 mole %) was prepared and used in a visual demonstration of the fluid fuel concept of molten-salt nuclear reactors. A smaller-scale production capability was exercised in the preparation of approximately 15 kg of various compositions in nine batch operations.

In addition to these production operations, a processing method for preparing LiF-UF₄ (73-27 mole %) directly from LiF and U₃O₈ by HF-H₂ treatment was developed for use by the Chemical Technology Division in preparing a ²³³U fuel concentrate charge for the MSRE. The chemical feasibility of the method was established in four small-scale preparations with ²³⁸U₃O₈, which served also as a training program for operating personnel.

PHASE RELATIONS IN FLUOROBORATE SYSTEMS

C. J. Barton L. O. Gilpatrick
J. A. Bornmann⁹ H. H. Stone
H. Insley¹⁰ T. N. McVay¹⁰

It was stated in the previous progress report¹¹ that an investigation of phase relations in fluoroborate systems had begun because of interest in the possible use of this type of material as the coolant medium in molten-salt reactors. We have prepared NaBF₄ and KBF₄ with a higher degree of purity than had been achieved by previous investigators, completed a reinvestigation of the NaF-KBF₄ and KF-KBF₄ binary systems reported earlier,^{12,13} and made progress in understanding phase relations in the system NaF-NaBF₄-KBF₄-KF. This work was discussed in greater detail in an earlier report.¹⁴

⁹Research participant from Lindenwood College, St. Charles, Mo.

¹⁰Consultant.

¹¹L. O. Gilpatrick, R. E. Thoma, and S. Cantor, *Reactor Chem. Div. Ann. Progr. Rept. Dec. 31, 1966*, ORNL-4076, pp. 5-6.

¹²V. G. Selivanov and V. V. Stender, *J. Inorg. Chem. USSR*, III(2), 447-49 (1958).

¹³S. Pawlenko, *Z. Anorg. Allgem. Chem.* **336**, 172-78 (1965).

¹⁴C. J. Barton et al., *MSR Program Semiann. Progr. Rept. Aug. 31, 1967*, ORNL-4191, p. 158.

Preparation of Purified NaBF_4 and KBF_4

Different values for the melting points of the compounds NaBF_4 and KBF_4 reported in the literature and our own experience with different preparations indicated a need for purer compounds than are available commercially. We found that compounds having considerably higher melting points than reported previously could be prepared by dissolving the commercial preparations in 0.5 M HF, filtering off any insoluble material, and recrystallizing the dissolved material by evaporation. We believe that the KBF_4 produced by this procedure has adequate purity, but we are not satisfied that the ultimate purity of NaBF_4 has been achieved, although the melting point of our best preparation ($405 \pm 2^\circ\text{C}$) is much higher than has been previously reported for this material. We have found that purer NaBF_4 can be produced by treating molten NaBF_4 at 425°C with a mixture of anhydrous HF, BF_3 , and helium (2 volumes of BF_3 per volume of HF). This treatment apparently removes oxygen, probably present as NaBF_3OH , introduced through hydrolysis. We have obtained by special purchase from a commercial producer a large batch of NaBF_4 which has a melting point only about 1°C lower than that of our best laboratory preparation.

The Binary Systems NaF-NaBF_4 and KF-KBF_4

Phase diagrams for the systems NaF-NaBF_4 and KF-KBF_4 have been published,^{12,13} but we reinvestigated both systems using the purified materials described in the previous section and the presently available NaF and KF (recrystallized from melted material). We used the differential thermal analysis (DTA) equipment described earlier¹¹ and the gradient quenching technique¹⁵ that has been in use in this laboratory for a number of years. The resulting phase diagrams, shown in the earlier report,¹⁴ indicate that both systems have single eutectic compositions with higher melting points than found by earlier investigators.^{12,13}

The System $\text{NaF-NaBF}_4\text{-KBF}_4\text{-KF}$

Unpublished work by other investigators at this laboratory demonstrated that fluoroborate preparations containing more than 50 mole % BF_3 exist only in equilibrium with a high pressure of BF_3

gas. Consequently, investigation of phase relations in the system NaF-KF-BF_3 at ordinary pressures is limited to the portion of the system bounded by the compounds $\text{NaF-NaBF}_4\text{-KBF}_4\text{-KF}$. As was indicated in the previous section, two of the binary systems forming sides of this portion of the ternary diagram were redetermined in this laboratory. The reported diagram¹⁶ for the system NaF-KF is assumed to be correct. The fourth side of the diagram is formed by the system $\text{NaBF}_4\text{-KBF}_4$. We confirmed earlier indications¹⁷ from thermal analysis data showing that the high-temperature forms of the two compounds make a continuous series of solid solutions with a minimum melting composition containing approximately 85 mole % NaBF_4 . We could not "quench in" the high-temperature form of the pure compounds or their mixtures and, consequently, have not been able to elucidate the interesting subsolidus behavior indicated by DTA data. Liquidus and solidus relations are shown in the published diagram.¹⁴

The diagonal join NaF-KBF_4 was found to be a quasi-binary system with a eutectic composition containing about 96 mole % KBF_4 melting at $540 \pm 5^\circ\text{C}$.

Study of the interior of the $\text{NaF-NaBF}_4\text{-KBF}_4\text{-KF}$ system is not complete, but it is quite clear that the NaF primary phase field covers a large fraction of the interior area. There is a ternary eutectic composition in the triangle $\text{NaF-KBF}_4\text{-KF}$ near the KF-KBF_4 binary eutectic. There also appears to be a valley forming the boundary between the NaF and $\text{NaBF}_4\text{-KBF}_4$ solid solution primary phase fields, approximately parallel to the $\text{NaBF}_4\text{-KBF}_4$ join and quite close to it. There is probably a minimum melting composition along this boundary curve, the exact composition of which has not yet been determined, giving the lowest melting composition in the system. Quenching data on the mixture NaF-KF-BF_3 (50-3-47 mole %) indicate liquidus and solidus temperatures of 367 and 350°C respectively. The minimum melting composition is believed to be quite close to this composition. It is anticipated

¹⁵C. J. Barton *et al.*, *J. Am. Ceram. Soc.* 41(2), 63 (1958).

¹⁶A. G. Bergman and E. P. Dergunov, *Compt. Rend. Acad. Sci. U.R.S.S.* 31, 753-54 (1941).

¹⁷R. E. Moore, J. G. Surak, and W. R. Grimes, *Phase Diagrams of Nuclear Reactor Materials*, ed. by R. E. Thoma, ORNL-2548, p. 25 (1959).

that a completed diagram for the ternary system will be available in the near future.

Liquidus Temperatures and Phase Changes in the System NaBF_4 -BULT4

A pump loop that had contained BULT4 (LiF - BeF_2 - UF_4 - ThF_4 , 65-30-1-4 mole %), representing a fuel mixture for a one-region reactor, from which this salt mixture had been incompletely drained, was needed for engineering development studies with NaBF_4 . The question was raised whether high-melting solid phases might be formed when the NaBF_4 was loaded and melted in contact with the BULT4 residue. We prepared two mixtures, one containing 90% NaBF_4 -10% BULT4 and the other 10% NaBF_4 -90% BULT4. Differential thermal analysis and quenching data showed no evidence of solid-phase separation at temperatures above the loop operating temperature. It appears from these data that mixing of fuel and coolant streams in a one-region breeder reactor fueled with a BULT4-type mix and cooled with fluoroborate would also not lead to the deposition of high-melting solid phases. Two-liquid formation in mixes of this type is discussed elsewhere in this report.

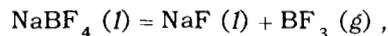
CORROSION OF HASTELLOY N AND ITS CONSTITUENTS IN FLUOROBORATE MELTS

Stanley Cantor C. E. Roberts

Melts composed mainly of NaBF_4 , because they possess attractive thermal properties, are under consideration as coolants for molten-salt reactors. Since it is planned to test this type of coolant in the MSRE, it is necessary to determine, out of pile, the corrosivity of the melt toward Hastelloy N, the alloy from which the MSRE coolant circuit is constructed.

A preliminary corrosion test showed that metallic chromium (the component of Hastelloy N most readily oxidized in molten fluoride media) reacted with a melt consisting of 91 mole % NaBF_4 -9 mole % NaF ; two products of the reaction were crystalline Na_3CrF_6 and gaseous BF_3 . The component which is reduced when chromium is oxidized is believed to be BF_3 , which is converted to elemental boron. In all probability, the removal of NaF from the melt in forming Na_3CrF_6 caused a

shift in the equilibrium



thereby establishing a higher vapor pressure of BF_3 .

A program of tests is in progress to determine whether Hastelloy N itself reacts unfavorably with NaBF_4 melts and to verify the initial results with pure chromium. In each test a salt sample of about 100 g partially decomposes (according to the above reaction) in an evacuated container fabricated from the test metal; the gas pressure and temperature are continuously monitored. On the basis of the preliminary study, we anticipated that for a constant temperature, the gas pressure would increase at a rate proportional to the chromium corrosion rate. After runs are completed, the containers are cut open and the contents examined. A summary of four tests is given in Table 1.9.

The condition of the Hastelloy N containers and specimens following tests 1 and 2 (see Table 1.9) indicated rather sluggish reaction with NaBF_4 . On the other hand, the increase in nickel and chromium in the salt implies that moderate corrosion had occurred; taking into account the surface area of metal exposed to the melt, the concentration of nickel and chromium in the salt was equivalent to a corrosion rate of 1.5 to 3 mils/year. Further study will be necessary to determine: (1) if impurities in the salt are partially responsible for the corrosion, (2) if longer exposures yield the same rate of attack, and (3) what is the exact nature of the corrosion reaction.

In addition to the tests described above, long-term (approximately one year) thermal convection loops constructed from Hastelloy N and containing sodium fluoroborate melts are being studied by the Metals and Ceramics Division.

COMPATIBILITY OF BF_3 WITH GULFSPIN-35 PUMP OIL AT 150°F

F. A. Doss J. H. Shaffer

The proposed use of a fluoroborate mixture as the secondary coolant in the MSRE will require that a covering atmosphere containing BF_3 be maintained above the salt in the pump bowl. Since BF_3 is known to catalyze the polymerization of

Table 1.9. Summary of Corrosion Tests with Fluoroborate Salts

Test No.	Metal Exposed	Salt Composition when Loaded ^a	Time at Temperature	Vapor Pressure	Other Observations
1	Hastelloy N	92 mole % NaBF ₄ , 8 mole % NaF	284 hr at 560°C	Rose from 100 to 210 mm over four days; remained at 210 mm thereafter	At end of test, metal had blackened appearance; Hastelloy N specimens immersed in melt had not changed weight; salt phase white with black scum at interfaces; concentrations of Cr and Ni in salt have increased by 99 and 652 ppm respectively
2	Hastelloy N	Pure NaBF ₄	449 hr at 580°C	585 mm continuously	Slight blackening of metal surfaces; no change in weight of Hastelloy N specimens; Cr and Ni in salt phase increased by 230 and 1590 ppm respectively
3	Hastelloy N	Same as 1	603 hr at 605°C; then 191 hr at 657°C	150 mm continuously Slow rise from 370 to 400 mm	Analysis of vapor shows essentially all BF ₃ ; test still in progress at 657°C
4	Chromium specimens, nickel containers	Same as 1	146 hr at 600°C	Slow rise from 170 to 210 mm	Test in progress

^aThe melt in equilibrium with BF₃ vapor contains a slightly lower concentration of NaBF₄. At the temperatures in tests 1, 3, and 4 the equilibrium compositions are each approximately 91 mole % NaBF₄, 9 mole % NaF.

certain organic materials, its effect on the lubricating properties of the pump oil needs to be evaluated. Although these effects will be observed directly during the planned operation of an engineering pump loop test with a fluoroborate salt mixture, a preliminary experiment is in progress to determine relative polymerization rates of Gulfspin-35 oil under conditions which can be related to actual pump operations. The degree of polymerization should be indicated by changes in oil viscosity during the experiment.

MSRE-type pumps use a helium purge down the pump shaft to isolate the lubricated parts of the pump assembly from the gas environment of the pump bowl. Previous tests on the prototype pump loop, using ^{85}Kr as an indicator, showed that this isolation technique reduced the concentration of pump bowl gases at the oil-gas interface to about 1 part in 20,000.¹⁸ Accordingly, this current study provides accelerated test conditions by contacting the pump oil with helium containing about 1000 ppm BF_3 at a maximum operating temperature of 150°F .

Two experimental assemblies have been operated concurrently to provide comparative data. In each assembly, helium was bubbled at a rate of about 1 liter/min through 1.5 liters of pump oil, and BF_3 was introduced into the helium influent stream to one experiment at a rate of about $1\text{ cm}^3/\text{min}$. Samples of the oil were drained from each experiment periodically and submitted to the Analytical Chemistry Division for viscosity measurements. Concentrations of BF_3 in the gas influent and effluent of the experiment are recorded from the output signal of a thermal conductivity cell. The light-hydrocarbon content (products of oil polymerization) is also monitored on a semicontinuous basis.¹⁹

The results obtained during approximately 1250 hr of continuous operation of the experiments show that the increase in oil viscosity thus far is no more than 0.3 centistoke at 25°C in either the helium-purged oil or the He-BF_3 -purged oil. Some discoloration of the oil exposed to BF_3 has been noted. An evaluation of the infrared spectra over a range of 650 to 4000 cm^{-1} with a Beckman IR-12

spectrophotometer has been made.²⁰ Loss of intensity of the bands in the 3300 to 3500 cm^{-1} region was probably due to the removal of water by gas sparging. Loss of intensity at 980 cm^{-1} in the sample exposed to BF_3 was probably due to the degradation of one or more of the oil additives. Materials which created broad bands at 1000 to 1250 cm^{-1} in the oil exposed to BF_3 have not been identified. The experiment will be continued to examine long-term effects of BF_3 on the pump oil.

COMPATIBILITY AND IMMISCIBILITY OF MOLTEN FLUORIDES AND FLUOROBORATES

C. E. Bamberger J. P. Young
C. F. Baes, Jr. C. S. Sherer²¹

In connection with the investigation of fluoroborates as a coolant for molten-salt reactors, some tests of compatibility and solubility of KBF_4 and NaBF_4 with various fluoride mixtures and with B_2O_3 were carried out. It was found that silica and, at lower temperatures, even Pyrex containers were suitable for these tests, thus providing the great advantage of direct visual examination. As a result the occurrence of liquid-liquid immiscibility was quickly detected, a phenomenon which had not been revealed by less-direct DTA and quenching techniques. In all tests the samples were evacuated several times and flushed with helium prior to melting.

In the following solubility tests, except No. 5, the temperature was 480°C and the containers were Pyrex. Samples remained molten for periods up to 12 hr.

1. $\text{NaBF}_4 + \text{CrF}_2$ (0.3 wt %). No solubility detected; after 1 to 2 hr the insoluble CrF_2 changed to a bright green color, possibly $3\text{NaF}\cdot\text{CrF}_3$.
2. $\text{NaBF}_4 + \text{CrF}_3$ (~ 1 wt %). No solubility detected; change of color possibly indicated $3\text{NaF}\cdot\text{CrF}_3$.
3. $\text{NaBF}_4 + \text{UF}_4$. Neither solubility of UF_4 nor formation of UO_2 was detected, even after adding B_2O_3 .

¹⁸A. G. Grindell and P. G. Smith, *MSR Program Semiann. Progr. Rept. July 31, 1964*. ORNL-3708, p. 155.

¹⁹From a hydrocarbon analyzer installed and calibrated by A. S. Meyer, Jr., and C. M. Boyd, Analytical Chemistry Division.

²⁰Personal communication from M. Murray, Analytical Chemistry Division, Dec. 5, 1967.

²¹Research participant, Alabama College, Montevallo, Ala.

Table 1.10. Liquid-Liquid Distribution Behavior for Li_2BeF_4 - NaBF_4 Mixtures at $\sim 600^\circ\text{C}$

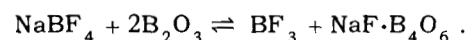
Initial Phase Ratio, g NaBF_4 /g Li_2BeF_4	Phase	Mole Fraction			
		NaF	LiF	BF_3	BeF_2
3	Top	0.391	0.139	0.419	0.052
	Bottom	0.165	0.435	0.129	0.271
2	Top	0.365	0.174	0.406	0.055
	Bottom	0.156	0.448	0.138	0.257
1	Top	0.373	0.164	0.432	0.031
	Bottom	0.110	0.545	0.044	0.300

- $\text{NaBF}_4 + \text{HoF}_3$. This rare earth was readily available, and its spectrum in molten fluorides is known; no measurable solubility was detected.
- $\text{KBF}_4 + \text{B}$ (amorphous) at 650°C in fused silica. No significant solubility was detected; the finely divided powder coagulated with time.

The following list summarizes the tests in which liquid immiscibility was observed; unless otherwise stated the container material was fused silica. Since UF_4 did not show spectrophotometrically any solubility in NaBF_4 or in KBF_4 , it was used for spiking other fluorides as a visual aid in the detection of phase separations. In some instances KBF_4 was used rather than NaBF_4 because its higher melting point was closer to the melting point of some fluoride mixtures.

- $\text{NaBF}_4 +$ blanket salt (0.71 LiF, 0.02 BeF_2 , 0.27 ThF_4), phase ratio $\sim 1:10$, temperature 585°C .
- $\text{KBF}_4 +$ blanket salt (0.71 LiF, 0.02 BeF_2 , 0.27 ThF_4), temperature 625°C .
- $\text{NaBF}_4 +$ BULT4 (0.65 LiF, 0.30 BeF_2 , 0.01 UF_4 , 0.04 ThF_4), phase ratio $\sim 1:10$, temperature 585°C .
- $\text{NaBF}_4 + 3\text{LiF}\cdot\text{UF}_4$, phase ratio $\sim 1:30$, temperature 480°C , Pyrex container.
- $\text{NaBF}_4 + 2\text{LiF}\cdot\text{BeF}_2$, phase ratio 10:1, temperature 480°C , Pyrex container.
- $\text{NaBF}_4 +$ MSRE salt (0.64 LiF, 0.29 BeF_2 , 0.015 ZrF_4 , 0.009 UF_4), phase ratio $\sim 1:10$ and 4:1, temperature 480°C , Pyrex container.

It has been reported²² that mixtures of NaBF_4 and B_2O_3 react vigorously on heating to produce BF_3 :



Indeed this is a commonly used method to generate BF_3 . Nonetheless, we decided to explore the effect of B_2O_3 additions to immiscible liquids of NaBF_4 plus $\text{LiF}\cdot\text{BeF}_2$ - ThF_4 - UF_4 . Gas evolution was detected in all tests where B_2O_3 was added directly, and no extraction of UF_4 or precipitation of UO_2 was noted. The resulting borate phases were very viscous.

Finally, in another series of tests $2\text{LiF}\cdot\text{BeF}_2$ was equilibrated with NaBF_4 in sealed nickel containers at $\sim 600^\circ\text{C}$. The capsules were quenched, and the two phases were sampled and analyzed. The results (Table 1.10) show appreciable distribution of all the components (NaF , LiF , BF_3 , and BeF_2) between the two phases. In each phase, $n_{\text{LiF}} + n_{\text{NaF}} \sim n_{\text{BF}_3} + n_{\text{BeF}_2}$, suggesting that the phases may be represented approximately as reciprocal mixtures of the ions Li^+ , Na^+ , BF_4^- , BeF_4^{2-} . In terms of these ions there is a tendency for Li^+ and BeF_4^{2-} to favor one phase and Na^+ and BF_4^- to favor the other phase.

²²W. Hellriegel, *Ber.* 70B, 689-90 (1937).

2. Behavior of Fission Products and Protactinium in Molten Fluorides

MOLTEN-SALT IRRADIATION EXPERIMENTS

E. L. Compere E. G. Bohlmann
H. C. Savage J. M. Baker

Irradiation of molten-salt fuel circulating in contact with graphite and Hastelloy N continued during the past year with the operation of a second molten-salt convection loop experiment in the Oak Ridge Research Reactor. These experiments are directed at study of graphite-salt compatibility, Hastelloy N-salt compatibility, fuel-salt stability, and fission product behavior.

In-pile operation and results of postirradiation examination of the second loop experiment are reported below, as well as elsewhere.¹

Loop Description

A diagram of the second in-pile molten-salt convection loop is shown in Fig. 2.1. All loop components, except for the graphite in the core, were fabricated² of Hastelloy N, as was the 12-ft-long sample tube which connected the loop to the sample station at the ORR shield face.

Operation

After assembly the loop was vacuum pumped at 600°C for 20 hr to remove air and moisture. The loop was flushed with solvent salt, recharged with fresh solvent salt, and operated at temperature for 248 hr in the mockup facility at Y-12. The loop containing the solvent salt used in the pre-

irradiation test period was then placed in beam hole HN-1 of the ORR. Operation was continued with solvent salt under irradiation at temperatures ranging between 550 and 650°C to evaluate the loop performance. Reactor gamma heat was determined as a function of the distance of the loop from the reactor lattice.

On January 30, 1967, ⁷LiF-UF₄ (63-37 mole %) eutectic fuel salt was added to the loop, resulting in a fuel composition of ⁷LiF-BeF₂-ZrF₄-UF₄ of 65.26-28.7-4.84-1.73 mole %. The nuclear heat generated in the loop (fission plus gamma) was again determined as a function of loop position, and on February 21, 1967, operation at the fully inserted, highest flux position was achieved.

While the ORR was shut down, the uranium concentration of fuel salt in the loop was increased to the composition ⁷LiF-BeF₂-ZrF₄-UF₄ (65.4-27.8-4.8-2.0 mole %) to increase the fission power densities in the fuel salt in an attempt to reach the experimental objective of 200 w/cc. Immediately after reactor startup on March 4 a small amount of radioactivity was detected in the secondary containment system. However, loop operation was continued with careful monitoring of the activity level until March 17, when a rapid increase in this radiation level indicated a leakage of fission products from the loop. The loop was retracted from the high flux, and the fuel salt in the loop was frozen by reducing the temperature to 320°C.

Subsequent investigation indicated that the fission product leak was in the vicinity of the gas separation tank, and beginning on March 27 the fuel salt was drained from the loop. On April 4, 1967, the loop was removed from the ORR and transferred into a hot cell for cutup and examination.

¹MSR Program Semiann. Progr. Rept. Aug. 31, 1967, ORNL-4191, p. 176.

²Reactor Chem. Div. Ann. Progr. Rept. Dec. 31, 1966, ORNL-4076, p. 41.

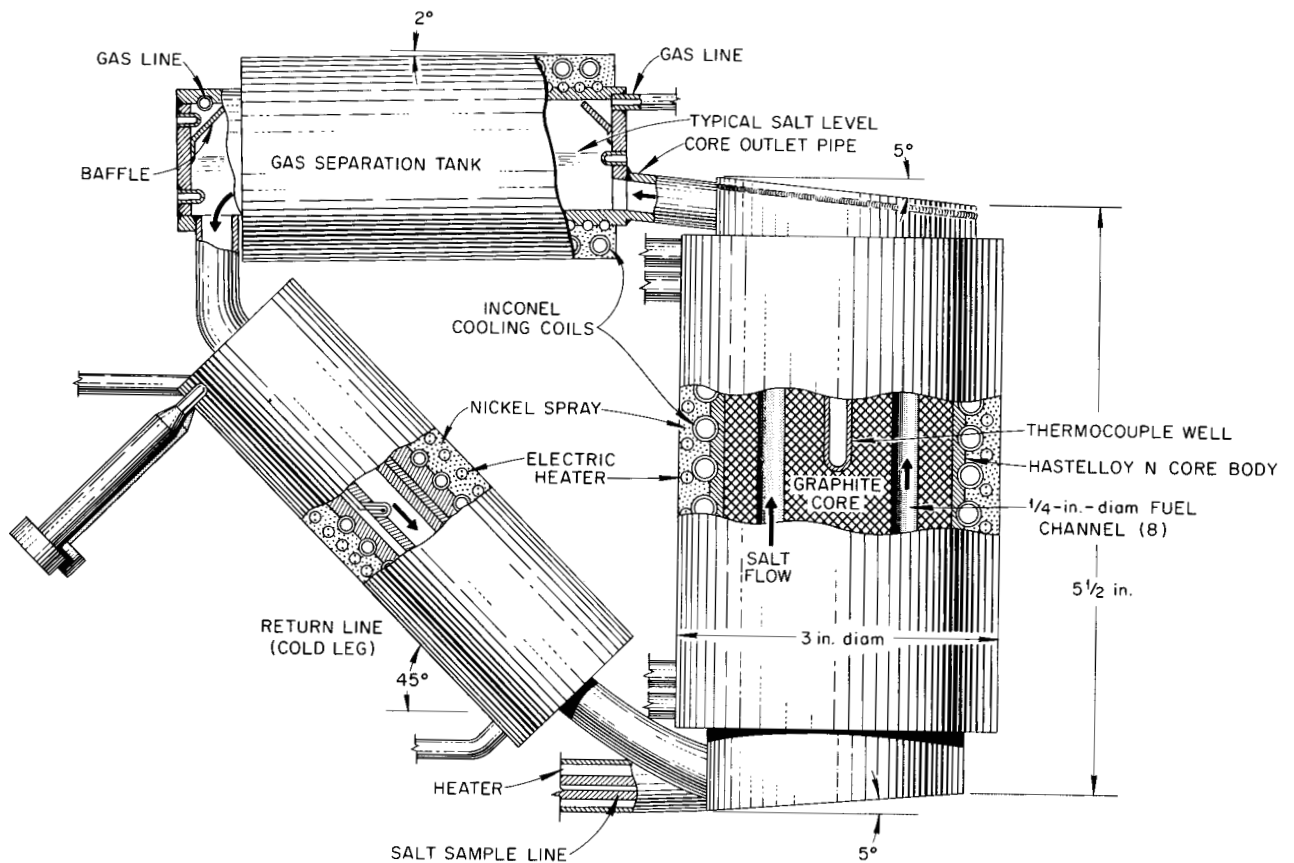


Fig. 2.1. Diagram of Molten-Salt Loop No. 2.

Table 2.1. Summary of Operating Periods for In-Pile Molten-Salt Loop No. 2

	Operating Period (hr)			Inventory Changes		
	Total	Irradiation	Full Power Dose Equivalent	Additions	Samples	Salt Removal
Out-of-pile						
Flush	77.8			7	1	13
Solvent salt	171.9			5	1	0
In-pile						
Preirradiation	73.7			1	2	0
Solvent salt	343.8	339.5	136.0	1	2	0
Fueled salt	1101.9	937.4	547.0	2	3	0
Retracted-fuel removal ^a	435.0	428.3	11.2	0	4	9
Total	2204.1	1705.2	694.2	16	13	22

^aMaintained at 350 to 400°C (frozen) except during salt removal operations and fission product leak investigations.

A summary of the loop operating periods at various conditions is shown in Table 2.1.

Nuclear Heat, Neutron Flux, and Salt Power Density

Nuclear heat was measured by comparing electrical heat requirements under similar conditions with the reactor at zero and at full power. Reactor gamma heat with the loop in the fully inserted position was 4200 w (with unfueled salt). With fuel salt containing 1.73 mole % (93% enriched), fission heat in the fully inserted position was 8600 w. The corresponding overall average fuel-salt fission heat density was 113 w/cc at 650°C, and the average in the core salt (43 cc volume) was 150 w/cc. It is estimated that the fission power density in the fuel salt in the forward core graphite tubes was 180 w/cc. During the in-pile operating period 8.2×10^{18} fissions/cc (1.2% uranium burnup) was developed in the fuel salt.

Operating Temperatures

The salt in the loop was kept molten ($>490^\circ\text{C}$) during all in-pile operations until it was frozen on March 17 following the fission product leak. At full power, temperatures in the fuel salt ranged from $\sim 545^\circ\text{C}$ in the cold leg return line up to $\sim 730^\circ\text{C}$ (750°C initially) in the core outlet pipe. Since nuclear heat was removed through the core graphite to the cooling coils around the outside of the Hastelloy N core body, the graphite temperature was $\sim 550^\circ\text{C}$, or some 70°C below the average fuel-salt temperature in the core.

Salt Circulation. – Convective salt circulation was estimated to be 30 to 40 cc/min. Nominal salt volume in the loop was about 80 cc at operating temperatures. Occasional loss of flow was readily overcome by adjustment of the temperature difference between the salt in the core and in the cold leg.

Crack in the Core Outlet Pipe. – When the loop assembly was examined in hot-cell facilities, a crack was found in the core outlet pipe from which gaseous fission product leakage had caused the experiment to be terminated. Subsequent metallographic examination revealed that the crack extended through the pipe wall and almost com-

pletely around the circumference of the pipe (0.40 in. OD \times 0.30 in. ID).

Analysis of the cause of failure in the core outlet pipe indicates that it was caused by stresses resulting from differential thermal expansion of the loop components. Piping stress analysis indicated that the maximum stress point was in the core outlet pipe where the failure occurred. For the normal operating temperatures in-pile, a stress of $\sim 10,000$ psi was produced in the pipe wall (tension on the top and compression on the bottom). When a reactor setback occurred, the temperature distribution was changed rapidly, and the direction of stress was reversed such that a stress of $\sim 17,000$ psi was produced in the pipe wall (compression on top and tension on bottom).

At the time of failure of the core outlet pipe, the Hastelloy N pipe had accumulated an irradiation dose of $\sim 5 \times 10^{19}$ nvt. For the pipe temperature of 1350°F (732°C) and an accumulated irradiation dose of $\sim 5 \times 10^{19}$ nvt, the stress-rupture properties of Hastelloy N are reduced such that stresses of about 10,000 psi could produce rupture.³ Further, a reactor setback and resultant loop thermal cycle occurred on March 3 after a dose accumulation of $\sim 2 \times 10^{19}$ nvt, and it was on March 11 that evidence of fission product leakage from the loop was first observed.

It is evident that for future in-pile loops with similar configuration and temperatures, a material superior to the present Hastelloy N in high-temperature strength is required. Improvement in the physical properties of Hastelloy N, especially improving its resistance to neutron irradiation, is being given major attention.⁴ Work has shown that additions of titanium, zirconium, hafnium, and possibly other elements will reduce the radiation damage of Hastelloy N. Therefore, the next in-pile molten-salt loop will be constructed of a modified Hastelloy N containing titanium and tungsten as additives for improved resistance to radiation-induced high-temperature embrittlement. The required shapes for construction of the next loop components are being made from an ingot of the modified ($\sim 0.5\%$ Ti, 2% W) Hastelloy N.

³H. E. McCoy, Jr., and J. R. Weir, Jr., *In- and Ex-Reactor Stress-Rupture Properties of Hastelloy N Tubing*, ORNL-TM-1906 (September 1967).

⁴H. E. McCoy, Jr., and J. R. Weir, Jr., *Materials Development for Molten-Salt Breeder Reactors*, ORNL-TM-1854 (June 1967).

Corrosion

Evidence of corrosion was obtained from chemical analysis of salt samples withdrawn from the loop and from metallographic examination. A total of 87 mg of chromium was found in the salt; this corresponds to the removal of chromium to a depth of half a mil over the 110-cm² metal loop surface. Metallographic examinations were in accord with this, although the depth of attack varied in the several components. The largest increases in dissolved chromium came during the first part of the run, consistent with out-of-pile behavior reported by DeVan and Evans.⁵ There was no indication of any aggravation of corrosion by irradiation.

Oxygen Analysis

Three oxygen determinations on salt samples were made. The original solvent salt contained 115 ppm. Solvent salt withdrawn from the loop after 353 hr of in-pile circulation contained ~260 ppm. The increase is equivalent to about 25 mg of oxygen (or 80 mg of chromium oxidized to Cr²⁺). Fueled salt withdrawn from the loop after retraction and freezing showed 241 ppm of oxygen. These values are well below levels expected to cause precipitation of zirconium or uranium oxides. However, some or all of the 69-mg increase in chromium content of the salt noted during the solvent-salt operation could have been due to corrosion if the oxygen increase in this period is attributed to moisture, all of which reacted to dissolve chromium from the metal.

Cutup of Loop and Preparation of Samples

Promptness in the examination of the loop was essential, since such short-lived isotopes as 66-hr ⁹⁹Mo and 78-hr ¹³²Te were of interest, and major irradiation of the loop had ceased on March 17, 1967.

On April 5, 1967, the loop package was removed from the beam hole and transferred to hot cells for cutup and sampling. The leak location was established with gas pressurization and Leak Tec (bubbles) solution. Representative samples of all

components were removed for analysis to establish the fates of the various fuel constituents; considerable redundancy was practiced in an effort to obtain reasonable material balances.

In order to determine the penetration profiles of the various fission products in graphite, concentric thin shavings of core graphite from representative fuel tubes were obtained for radiochemical analysis. Fourteen broaching tools permitted sampling of the core graphite fuel channels ($\frac{1}{4}$ in. ID) to a depth of 45 mils in steps ranging from 0.5 mil up to 10 mils each. The cutup and sampling were completed April 14, 1967.

Metallographic Examination

Samples of loop metal taken from the core, core outlet, gas separation tank, cold leg, and other regions were subjected to metallographic examinations reported in greater detail elsewhere.¹ In addition to establishing the nonductility of the break in the core outlet tube, some evidence was obtained of mild carburization of core regions in contact with graphite. Slight corrosion of the core outlet and cold-leg tubing (which were from the same original piece of tubing) was of a magnitude consistent with the chromium uptake of the salt. Results of examination of the graphite will be presented in a section below.

Salt-Graphite Interactions

Various items of evidence show that fuel salt adhered to some of the graphite surfaces and also penetrated cracks in the graphite. The entry into cracks was doubtless associated with the changes in overpressure used in transferring salt. The adherence to graphite surfaces is believed to have resulted from interaction with traces of moisture in the argon cover gas as discussed below.

Uranium-235 was determined in the various samples by an activation technique sensitive to less than 1 μ g of ²³⁵U, in which delayed neutrons were counted. In seven of the eight graphite channels from which samples were taken, the quantity of ²³⁵U found ranged from 1.6 to 2.8 mg (in 8.3 to 9.5 cm²), with over half being found within the first mil and over 80% generally within the first 3 mils. However, some uranium was detected even in the 35- to 45-mil cuts. The first sample from the remaining channel weighed 290 mg and contained 18.9 mg of ²³⁵U, equivalent to 190 mg of

⁵J. H. DeVan and R. B. Evans III, "Corrosion Behavior of Reactor Materials in Fluoride Salt Mixtures," pp. 557-79 in *Conference on Corrosion of Reactor Materials*, June 4-8, 1962, vol. II, IAEA, Vienna, 1962.

Table 2.2. Salt Constituents in Graphite at Given Depths

	Mass Spectrograph (MS-7)					Activation
	Li (mole %)	Be (mole %)	Zr (mole %)	U (mole %)	U ($\mu\text{g}/\text{mg}$)	U ($\mu\text{g}/\text{mg}$)
Loop inventory	27.8	65.3	4.8	2.0		
Graphite — top section, next-to-front channel						
0.2 to 0.4 mil	22	71	5.3	1.8	39	49
0.4 to 2.05 mils	21	73	3.8	2.2	2.6	3.6
2.05 to 4.4 mils	15	80	3.5	1.7	2.2	0.91
4.4 to 9.8 mils	16	80	4.5	<i>a</i>	(<0.34)	0.32

^aNot determined.

fuel salt, probably from a small piece of fuel salt on the graphite surface. The samples from deeper cuts contained uranium at levels only moderately higher than those from the other channels.

The MS-7 spark mass spectrograph was used to examine solutions of graphite shaved from a typical fuel tube for salt constituents. Total amounts used were at the microgram level. Results are shown in Table 2.2. The salt ingredients, Li, Be, Zr, and U, are in the proper molar ratio (with the proper total of ⁷Li and ⁹Be) but with some drift in their ratios. Furthermore, the absolute quantity of uranium determined agreed reasonably with the value from the activation analysis; consequently, the uranium found in the graphite resulted from salt wetting and penetration rather than from some interaction.

Examinations of autoradiographs indicate that several fuel channels had one or two cracks extending from them and that appreciable radioactivity was located along such cracks. In addition, alpha radiography showed the presence of ²³⁵U in cracks as well as on hole surfaces.

A $\frac{1}{8}$ -in.-thick cross section of the 2-in.-diam graphite core was examined by soft x-ray transmission. This is shown in Fig. 2.2. Darkened areas indicate penetration of salt into many cracks and adherence as small slumped granules to fuel channel walls. Near some channels, apparently, porous regions were penetrated by salt.

The minimum "radius" of a crack which may be entered by fuel salt is estimated from the equation $r = 2\gamma \cos \theta / P$ as being about 3.7μ (0.00015 in.) for a net pressure of 1 atm, a surface tension of 230 dynes/cm, and assuming a contact angle (for clean, dry, nonwetting salt) of 145°. Our obser-

vations above on the penetration of cracks and coarse pores by salt are not inconsistent with a limiting pore diameter of 0.3 mil. Since a net pressure differential of about 1 atm existed during salt transfer operations, no elaborate explanation appears to be required.

Evidence was obtained indicating that salt adhered to our graphite surfaces after draining. X-ray diffraction patterns obtained from the surface of a specimen of graphite cut from an exit fuel channel surface showed patterns of Li_2BeF_4 and Li_2ZrF_6 with no indication of oxides or uranium compounds. This is characteristic of normally frozen fuel salt (including uranium), indicating that fuel-salt droplets had adhered to the graphite surface after the salt was drained from the loop. It was later seen there by microscopic observation. Possible factors related to such adherence are considered below.

Prior to admission of any salt to the loop, the graphite was heated at 600°C for 20 hr under vacuum, whereas evacuation for several minutes at 400°C has been shown to be sufficient to remove normal moisture from graphite. Thus, internal moisture in the graphite is not believed to account for adherence of the salt to the graphite.

We have recently studied in a vacuum box the wetting characteristics of droplets of our solvent salt on a platelet of our graphite. We confirm generally the observation of Kreyger, Kirslis, and Blankenship⁶ that wetting is due to three-phase

⁶P. J. Kreyger, S. S. Kirslis, and F. F. Blankenship, *Reactor Chem. Div. Ann. Progr. Rept. Jan. 31, 1964*, ORNL-3591, pp. 38-42.

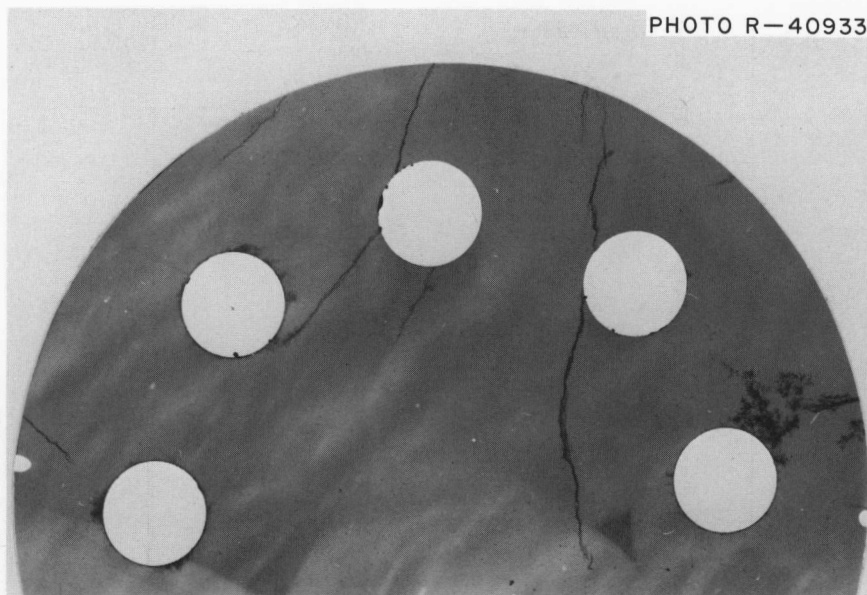


Fig. 2.2. Penetration of Salt into Graphite (2 \times).

contact of gas, graphite, and molten salt at moisture levels of 10 ppm or lower.

In an atmosphere of tank helium (below 4 ppm of water), the droplet on melting did not wet the graphite. However, in a few minutes it developed a translucent crust, and in 1 to 2 hr after melting had slumped and spread sporadically over the graphite surface. Another droplet was melted on graphite under good vacuum (less than 10^{-4} torr, the present gage limit), and it remained clear and round for about 20 hr. However, when tank helium was admitted to a pressure of 0.2 torr, the molten droplet promptly slumped and wetted the graphite.

The lack of wetting in the experiment under vacuum indicates that the prior condition of graphite or salt did not control the wetting behavior. The wetting behavior of the salt appears to be very sensitive to very slight impurities (presumably water) in the helium when three-phase contact exists. This could have been accentuated in the box experiments because of the small amount of salt and the large volume of gas. However, we are consequently led to believe that the wetting of loop graphite by salt occurred when a gas phase containing traces of moisture was present in contact with both salt and graphite. This could have occurred during periods of salt removal, either removal of the first flush salt or the final removal of irradiated salt from the loop.

Isotope Activity Calculation from Flux and Inventory History

The activity of a given isotope to be expected in the system at a particular time was estimated by a detailed application of standard equations^{1,7} to the individual irradiation and inventory periods, with adjustment for decay to final ORR shutdown for the experiment.

The activities of the fission products ^{137}Cs , ^{144}Ce , and ^{95}Zr were used as internal standards to estimate the average flux received by the salt under the assumption that they were not appreciably lost from the salt. A mean flux to the salt of 0.88×10^{13} was thus estimated. From this value, total activities of the various isotopes produced in the experiment were calculated.

The mean flux was also estimated from the fission heat measurement reported above, giving a flux of 1.18×10^{13} , and from the dosage received by type 304 stainless steel monitor wires attached to the loop which, when corrected for position, attenuation, etc., gave an estimated mean flux of 1.15×10^{13} .

⁷J. M. West, pp. 7-14 in *Nuclear Engineering Handbook*, ed. by H. Etherington, McGraw-Hill, New York, 1958.

Table 2.3. Comparison of Fission Product Activity Produced with Activity Found in Various Loop Regions

All activities in units of 10^{10} dis/min, referred to ORR shutdown, 4/4/67, 0800

Isotope	^{99}Mo	^{103}Ru	^{132}Te	$^{95}\text{Nb}^a$	^{95}Zr	^{131}I	^{140}Ba	^{89}Sr	^{91}Y	^{137}Cs	^{141}Ce	^{144}Ce	^{147}Nd
Half-life	66 hr	39.7 days	77.7 hr	35 days	65 days	8.05 days	12.8 days	50.4 days	58.3 days	30 years	32.8 days	284 days	11.1 days
Fission yield, %	6.1	3.0	4.3	6.2	6.2	2.93	6.35	4.79	5.8	6.0	6.0	5.6	2.6
Total activity formed ^b	940	8100	1140	7400	12800	5000	16500	11500	12900	108	17300	3500	6100
Found in salt samples ^c	2	6 7	9 20	1530 1290	8900 13300	1520 1570	4800 5000	7550 9370	15600 7900	94 103	12100 13500	3830 4330	4400 3900
Found in graphite ^d	385	485	360	993	57	16	385	1000	386	1.9 ^d	219	47	122
Found in loop metal	220	363	160	1300	77	80	220	122	79	2.4 ^d	77	16	42
Found in salt sample line	93	52	82	246	104	57	150	84	79	0.02 ^d	114	23	115
Found in hot gas sample line	0.2	0.04	0.4	<1	<1	5	<1	15	0.4	0.15 ^d	<1	0.01	<1
Found in cold gas inlet line	<0.1	0.01	<0.1	<1	<1	1	<1	1	<0.001	0.02 ^d	<1	<0.01	<1

^aDaughter of ^{95}Zr .

^bAssuming a mean flux to salt of 0.88×10^{13} based on average of values from ^{95}Zr , ^{137}Cs , and ^{144}Ce in final salt samples.

^cEstimated for total salt based on each of two final samples.

^dCorrected for salt content.

Isotope Activity Balance

The calculations described above provided an estimate of the amount of each isotope to be accounted for. We determined the total amount of isotope actually found in the system by dividing the loop into regions, analyzing a specimen from each region, and allocating a proportionate amount of activity to the region.

For the various samples obtained from the loop, activity determinations for the 13 isotopes shown in Table 2.3 were made as well as sensitive determinations of ^{235}U . The activities have been totaled for each isotope under the categories of graphite, loop metal, salt sample lines, gas lines, and salt. These values, plus the estimated total activities calculated from inventory and irradiation history, are also shown in Table 2.3.

It may be seen that over half (but generally less than all) the expected activity was accounted for in the cases of ^{99}Mo , ^{132}Te , ^{95}Nb , ^{95}Zr , ^{89}Sr , ^{137}Cs , ^{141}Ce , ^{144}Ce , ^{91}Y , and ^{147}Nd .

A substantial proportion, although less than half, was accounted for in the cases of ^{140}Ba and ^{131}I . Inasmuch as iodine readily volatilizes from all samples (without doubt from powdered graphite in particular), it is to be expected that iodine determinations would be low.

Only about 11% of the ^{103}Ru was found, although proper traps were used to recover any ruthenium compounds volatilized during the preparation of radiochemical samples.

Molybdenum, tellurium, and ruthenium are almost entirely departed from the salt along with substantial proportions of ^{89}Sr , ^{95}Nb , ^{140}Ba , and probably considerable ^{131}I . Except for ^{89}Sr and possibly ^{140}Ba , which favor graphite, these elements showed no strong preference for graphite or metal but seemed to deposit on whatever surface was available. The alkali and rare-earth isotopes, including ^{91}Y , ^{137}Cs , ^{141}Ce , ^{144}Ce , ^{147}Nd , and also ^{95}Zr , remained almost completely in the salt.

Penetration of Fission Products into Graphite and Deposition onto Surfaces

The amounts of the respective fission product isotopes which penetrated the graphite to given depths were obtained from the samples shaved from the fuel tubes. Data for each isotope and each cut depth were summed over all the fuel

channels. The value was corrected for the amount of isotope in salt in the sample based on the amount of ^{235}U which was found and on the concentration of isotope in regular salt samples. This correction was appreciable only for those isotopes found principally in salt and was never dominant.

The net amount of isotope in the graphite up to a given depth (for the total exposed graphite surface) was then divided by the total amount of isotope found in the loop, yielding a value for each depth of the percentage of the particular fission product that penetrated to that depth in the graphite. Thus, about 43% of the fission product ^{132}Te was found within 1.3 mils of the graphite surface and about 58% within the first 35 mils.

Values so obtained are shown in Fig. 2.3, where the percentage of each respective fission product present which penetrated to given depths is shown as a function of depth.

The fission products ^{95}Zr , ^{141}Ce , ^{144}Ce , ^{91}Y , and ^{147}Nd range between about 0.4 and 3% in the graphite, with nearly all of that entering the graphite being found within the 3.1-mil cut and thereby possibly being deposited as fission product recoils directly from the salt.

On the other extreme are ^{132}Te , ^{99}Mo , and ^{103}Ru . These isotopes showed 35 to 43% in the first 1.3 mils, 52 to 56% within 3.1 mils, and not much more at greater depths. These isotopes are thus indicated to deposit strongly from the salt onto the graphite surface but migrate only weakly if at all after deposition.

Other isotopes appear to move within the graphite; these include ^{131}I , ^{140}Ba , ^{95}Nb , and ^{89}Sr . About 0.4% of the iodine was found within 3.1 mils, 0.6% within 20 mils, and about 0.8% within 40 mils – a fairly regular increase showing fairly equal concentration at each depth with the implication of free migration (presumably gaseous) of such as was found. This could, however, have occurred during the period after the experiment was frozen.

Niobium-95 clearly is present at concentrations far in excess of its parent ^{95}Zr , and concentrations increase rapidly for the first 5 mils from 7 to 21%, then regularly but more slowly up to about 25% at 35 mils. Its action does not appear coupled to that of ^{95}Zr . Apparently this isotope moved readily in the graphite, probably in the form of a gaseous molecule (NbF_5 ?).

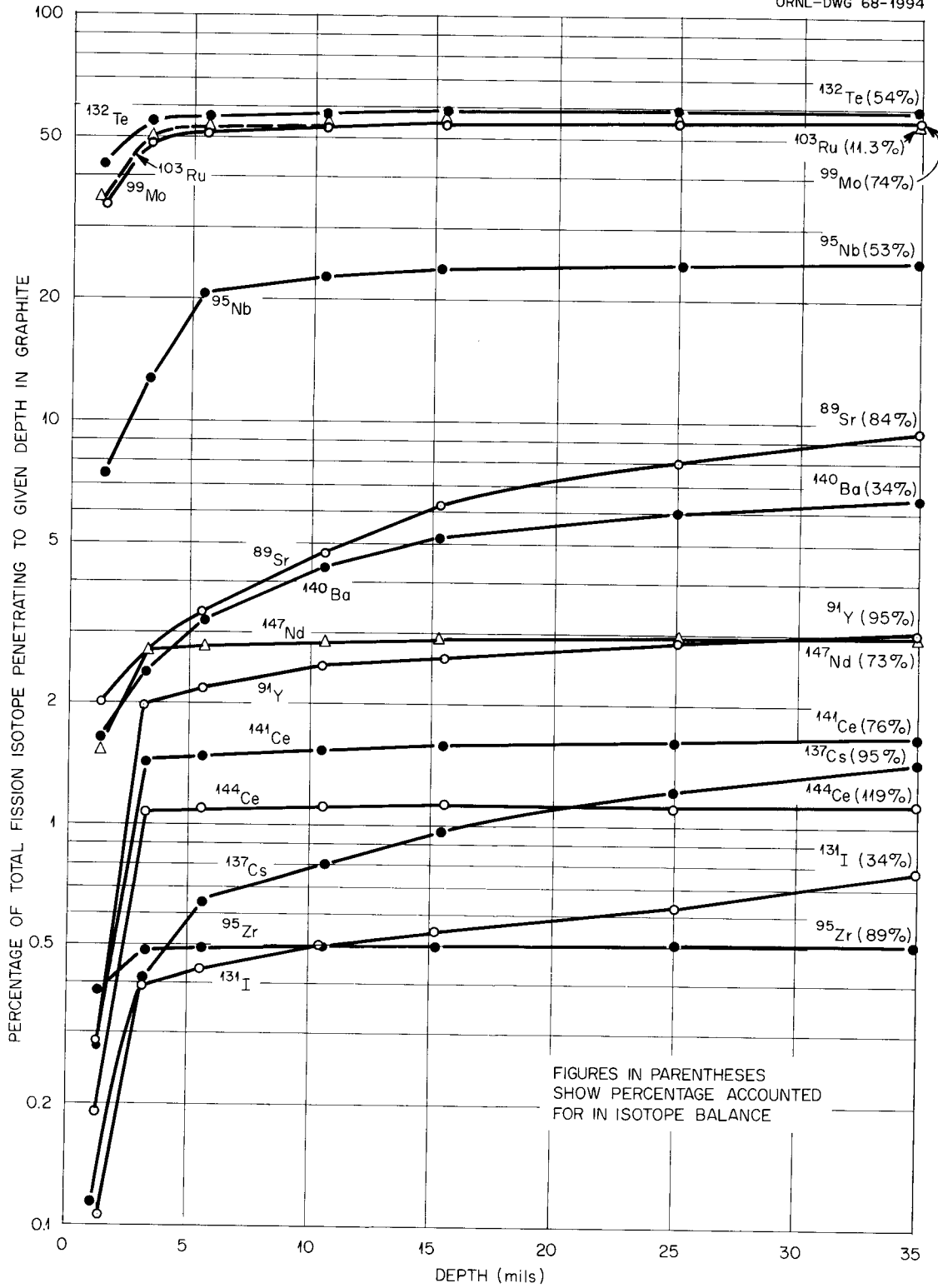


Fig. 2.3. Penetration of Various Fission Product Isotopes into Graphite as a Percentage of Total Isotope in Loop.

The isotopes ^{89}Sr , ^{137}Cs , and ^{140}Ba each show regularly increasing percentages with depth, as would be expected with mobile gaseous precursors⁸ (3.2-min ^{89}Kr , 3.8-min ^{137}Xe , and 16-sec ^{140}Xe).

Gamma Irradiation of Fuel Salt in the Solid Phase

Since the fuel salt in the in-pile loop was kept frozen for a number of days before salt was removed from the loop, radiolysis could produce atomic fluorine which could oxidize various species (U, Mo, Ru, Nb, etc.) which could be transported to other parts of the system. Temperatures of the frozen salt were generally kept above 300°C. Gaseous fluorine (F_2) has been observed to result from the radiolysis of frozen salt at temperatures below 100°C, but no direct information was available at 300°C.

Solid MSR fuel salt ($\text{LiF}\text{-BeF}_2\text{-ZrF}_4\text{-UF}_4$, about 65-28-5-2 mole %) as used in the in-pile loop was irradiated at a temperature of 320°C in a Hastelloy N capsule for 25 days in the center of a freshly spent HFIR fuel element. The gamma dose rate at the beginning of the period was about 0.2 w/g, decaying by a factor of about 4 over the period. A total of 1.5×10^{24} ev per g of salt was absorbed.

No significant pressure changes were noted. Examination of the salt, metal, and a contained graphite specimen gave no evidence of radiolytic generation of fluorine, transport of uranium, or other substances due to irradiation at 320°C.

With respect to the loop experiment, it is thus indicated that radiolytic production of fluorine during the interval in which the loop was held at temperatures of $\sim 300^\circ\text{C}$ did not occur.

Discussion and Conclusions

The power density (about 150 w/cc average in the core fuel) achieved in this experiment is of the magnitude to be developed in molten-salt breeder reactors, and the burnup (8×10^{18} fissions/cc) corresponds roughly to about several weeks of operation, so that fission product concentrations corresponding to MSBR levels were attained.

Embrittlement of unmodified Hastelloy N at elevated temperatures after thermal neutron doses

above 10^{19} nvt was encountered. Necessary changes in future experiments appear to include modified alloy composition to reduce the high-temperature embrittlement caused by irradiation, design to minimize stress, lower maximum temperatures, and minimization of the range and frequency of temperature cycles.

Reasonable balances of most fission products were obtained, and thereby their behavior is usefully delineated. Considering that about 80 graphite samples and over 40 metal samples were analyzed, the answers weighted by area factors, and the totals then compared with the resultant of many changes in irradiation conditions, the agreement was generally satisfactory.

The behavior of the various fission products was in reasonable agreement with results reported on MSRE surveillance specimens, though our fractions of such isotopes as ^{99}Mo , ^{132}Te , and ^{103}Ru on the graphite are higher. This is possibly because of a longer circuit time as well as a greater proportion of time in the core in our case. We believe that deposition occurs rather promptly on whatever metal or graphite surface is available, and these fission products are immobilized near the surface.

Niobium-95 enters the graphite in substantial proportions and penetrates rather deeply; thus, conceivably, it moves as a gaseous molecule. It deposits with comparable facility on metal contacted by the salt.

No radiation effects on graphite or salt-graphite interaction that could be ascribed to radiation were noted, except fission product deposition.

Salt can enter rather minute cracks in the graphite, including some occasional grossly porous areas, as a result of varying the overpressure, but otherwise it does not penetrate the regular pores.

The salt and graphite are indicated to be quite sensitive to the very low levels of impurity in the gas phase contacting them, and droplets or salt films remain on the graphite when interaction occurs.

Corrosion was not affected by irradiation. Such corrosion as occurred is indicated to have taken place in the early parts of the run and appears related to increase in oxygen content of the salt.

Intense gamma irradiation of solid fluoride fuel at 320°C did not appear to result in radiolytic effects in the salt.

⁸R. J. Kedl, *A Model for Computing the Migrations of Very Short-Lived Noble Gases into MSRE Graphite*, ORNL-TM-1810 (July 1967).

BEHAVIOR OF MOLYBDENUM FLUORIDES

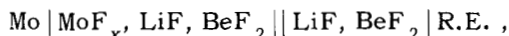
In both the Molten Salt Reactor Experiment (see Chap. 1) and in the ORR Loop Experiments (see preceding section of this chapter), the behavior of the relatively noble fission products has been surprising. Analysis of the molten fluoride fuel mixture has shown, in each case, very small concentrations of ^{99}Mo , ^{132}Te , ^{95}Nb , and ^{103}Ru . In both these experimental assemblies appreciable fractions of such fission products are found in or on the graphite and the container metal, and in the MSRE, where equilibration of a part of the molten fuel with the helium cover gas is attempted, appreciable fractions of these fission products are found in the gas phase.

The mechanisms by which these fission products distribute as they do are still unknown. We consider it unlikely, but still possible, that the phenomena observed are the consequences of chemical reactions of (poorly known and relatively unstable) lower fluorides of these elements. We have, therefore, begun a study of such compounds with special emphasis on their behavior in solutions similar to the MSRE fuel. Initial experiments have been limited almost entirely to the lower fluorides of molybdenum.

Potentiometric Study of Molybdenum in LiF-BeF₂ (67-33 mole %)

N. J. Meyer⁹ C. F. Baes, Jr.
K. A. Romberger

Molybdenum is not only a major constituent of the container alloy of the MSRE, but it is also an important fission product whose chemical behavior in a molten-salt reactor is not sufficiently well understood. As a means of studying the chemistry of molybdenum in MSR fluoride solutions, potentiometric measurements have been initiated on cells of the type

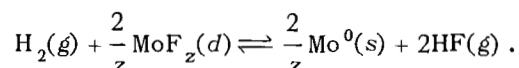
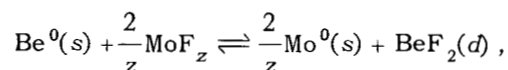


in which the solvent is LiF-BeF₂ (67-33 mole %).
Three different reference electrodes $\text{Be}^{2+} | \text{Be}^0, ^{10}$

$\text{HF} | \text{H}_2, \text{F}^-$,¹⁰ and $\text{NiF}_2(s) | \text{Ni}^0$ have been used in this study.

In a preliminary experiment performed in a cell constructed of fused silica, a dark, finely divided precipitate appeared at the molybdenum electrode when electrolysis was started with this electrode as the anode. From the amount of current passed and the weight loss of metal, the oxidation product appeared to be insoluble MoF_3 .

Subsequent experiments were performed in a copper-lined vessel with copper, graphite, or gold electrode compartments. With $\text{Be}^{2+} | \text{Be}^0$ or $\text{HF} | \text{H}_2, \text{F}^-$ reference electrodes, cell potentials were found to decrease with time. This decrease was probably due to direct reaction between inadequately separated electrode materials in cells in which the reactions were

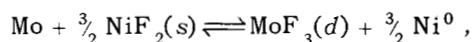


The results suggested that MoF_z produced by electrolysis was considerably more soluble than was indicated by the preliminary experiment, and showed that H_2 readily reduced MoF_z , while HF oxidized molybdenum. Thus the $\text{MoF}_z | \text{Mo}^0$ couple probably has a potential near that of the $\text{HF} | \text{H}_2, \text{F}^-$ couple. It was also noted that the molybdenum electrode was sluggish and easily polarized.

A great improvement in the stability of the cell potential was obtained by use of an $\text{NiF}_2(s) | \text{Ni}^0$ reference electrode in a silica compartment with a fine-porosity frit at the lower end. Nernstian behavior was observed with this cell assembly when, in a series of electrolysis steps at 496°C, the amount of current passed – assumed to be equivalent to the molybdenum anodized – was compared with the cell potential reached after each electrolysis step.

Current (coulombs)	Concentration of MoF_x (equivalents/kg)	E (v)
0.360	0.0015	0.286
3.36	0.014	0.232
45.0	0.187	0.185

These data suggest the formation of soluble MoF_3 as the oxidation product of molybdenum,



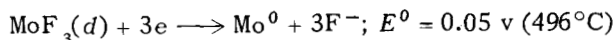
⁹Summer faculty employee, Bowling Green State University, Bowling Green, Ohio.

¹⁰Reactor Chem. Div. Ann. Progr. Rept. Jan. 31, 1965, ORNL-3789, pp. 76-79.

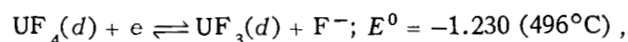
with

$$E_{\text{cell}} = 0.046 - \frac{RT}{3F} n x_{\text{MoF}_3}$$

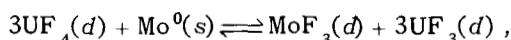
From the potential of the saturated $\text{NiF}_2|\text{Ni}$ electrode¹¹ (0.097 v vs $\text{HF}|\text{H}_2, \text{F}^-$) we obtain, as a preliminary estimate,



[vs the $\text{HF}|\text{H}_2, \text{F}^-$ electrode and for the mole fraction standard state in $\text{LiF}-\text{BeF}_2$ (66-34 mole %)]. Comparing this with the UF_4/UF_3 couple,



the equilibrium position of the following reaction should be far to the left:



$$K = x_{\text{UF}_3}^3 x_{\text{MoF}_3} | x_{\text{UF}_4}^3 a_{\text{Mo}^0} \sim 10^{-25}.$$

For a UF_3/UF_4 ratio of 0.01, which is typical of recent MSRE operation, the concentration of dissolved MoF_3 in redox equilibrium with molybdenum metal thus should be $\sim 10^{-19}$ mole fraction. In the MSRE, where the activity of molybdenum metal is probably less than unity, this concentration should be even lower.

The cause and the nature of the precipitate seen in the first experiment remain to be determined. We suspect it was an oxide or oxyfluoride of molybdenum. The role of oxide in the electrochemistry of molybdenum will be explored as a part of future measurements.

Preparation and Properties of Molybdenum Fluorides

C. F. Weaver H. A. Friedman
D. N. Hess

A literature survey of the known fluorides and oxyfluorides of molybdenum has been prepared,¹² a study of methods of synthesis of molybdenum fluorides has been conducted, and a research effort to define the nature, extent, and rate of the

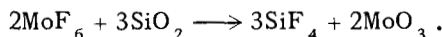
¹¹C. F. Baes, Jr., *Thermodynamics*, p. 427, vol. 1, IAEA, Vienna, 1966.

¹²C. F. Weaver and H. A. Friedman, *A Literature Survey of the Fluorides and Oxyfluorides of Molybdenum*, ORNL-TM-1976 (October 1967).

pertinent reactions of these materials has been started.¹³

Synthesis of MoF_3 and MoF_5 . – The fluorides of molybdenum have been variously reported to include MoF_3 , MoF_4 , Mo_2F_9 , MoF_5 , and MoF_6 , with MoF_6 the only compound of this class that is easily available. We have examined the several reported methods¹⁴⁻²¹ for synthesis of the lower fluorides and have developed procedures for preparation of MoF_3 and MoF_5 which are much more convenient than those previously described. In all cases the commercially available MoF_6 serves as the raw material for our synthesis.

Molybdenum hexafluoride and the lower fluorides react rapidly with traces of moisture, and HF (a reaction product) is known²² to catalyze the reaction



However, if the reaction vessels are carefully dried (by flaming under vacuum) and if the MoF_6 is freed from HF by distillation over anhydrous NaF, the preparations can be safely conducted in vessels of pyrex. (Failure to observe these precautions has led in our experiments to explosive rupture of the equipment, but careful attention to

¹³MSR Program Semiann. Progr. Rept. Aug. 31, 1967, ORNL-4191, p. 142.

¹⁴D. E. LaValle, et al., "The Preparation and Crystal Structure of Molybdenum(III) Fluoride," *J. Am. Chem. Soc.* **82**, 2433-34 (1960).

¹⁵R. D. Peacock, "Two New Fluorides of Molybdenum," *Proc. Chem. Soc.* **1957**, p. 59.

¹⁶G. H. Cady and G. B. Hargreaves, "Vapor Pressures of Some Fluorides and Oxyfluorides of Molybdenum, Tungsten, Rhenium, and Osmium," *J. Chem. Soc.* **1961**, p. 1568-74.

¹⁷A. J. Edwards, R. D. Peacock, and R. W. H. Small, "The Preparation and Structure of Molybdenum Pentafluoride," *J. Chem. Soc.* **1962**, p. 4486-91.

¹⁸T. A. O'Donnell and D. F. Stewart, "Chemical Reactions of Molybdenum Hexafluoride," *J. Inorg. Nucl. Chem.* **24**, 309-14 (1962).

¹⁹T. A. O'Donnell and D. F. Stewart, "Reactivity of Transition Metal Fluorides. I. Higher Fluorides of Chromium, Molybdenum, and Tungsten," *Inorg. Chem.* **5**, 1434-37 (1966).

²⁰T. A. O'Donnell and D. F. Stewart, "Reactivity of Transition Metal Fluorides. Uranium Hexafluoride," *Inorg. Chem.* **5**, 1438-41 (1966).

²¹M. K. Wilkinson et al., "Neutron Diffraction Investigation of Magnetic Ordering in the Trifluorides of 4-d-Transition Elements," *Phys. Rev.* **121**, 74-77 (1961).

²²A. P. Brady, O. E. Myers and J. K. Clauss, "Thermodynamic Properties of Higher Fluorides. I. The Heat Capacity, Entropy, and Heats of Transition of Molybdenum Hexafluoride and Niobium Pentafluoride," *J. Phys. Chem.* **64**, 588-91 (1959).

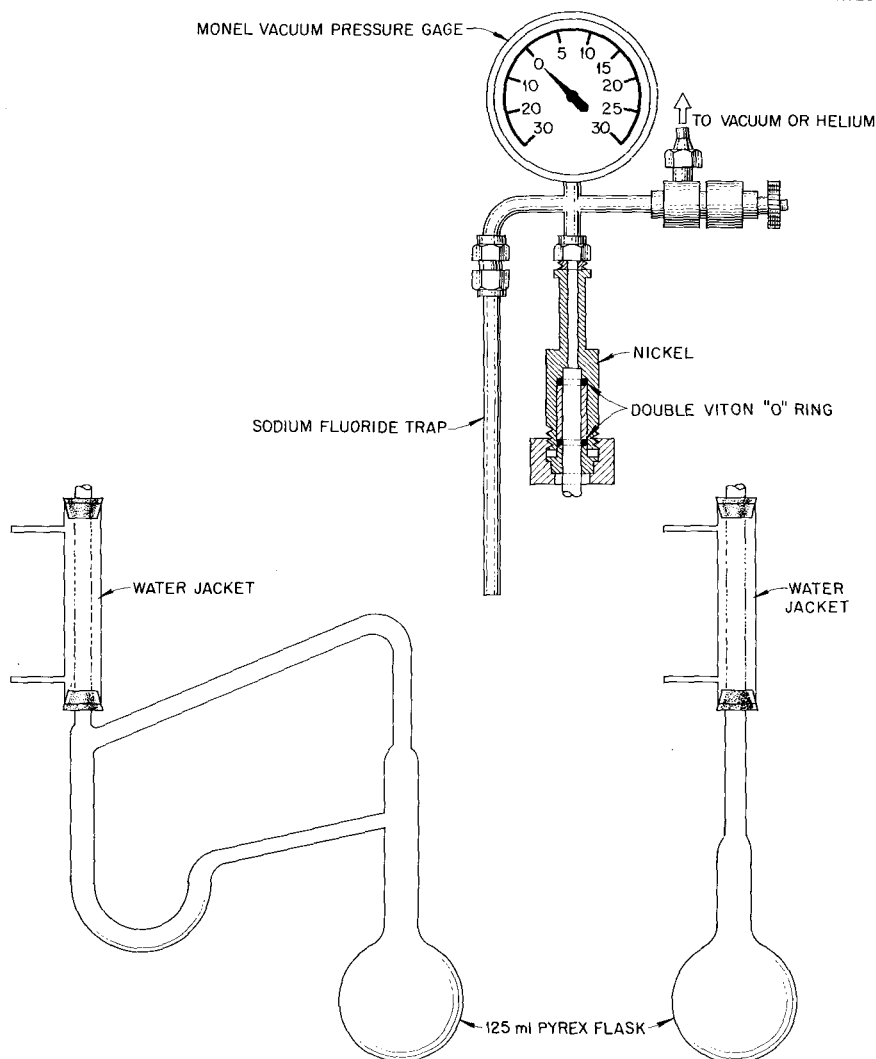


Fig. 2.4. Apparatus for the Synthesis of Molybdenum Fluorides.

these purification procedures permits containment of MoF_6 in glass for weeks without pressure increase.)

Commercially available MoF_6 is distilled over NaF in the apparatus shown at the left in Fig. 2.4. The purified MoF_6 is transferred to dry pyrex equipment (right side of Fig. 2.4) and refluxed with a predetermined quantity of clean molybdenum metal to prepare a solution of MoF_5 in the MoF_6 . After complete reaction of the added molybdenum, the system is evacuated, and the temperature is slowly increased. Excess MoF_6 leaves the equipment, and a residue of MoF_5 remains. Further heating causes sublimation of the MoF_5 to the cooler neck of the reaction vessel and, if the

temperature is sufficiently high, some disproportionation of the MoF_5 to MoF_3 and MoF_6 (which is lost by vaporization). Experiments in which the terminal temperature was 200 and 150° produced MoF_3 as a tan residue in the bulb and MoF_5 as a bright yellow deposit in the neck of the flask. The ratio of MoF_3 to MoF_5 was higher at 200 than at 150°. An experiment which was heated only to 100° produced the MoF_5 in the neck of the container, but left a viscous residue with a ratio of molybdenum to fluorine slightly higher than MoF_5 . This residue did not solidify upon cooling to room temperature and storing for several days.

The MoF_3 and MoF_5 were both identified by x-ray diffraction and by chemical analysis. Their

Table 2.4. X-Ray Diffraction Lines^a

MoF ₃ Powder Pattern		MoF ₅ Debye-Sherrer	
2θ	100I/I ₀	2θ	Intensity
23.3	100	11.10	w
31.8	25	16.73	m
34.4	13	19.65	w
39.3	5.4	20.64	m
41.9	8.2	22.31	s
47.5	8.1	24.31	vw
51.7	12	25.11	vw
54.9	3.2	26.53	ms
55.3	6.5	27.49	vw
60	4.7	28.61	vw
61.6	4.4	31.11	vw
66	2.1	32.64	w
68.2	1.9	33.81	vw
72.6	0.7	37.22	w
74.3	1.1	39.55	w
77.3	2.5	42.51	vw
81.3	1.4	45.37	ms
		47.35	vw
		48.77	vw
		51.51	vw
		53.37	vw

^aCu target.

diffraction lines are listed in Table 2.4. Those for MoF₃ were identical to those obtained by LaValle *et al.*¹⁴⁻²³ in their synthesis and structure studies. The pattern for MoF₅ corresponds to that calculated²⁴ from structural data in the literature.¹⁷ The analytical results²⁵ confirming the stoichiometry are shown in Table 2.5. The impurity level determined by emission spectroscopy²⁶ is also shown in Table 2.5. The optical properties of these substances and of NbF₅ (ref. 27) were determined to provide a rapid and convenient means for future identification and are summarized in Table 2.6.

²³R. M. Steele, Metals and Ceramics Division, personal communication.

²⁴Pattern calculated by G. D. Brunton, Reactor Chemistry Division.

²⁵Analyses performed by E. C. Lynn and Dave Canada, Analytical Chemistry Division.

²⁶Analyses performed by J. A. Carter *et al.*, Analytical Chemistry Division.

²⁷Sample prepared by L. M. Toth (Reactor Chemistry Division) by vacuum distillation of impure NbF₅.

Table 2.5. Analyses of the Molybdenum Fluorides

Elements Present	MoF ₃	MoF ₅
Mo, wt %	62.7	49.6
Mo (calculated), wt %	62.7	50.2
F, wt %	37.9	49.9
F (calculated), wt %	37.3	49.8
Al, ppm	≤200	
B, ppm		500
Be, ppm		10
Ca, ppm	<100	≤500
Cu, ppm	50	3000
Li, ppm	500	100
Mg, ppm	50	<100
Mn, ppm	30	
Na, ppm	300	500
Si, ppm	300	200
W, ppm	≤500	

Table 2.6. Optical Properties of the Molybdenum Fluorides and Niobium Pentafluoride

MoF ₃	Uniaxial positive $N_{\omega} = 1.592$ $N_{\epsilon} = 1.624$ Golden yellow
MoF ₅	Biaxial Optic angle = 90° $N_{\alpha} = 1.520$ $N_{\beta} = 1.534$ $N_{\gamma} = 1.548$ Lemon yellow
NbF ₅	Biaxial negative Optic angle ≈ 50° $N_{\alpha} = 1.484$ $N_{\gamma} = 1.516$

The absorption spectrum of MoF₅ is being investigated.²⁸ Preliminary results show absorption in the region of 1260 nm and an intense ultraviolet shoulder near 340 nm.

Lithium Fluoromolybdates (III). — The relative stability of MoF₃ at temperatures of reactor operation and the fact that it can produce both molybdenum metal and volatile molybdenum products

²⁸In cooperation with Jack Young, Analytical Chemistry Division.

Table 2.7. Optical Properties of the Lithium Fluoromolybdates

$\text{LiF}\cdot\text{MoF}_3$	Uniaxial positive $N\omega = 1.512$ $N\epsilon = 1.524$
$5\text{LiF}\cdot 2\text{MoF}_3$	Biaxial negative Optic angle $\approx 60^\circ$ $N_\alpha = 1.472$ $N_\gamma = 1.490$

Table 2.8. X-Ray Diffraction Powder Patterns

$5\text{LiF}\cdot 2\text{MoF}_3$		$\text{LiF}\cdot\text{MoF}_3$	
2θ	$100I/I_0$	2θ	$100I/I_0$
20.2	100	19.3	29
21.4	72	21.3	100
25.9	34	26.9	37
32.9	33	30.1	4
35.2	6	33.3	27
35.8	11	35.0	11
40.1	21	38.2	4
40.9	10	40.0	12
41.6	12	42.3	10
43.5	23	44.3	19
44.7	3	44.6	12
48.7	7	52.9	16
51.1	9		
52.8	18		
55.1	7		
57.1	4		
61.1	6		
63.1	4		
68.9	6		

upon disproportionation suggested that behavior of Mo^{3+} in MSRE-type solvents should be investigated. Melts along the join $2\text{LiF}\cdot\text{BeF}_2\text{-MoF}_3$ have produced two previously unknown compounds. They have been shown to belong to the system $\text{LiF}\cdot\text{MoF}_3$. Their optical properties and x-ray diffraction patterns are given in Tables 2.7 and 2.8 respectively. Attempts to determine the stoichiometry and melting behavior of these phases have been complicated by corrosion of container materials such as nickel and copper.

However, the formulas are certainly close to $5\text{LiF}\cdot 2\text{MoF}_3$ and $\text{LiF}\cdot\text{MoF}_3$, and the compounds have been so labeled in the tables. These studies are being continued to establish the formulas and melting behavior of these compounds, and the liquidus values and primary phases along the join $2\text{LiF}\cdot\text{BeF}_2\text{-MoF}_3$. Analogous studies of other fluorides, such as those of ruthenium and niobium, will be made if such information seems of value to the program.

Behavior of MoF_3 in Molten $\text{LiF}\text{-BeF}_2$ (67-33 mole %). — By proper control of the system pressure, pure MoF_3 at 500 to 700°C may be kept essentially unchanged for many days or may be disproportionated to MoF_6 and molybdenum in a few hours. This compound has been shown¹³ to be somewhat less stable in the presence of molten $\text{LiF}\text{-BeF}_2$ (67-33 mole %); nickel containers are appreciably corroded, but copper containers are reasonably stable in contact with such melts. Dissolved MoF_3 (1 mole %) reacted readily with dissolved UF_3 (4 mole %) at 500°C in the $\text{LiF}\text{-BeF}_2$ solutions.¹³ While such observations cast doubt upon the importance of MoF_3 in the MSRE, it has still seemed worth while to examine the behavior of this compound in dilute fluoride solution.

These experiments have been performed in vessels of copper; MoF_3 was added to the $\text{LiF}\text{-BeF}_2$ mixture as a previously fused preparation of $\text{LiF}\text{-MoF}_3$ (75-25 mole %). Pure helium was passed through the assembly at 8 liters/hr per kg of melt. Filtered samples of the molten mixture were drawn in hydrogen-fired copper tubes closed with sintered copper filters; unfiltered samples were drawn in open tubes of copper. Molybdenum concentrations in the samples were determined by spectrographic techniques, by activation analysis,²⁹ and by standard wet chemical methods. Agreement among the three methods was generally satisfactory; the simple wet chemical method yielded the most consistent data.

When the molten mixture containing about 800 ppm of Mo^{3+} was maintained at 500°C, both filtered and unfiltered samples showed no change in molybdenum concentration over a 23-hr period. It appeared, therefore, that the MoF_3 solution was essentially stable.

²⁹Analyses performed by E. I. Wyatt *et al.*, Analytical Chemistry Division.

Table 2.9. Stability of MoF_3 in $\text{LiF}\cdot\text{BeF}_2$ (67-33 mole %) Under Flowing Helium

Temperature (°C)	Reaction Time (hr)	Molybdenum Concentration (ppm)	
		Filtered Sample	Unfiltered Sample
500	2	690	
500-700	2.5	510	
700	3.5	440	
700	7	390	
700	24	190	250
700 ^a	27	<10	20

^aMelt treated with H_2 between 24- and 27-hr samples.

A second experiment with all conditions similar but with the temperature at 700°C showed a marked decrease in molybdenum concentration with time (see Table 2.9). The unfiltered sample shows a higher concentration of molybdenum than its filtered counterpart; this suggests that some metallic molybdenum was present in the salt and was removed by the filter. Treatment of the melt with excess H_2 served to reduce the molybdenum concentration to low levels; concentration in the filtered sample was below the determinable limit, while the unfiltered samples contained an appreciable quantity (presumably as metal). Attempts to collect and determine a volatile species by trapping it in aqueous caustic solution were unsuccessful. Such a species (presumably MoF_6) may well be reacting with the vapor regions of the apparatus before reaching the trap system.

The melts were analyzed for Cu^{2+} in an attempt to establish whether reaction with the container was responsible for loss of MoF_3 . The data obtained ranged from 50 to 200 ppm of copper and showed no increase with reaction time. It does not appear that reduction of the MoF_3 by copper can have contributed markedly to the observed loss.

These data make it likely but not certain that disproportionation of MoF_3 at 700°C is responsible for its disappearance from solution. Further attempts will be made to demonstrate and identify the volatile product and to determine the effect of UF_4 , UF_3 , and other pertinent reagents on the course of this reaction.

Mass Spectrometric Studies of Molybdenum Fluorides

J. D. Redman R. A. Strehlow

The mass spectrometer is of particular value in investigations involving volatilization. Studies of the fluorides of molybdenum have been initiated with a Bendix time-of-flight spectrometer and a Knudsen cell inlet system. Initial objectives were to assess purity of the compounds, to establish the mass spectrometric cracking patterns for these materials, and to obtain relevant thermodynamic information. Two samples of MoF_3 and one of MoF_5 were examined. The first sample of MoF_3 had been exposed to air for several years. When heated from 400°C to 725°C , this specimen yielded peaks which were attributed to MoO_2F_2^+ , then MoOF_4^+ , and finally, at the highest temperatures, MoF_5^+ and MoF_4^+ . Assignment of the peaks to these species is based on the assumption that the dominant peaks for MoF_m^+ ($m = 4, 5, 6$) were respectively the ions MoF_{m-1}^+ . On the basis of this assumption, the cracking patterns for MoF_5 and MoF_4 were determined. These are shown with patterns for $\text{MoOF}_4(?)$ and MoO_2F_2 in Table 2.10.

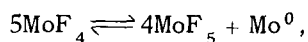
The oxyfluoride MoO_2F_2 was found to be present in a sample of MoF_3 which had been exposed to air for several years. It was also observed as the sole compound over a sample of MoF_5 which was exposed to laboratory air for 30 min and then heated to 525°C (the observation temperature). The mass spectra of the oxyfluoride and of MoF_5 are shown in Fig. 2.5. This figure serves to illustrate the two reasons why the apparently complex spectra can be resolved with reasonable facility. These are the unique isotopic abundance patterns for molybdenum coupled with the 3-amu difference between fluorine and oxygen. One finds a characteristic "slot" corresponding to the two isotopes 93 and 99. This yields, if one selects adjacent pairs of species from the MoO_2F_2^+ , MoOF_3^+ , MoF_4^+ family of peaks, three unique peaks for each species. A precise calculation of the peak-height ratios for the overlapping peaks can then be made. The dimer Mo_2F_9 has the 15 peaks which would be expected from the seven stable molybdenum isotopes. The ion Mo_2F_9^+ is believed to be both parent and principal ion peak. This compound is assumed to be an exception to the assumption calling for fluorine loss

during ionization, since Mo_2F_9 has been reported as a stable compound. There is no evidence to indicate that a significant fraction of the MoF_4^+ or MoF_5^+ peaks is due to Mo_2F_9 .

A new approach to the study of the volatile fluorides was made using a Knudsen cell constructed to permit introduction of gases during operation to 1000°C . Over the temperature range 75 to 900°C , MoF_6 was admitted into the cell containing molybdenum metal. A set of mass

spectra was obtained, and by successive subtraction the relative gaseous compositions shown in Table 2.11 were obtained.

If the relative constancy of MoF_6 is presumed to be due to leakage and the $\text{MoF}_4/\text{MoF}_5$ ratio is assumed to reflect equilibrium ratios for the reaction



the equilibrium constants can be calculated for

Table 2.10. Mass Spectrometric Cracking Patterns for Several Molybdenum Fluorides

MoF_5		MoF_4		MoF_6		MoOF_4^a		MoO_2F_2	
Fragment	Normalized Intensity	Fragment	Normalized Intensity	Fragment	Normalized Intensity	Fragment	Normalized Intensity	Fragment	Normalized Intensity
MoF_5^+	<7	MoF_3^+	100	MoF_5^+	100	MoOF_3^+	100	MoO_2F_2^+	100
MoF_4^+	100	MoF_2^+	15	MoF_4^+	32	MoF_3^+	6	MoO_2F^+	65
MoF_3^+	56	MoF^+	10	MoF_3^+	19	MoOF_2^+	10+	MoOF_2^+	6
MoF_2^+	18	Mo^+	10	MoF_2^+	15	MoF_2^+	11	MoF_2^{2+}	2
MoF^+	8			MoF^+	11	MoOF^+	10	MoOF^+	23
Mo^+	8			Mo^+	8	MoF^+	9	MoF^+	5
						MoO^+	3.5	MoO^+	7
						Mo^+	5	Mo^+	16

^aMay be MoOF_3 .

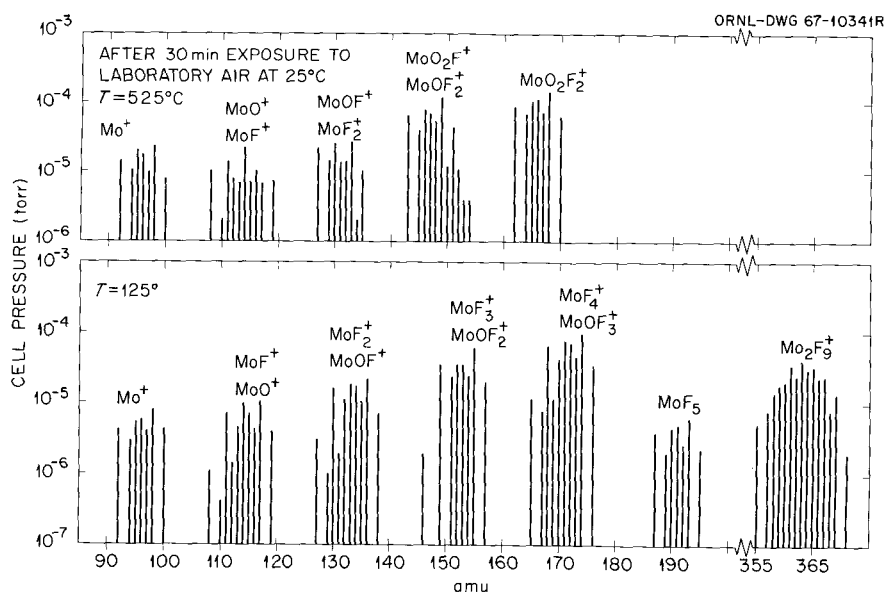


Fig. 2.5. Mass Spectra of MoF_5 at 125°C and at an Elevated Temperature After Exposure to Air.

Table 2.11. Composition of Vapor Resulting from Reaction of MoF_6 and Molybdenum (Metal) at Various Temperatures

Compound	Vapor Composition (%) at Temperatures ($^{\circ}\text{C}$) of					
	75	200	450	650	750	850
MoF_6	100	62	11	8	9	11
MoF_5		38	89	81	62	38
MoF_4				11	29	51

the temperatures from 650 to 850 $^{\circ}\text{C}$. They yield a derived enthalpy change of near $-5 \text{ kcal/F}^{\circ}$. This relatively low value is concordant with the observed volatility behavior. This promising approach will be pursued.

BEHAVIOR OF RARE-EARTH FLUORIDES IN MOLTEN LiF-BeF_2 MIXTURES

Solubilities of SmF_3 and NdF_3 in Molten LiF-BeF_2 (66-34 mole %)

F. A. Doss F. F. Blankenship
J. H. Shaffer

Measurements of rare-earth fluoride solubilities in molten LiF-BeF_2 mixtures have been resumed to supplement earlier data on rare-earth trifluoride solubility behavior in molten fluoride systems.³⁰ This experimental program will examine the behavior of those rare earths which are of interest to fuel reprocessing studies for the reference design MSBR and whose solubilities in the proposed MSBR fuel solvent have not been previously measured. The solubility of SmF_3 in LiF-BeF_2 (66-34 mole %) was determined for comparison with previous data in a similar fluoride solvent.

The experimental method essentially duplicated that of the earlier investigation. Filtered samples of the saturated solvent were withdrawn at 50 $^{\circ}$ temperature intervals while heating and cooling the molten mixture between 550 and 800 $^{\circ}\text{C}$. Rare-earth concentrations in the filtered samples were determined by radiochemical techniques. In the

³⁰Reactor Chem. Div. Ann. Progr. Rept. Jan. 31, 1960, ORNL-2931, p. 77.

current study, rare earths were labeled in situ with an appropriate radioisotope at temperatures in excess of that required for complete dissolution of the added rare-earth fluoride. Earlier studies incorporated the radiotracer during the preparation of the rare-earth trifluoride.

Experimental values of the solubility of SmF_3 in LiF-BeF_2 (66-34 mole %) at 600, 700, and 800 $^{\circ}\text{C}$ were 0.013, 0.024, and 0.040 mole fraction respectively. Solubilities of NdF_3 in the same solvent were 0.010, 0.019, and 0.035 mole fraction at 600, 700, and 800 $^{\circ}\text{C}$ respectively. Heats of solution of 10.5 kcal/mole for NdF_3 were calculated from the linear dependence of the logarithm of the solubility values on the reciprocal of the absolute temperature, as shown in Fig. 2.6.

Current solubility values for SmF_3 coincide with those obtained previously in the solvent $\text{LiF-BeF}_2\text{-UF}_4$ (62.8-36.4-0.8 mole %) only at 650 $^{\circ}\text{C}$. The heat of solution of SmF_3 by the previous data is about 13.9 kcal/mole. Although no discrepancies in the two experimental procedures are apparent, further studies would be required to resolve possible solvent effects.

Reductive Extraction of Rare Earths from Molten Fluorides into Molten Metals

D. M. Moulton W. K. R. Finnell
W. P. Teichert W. R. Grimes
J. H. Shaffer

The reductive extraction of active metal fission products, mainly rare earths, from molten fluoride salts into liquid bismuth has promise as a step in reprocessing the salt streams of a molten-salt reactor. The distribution equilibria of rare earths between LiF-BeF_2 (67-33 mole %) and Bi-Li alloys at 600 $^{\circ}$ have been reported in the preceding volume of this series.³¹ These studies have been continued and extended to cover other elements and the temperature range 500 to 800 $^{\circ}$ as well. The experimental procedure was more or less as described with the addition, in some cases, of a beryllium metal rod inserted into the salt phase so that the electrochemical potential of the liquid bismuth could be measured against this known electrode, affording an extra and rapid check on the progress of the extraction.

³¹Reactor Chem. Div. Ann. Progr. Rept. Dec. 31, 1966, ORNL-4076, pp. 34-36.

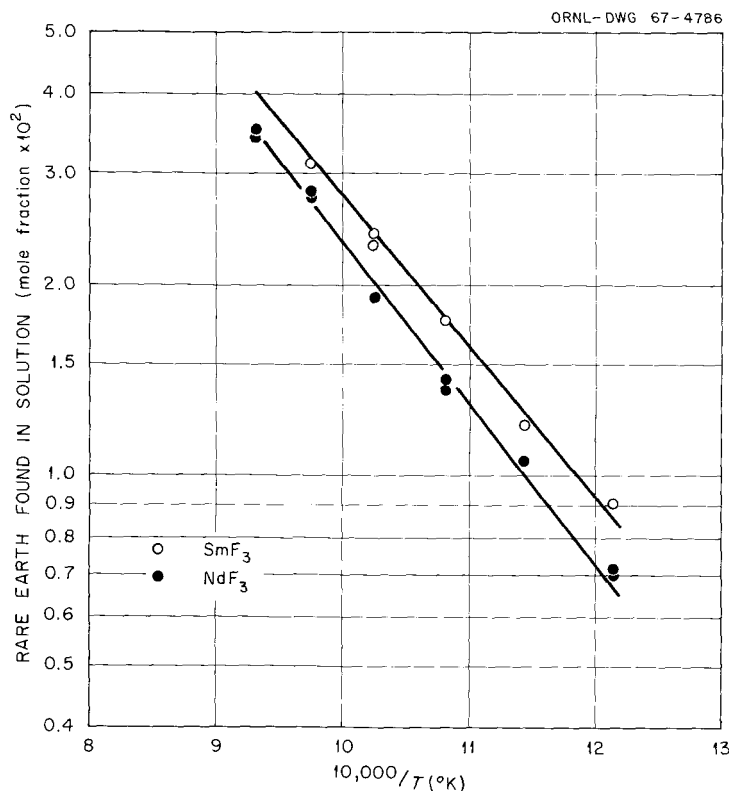


Fig. 2.6. Temperature Dependence of the Solubility of SmF_3 and NdF_3 in Molten LiF-BeF_2 (67-33 mole %).

The previous report showed clearly that all of the rare earths studied could be extracted into bismuth. Data were presented in the form of distribution coefficients as a function of the lithium concentration in the metal phase. The possibility of using several extraction stages to selectively remove certain components of the salt (e.g., uranium or protactinium in a fertile salt) suggests an alternate form to express the distributions. A convenient method is the use of an electromotive series where the relative positions of metals indicate their order of extraction. Since bismuth forms strong intermetallic compounds with most of the subject metals, defining the standard reduced state as the infinitely dilute solution in bismuth extrapolated to unit mole fraction, as in the salt phase, allows the use of the unit activity coefficient at low concentration. Thus we define

$$\mathcal{E} = \mathcal{E}'_0 - \frac{RT}{nF} \ln \frac{X_{\text{metal}}}{X_{\text{salt}}},$$

$$\mathcal{E} = \mathcal{E}'_0 \text{ at } X_{\text{metal}} = X_{\text{salt}}.$$

The prime indicates that the standard reduced

state is a solution and not the pure metal. The beryllium electrode can be related to the $\text{H}_2\text{-HF}$ electrode at $\mathcal{E}_0 = 0.00$ to give a point of reference to the system. Beryllium is now used as the standard against which other metals are measured, since it seems more reproducible than the lithium concentration. At any equilibrium point the potentials of all metals are equal, so that \mathcal{E}'_0 can be readily calculated from the distributions if one standard potential is used as a reference. Table 2.12 is a summary of the data to this time.

These values were obtained in several ways. The beryllium potential is taken from Baes;³² Li, Ce, Eu, and Th values were obtained in experiments using this electrode and assuming X_{Li^+} constant. This value of \mathcal{E}'_0 for lithium was then used to give the positions of La, Sm, and Nd from the earlier work³¹ and of barium from the Ba-Li equilibrium. The cerium value and the U-Ce equilibrium yielded the uranium potential (no lithium analyses were used). This then gave the zirconium value in a U-Zr experiment and

³²C. F. Baes, Jr., and B. F. Hitch, personal communication.

agreed quite well with the lithium distribution data. Mass balance problems with both uranium and zirconium, however, make the numbers somewhat less reliable than the others, which are hopefully within 0.01 to 0.02 v.

The valences shown are those used in the calculations. For all but zirconium and thorium they have been determined experimentally. The fractional rare-earth valences reported previously are

Table 2.12. Extraction Potentials of Fission Products from $2\text{LiF}\cdot\text{BeF}_2$ into Bismuth

Element	Valence	$E_0'(v)$ at			
		500°	600°	700°	800°
Li	1	2.00	1.93	1.88	1.83
Be ^a	2	1.93	1.85	1.78	1.71
Ba	2		1.80		
Eu	2		1.61	1.54	
Th	4		1.56	1.50	
Nd	2.5		1.52		
Ce	3	1.57	1.50	1.43	1.35
Sm	1.6		1.50		
Zr	4		1.49		
La	2.7		1.48		
U	4		1.39		

^a E_0' as referred to pure metal (ref. 32). Beryllium is insoluble in bismuth.

not confirmed in the present work on cerium and europium, although the scatter of the data does not allow unequivocal rejection of them. The value of 4 for uranium is rather surprising. It was obtained in an $\text{LiF}\cdot\text{ThF}_4\cdot\text{BeF}_2$ (73-25-2 mole %) salt and is not considered final.

It has been shown that uranium can be quantitatively separated from cerium by this method. Such a procedure could perhaps eliminate the need for fluorination to remove uranium prior to other fuel salt reprocessing steps. A similar experiment with uranium and zirconium (followed with a hafnium tracer) showed separation that was less complete but was still good enough if two or more stages were used. The U-Ce separation is shown in Fig. 2.7.

In a number of old experiments there seemed to be a rather poor balance of the total amount of reductant. This question has been investigated fairly carefully during this period. Most of this investigation came as part of other experiments and will not be described separately. Although it is a hard point to prove, the evidence indicates that the losses were due to faulty experimental technique (letting air in during sampling or lithium additions, for example) and not to any extraneous process such as the formation of a new phase or dissolved reduced material. This is the sort of problem which is probably worse in the laboratory than in large-scale processing, so it is not now considered a threat to the application of this process.

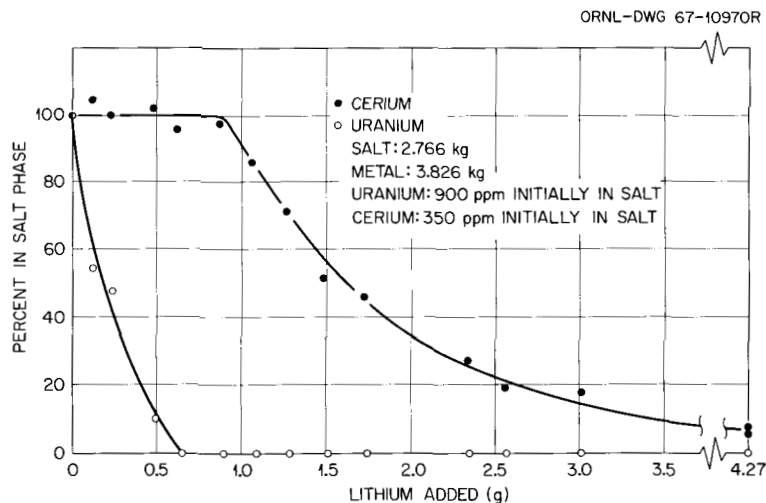


Fig. 2.7. Separation of Uranium from Cerium by Reductive Extraction with Lithium from $\text{LiF}\cdot\text{BeF}_2$ (67-33 mole %) into Bismuth at 600°C.

METALLIC COLLOIDS IN MOLTEN SALTS

H. W. Kohn³³

Until now there has been little experimental³⁴ or theoretical³⁵ reason to give credence to the existence of metallic colloids in molten salts. However, if they did exist, such colloids would almost surely be unwelcome intruders in large-scale molten-salt reactor experiments and would also have considerable impact on our ideas concerning lyophobic colloids.

We found it pretty easy to prepare such colloids. Photolysis of silver nitrate in sodium-potassium nitrate eutectic in the temperature range 300 to 400°C produced a silver metal colloid which gave an easily observable Tyndall beam. A Hanovia 125-w medium-pressure mercury arc was used. The rates of formation and of coagulation were followed using a Beckman D.U. spectrophotometer modified to serve as a high-temperature tyndallometer.

The initial rate of formation appeared to be a linear function of lamp intensity and to be independent of silver ion concentration. The temperature dependence, if one uses the initial slope of the formation curves, showed an activation energy of 2.7 kcal. The photolysis showed an induction period which, in some instances, was quite long (see Fig. 2.8). Water, added by sparging the molten salt with wet helium, discouraged the formation of metallic silver and produced a long induction period but did not inhibit silver formation entirely. When the illumination ceased, a limited dark reaction sometimes followed.

We are sure of the identity of the particles. For one thing, on standing, a silver ring sometimes

formed on the glass at the solution interface. The particles have also been examined by electron microscopy and electron diffraction³⁶ and showed the electron diffraction pattern of silver. To prepare these samples, a representative portion of the nitrate melt was dissolved in water; the resulting precipitate was removed by centrifugation and washing and was then redispersed in butanol with an ultrasonic stirrer. Hence the particles observed were water-washed coagulations of the original molten-salt colloids. Nevertheless, it can be seen that the particles agglomerated in blobs about 200 Å across. A fine structure of tiny blobs about 10 to 15 Å across could sometimes be detected.

Silver produced by photolysis was very slow to settle. Settling half-times of hundreds of minutes have been observed, and one preparation showed only a 10% diminution in tyndallometer reading³⁷ after standing overnight. Substituting appropriate numbers into Von Smoluchowski's³⁸ equation gives coagulation times of the order of milliseconds. Hence it appears that the colloid is stabilized by forces which we do not yet understand.

³³Chemistry Division.

³⁴M. A. Bredig, "Mixtures of Metals with Molten Salts," in *Molten Salt Chemistry*, ed. by M. Blander, Interscience, Wiley, 1964.

³⁵E. J. W. Verwey and J. Th. G. Overbeek, *Theory of the Stability of Lyophobic Colloids*, Elsevier, 1946.

³⁶Work performed by T. E. Willmarth, Analytical Chemistry Division.

³⁷It should be pointed out that the "settling," having been measured by tyndallometer reading, actually includes a loss due to growth of small particles and plating on the walls.

³⁸M. Von Smoluchowski, *Physik. Z.* 17, 585 (1916); *Z. Physik. Chem.* 82, 129 (1917).

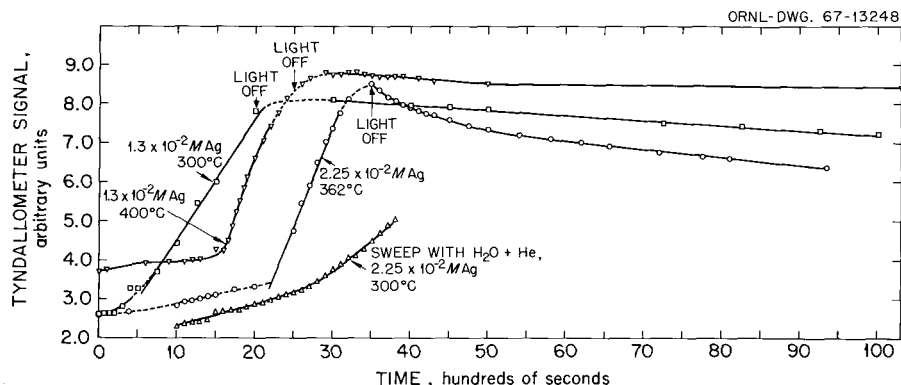


Fig. 2.8. Formation and Coagulation of Colloidal Silver in Molten $\text{NaNO}_3\text{-KNO}_3$ Eutectic.

The formation of the colloids is no clearer than their apparent stability. Most of the uv is absorbed by the nitrate ion, and somewhere along the line electrons are released and captured by the silver. Since the precipitate shows, however, none of the morphological peculiarities observed by Mahlman and Willmarth,³⁹ we can only conclude that the mechanism of formation in molten salts must be quite different from that in aqueous solutions.

Silver colloid formation in molten salts showed several peculiar phenomena. We have been unable so far to produce any colloidal silver by irradiating molten salt solutions with ⁶⁰Co gamma rays up to doses of 10²⁰ ev/g. However, irradiation of the solidified melt followed by melting produced particulate silver, but this settled comparatively rapidly. We have also been unable to produce colloidal silver by photolysis of the lithium-potassium nitrate eutectic or by radiolysis of chloride melts.

RECOVERY OF PROTACTINIUM FROM MOLTEN LiF-BeF₂-ThF₄ MIXTURES

Studies of the reductive extraction of protactinium and uranium from molten fluorides into molten metals continue to yield results which favor its application for reprocessing fluoride mixtures in the various molten-salt breeder reactor concepts.⁴⁰ Although studies thus far have been directed toward application to a two-region breeder reactor, the process appears equally applicable for removing protactinium and uranium from a single-region machine. The proposed process provides basically for the extraction of protactinium and uranium from molten mixtures of LiF, BeF₂, and ThF₄ by reduction into molten bismuth, followed by their back-extraction by oxidation into a second salt mixture.

Reductive Extraction of Protactinium at Tracer Levels from Molten Fluorides into Molten Metals

D. M. Moulton W. K. R. Finnell
W. P. Teichert W. R. Grimes
J. H. Shaffer

As reported previously,⁴¹ the results obtained by extracting trace quantities (<50 ppb) of ²³³Pa from LiF-BeF₂-ThF₄ (73-2-25 mole %) into either lead or bismuth contained in mild steel at 650°C

showed that ²³³Pa removal from the salt, upon addition of a reducing agent, was essentially complete; however, only minor fractions of the reduced ²³³Pa were found in the metal phase. By recirculating bismuth containing dissolved thorium through a similar salt mixture in a small pump loop experiment, approximately 43% of the ²³³Pa initially in the salt mixture was recovered from the bismuth on steel wool columns after 96% of the ²³³Pa had been removed from the salt phase. Examination of these columns indicated that ²³³Pa was transported primarily on solids in the molten metal phase. The results of spectrographic analyses of these solids showed relatively high concentrations of thorium with iron and chromium.

Since the extraction method utilizes the molten metal only as a transport medium, a very low solubility of protactinium or that of its carrier in the molten metal would not necessarily be detrimental to the process. The apparent adsorption of ²³³Pa on the transported solids may also have resulted from the extremely low chemical concentrations of ²³³Pa in the experimental assemblies and may not be encountered with realistic quantities of ²³³Pa in the actual application of the extraction process. Nevertheless, continued studies have been directed toward an examination of the stability of protactinium-bismuth solutions, demonstrations of the overall extraction process, and determinations of extraction potentials for various chemical components of the two-liquid-phase system. The liquid phases of some of these experiments were contained in graphite to avoid their further contamination with structural metals.

Stability of Protactinium-Bismuth Solutions. — The stability of protactinium-bismuth solutions has now been examined in three experiments. In an early experiment, ²³³Pa was added as irradiated thorium metal to bismuth contained in mild steel.⁴² The ²³³Pa concentration initially approached 75% of the value estimated for complete dissolution and then decreased to about 40% of

³⁹H. A. Mahlman and T. E. Willmarth, *Nature* **202**, 590 (1964).

⁴⁰MSR Program Semiann. Progr. Rept. Aug. 31, 1967, ORNL-4191, p. 148.

⁴¹Reactor Chem. Div. Ann. Progr. Rept. Dec. 31, 1966, ORNL-4076, p. 36.

⁴²MSR Program Semiann. Progr. Rept. Aug. 31, 1966, ORNL-4037, p. 148.

this value. The quantity of irradiated thorium corresponded to a concentration of 980 ppm in the molten bismuth, or about one-third of its solubility limit at 600°C. Analytical values for dissolved thorium ranged from 19 to 79% of the amount added. These values also showed a linear correlation with the ^{233}Pa which also remained in solution. Subsequent examination of the drained vessel for ^{233}Pa supported the conclusion that ^{233}Pa was lost as sedimentary deposits rather than by adsorption on the walls of the vessel.

A second experiment essentially duplicated the previous investigation except that the quantity of irradiated thorium added to the bismuth corresponded to a concentration of about 213 ppm. Filtered samples of the molten metal were taken periodically during a 350-hr equilibration period with intermittent helium sparging. The results of radiochemical analyses of these samples showed that ^{233}Pa concentrations during the first 100 hr varied at random between 85 and 96% of the maximum anticipated value. During the second 100-hr period ^{233}Pa concentrations decreased to about 60% of the maximum value. At the end of 350 hr about 31% of the ^{233}Pa remained in solution. A concluding phase of the experiment examined the effect of further additions of thorium on the ^{233}Pa concentration in bismuth. The addition of 1 g of thorium, which corresponded to a total maximum concentration of 1100 ppm, resulted in the reduction of the dissolved ^{233}Pa content to 19% of its original value. Two subsequent additions of 0.5 to 1.0 g of thorium had little or no further effect on the ^{233}Pa concentration in bismuth.

In the third experiment the molten bismuth was contained in graphite. Radiochemical analyses of a bismuth sample taken after the addition of irradiated thorium showed a ^{233}Pa content of about one-third of its anticipated value. However, this concentration remained constant at 600 and 750°C during an equilibration period of 16 days and further additions of thorium to its saturation value in bismuth. When the metal was cooled to 350°C so that 98% of the thorium would precipitate from the bismuth, the ^{233}Pa content decreased to about 12% of its initial value. Reheating to 725°C restored only 30% of the ^{233}Pa to solution in bismuth, although 82 to 86% was subsequently recovered in an added $\text{LiF}\cdot\text{BeF}_2$ (66-34 mole %) salt phase upon oxidation with BiF_3 . Metal specimens inserted into the bismuth

acquired ^{233}Pa activities in the order $\text{C} \ll \text{Fe} < \text{Be} < \text{Nb}$; however, the fraction of ^{233}Pa which deposited on the specimens was a negligible fraction of the total ^{233}Pa content in the bismuth.

Although the results of the three preceding experiments are inconclusive, they do associate instabilities of protactinium-bismuth solutions with the presence of saturating concentrations of thorium and the presence of metal surfaces.

Extraction Process Demonstrations. — On the basis of preceding results, an experimental program was conducted to attempt the extraction of protactinium and uranium from a simulated MSBR blanket mixture, $\text{LiF}\cdot\text{BeF}_2\cdot\text{ThF}_4$ (73-2-25 mole %), by reduction into bismuth and their recovery into a second salt mixture by hydrofluorination. The extraction vessel was designed to contain the blanket salt and the recovery salt in separate cylindrical shells of graphite arranged so that both salt phases would contact a common pool of the molten metal. Samples of the three liquid phases were obtained after incremental additions of thorium or beryllium to the blanket salt while the recovery salt was exposed to a gaseous mixture of anhydrous hydrogen fluoride and hydrogen. The objectives of three experiments were to investigate the concurrent transport of uranium and protactinium through the extraction system and to examine the effect of metal additives to bismuth on the transport of protactinium alone.

The first experiment involved 3.60 kg of bismuth; 0.50 kg of the ternary eutectic, $\text{LiF}\cdot\text{NaF}\cdot\text{KF}$ (46.5-11.5-42.0 mole %), as the recovery salt; and 2.52 kg of $\text{LiF}\cdot\text{BeF}_2\cdot\text{ThF}_4$ (73-2-25 mole %) containing about 1 mc of ^{233}Pa activity and 213 ppm of uranium as the simulated MSBR blanket mixture. The transport of uranium and protactinium in the extraction was followed during the addition of four gram-equivalents of beryllium in small increments to the blanket salt mixture. The experiment was terminated when the leak rate of HF through a graphite-metal seal into the gas phase above the blanket salt became excessive. Although the behavior of ^{233}Pa was somewhat erratic, approximately 65% of the amount originally in the blanket was found in the recovery salt, and about 80% of the ^{233}Pa was accounted for by material balance based on samples of the three liquid phases. The transport of uranium in the extraction system is illustrated in Fig. 2.9. Within the experimental precision, the appearance of protactinium in the

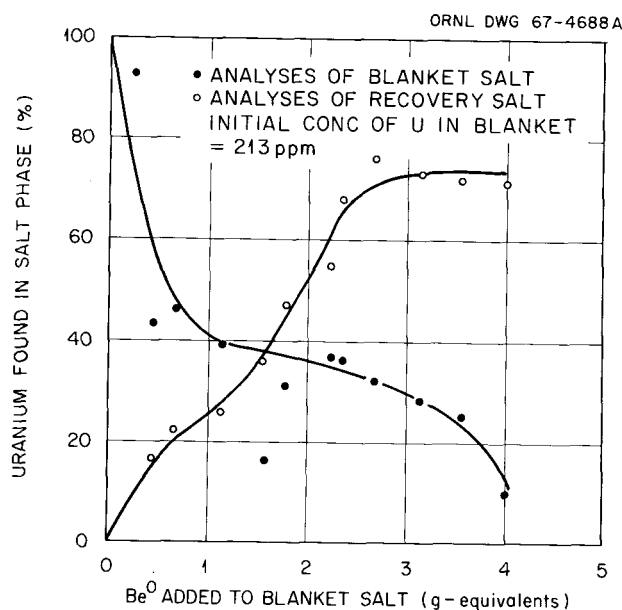


Fig. 2.9. Extraction of Uranium from $\text{LiF-BeF}_2\text{-ThF}_4$ (73-2-25 mole %) by Reduction with Beryllium Metal into LiF-NaF-KF (46.5-11.5-42.0 mole %) by Hydrofluorination via Molten Bismuth at 650°C During Simultaneous Extraction of ^{233}Pa .

recovery salt showed a linear relationship to that of uranium.

The next two experiments in this series were directed toward the evaluation of bismuth-copper and bismuth-tin alloys as the molten metal phase of the extraction process. Uranium was omitted from the blanket salt to simplify the interpretation of results, and the mixture LiF-BeF_2 (60-40 mole %) was substituted for the ternary alkali-metal fluoride eutectic mixture as the recovery salt. Thorium metal turnings were used as the reducing agent. A single experiment failed to demonstrate suitable ^{233}Pa transport through a copper-bismuth alloy. Results obtained after the addition of some 30 g of thorium and 60 hr of HF treatment showed ^{233}Pa concentrations in the blanket that varied at random from 12.6 to 37.4% and only gradual increases in the ^{233}Pa content of the recovery salt from 2.8 to 23.4%. The maximum concentration of ^{233}Pa in the metal phase was 18.6%, and the overall ^{233}Pa inventory in the three liquid phases at the conclusion of the experiment was about 55% of the amount originally in the blanket mixture.

Since the content of structural-metal difluorides in the blanket salt may be relatively large compared with that of protactinium, the third experiment attempted to improve ^{233}Pa extractability by in-

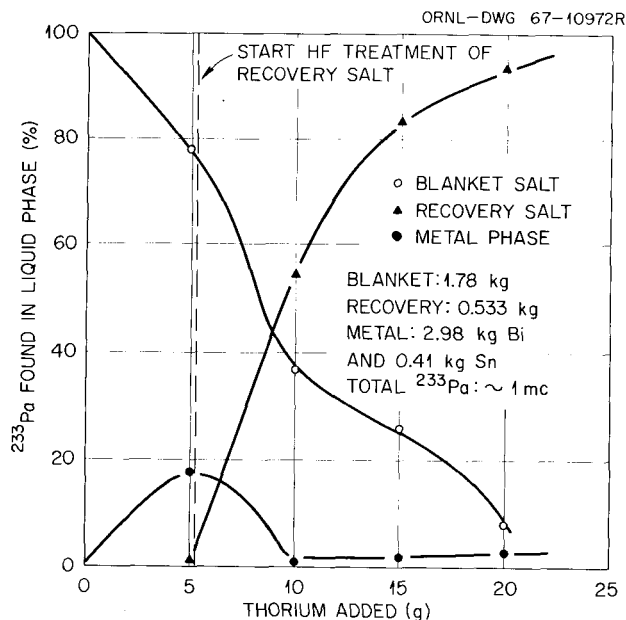


Fig. 2.10. Extraction of ^{233}Pa from $\text{LiF-BeF}_2\text{-ThF}_4$ (73-2-25 mole %) by Reduction with Thorium Metal into LiF-BeF_2 (60-40 mole %) by Hydrofluorination via Molten Bismuth-Tin Mixture at 650°C .

creasing the solubility of structural metals in the molten metal phase. Tin was chosen as an additive for several reasons: the solubility of iron is reported to be greater than 0.385 at. % at 500°C and to increase with temperature; no high-melting compounds of tin and bismuth are known, and the two metals are completely miscible; tin is essentially chemically inert in the system under study. The experiment involved 1.78 kg of the simulated MSBR blanket mixture with added ^{233}Pa activity and 0.53 kg of LiF-BeF_2 (60-40 mole %) as the recovery salt. The metal phase initially contained 207 g of tin in 2.98 kg of bismuth; another 201 g of tin was added later to increase further the solubility of iron in the molten metal phase. If bismuth behaved as an inert diluent, each addition of tin should have dissolved approximately half the iron initially contained in the blanket salt. Analytical results which demonstrate ^{233}Pa transport in the extraction system are shown in Fig. 2.10. At the conclusion of the experiment, approximately 90% of the ^{233}Pa activity was found in the recovery salt mixture, 2% was present in the molten metal phase, and 8% remained in the blanket salt. Thus the experiment demonstrated quantitative accountability of ^{233}Pa by analyses of samples taken from the three liquid phases.

The results of experiments 1 and 3 in this series demonstrate the chemical feasibility of recovering uranium and protactinium from the fertile blanket of a two-region molten-salt breeder reactor. Although the addition of tin to the metal phase was associated with greatly improved ^{233}Pa transport characteristics, the results of the first experiment indicate that an increased solubility of iron in the metal phase may not be required in the large-scale application of the extraction process.

Determination of Extraction Potentials. — Although the previous experiments have demonstrated the chemical feasibility of the extraction method, engineering development of the concept will require knowledge of the distribution relationships of the various chemical components of the extraction system under equilibrium conditions.

In a preliminary experiment, 2.35 kg of bismuth and 2.94 kg of the simulated blanket salt mixture, $\text{LiF}\cdot\text{BeF}_2\cdot\text{ThF}_4$ (73-2-25 mole %), with about 500 ppm of uranium and 1 mc of ^{233}Pa activity were contained at 650°C in a graphite-lined extraction vessel. Thorium was added to the two-liquid-phase system in several successive small increments. Samples of the liquid phases were taken after each thorium addition under assumed equilibrium conditions. Analytical results from these samples for Li, U, Th, and Pa in the bismuth and U and Pa in the salt (Li and Th in the salt stayed constant) provided a basis for determining relative extraction potentials of these metals.

As described for the extraction of rare earths from a reactor fuel solvent⁴³ the distribution of a specific metal in the extraction system can be expressed as a half-cell voltage by the equation

$$\mathcal{E} = \mathcal{E}'_0 - \frac{RT}{nF} \ln \frac{X_m}{X_s}, \quad (1)$$

where X_m and X_s denote mole fractions in the metal and salt phases; \mathcal{E}'_0 is an alternate standard potential and can be related to the ordinary standard potentials, \mathcal{E}_0 , as defined by Baes⁴⁴ if the activity coefficients, γ , are known; $\gamma_m X_m$ would here denote the metal activity compared

with the activity of the pure solid metal. Under these circumstances γ_m is many orders of magnitude less than unity but should stay constant. Thus, if all γ 's remain constant, \mathcal{E}'_0 is also constant and equal to the voltage of the half-cell when $X_m = X_s$. Here the standard states or hypothetical unit mole fraction solutions have the properties corresponding to infinite dilution.

A plot of the experimental data in the form $1/n[\ln(X_m/X_s)]$ vs the amount of thorium added gave four parallel lines. This was taken to mean that the metals were indeed in equilibrium; therefore, all of the \mathcal{E} 's were set equal to each other. The absolute value of \mathcal{E}'_0 for lithium was estimated from the data of Baes on activity coefficients of lithium ion as a function of its mole fraction in $2\text{LiF}\cdot\text{BeF}_2$ and from the metal-phase activity coefficients obtained at Brookhaven.⁴⁵ From this the other absolute values could be obtained. The absolute values are only estimates, and are irrelevant anyway; the differences, which are the measured quantities, are the only numbers of importance in determining liquid-liquid distributions in this system. Data obtained from this preliminary experiment yielded values for \mathcal{E}'_0 as shown in the accompanying table.

M	$-\mathcal{E}'_0$ (923°K) ^a	$-\mathcal{E}'_0$ ^b
Li	2.601	1.80
Th	1.772	1.47
Pa		1.32
U	1.368	1.28

^a $-\mathcal{E}'_0$ (v) at 923°K is half-cell potential for pure metal \rightarrow ion at hypothetical unit mole fraction in Li_2BeF_4 (except to 0.67 mole fraction for Li).

^b $-\mathcal{E}'_0$ (v) at 923°K is half-cell potential for amalgam \rightarrow ion in Li_2BeF_4 at $X_m = X_s$.

Although these values show the relative order of extraction potentials for the various metals of interest, they will be refined by further experimentation and development of laboratory techniques.

⁴³See "Reductive Extraction of Rare Earths," this report.

⁴⁴C. F. Baes, Jr., *Thermodynamics*, pp. 409-33, IAEA, Vienna, 1966.

⁴⁵Brookhaven National Laboratory Nuclear Engineering Progress Report, July-September 1958, January-April 1959; Annual Report, July 1, 1958.

Protactinium Studies in the High-Alpha Molten-Salt Laboratory

C. J. Barton H. H. Stone

The glove-box train in the High-Alpha Molten-Salt Laboratory described in a previous report⁴⁶ had seven glove boxes arranged in an L. During the past year this facility was expanded by adding two more stainless steel boxes. The box at one end of the original facility had a 12-in. bag-out port which required open space around it for proper operation. Consequently, we disconnected this box from the end of the train after careful decontamination, inserted an angle glove-box connection in its place, connected the two new boxes in series, and then placed the box with the 12-in. bag-out port at the end of the train. The final arrangement is a U-shaped train with the other end of the train connected to the laboratory hood. One of the new boxes is equipped with a furnace and with gas control valves (helium, hydrogen, HF, and vacuum) similar to that described earlier⁴⁶ except that most of the controls are placed outside the box to facilitate replacement. The original high-temperature box is being renovated. When this work is completed, we will have the capability of performing two protactinium recovery experiments simultaneously or of working with two different alpha-active materials. This facility permits us to supplement the tracer-level studies performed in other laboratories⁴⁷ by experiments in which the protactinium concentrations are as high as are expected for full-scale reactor operation.

Reduction of Protactinium by Thorium in the Presence of Iron Surface (Brillo Process). — Results of an experiment on the reduction of protactinium by thorium in the presence of steel wool were given in a previous report.⁴⁸ Several more experiments of this type have been completed since that time, making a total of six such experiments that we have performed. These experiments have been described in part in other reports.^{49,50} The data from the different experi-

ments show variations in the fraction of the protactinium reduced by thorium and retained by the steel wool surface, but it appears that 90% or more of the protactinium content of molten LiF-ThF₄ breeder blanket material can be concentrated on a comparatively small amount of steel wool having a large surface area (at least 80 curies of ²³³Pa per gram of steel wool).

Reduction of Iron Dissolved in Molten LiF-ThF₄. — The possible influence of iron impurity in melts on the behavior of reduced protactinium has been discussed in earlier reports⁴⁸⁻⁵⁰ and in the preceding section of this report. It was considered desirable, therefore, to obtain data on the reduction of iron in molten LiF-ThF₄ by both hydrogen and thorium. One experiment was conducted with ⁵⁹Fe tracer added, but without protactinium, so that a comparison could be made between analytical values for iron determined in different laboratories and results calculated from our own measurement of the ⁵⁹Fe activity of the samples. The results of this experiment have been reported⁵¹ in more detail and will only be summarized here.

More than 40 hr was required for nearly complete removal of iron from the melt by hydrogen reduction at about 600°C, while reduction of iron by metallic thorium at the same temperature was virtually complete after 3 hr. In a later test at 700°C, 95% of the iron was reduced by hydrogen in 6 hr and 99.5% in about 18 hr. Comparison of the data obtained by use of ⁵⁹Fe tracer counts with the results of colorimetric iron determinations by two different laboratories indicated that the colorimetric methods used when this test was performed did not give reliable results at low iron concentration.

It was concluded that use of ⁵⁹Fe tracer in molten-salt experiments permits rapid and sensitive measurements of the iron content of salt samples.

Thorium Reduction Followed by Filtration. — The finding⁵² that a large fraction of the thorium-reduced protactinium was absent from salt passed through a sintered copper filter suggested the possibility of collecting the reduced protactinium on a metal filter. Six experiments to test this possibility gave rather discouraging results, which were

⁴⁶C. J. Barton, *Reactor Chem. Div. Ann. Progr. Rept. Dec. 31, 1965*, ORNL-3913, p. 44.

⁴⁷D. M. Moulton *et al.*, "Reductive Extraction of Protactinium at Tracer Levels from Molten Fluorides into Molten Metals," this report.

⁴⁸C. J. Barton and H. H. Stone, *Reactor Chem. Div. Ann. Progr. Rept. Dec. 31, 1966*, ORNL-4076, p. 39.

⁴⁹C. J. Barton and H. H. Stone, *MSR Program Semiann. Progr. Rept. Feb. 28, 1967*, ORNL-4119, p. 153.

⁵⁰C. J. Barton and H. H. Stone, *MSR Program Semiann. Progr. Rept. Aug. 31, 1967*, ORNL-4191, p. 153.

⁵¹C. J. Barton and H. H. Stone, *Reduction of Iron Dissolved in Molten LiF-ThF₄*, ORNL-TM-2036 (Nov. 2, 1967).

⁵²C. J. Barton and H. H. Stone, *MSR Program Semiann. Progr. Rept. Aug. 31, 1966*, ORNL-4037, p. 156.

discussed briefly in another report.⁵⁰ A large part of the reduced protactinium, 20 to 57%, was found on the graphite liner and dip leg, while only 10 to 30% was on the transfer filter, the desired location from which it could presumably be recovered by hydrofluorination. Although it appears that a continuous reduction-filtration method could possibly be developed, the results of these experiments demonstrated that the batch reduction-filtration process was not a promising recovery method, and no further experiments of this type are planned.

Transfer of Reduced Protactinium to Liquid Bismuth. — Results of experiments reported earlier^{53,54} showed that protactinium can be readily removed from molten fluoride mixes by equilibration with liquid lead-thorium or bismuth-thorium alloy. However, transfer of the reduced protactinium to the molten metal phase was found to be incomplete. More recent experiments⁵⁵ demonstrated that transfer of protactinium from one fluoride melt to another can be effected using molten bismuth as the transfer medium. This finding encouraged further study of molten bismuth as a processing medium for protactinium recovery. Uranium will be present at a low concentration in the breeder blanket of a two-region reactor and at a higher concentration in the fuel mix of a one-region reactor. It is important, therefore, to determine the effect of uranium dissolved in bismuth on the distribution of protactinium between bismuth and salt phases.

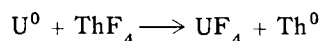
In one experiment, the first to be performed in the new stainless steel glove box described above, only a trace amount of ²³³Pa was added in order to minimize alpha contamination of the box during the first trial. One millicurie of ²³³Pa and 1 mc of ⁵⁹Fe were mixed with 255 g of LiF-ThF₄ (73-27 mole %) in a nickel reactor vessel, sparged with HF and H₂ to remove oxygen, and sparged with H₂ to reduce nickel and iron present in the melt. The hydrogen treatment removed only about 40% of the initial ⁵⁹Fe activity; in the process, about 15% of the initial ²³³Pa activity was lost from solution, possibly as a result of a trace of water in the system.

⁵³J. H. Shaffer *et al.*, *MSR Program Semiann. Progr. Rept. February 28, 1966*, ORNL-3936, p. 147.

⁵⁴C. J. Barton and H. H. Stone, *Removal of Protactinium from Molten Fluoride Breeder Blanket Mixtures*, ORNL-TM-1543 (June 1, 1966).

⁵⁵D. M. Moulton *et al.*, "Reductive Extraction of Protactinium at Tracer Levels from Molten Fluorides into Molten Metals," this report.

The treated salt was transferred through a sintered nickel filter into a graphite-lined vessel fitted with a graphite dip leg. This vessel contained 171.4 g of bismuth and 1.98 g of freshly cleaned uranium turnings (1 at. %) which had been mixed at 750° and then cooled to 650°C. Samples of salt and bismuth phases were removed at intervals for analysis. The data are displayed in Table 2.13. The graphite rod sampler that was used to take unfiltered samples of bismuth intended to be free of salt contamination failed to perform as expected. Consequently, no samples of the bismuth phases were obtained until late in the experiment. The uranium content of the salt phase, both filtered and unfiltered samples, showed a sharp increase after only a few minutes contact of the salt and bismuth phases. The rate of change in uranium concentration of the salt over the remaining 20 hr of contact was slow compared with the initial increase. As expected, only a small fraction (about 1.0%) of the protactinium activity transferred to the bismuth phase. The free energy change calculated for the reaction



is +45.4 kcal per gram-atom of uranium at 900°K. The corresponding change for the reduction of PaF₄ by uranium is undoubtedly less than that for ThF₄ but is almost certainly positive. The uncertainty in the amount of metallic uranium present in the bismuth and the unknown effect of possible UO₂ present make calculations based on thermodynamic estimates of doubtful value in this experiment, but it appears that the protactinium distributed more or less as expected and that the unexpected high concentration of uranium in the salt phase could have been due to partial conversion of uranium metal to UO₂ which subsequently reacted with ThF₄ to give UF₄.

The second experiment involving equilibration of liquid bismuth and molten fluoride salt was designed to simulate reactor processing conditions more closely. The salt phase in this experiment was 255 g of LiF-BeF₂-ThF₄ (73-2-25 mole %) containing approximately 100 ppm ²³¹Pa and 50 ppm ²³⁵U (added as ⁷LiF-²³⁵UF₄), with 1 mc each of ²³³Pa and ⁵⁹Fe added as tracers. The bismuth (300 g) contained initially 2220 ppm of Th⁰ by analysis (2500 ppm of metal had been added). During each of three efforts to reduce Fe²⁺ by hydrogen treatment of the melt, precipitation of protactinium occurred. At the end of this

Table 2.13. Distribution of ^{233}Pa and Uranium Between Uranium-Bismuth Alloy and Molten LiF-ThF_4

Contact Time (hr)	Phase	$^{233}\text{Pa}^a$ c/m-Total	U (%)	Bi (%)
		$\times 10^6$		
0	Filtered salt	3.53	0.007	11.0-12.9
0	Unfiltered salt	3.80	0.012	0.19
$\frac{1}{4}$	Filtered salt	2.67	0.13	4.05
$\frac{1}{4}$	Unfiltered salt	3.34	0.19	1.63
5	Filtered salt	2.56	0.19	3.90
5	Unfiltered salt	2.62	0.39	1.08
5	Unfiltered salt	2.63	0.23	0.95
16	Unfiltered Bi	0.017	0.14	
16	Filtered salt	2.37	0.23	7.31
16	Unfiltered salt	2.40	0.24	0.30
20	Filtered Bi	0.015	0.10	
20	Filtered salt	2.31	0.29	6.65
20	Unfiltered salt	2.36	0.27	0.17
	Frozen unfiltered salt	2.03	0.83	0.21
	Frozen unfiltered Bi	0.012	0.22	
	Transfer filter	0.020		

^aCalculated assuming no salt or bismuth removed in samples.

prolonged treatment of the salt, the thorium content of the bismuth phase had dropped to 220 ppm. Nevertheless, after returning the precipitated protactinium to solution by H_2 -HF treatment, the bismuth and salt phases were mixed without reduction of iron. Only preliminary results on protactinium distribution in the experiment are available; they are based on ^{233}Pa counts of weighed portions of the solid salt and bismuth samples. The principal uncertainty in using these counts as a direct measure of ^{231}Pa concentration is the factor used to compensate for the different self-absorption values for ^{233}Pa in the salt and bismuth samples. We multiplied ^{233}Pa counts in bismuth by 2 to provide approximate compensation for this difference. The data indicate that about 6% of the total ^{233}Pa activity was transferred to the bismuth phase after $3\frac{1}{2}$ hr contact with 220 ppm initial Th^0 concentration in bismuth. The ^{233}Pa activity in a filtered salt sample at the same time dropped to 51% from the previous value of 83%, suggesting that ThO_2 present in the partially oxidized thorium-bismuth alloy may have converted part of the protactinium to an insoluble form.

At this point an additional 0.75 g of thorium metal chips was added to the reaction vessel, and samples were taken 1 hr later. Mixing of phases was accomplished by helium sparging. A marked increase in the ^{233}Pa content of the bismuth occurred during this period (to about 45% of the original ^{233}Pa activity present), and a corresponding decrease in the ^{233}Pa content of an unfiltered salt sample was also observed. After standing overnight under flowing helium the ^{233}Pa concentration in filtered bismuth was approximately half of the maximum value, and a further decrease occurred when the phases were mixed for $1\frac{1}{4}$ hr with helium. Only a few percent of the original ^{233}Pa activity remained in the filtered salt at this juncture.

A more thorough evaluation of this experiment will be attempted when the analyses of the various samples are completed, but the presently available data indicate that equilibration of bismuth-thorium alloys with salt phases containing realistic concentrations of ^{231}Pa results in a significant transfer of protactinium to bismuth.

3. Chemical Studies of Molten-Salt Systems

RELATIONS BETWEEN DEVIATIONS FROM IDEALITY AND ASSOCIATION IN BINARY MIXTURES

Jerry Braunstein

In mixtures of charge-unsymmetrical molten salts (e.g., KCl-MgCl_2 , LiF-BeF_2), simple physical models have been unable to account entirely for observed deviations from ideality, and additional contributions from the formation of associated species have been proposed.¹ The representation of deviations from ideality in terms of the formation of associated species may be useful in some systems if the association constants can be defined unambiguously and evaluated uniquely, as for dilute solutes in reciprocal molten-salt systems.² To determine the extent to which association can contribute to deviations from ideality, relations were derived between the coefficients in the Margules expansion of the activity coefficients and the association constants, under the assumption that the associated and unassociated species mix ideally. Mixtures of nonelectrolytes, for example, liquid metals, were considered as well as mixtures of molten salts.

The Margules expansions of the activity coefficients in a two-component system (mole fraction $1-x$ of A and mole fraction x of C) are

$$\ln \gamma_A = \alpha x^2 + \beta x^3 + \dots,$$

$$\ln \frac{\gamma_C}{\gamma_C(x=0)} = -2\alpha x + \left(\alpha - \frac{3}{2}\beta\right)x^2 + \dots$$

The activity coefficients may be written for nonelectrolytes as

¹O. J. Kleppa and F. G. McCarty, *J. Phys. Chem.* **37**, 451 (1962).

²J. Braunstein, M. Blander, and R. M. Lindgren, *J. Am. Chem. Soc.* **84**, 1529 (1962).

$$\gamma_A = \frac{a_A}{1-x} = \frac{N_A}{1-x},$$

$$\gamma_C = \frac{a_C}{x} = \frac{N_C}{x},$$

where the a 's are the activities and N_A and N_C are the mole fractions of unassociated A and C. If AC is the only associated species, and its association constant is

$$K = \frac{N_{AC}}{N_A N_C},$$

a Taylor's series expansion gives

$$\ln \gamma_A = -(K/K+1)x^2 - 2(K/K+1)^2x^3 + \dots$$

The coefficient of the quadratic term may be obtained from the limiting slope of a plot of $\ln \gamma_A$ vs x^2 or as the intercept of a plot of $(\ln \gamma_A)/x^2$ vs x . The limiting slope of the latter plot gives the coefficient of the cubic term.

For mixtures of molten salts, the ion fractions generally are used as the concentration units. Thus, in a mixture of mole fraction x of A^+C^- and mole fraction $(1-x)$ of A^+D^- in which the "associated species" A_2C^+ are considered to mix randomly with the unassociated cations A^+ while the anions C^- and D^- mix randomly with each other but not with the cations, we have

$$\gamma_{AD} = \frac{a_{AD}}{1-x}, \quad \gamma_{AC} = \frac{a_{AC}}{x},$$

$$a_{AD} = N_A N_D, \quad a_{AC} = \frac{N_A N_C}{N_A(x=1)},$$

$$N_A = 1 - N_{A_2C} = \frac{n_A}{n_A + n_{A_2C}},$$

Table 3.1. Relations Between α and K for Several Modes of Association

	Solvent		Solute		Associated Species	
	A	C	AC	A_2C	A_nC	AC_2
α			$-K/K + 1$	$-2K/K + 1$	$-nK/K + 1$	$+K$
(a) $\alpha(K=0)$			0	0	0	0
$\alpha(K=\infty)$			-1	-2	-n	∞
	A^+D^-	A^+C^-	AC	A_2C^+	AC_2^-	
α			0	$-(K/K + 1)^2$	0	
(b) $\alpha(K=0)$			0	0	0	
$\alpha(K=\infty)$			0	-1	0	
	A^+D^-	H	AH^+			
α			$-K/K + 1$			
(c) $\alpha(K=0)$			0			
$\alpha(K=\infty)$			-1			
	L^+C^-	$M^{2+}C_2^-$	MC^+	MC_3^-		MC_4^{2-}
α			0	$-K(K-1)/(K+1)^2$		$-K(2K-1)/(K+1)^2$
(d) $\alpha(K=0)$			0	0		0
$\alpha(K=\infty)$			0	-1		-2

$$N_D = 1 - N_C = \frac{n_D}{n_C + n_D},$$

$$K = \frac{N_{A_2C}}{N_A^2 N_C}.$$

The expressions for α in terms of the association constants for various associated species are listed in Table 3.1 along with the range of values of α consistent with the various modes of association.

The results of Table 3.1 indicate that unique evaluation of the association constants from the limiting thermodynamic behavior, which was possible with dilute reciprocal molten-salt systems, is not here possible because different species give similar concentration dependence of γ . Table 3.1 (a) indicates, however, that if associated species alone are responsible for the deviations from ideality, and $\alpha = -n$, species at least as complex as A_nC must be present.

The artificiality of the Temkin activities for mixtures of ions of widely different size (complexity) and charge type is indicated by the absence of con-

tributions to nonideality from AC and AC_2^- in case (b) and from MC^+ in case (d). Neutral species which "solvate" cations [case (c)] do contribute to deviations from ideality.

For partial association to anionic species $MC_n^{(n-2)-}$ in mixtures of the type $(1-x)LC-xMC_2$, the activities of both components,

$$a_{LC} = (1 - N_M)N_C$$

and

$$a_{MC_2} = \frac{N_M N_C^2}{N_C^2(x=1)},$$

may be calculated from the equations

$$KN_C^{n+1}(1-lx) + KN_C^n(mx-1) + N_C^2(x-l) + N_C(l+m-2x) + (x-m) = 0,$$

$$N_M = \frac{1 - N_C}{KN_C^n},$$

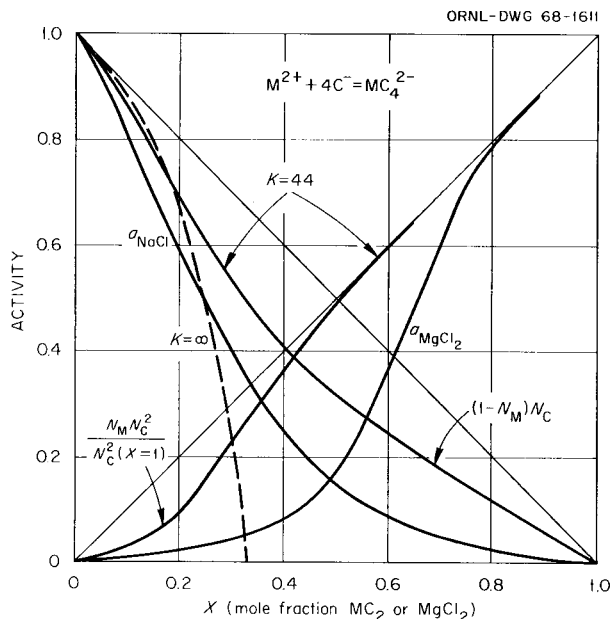


Fig. 3.1. Activities of NaCl and MgCl₂ vs Composition (ref. 3) and Activities Calculated on the Basis of Association with $K = 44$.

where $l = n - 2$ and $m = n - 1$. Figure 3.1 shows calculated values of the activities for the case $n = 4$ (species MC_4^{2-}), $K = 44$. This species and association constant have been proposed to account for the excess chemical potentials in the system NaCl-MgCl₂.³ The dashed line corresponds to $K = \infty$ (complete association to $MgCl_4^{2-}$). It is apparent that this model is not applicable.

Figure 3.2 shows plots of the activities in the molten-salt system LC-MC₂ and the nonelectrolyte system A-C for association of two solvent particles with one solute particle. In the molten-salt system the calculated deviations from ideality are much smaller than for the nonelectrolyte because of the form of the Temkin activities. Systematization of the thermodynamics of association in binary molten-salt mixtures requires additional attention to suitable models of ideality.⁴

THERMODYNAMICS OF LiF-BeF₂ SYSTEM BY EMF MEASUREMENTS

B. F. Hitch C. F. Baes, Jr.

The development of HF, H₂|F⁻ and Be²⁺|Be⁰ electrode half cells for use in Li₂BeF₄ melts has been described previously.⁵ In the present investi-

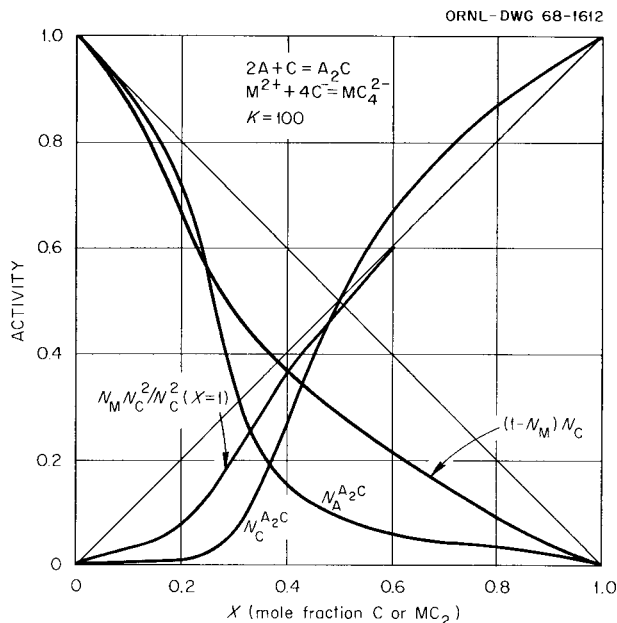
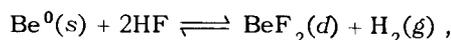


Fig. 3.2. Activities Calculated with $K = 100$ for the Modes of Association $2A + C = A_2C$ and $M^{2+} + 4C^- = MC_4^{2-}$.

gation these two electrodes were used in the following cell:



The cell reaction is assumed to be



and hence the measured cell potential E may be related to the activity of BeF₂ in the melt:

$$E = E^0 - \frac{RT}{2F} \ln \left[\frac{a_{\text{BeF}_2} P_{\text{H}_2}}{P_{\text{HF}}^2} \right] \quad (2)$$

For a fixed composition the activity of BeF₂ can be considered to be constant; thus Eq. (2) is reduced to

$$E = E_c^0 - \frac{RT}{2F} \ln \frac{P_{\text{H}_2}}{P_{\text{HF}}^2}, \quad (3)$$

³D. E. Neil, H. M. Clark, and R. H. Wiswall, *J. Chem. Eng. Data* 10, 21 (1965).

⁴L. S. Darken and R. W. Gurry, *Physical Chemistry of Metals*, p. 282, McGraw-Hill, New York, 1953.

⁵G. Dirian, K. A. Romberger, and C. F. Baes, Jr., *Reactor Chem. Div. Ann. Progr. Rept. Jan. 31, 1965*, ORNL-3789, pp. 76-79.

where

$$E_c^0 = E^0 - \frac{RT}{2F} \ln a_{\text{BeF}_2} \quad (4)$$

(E^0 being a function of temperature and E_c^0 being a function of both composition and temperature).

Improvements were made in the design of the electrodes which reduced potential fluctuations to ± 0.1 mv. Cell potentials were determined over a composition range of 0.30 to 0.90 mole fraction BeF_2 and a temperature range of 500 to 900°C. An attempt was made to measure the potential of pure BeF_2 , but results of useful accuracy could not be obtained because of high melt viscosity. The cell potentials, E_c^0 , for various compositions and temperatures were determined by passing a known mixture of HF-H_2 through the HF-H_2 electrode, measuring the cell voltage, E , and evaluating E_c^0 from Eq. (3). Plots of E_c^0 as a function of temperature at each composition studied as well as lines which have been least squared to the data at each composition are shown in Fig. 3.3.

The activity of BeF_2 may be calculated from Eq. (4) if the standard cell potential, E^0 , is known; however, the data obtained for various BeF_2 concentrations do not lend themselves to direct extrapolation to obtain E^0 . Instead the standard cell potential was calculated from Eq. (4), using values for a_{BeF_2} derived from the liquidus data⁶ and the heat of fusion of BeF_2 . While the values reported for the heat of fusion of BeF_2 vary widely,⁷ values below 2 kcal/mole are clearly indicated by the present data, and a value of 1.13 kcal/mole reported by Taylor and Gardner⁸ was actually used in the calculation of E^0 , giving

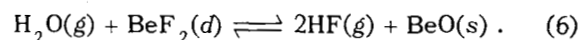
$$E^0 = 2.443 - 0.0007952T.$$

Next, a power series was assumed for $\log \gamma_{\text{BeF}_2}$ and the coefficients determined by a least-squares fit to the data using the above expression for E^0 . This gave

$$\begin{aligned} \log \gamma_{\text{BeF}_2} = & \left(3.8780 - \frac{2353.5}{T} \right) X_{\text{LiF}}^2 \\ & + \left(-40.7375 + \frac{36292.8}{T} \right) X_{\text{LiF}}^3 \\ & + \left(94.3997 - \frac{84870.9}{T} \right) X_{\text{LiF}}^4 \end{aligned}$$

$$+ \left(-67.4178 + \frac{52923.5}{T} \right) X_{\text{LiF}}^5 \quad (5)$$

Mathews and Baes⁹ measured the equilibrium quotient for the reaction



If Eq. (6) is combined with the reaction in Eq. (1) the resulting reaction is



The free energy and heat of this last reaction thus were obtained by combining the two sets of measurements, and, since the thermochemical data for H_2O is accurately known, improved free energy and heats of formation values for BeO could then be calculated. These are shown in Table 3.2. The free energy and heat were also derived for the reaction in Eq. (1) (assuming a heat of fusion for $\text{BeF}_2 = 1.13$ kcal/mole). These values combined with the thermochemical values for HF ⁶ were used to derive the free energy and heat of formation for liquid BeF_2 (Table 3.2). These calculations were all made for a temperature of 900°K. Values for the other temperatures were generated using the heat capacity data in JANAF.¹⁰

Smoothed values of γ_{BeF_2} are shown as a function of composition at several temperatures in Fig. 3.4. These new results are quite consistent with the previous estimates based on reaction (6)⁹ over the composition range 0.3 to 0.6 X_{BeF_2} . At $X_{\text{BeF}_2} > 0.6$ the older data appear to be less reliable, the newer results being more consistent with the phase data and a low heat of fusion for BeF_2 .

⁶R. E. Thoma *et al.*, submitted for publication in *Journal of Nuclear Materials*.

⁷A. L. Mathews and C. F. Baes, Jr., to be published in *Journal of Physical Chemistry* (February 1968).

⁸A. R. Taylor and T. E. Gardner, *Some Thermal Properties of Beryllium Fluoride from 8° to 1200°K*, U.S. Bur. of Mines, Rept. No. RI-6644 (1965).

⁹A. L. Mathews and C. F. Baes, Jr., *Oxide Chemistry and Thermodynamics of Molten Lithium Fluoride-Beryllium Fluoride by Equilibration with Gaseous Water-Hydrogen Fluoride Mixtures*, ORNL-TM-1129 (May 7, 1965), p. 83.

¹⁰JANAF Thermochemical Tables, Clearing House for Federal Scientific and Technical Information, U.S. Dept. of Commerce, August 1965.

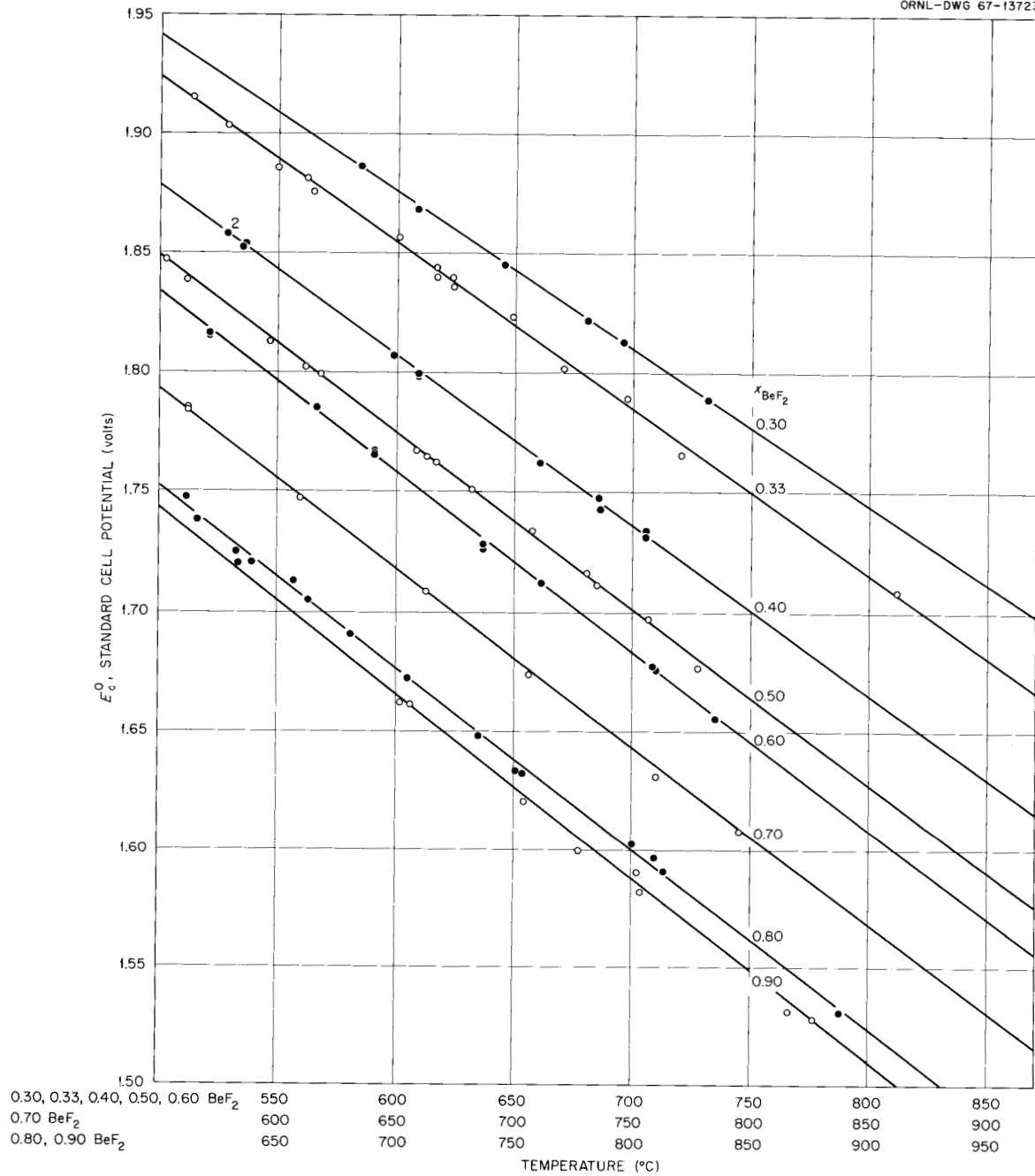
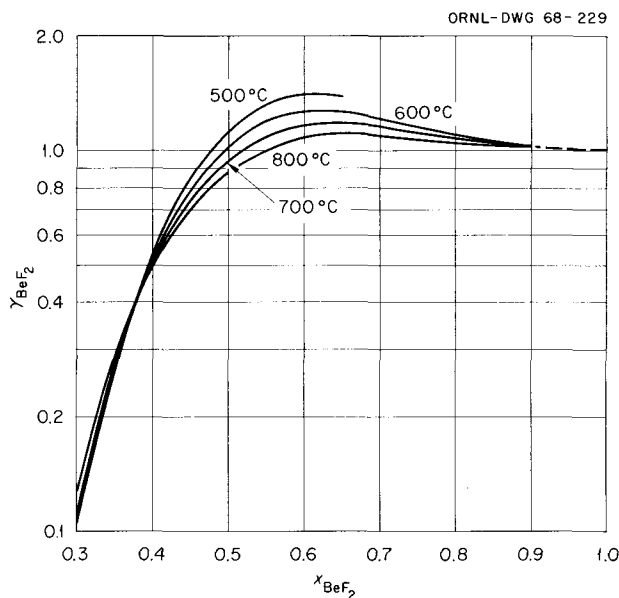


Fig. 3.3. Correlation of E_c^0 for Various BeF_2 Concentrations as a Function of Temperature.

Table 3.2. Formation Heats and Free Energies of BeF_2 and BeO

Compound	Temperature (°K)	State	ΔH_f (kcal/mole)	ΔG_f (kcal/mole)
BeF_2	298	Crystalline	-246.01 (-242.30) ⁶	-234.39 (-230.98) ⁶
	800	Crystalline	-244.75	-215.50
	900	Liquid	-243.12 (± 2.0)	-211.90 (± 1.1)
	1000	Liquid	-242.54	-205.09
BeO	298	Crystalline	-145.85 (-143.10) ⁶	-138.36 (-136.12) ⁶
	800	Crystalline	-145.68	-125.70
	900	Crystalline	-145.57 (± 1.0)	-123.20 (± 1.0)
	1000	Crystalline	-145.46	-120.73

Fig. 3.4. Activity Coefficients of BeF_2 in LiF-BeF_2 Mixtures.

In a closed apparatus of known volume, BF_3 pressures in equilibrium with the melt were measured manometrically in the composition range 5 to ~ 100 mole % NaBF_4 . For each composition, pressures were measured over at least a 150° temperature interval within overall limits of 425 to 1200°C . Vapor pressures vs composition for three temperatures are shown in Fig. 3.5.

For the pure NaBF_4 that was loaded into the apparatus (at room temperature), our observed BF_3 pressures were at least a factor of 3 higher than those previously reported.^{11,12} Previous measurements did not take into account the bivalence of the system — molten NaBF_4 and NaF plus gaseous BF_3 . In particular, when stoichiometric NaBF_4 partly dissociates into NaF and BF_3 , the number of moles of BF_3 in the vapor formed at equilibrium also equals the number of moles of NaF dissolved in the melt. In the previous work, it is most likely that a higher percentage of the NaBF_4 was dissociated than was the case in our measurements.

From the pressure data over the range of composition, the activity coefficients of NaBF_4 and NaF

VAPOR PRESSURES AND DERIVED THERMODYNAMIC INFORMATION FOR THE SYSTEM $\text{NaBF}_4\text{-NaF}$

Stanley Cantor C. E. Roberts
H. F. McDuffie

In this investigation we sought to determine: (a) the vapor pressures of the system in support of the development of fluoroborate melts as reactor coolants, and (b) the thermodynamic behavior of this system, primarily to establish how closely fluoroborate anions resemble halide ions in fused salt media.

¹¹L. J. Klinkenberg, doctoral dissertation, University of Leiden, Netherlands (1937).

¹²L. J. Klinkenberg, *Rec. Trav. Chim.* 56, 36 (1937).

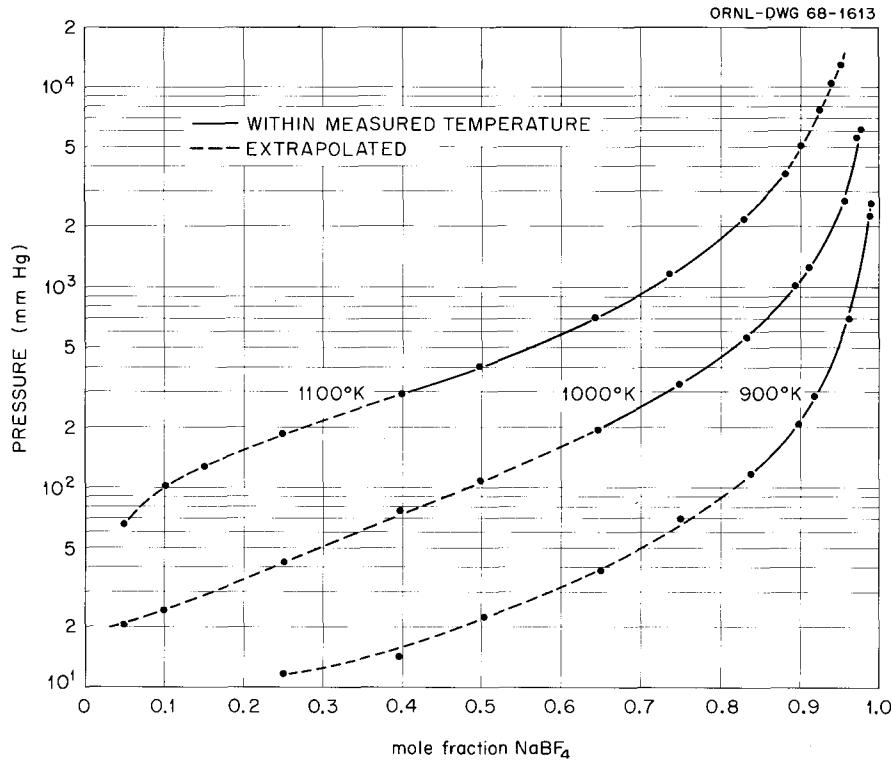


Fig. 3.5. Vapor Pressure of BF_3 vs Composition in the System NaBF_4 - NaF .

were evaluated from the expressions

$$\ln \gamma_1 X_1 = \int_{X_2 \rightarrow 0}^{X_2} X_2 d \ln P_{\text{BF}_3}, \quad (1)$$

$$\ln \gamma_2 X_2 = - \int_{X_2 \rightarrow 1}^{X_2} \frac{X_1}{X_2} d \ln \gamma_1 X_1, \quad (2)$$

where subscripts 1 and 2 refer to NaBF_4 and NaF respectively, X is mole fraction, γ is activity coefficient, and P_{BF_3} is the BF_3 vapor pressure.

Equation (1) was derived from the statement of the equilibrium



in terms of chemical potentials and the Gibbs-Duhem equation. Equation (2) is the Gibbs-Duhem equation itself. The integrals of (1) and (2) were evaluated graphically using Simpson's rule.

Activity coefficients have been calculated at 1000 and 1100°K. At these two temperatures, the components in the melt do not deviate greatly from

ideal solution behavior. The activity coefficients at 1000°K are given in Fig. 3.6.

By combining BF_3 pressures, activity coefficients, and mole fractions, the equilibrium constant K_p is obtained for the reaction



where

$$K_p = P_{\text{BF}_3} \frac{\gamma_2 X_2}{\gamma_1 X_1}. \quad (3)$$

At 1000°K, K_p equals 0.181₆ atm; at 1100°K, K_p is 0.709₂ atm.

From the two values of K_p , the enthalpy of the reaction, ΔH° , can be calculated from the expression

$$\Delta H^\circ = \frac{2.303RT_b T_a}{(T_b - T_a)} \log \frac{K_p(\text{at } T_b)}{K_p(\text{at } T_a)},$$

where the subscripts a and b refer to two different data points, that is, two different temperatures.

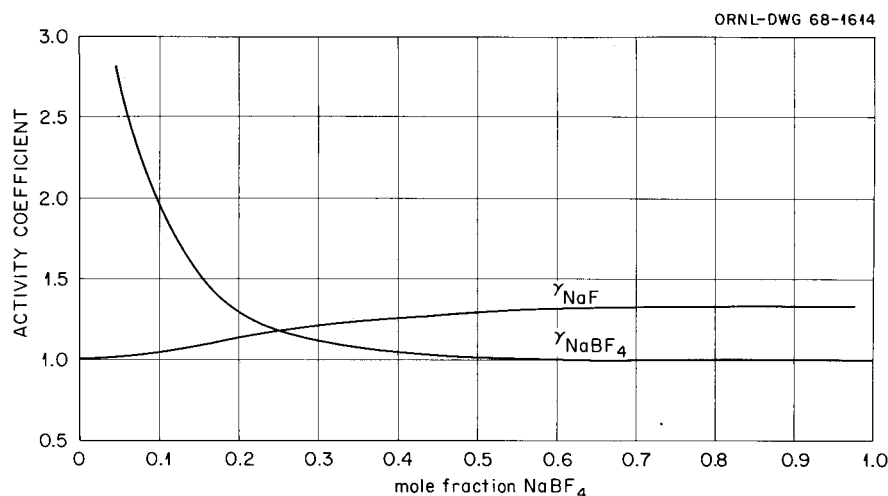


Fig. 3.6. Activity Coefficients of NaBF_4 and NaF at 1000°K .

Substituting the values obtained at 1000 and 1100°K yielded $\Delta H^\circ = 29.8$ kcal.

Much remains to be done in treating the experimental data collected for this system. In particular, we shall evaluate activity coefficients and other thermodynamic information at other temperatures and interpret the thermodynamic data in terms of structural models in pursuance of the second purpose of this investigation given at the beginning of this report.

VISCOSITY AND ITS TEMPERATURE DEPENDENCE IN MOLTEN BeF_2

C. T. Moynihan¹³ Stanley Cantor

Measurements of the viscosity of pure BeF_2 were reported previously.¹⁴ The interpretation of these results in terms of a recent theory of liquid transport is given in an article in press with the *Journal of Chemical Physics*. The following is the abstract of this article:

The viscosity of molten beryllium fluoride has been measured with coaxial cylinder viscometers over five orders of magnitude (limits: 979°C , 28.6 poises; 574°C , 2.24×10^6 poises). Over the experimental range of shear stresses BeF_2 behaves as a Newtonian fluid. Like SiO_2 , its high-tempera-

¹³Chemistry Department, California State College at Los Angeles.

¹⁴C. T. Moynihan and S. Cantor, *Reactor Chem. Div. Ann. Progr. Rept. Dec. 31, 1966*, ORNL-4076, pp. 25-26.

ture analog, BeF_2 shows an Arrhenius temperature dependence over several orders of magnitude in viscosity. Reported heat capacity data for BeF_2 and SiO_2 and the Adam-Gibbs theory indicate that the Arrhenius viscosity behavior of these liquids may be explained in terms of the configurational entropy, which is virtually constant at temperatures above the glass transition temperature.

ELECTRICAL CONDUCTIVITY OF MOLTEN SALTS

G. D. Robbins Jerry Braunstein

We have carefully examined the published methods for measuring electrical conductivity, especially in fused salt systems, have designed and constructed a conductance bridge for such measurements, and have made improved measurements of the conductivity of a molten LiF-BeF_2 mixture containing 34 mole % BeF_2 .

Discussion of Method

Investigators of aqueous media almost invariably use some form of the Wheatstone bridge arrangement shown in Fig. 3.7, with the balancing resistance, R_p , and capacitance, C_p , connected in parallel. This parallel arrangement is used despite the fact that in the most simple electrical representation of the cell the resistance of the solution, R_s , is in series with the double-layer capacitance, C_s

ORNL-DWG 68-1615

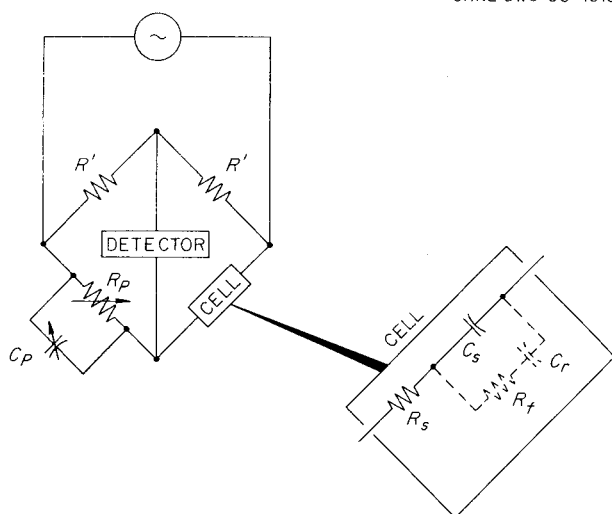


Fig. 3.7. Impedance Bridge and Equivalent Circuit of Conductance Cell.

(Fig. 3.7, inset, solid lines). The high degree of precision reported in aqueous investigations (up to $\pm 0.001\%$)¹⁵ is explained by analysis of the impedance balance conditions

$$R_s = \frac{R_p}{1 + R_p^2 C_p^2 (2\pi f)^2},$$

$$(2\pi f)^2 R_s R_p C_s C_p = 1,$$

where f is the measuring frequency. Thus, R_s is well represented by R_p in aqueous solutions, where C_p is of the order of 10^{-12} for the cell designs generally used.

In molten salts the values of capacitance are not such as to result always in $R_p^2 C_p^2 (2\pi f)^2$ being negligibly smaller than unity.¹⁶ For an electrode capacitance of 20 μf , Table 3.3 shows the minimum values of melt resistance which will result in the accuracy obtained in aqueous investigations, as a function of measuring frequency. Because of the high conductivity of molten salts and the problems of containment and temperature control, measured resistances are often less than 10 ohms. For the error in the resistance to be less than 1%, the fre-

Table 3.3. Minimum R_s vs f for Validity of Approximation $R_p = R_s$ to 0.001%

f (hertz)	R_s (ohms)
500	5040
1,000	2520
2,000	1260
4,000	630
8,000	315
10,000	252
12,000	210
16,000	157
20,000	126
30,000	84

quency must be greater than 7900 hertz. Resistances below 1 ohm have been reported, at frequencies below 4000 hertz.¹⁷ This can lead to spurious frequency dispersion beyond that due to the polarization resistance, and can cause errors in the extrapolation to infinite frequency.

When charge is transferred across the solution-electrode interface (a reaction), the simple model shown in Fig. 3.7 does not hold, and the model should include the Faradaic impedance, R_f , and reaction capacitance, C_r , also shown in Fig. 3.7. With increasing frequency, the impedance approaches that of the simple model (R_s in series with C_s). From an argument based on Fick's law of diffusion, it has been proposed¹⁸⁻²¹ that the added resistance due to polarization varies approximately as $f^{-1/2}$. This functional form often is used to extrapolate to infinite frequency, although some systems have been observed to exhibit an entirely different frequency dispersion.²² In pure molten salts it is difficult to envision the diffusion-limited condition, since the bulk medium

¹⁷N. D. Greene, ORNL-CF-54-8-64.

¹⁸E. Warburg, *Wied. Ann. Physik* **67**, 493 (1899).

¹⁹E. Warburg, *Drude Ann. Physik* **6**, 125 (1901).

²⁰E. Neumann, *Wied. Ann. Physik* **67**, 500 (1899).

²¹E. Jones, and S. M. Christian, *J. Am. Chem. Soc.* **57**, 272 (1935).

²²O. V. Brody and R. M. Fuoss, *J. Phys. Chem.* **60**, 177 (1956).

¹⁵G. Jones and R. C. Josephs, *J. Am. Chem. Soc.* **50**, 1049 (1928).

¹⁶C. H. Liu, K. E. Johnson, and H. A. Laitinen, p. 715 in *Molten Salt Chemistry*, ed. by M. Blander, Interscience, New York, 1964.

is charge carrying. Yet we observe frequency dispersion, which has also been reported at polarizing potentials much lower than required for Faradaic processes.²³

A conductance bridge having the balancing resistance in series with the variable capacitance has been constructed in order to reduce errors due to low resistivity of the salts. Frequency dispersion studies in molten salts are under way to elucidate problems of this type in molten mixtures.

Electrical Conductivity of Molten LiF-BeF₂ (66-34 Mole %)

The electrical conductivity of LiF-BeF₂ (66-34 mole %) has been measured at 470 to 500°C, employing the series RC conductance bridge described above. A specially designed silica cell (Fig. 3.8) resulted in a cell constant of 129 cm⁻¹, as determined in molten potassium nitrate. The cell consisted of two silica tubes (3 mm inside diameter) attached to a silica rod. This assembly, with platinum wire electrodes (~1 mm diameter) inserted in the tubes, passed through a Teflon cap and dipped in the molten salt so that the total conducting path through the tubes was about 11 cm. The electrodes were platinized before use to reduce the polarization resistance. The salt in the cell was melted and maintained under a helium blanket. Analysis of the salt after completion of the measurements indicated an oxide content of 0.09%, which should not have affected the measured conductivity. Measurements were made at 600 to 4000 hertz and extrapolated to infinite frequency. The results, shown in Table 3.4, confirm an earlier preliminary estimate of the magnitude of the conductivity, but they indicate a higher temperature coefficient than estimated.²⁴

Using the density data of Cantor,²⁵ the calculated equivalent conductance,

$$\Lambda = \frac{\text{equiv. wt.}}{\text{density}} \kappa,$$

²³G. J. Hills and K. E. Johnson, *J. Electrochem. Soc.* **108**, 1013 (1961).

²⁴J. Braunstein and K. A. Romberger, *MSR Program Semiann. Progr. Rept. Aug. 31, 1967*, ORNL-4191, p. 141.

²⁵S. Cantor, personal communication.

leads to an apparent enthalpy of activation

$$-R \frac{d \ln \Lambda}{d(1/T)} = 4.7 \text{ kcal/mole.}$$

Table 3.4. Specific Conductance of 2LiF-BeF₂

T (°C)	κ (ohms ⁻¹ cm ⁻¹)
470	1.36
485	1.47
500	1.54

ORNL-DWG 68-1616

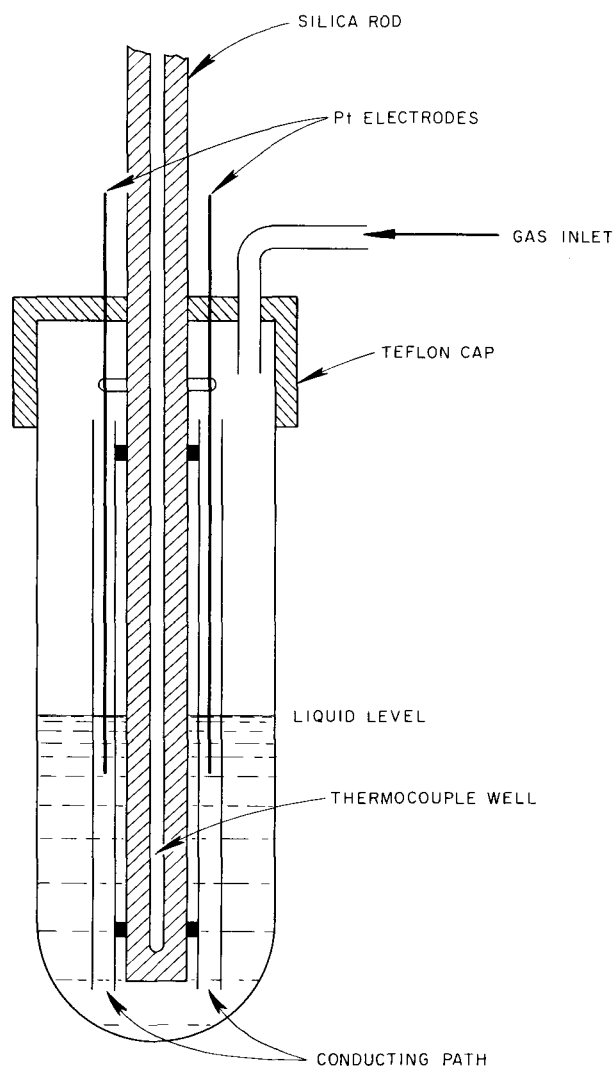
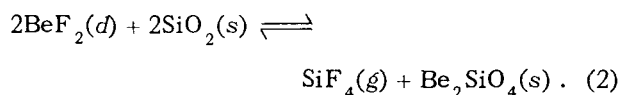
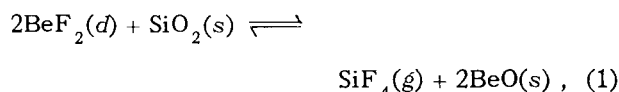


Fig. 3.8. Conductance Cell for Molten Salts.

CHEMISTRY OF SiO₂ IN MOLTEN FLUORIDES

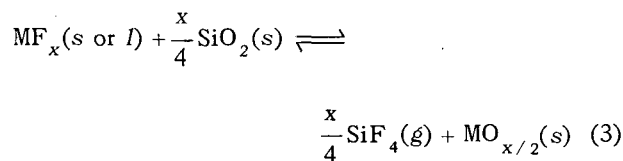
C. E. Bamberger R. B. Allen²⁶
C. F. Baes, Jr.

The advantages of silica as a container material for molten salts in spectrophotometric, emf, and other measurements are many. For the containment of molten LiF-BeF₂ mixtures, an obvious disadvantage is the possible chemical attack as a result of the reactions

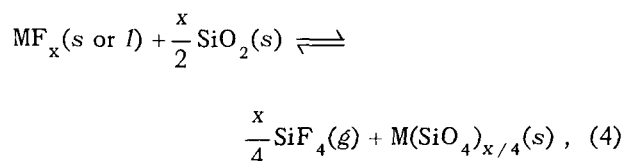


However, when the equilibrium partial pressure of SiF₄ was calculated from available free energies of formation, the values were slightly more positive for reaction (2) but were surprisingly low for both reactions. This suggested that an overpressure of SiF₄ might prevent or at least reduce the attack on the silica container and prevent the precipitation of BeO or the formation of Be₂SiO₄.

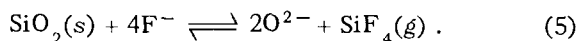
The compatibility of SiO₂ with these LiF-BeF₂ melts is primarily associated with the relative stability of BeF₂ compared with that of BeO. Since many other metallic fluorides show even greater stability compared with their corresponding oxides, it seems that SiO₂ should not be ruled out as a container material for molten fluorides without first estimating the equilibrium position of such reactions as



or



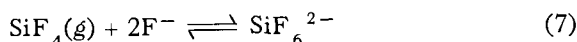
which involve the pure metal fluoride and the metal oxide or silicate, and



The last reaction is of special interest since it gives the level of oxide contamination of the fluoride melt. Its equilibrium position may be judged if activity coefficients or solubilities can be assigned to MF_x and MO_{x/2} in the melt under consideration. In the present case the activity of BeF₂ in 2LiF-BeF₂ (~0.03) and the solubility of BeO (~0.01 mole of O²⁻ per kilogram of salt at 600°C) have been measured.²⁷ From these and the available thermochemical data the following equilibrium quotient may be estimated for the above reaction [Eq. (5)] in 2LiF-BeF₂ at 600°C:

$$Q = [\text{O}^{2-}]^2 P_{\text{SiF}_4} = 4 \times 10^{-7} \text{ atm mole}^2 \text{ kg}^{-2}. \quad (6)$$

The solubility of SiF₄ in the molten fluoride must be considered because possible reactions such as



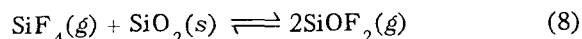
could cause the solubility to be appreciable. This would not only alter the salt phase but also cause the reaction with SiO₂ to proceed further than otherwise expected. Accordingly, the solubility of SiF₄ in 2LiF-BeF₂ was estimated by means of transpiration measurements. The results, expressed as Henry's law constants, were

$$K_H = 0.032 \pm 0.005 \text{ mole kg}^{-1} \text{ atm}^{-1} \text{ at } 499^\circ\text{C},$$

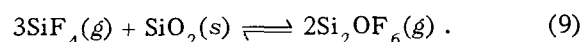
$$K_H = 0.035 \pm 0.005 \text{ mole kg}^{-1} \text{ atm}^{-1} \text{ at } 540^\circ\text{C}.$$

These solubilities are of the same order of magnitude as the solubility of HF in 2LiF-BeF₂ (<0.01 mole kg⁻¹ atm⁻¹).²⁸

Another possible reaction that should be considered in these systems is the formation of silicon oxyfluorides, for example,



and



²⁶Temporary summer employee, 1967.

²⁷C. F. Baes, Jr., "The Chemistry and Thermodynamics of Molten Salt Reactor Fluoride Solutions," p. 409 in *Thermodynamics*, vol. 1, IAEA, Vienna, 1966.

²⁸P. E. Field and J. H. Shaffer, *J. Phys. Chem.* 71, 3218 (1967).

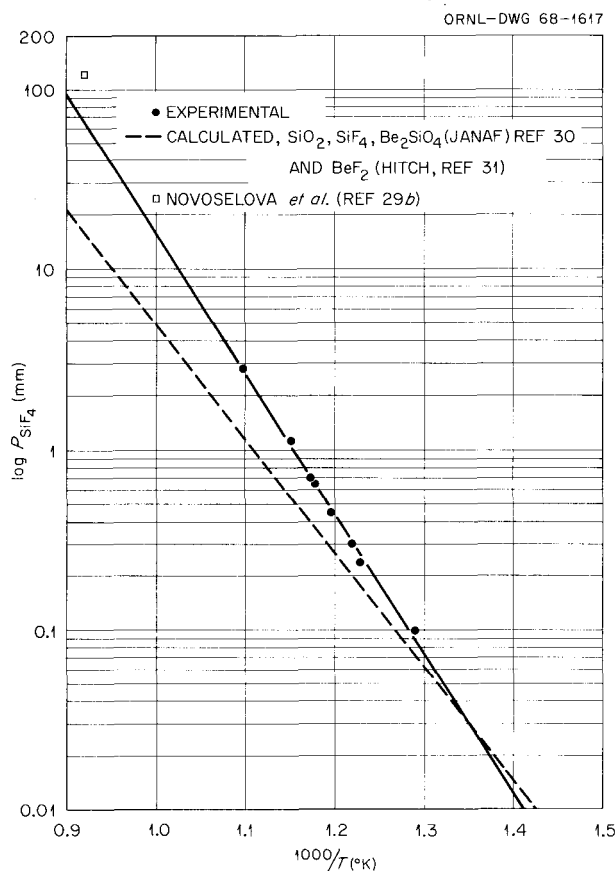


Fig. 3.9. Arrhenius Plot for SiF_4 Pressures in the Reaction $2\text{BeF}_2(\ell) + 2\text{SiO}_2(\text{s}) \rightleftharpoons \text{Be}_2\text{SiO}_4(\text{s}) + \text{SiF}_4(\text{g})$.

These silicon oxyfluorides have been reported by Novoselova *et al.*²⁹ during the synthesis of phenacite from SiO_2 , BeO , and Na_2BeF_4 . They observed^{29a} SiOF_2 pressures of 54 mm in the presence of 123 mm of SiF_4 at 813°C (see Fig. 3.9). We performed tests using a system in which helium was sparged through molten $2\text{LiF}\cdot\text{BeF}_2$ containing powdered BeO and SiO_2 at temperatures up to 650°C . The gas samples were analyzed by means of a mass spectrometer, but no silicon oxyfluorides were detected (limit <0.05 mole %).

In the temperature range of interest (500 to 700°C), phenacite (reaction 2) should be stable with respect to $\text{BeO} + \text{SiO}_2$, but the available thermodynamic data for phenacite are only estimates.³⁰ Therefore, we measured the equilibrium pressure of SiF_4 in a system containing molten $2\text{LiF}\cdot\text{BeF}_2$, phenacite, and silica (as α -cristobalite). The experiment was carried out in a nickel container through which SiF_4 in helium carrier gas was bubbled by means of a recirculating pump. The gas

circulation was continued until constant values of P_{SiF_4} were obtained as indicated by measuring the infrared spectra of the gases. The following expression reproduced the data within their estimated error ($\pm 10\%$):

$$\log P_{\text{SiF}_4} (\text{mm}) = 8.745 - 7576/T. \quad (10)$$

The observed partial pressures are in general slightly higher than may be predicted from available thermodynamic data (see Fig. 3.9). The equilibrium constant of reaction (2) can be expressed as

$$K = P_{\text{SiF}_4} / a_{\text{BeF}_2}^2. \quad (11)$$

Defining a_{BeF_2} as unity in $2\text{LiF}\cdot\text{BeF}_2$,

$$\Delta G_{R(2)} = -RT \ln P_{\text{SiF}_4}, \quad (12)$$

and

$$\Delta G_{\text{Be}_2\text{SiO}_4} = -RT \ln P_{\text{SiF}_4} + 2\Delta \bar{G}_{\text{BeF}_2} + 2\Delta G_{\text{SiO}_2} - \Delta G_{\text{SiF}_4}, \quad (13)$$

where

$$\Delta \bar{G}_{\text{BeF}_2} = -243.5 + 29.8T/1000 \text{ (ref. 31)}, \quad (14)$$

$$\Delta G_{\text{SiO}_2} = -216.5 + 42.2T/1000 \text{ (ref. 30)}, \quad (15)$$

$$\Delta G_{\text{SiF}_4} = -386.3 + 34.7T/1000 \text{ (ref. 30)}. \quad (16)$$

Using Eqs. (12–15), the free energy of formation of Be_2SiO_4 was calculated, giving

$$\Delta G_{\text{Be}_2\text{SiO}_4} = -499.1 + 82.4T/1000. \quad (17)$$

Resulting values (Table 3.5) compare favorably with estimated values given in the JANAF

²⁹(a) A. V. Novoselova *et al.*, *Acad. Sci. USSR Proc. Chem., English Trans.* 159(6), 1370 (1964); (b) A. V. Novoselova and Yu. V. Ashikina, *Inorg. Materials USSR, English Trans.* 2(9), 1375 (1966).

³⁰JANAF Thermochemical Tables, Clearing House for Federal Scientific and Technical Information, U.S. Dept. of Commerce, Aug. 1965. The quartz data was corrected for cristobalite using the differences of enthalpy and of entropy reported by Rossini *et al.* (NBS, Circ. 500, 1952) for the fusion of crystalline quartz and crystalline cristobalite.

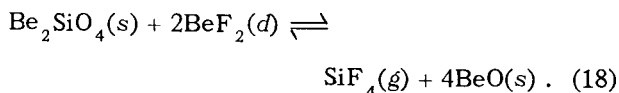
³¹B. F. Hitch, this report, p. 52.

Table 3.5. Free Energy of Formation of Be_2SiO_4

Temperature (°C)	$\Delta G_{\text{Be}_2\text{SiO}_4}$ (kcal/mole)	
	This Study	JANAF Value ^a
700	-441.4	-441.7
800	-433.1	-432.6
900	-424.9	-423.6
1000	-416.6	-414.7

^aJANAF Thermochemical Tables, Clearing House for Federal Scientific and Technical Information, U.S. Dept. of Commerce, Aug. 1965. The quartz data was corrected for cristobalite using the differences of enthalpy and of entropy reported by Rossini *et al.* (NBS, Circ. 500, 1952) for the fusion of crystalline quartz and crystalline cristobalite.

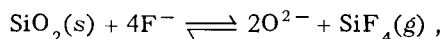
Tables.³⁰ Similar measurements of SiF_4 partial pressures generated by Be_2SiO_4 plus BeO in $2\text{LiF}\cdot\text{BeF}_2$ are presently in progress:



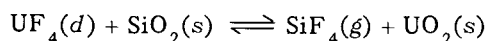
SPECTROPHOTOMETRIC MEASUREMENTS OF MOLTEN FLUORIDES IN SILICA

C. E. Bamberger J. P. Young³²
C. F. Baes, Jr.

To estimate the extent to which an SiF_4 overpressure would prevent the reaction



UF_4 was added to $\text{LiF}\text{-BeF}_2$ melts in SiO_2 containers as a colored solute which would produce an even less soluble oxide than does BeF_2 . Tetravalent uranium thus should act as a sensitive "internal indicator" of the reaction of F^- with SiO_2 . It has a known absorption spectrum of suitable intensity,³³ and hence its concentration can be followed spectrophotometrically. Although for the reaction



higher equilibrium partial pressures of SiF_4 were

predicted than for reactions of SiO_2 with dissolved BeF_2 , these pressures were still reasonably low; for example, with 0.002 mole fraction UF_4 in $2\text{LiF}\text{-BeF}_2$, calculated SiF_4 pressures varied from 3 mm at 700°K to 115 mm at 1000°K. Thus spectrophotometric monitoring of the concentration of U(IV) provides a very good means for studying the stability of the system: molten fluoride, silica, silicon tetrafluoride.

Melts of $2\text{LiF}\text{-BeF}_2$ containing variable concentrations of UF_4 (0.0053–0.13 mole % or 0.003–0.008 mole/liter) were held under SiF_4 (~400 mm) at temperatures ranging from 490 to 700°C in sealed silica tubes. The tubes were placed in a special furnace³⁴ located in the light path of a Cary spectrophotometer model 14M, or in a heated nickel metal block and later transferred to the furnace inside the instrument. Temperatures were controlled to $\pm 1^\circ\text{C}$.

Based on the constancy of absorbance of the U(IV) absorbance peaks at 1090 and 640 nm, the uranium concentration in the melt remained constant within the precision of the spectral measurement (ca. 1%) during at least 48 hr, thus indicating no significant attack on, or contamination by, the silica container. During longer periods of time (up to one week) the transparency of the containers was noticeably affected, and the base lines of the spectrum rose. The net absorbance of the U(IV) peaks remained reproducible even though in some experiments the temperature was cycled from 500 to 700°C in order to study the effect of temperature on the absorbance of U(IV). No spectral experiments were continued for longer than a week, but in other studies melts of $2\text{LiF}\text{-BeF}_2$ were maintained as long as one month at 500°C without noticeable damage except loss of transparency of the cell.

The precision of these spectral measurements of U(IV) was better than that possible with windowless cells.³⁵ The molar absorptivity (A_m) of U(IV) previously had been observed³³ to be $14 \pm 10\%$ and $7 \pm 10\%$ at 1090 and 640 nm, respectively, in molten $\text{LiF}\text{-BeF}_2$ at 550°C in windowless cells. With the present silica cells the A_m of U(IV) was observed to be 14.4 ± 0.5 and 7.3 ± 0.3 at 1090 and 650 nm, respectively, in molten $2\text{LiF}\text{-BeF}_2$.

The effect of temperature on the A_m of several absorption peaks of U(IV) in $2\text{LiF}\text{-BeF}_2$ was studied. The results are summarized in Table 3.6.

³²Analytical Chemistry Division.

³³J. P. Young, *Inorg. Chem.* **6**, 1486 (1967).

³⁴J. P. Young, *Anal. Chem.* **31**, 1892 (1959).

³⁵J. P. Young, *Anal. Chem.* **36**, 390 (1964).

Table 3.6. Effect of Temperature on the Molar Absorptivity of Several Peaks of U(IV) in Molten 2LiF-BeF₂

Temperature (°C)	Molar Absorptivity at —	
	1090 nm	640 nm
498	16.4	8.0
560	14.4	7.3
650	13.8	6.2
698	12.9	5.7

The solubility of CrF₃ in LiF-BeF₂ was investigated spectrophotometrically with the melts contained in SiO₂ cells. The solubility was found to exceed 0.43 mole %; at this concentration the solutions were too opaque for absorbancy measurements in a cell of 1 cm path length. The spectrum of Cr(III) in LiF-BeF₂ at 500°C consists of 3 peaks at 302, 442, and 690 nm, all arising from transitions within the 3d level. The molar absorptivity of the 690 nm peak was calculated to be 6.6. This value compares favorably with an approximate value of 7 reported from a cursory study of the system in windowless cells.³⁶ The molar absorptivity of the two other peaks is somewhat higher, ca. 10, but further work will be necessary to establish a more precise value.

EVALUATION OF SPECTROPHOTOMETRIC CONTAINERS FOR MOLTEN FLUORIDES

L. M. Toth G. P. Smith³⁷

The unavailability of a convenient and economical optical system for containing molten fluorides has been a serious obstacle to quantitative fluoride absorption spectroscopy. The potential which such quantitative spectroscopy offers, however, has encouraged another examination of the problem.

A material which is reasonably transparent from 2600 to 200 μm and resistant to the attack of the molten fluorides is desired. The material should be inexpensive and easy to handle, so that the resulting cost per sample is not prohibitive. A

³⁶MSR Program Semiann. Progr. Rept. Aug. 31, 1966, ORNL-4037, p. 194.

³⁷Metals and Ceramics Division.

survey³⁸ has been made of all available materials and techniques. It has been concluded that fused silica should be used as much as possible because of the convenience which it offers. However, it is recognized that few fluorides can be contained in silica for short periods at temperatures of 500°C and above.

Chemical inhibition of the silica corrosion process had been previously suggested³⁹ and tested for direct application to the absorption spectroscopy problem. The technique is intended to decrease the equilibrium concentration of oxides such as BeO by the addition of excess SiF₄,



and hence reduce SiO₂ corrosion.

The procedure has been tested by comparing melts of LiF-BeF₂ (66-34 mole %) in fused silica tubes exposed to SiF₄ with similar samples exposed to dry helium. Pressures of SiF₄ from 0 to 300 mm Hg in LiF-BeF₂ (66-34 mole %) have been introduced in the silica tubes and their optical properties observed at temperatures from 500 to 700°C.

The reference cells containing helium atmospheres remained optically transparent for longer periods of time than cells with various pressures of SiF₄. Cells which contain SiF₄ atmospheres over molten LiF-BeF₂ (66-34 mole %) do, in fact, remain optically transparent for periods of 10 to 20 hr at 500°C, but cells which contain helium atmospheres over the same melts and temperatures demonstrate optical transparencies for 20 to 60 hr duration. As a result of these tests, it was concluded that at the present development stage of the chemical inhibition process, commercial SiF₄ does not extend the usefulness of silica for absorption spectroscopy at truly high precision and accuracy.

As an alternative, coated silica has been investigated with the hope of screening the reactive silica from the melt by an unreactive coating substance. The inner surfaces of silica cells have been covered with thin, semitransparent layers of vapor-deposited platinum. Such a container has been found to remain optically clear in the coated region and yet was severely etched in the uncoated region when subjected to approximately 1 wt % NiF₂ in

³⁸L. M. Toth, *Containers for Molten Fluoride Spectroscopy*, ORNL-TM-2047 (November 1967).

³⁹C. E. Bamberger, J. P. Young, and C. F. Baes, Jr., *MSR Semiann. Progr. Rept. Aug. 31, 1967*, ORNL-4191.

LiF-BeF₂ (66-34 mole %). These coatings are typically permeated with microscopic voids and therefore do not totally eliminate corrosion. However, an extension of the silica lifetime is feasible by limiting the contact of the fluoride melt and silica.

Further development of the coating technique is in progress to determine what practical application it may yield to spectroscopy.

SPECTROSCOPIC INVESTIGATION OF NIOBIUM FLUORIDES IN MOLTEN SALTS

L. M. Toth G. P. Smith³⁷

The chemistry of NbF₅ and the lower fluorides of niobium is currently under examination. NbF₅ has been purified from existing supplies by sublimation in quartz vessels. The x-ray powder pattern of the resulting material agrees with the previously reported pattern,⁴⁰ and examination of the material under a polarizing-light microscope confirms the purity.⁴¹ The material gives no visible absorption spectrum and only a charge-transfer band in the ultraviolet below 260 mμ. NbF₅ is also being synthesized by direct combination of the elements in a Monel reaction vessel.

NbF₄ has been synthesized by the reduction of NbF₅ with niobium in quartz containers at 250°C. The black crystalline material which has been isolated gives an x-ray powder pattern which is identical to the previously reported pattern.⁴²

NbF₅, which melts at 80°C, can be used as a low-temperature solvent for lower-valent niobium fluorides. It can be contained in quartz cells at temperatures up to 250°C with no evidence of silica corrosion. A small amount of the solvent can be reduced by adding less than 0.1 wt % niobium metal, and the reaction can be monitored by spectroscopy. The metal is completely consumed, and the resulting solution is intensely colored due to a strong absorption at 320 mμ and a weak absorption at 1100 mμ. A solid phase which later appears is accompanied by a decrease in the intensity of these two peaks and the appearance of two new peaks at 410

and 580 mμ. None of these spectra has yet been characterized.

NbF₄ has also been dissolved in NbF₅ at 250°C and indicates similar anomalies. Complete dissolution of the NbF₄ is followed by precipitation of a black crystalline material. An x-ray powder pattern of the precipitate indicates it is neither NbF₅, NbF₄, Nb⁰, nor any reported oxyfluoride.

The reduction of NbF₅ can be qualitatively described as proceeding well in solution at 250°C with the formation of insoluble products. NbF₄, which dissolves easily in NbF₅, forms a similar insoluble product, which has not yet been identified. NbF₄ has been found to be more difficult to dissolve in LiF-BeF₂ (66-34 mole %).

Further work will endeavor to explain these reactions, as well as similar reductions of NbF₅ with Nb in molten LiF-BeF₂ and related solvents.

CRYSTAL STRUCTURES OF COMPLEX FLUORIDES

G. D. Brunton D. R. Sears

The crystal structures which follow were determined from partial x-ray data; a computer-operated automatic diffractometer, which will become operable very soon, will markedly facilitate data collection. At that time the structures of NaKThF₆, KCeF₄, and β₁-K₂UF₆, as well as NaBF₄, will be refined. The structures of KBF₄, Na₃CrF₆, LiTh₂F₉, CsU₆F₂₅, and Cs₂UF₆ will be the first to be investigated with the new instrument.

The crystal structure of a compound whose stoichiometry is either Na₃Li₃Th₆F₃₀ or (Na, Li)₇Th₆F₃₁ is in the final stages of refinement from available x-ray and neutron diffraction data.

KCeF₄

The low-temperature form of KCeF₄ crystallizes in space group *Pnma* with $a_0 = 6.28$ Å, $b_0 = 3.798$ Å, and $c_0 = 15.48$ Å. The x-ray density is 4.592 g/cm³ and $Z = 4$. The simple framework structure (Fig. 3.10) is a three-dimensional array of 9-coordinated cerium and potassium polyhedra, which share faces and edges in all directions. The Ce³⁺-F⁻ bond distances range from 2.33 to 2.52 Å and the K⁺-F⁻ bonds from 2.59 to 3.32 Å. The positional parameters are listed in Table 3.7.

⁴⁰A. N. Edwards, *J. Chem. Soc.* 1964, 3714 (1964).

⁴¹Microscope measurements by C. F. Weaver, Reactor Chemistry Division.

⁴²F. P. Gortsema and R. Didchenko, *Inorg. Chem.* 4, 182 (1965).

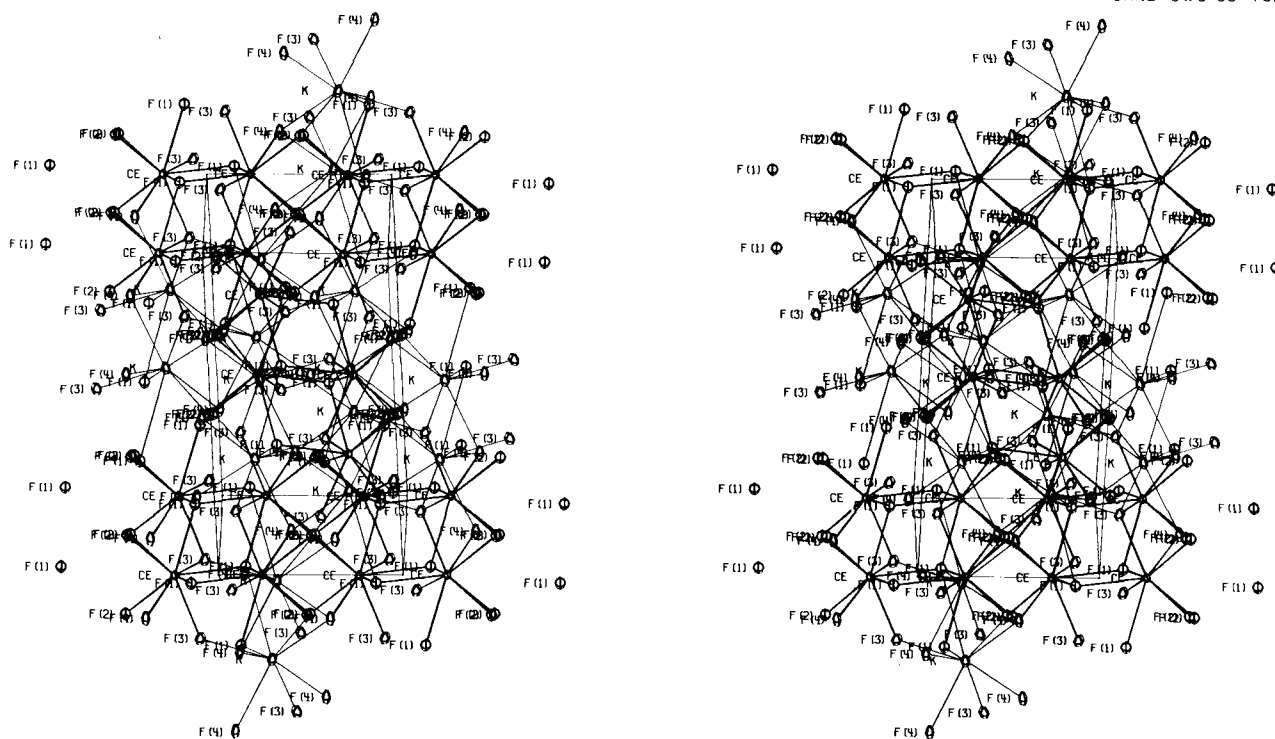
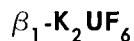


Fig. 3.10. A Stereoscopic Drawing of KCeF_4 . One unit cell is outlined.

Table 3.7. Atomic Parameters for KCeF_4

Atom	x	y	z	β_{11}	β_{22}	β_{33}	β_{13}
Ce	0.251	0.25	0.438	0.0031	0.0145	0.0008	-0.0001
K	0.281	0.75	0.202	0.0047	0.0334	0.0010	-0.0006
F(1)	0.139	0.25	0.036	0.0090	0.0402	-0.0001	0.00001
F(2)	-0.004	0.75	0.440	0.0089	0.0254	-0.0001	0.0014
F(3)	0.399	0.75	0.364	0.0057	0.0290	0.0010	0.0006

This structure differs from previously reported alkali-metal-rare-earth 1:1 fluorides^{43,44} in that there are no mixed cation sites and no partially occupied sites.



This compound was first described by Zachariasen.^{45,46} It crystallizes in space group $P\bar{6}2m$ with $a_0 = 6.54$ Å and $c_0 = 3.76$ Å. The x-ray density is 5.10 and $Z = 1$. The structure consists of

chains of face-sharing $\text{U}^{4+}\text{-F}^-$ polyhedra, with each U^{4+} ion coordinated by nine F^- ions. These chains are parallel to c_0 in the crystal. The chains

⁴³J. H. Burns, *Inorg. Chem.* 4, 881 (1965).

⁴⁴D. R. Sears, *Reactor Chem. Div. Ann. Progr. Rept. Dec. 31, 1966*, ORNL-4076, p. 11.

⁴⁵W. H. Zachariasen, *J. Am. Chem. Soc.* 70, 2147 (1948).

⁴⁶W. H. Zachariasen, *Acta Cryst.* 1, 265 (1948).

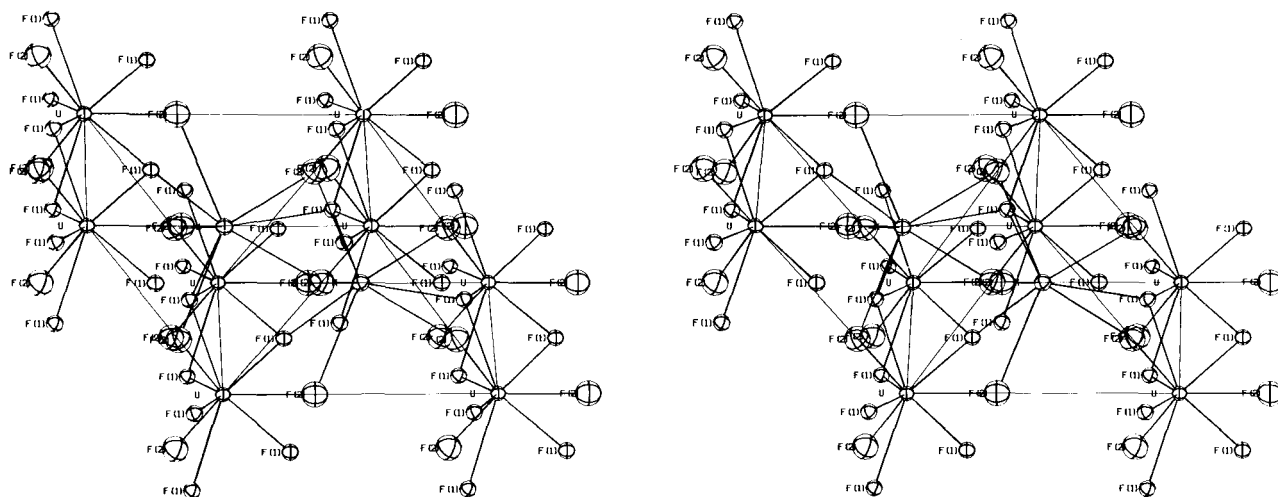


Fig. 3.11. A Stereoscopic View of β_1 - K_2UF_6 . One unit cell is outlined.

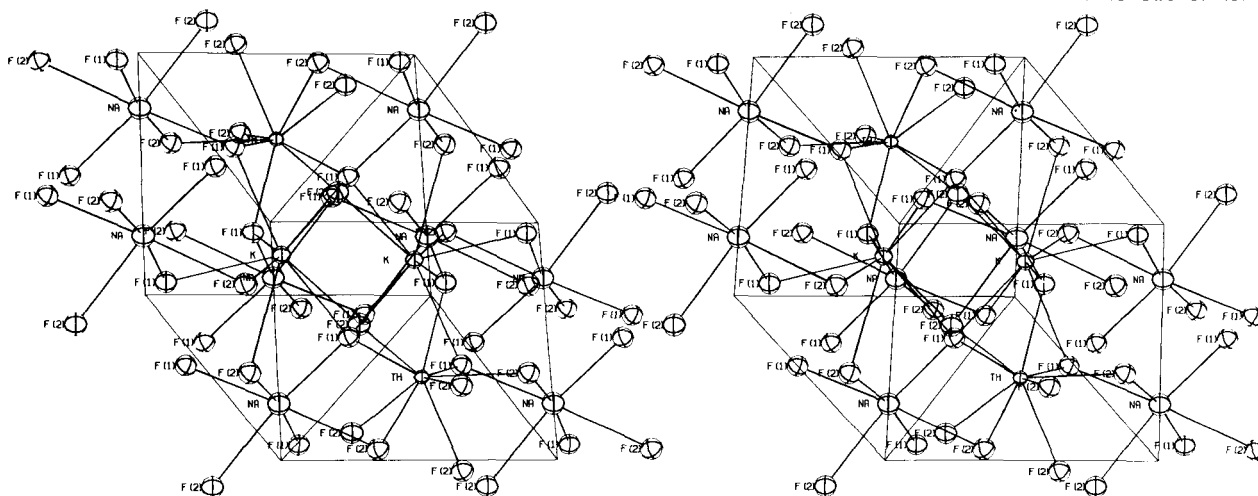


Fig. 3.12. A Stereoscopic View of $NaKThF_6$. One unit cell is outlined.

are cross linked by the K^+ ions at the centers of 9-coordinated F^- polyhedra (Fig. 3.11). The atomic parameters are listed in Table 3.8. The $U^{4+}-F^-$ distances range from 2.17 to 2.41 Å, and the K^+-F^- distances range from 2.57 to 2.88 Å.

$NaKThF_6$

$NaKThF_6$ crystallizes in space group $P\bar{3}$ with $a_0 = 6.303$ Å and $c_0 = 7.831$ Å. The calculated

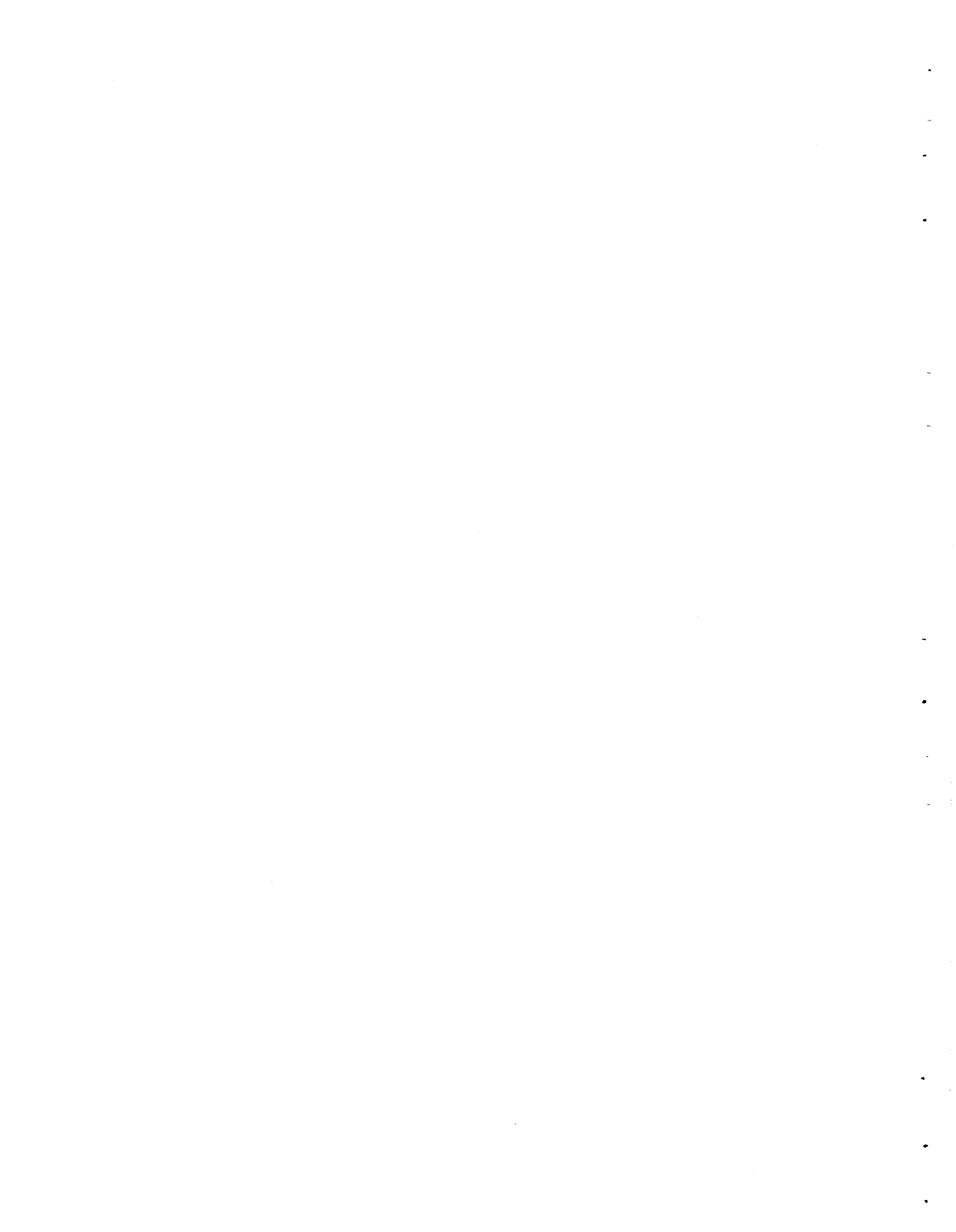
density is 5.02 g/cm³ and $Z = 2$. The structure is a framework of edge-sharing polyhedra of F^- ions coordinated around the cations (Fig. 3.12). The Na^+ ion is coordinated by six F^- ions at the corners of an irregular octahedron. The K^+ and Th^{4+} ions are coordinated each by nine F^- ions. The positional parameters are listed in Table 3.9. The $Th^{4+}-F^-$ distances range from 2.23 to 2.44 Å, the Na^+-F^- distances range from 2.29 to 2.53 Å, and the K^+-F^- distances range from 2.69 to 2.85 Å.

Table 3.8. Atomic Parameters for β_1 -K₂UF₆

Atom	x	y	z	B
U	0	0	0	1.015
K	0.333	0.667	0.50	1.342
F(1)	0.233	0	0.50	1.234
F(2)	0.332	0	0	3.114

Table 3.9. Atomic Parameters for NaKThF₆

Atom	x	y	z	B
Th	0.333	0.677	0.122	0.902
K	0.333	0.677	0.606	1.355
Na	0	0	0.237	2.168
F(1)	0.110	0.390	0.320	1.945
F(2)	0.395	0.316	0.097	2.107



Part II

Aqueous Reactors and Desalination



4. Corrosion and Chemical Behavior in Reactor and Desalination Environments

HERMETICALLY SEALED PRESSURIZED- AND BOILING-WATER REACTORS

G. H. Jenks J. C. Griess

Members of the Reactor Division have recently proposed several reactor systems, including both pressurized- and boiling-water types, aimed at accomplishing reduction in size, cost, and complexity of small nuclear power plants.¹ These reactors, collectively called Terrestrial Low-Power Reactors (TLPR), would be small, hermetically sealed units capable of unattended operation for extended periods. The elimination of water purification systems and the development of methods for handling the radiolytic gases generated in boiling-water reactors would greatly simplify such plants and increase the probability of unattended operation. We briefly reviewed the water chemistry of both pressurized- and boiling-water reactors, particularly as it relates to the necessity of purification systems, and considered means whereby small reactors could operate satisfactorily without water cleanup or special gas handling equipment. This work has been reported and is summarized below.¹

Although conventional aqueous reactors utilizing primarily stainless steel and Inconel as materials of construction have performed well, all such reactors rely on purification systems to prevent the buildup of corrosion products in the water which could cause fuel element fouling. From the standpoint of corrosion and accumulation of corrosion products in the water, titanium appears to be a better choice as a structural material than either

stainless steel or Inconel. Although only limited data are available on corrosion and corrosion product release rates for titanium in high-temperature water, those which are available appear favorable; corrosion rates of a few hundredths of a mil per year have been reported, with most, if not all, of the corrosion products adhering to the base metal. Furthermore, there are no indications that hydrogen embrittlement will be a problem. However, it should be emphasized that a rather extensive experimental program would be necessary to establish titanium as a structural material for aqueous reactors.

Radiolytic gases pose no problem in pressurized-water reactors if the water is sufficiently pure; addition of hydrogen reduces the concentration of oxygen in the water to an insignificant level. In boiling-water reactors, however, the radiolytic gases are swept out of the reactor and collect in the condenser. The proposed method of recombining the hydrogen and oxygen in the boiling system described by Fraas² involves returning the radiolytic gases along with excess hydrogen to the high-pressure system. This particular reactor concept is well suited to this method since only about 2 and 0.5% of the fast-neutron and gamma energy, respectively, are absorbed in boiling water; the remainder of the water within the core and reflector does not boil. The designs of the condenser and feed pump are such that large quantities of gas can be entrained in the condensate and pumped back into the nonboiling portion of the reactor, where the radiation field recombines the gases before the water reenters the boiling region. Analyses showed that this method of recombining

¹G. H. Jenks and J. C. Griess, *Water Chemistry in Pressurized and Boiling Water Reactors*, ORNL-4173 (November 1967).

²A. P. Fraas, internal memoranda and private conversation. Also, *Proposed Layouts for TLPR Plants with Boiling Water Reactors*, to be published.

radiolytic gas will perform satisfactorily in this type of reactor provided that gases can be circulated as required and that impurities which accumulate in the water do not seriously affect the radiolytic recombination. Experimental work would be required to evaluate these factors.

WATER CHEMISTRY IN A SMALL STATE-OF-THE-ART PRESSURIZED-WATER REACTOR

G. H. Jenks P. D. Neumann

As part of the Terrestrial Low-Power Reactor Program, ORNL is preparing plans and specifications for a small pressurized-water reactor in which the design will be based on state-of-the-art information. In particular, all aspects of the technology comprising the present state of the art are to be considered for possible inclusion in this design. We have the responsibility for providing specifications or recommendations in areas related to water technology in this design, that is, in such areas as selection of materials and treatment, purification, and analyses of water in primary, secondary, and shield systems. In this connection, we have been reviewing available information on reactor water technology in much more detail than was done in the review mentioned above.¹

No firm recommendations regarding water treatment in the primary system have been made as yet since some design features which affect water chemistry considerations have not yet been fixed by the designers. In particular, the use of boric acid in the coolant and the use of local boiling on fuel element surfaces are being considered by the designers. It is expected that water chemistry features which are common to the primary system of all pressurized-water reactors will be used in this reactor, for example, use of pure makeup water, use of excess hydrogen in the coolant, and continuous purification of the coolant during reactor operation by passage of a cooled bypass stream through resin beds. Inconel is an obvious choice of material for the steam generator on the basis of stress corrosion cracking consideration. Fuel element cladding may be Zircaloy-4, and the remainder of the surfaces in contact with water will be stainless steel or Inconel.

The secondary, or steam, system may be conventional in the use of carbon steel along with

pH 9 to 10 deoxygenated water. However, we are also considering whether the use of stainless steel rather than carbon steel would result in significant advantages from the standpoint of simplicity and reliability of operation.

WATER RADIOLYSIS IN THE HFIR

G. H. Jenks

Estimates of the extent of radiolytic decomposition of the moderator-coolant water in the HFIR were made prior to the start of that reactor.³ These were based on a new analysis of available radiation chemistry information, and, accordingly, it was of interest to compare predicted and experimental values for the HFIR in order to evaluate the method of analysis as well as to determine whether unrecognized factors are affecting the radiolysis. Unfortunately, the available results of analyses of the HFIR moderator are of uncertain validity in some respects, so that the comparisons which can be made are limited to those for hydrogen. However, these comparisons are of interest and are discussed below.

The products of water radiolysis which persist after termination of radiation are hydrogen, oxygen, and hydrogen peroxide. The steady-state concentrations of these in the HFIR are expected to depend upon several factors, including principally: (1) temperature, (2) ratio, R , of rate of energy deposition in core water by neutrons to that by beta-gamma radiation, (3) total radiation intensity, I , and (4) concentration, α , of excess oxidant. The temperature of the core water is, of course, nonuniform. The radiation intensity is also nonuniform. It was estimated³ that the steady-state concentrations of the radiolytic products mentioned above would correspond to those formed during continuous irradiation at a temperature slightly below the core exit temperature (66°C in HFIR)⁴ and at the average radiation intensity. Estimated values of R were in the range 0.48 to 1, and the corresponding values of I at 100 Mw reactor power were 125 and 100 w/cm³. The concentration of excess oxidant in the reactor water is set by the concentrations of oxygen and hydrogen peroxide in the feedwater. However, these are not determined,

³G. H. Jenks, *Effects of Reactor Operation on HFIR Coolant*, ORNL-3848 (October 1965).

⁴Based on information obtained from B. L. Corbett.

and the addition method is such that they are not necessarily constant. Accordingly, α at the time of sampling must be evaluated from the analytical data for hydrogen and for oxidants in the sample.

Analytical results for hydrogen, oxygen, and hydrogen peroxide in the HFIR moderator have been reported by McCord and Corbett. The most recent results, which are for the period May 12, 1967, to September 14, 1967, are listed in Table 4.1. Water samples for these analyses were taken in a large stainless steel high-pressure autoclave. Analyses were performed by the Analytical Chemistry Division. There was apparently no information regarding the extent of decomposition of hydrogen peroxide prior to analysis of a sample.

Boyle⁵ has conducted analyses on two water samples using microtechniques and equipment developed for previous work of similar nature. One of these was a high-pressure sample collected in a 3-cm³ stainless steel autoclave.⁶ This sample was analyzed for hydrogen, oxygen, and hydrogen peroxide. A second, later, sample⁶ was collected in an open polyethylene flask and was analyzed for hydrogen peroxide. Boyle's reported results⁵ are listed in Table 4.2.

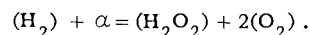
The data in Table 4.2 indicate that considerable decomposition of hydrogen peroxide occurred in the small stainless steel autoclave prior to

analysis and, accordingly, that the relative amounts of oxygen and hydrogen peroxide in the autoclave sample differed from those in the reactor water. However, this does not affect the evaluation of α , so that the data can be used in comparisons between predicted and experimental values for hydrogen. Similarly, the data in Table 4.1 can be used for making these comparisons although the values for relative amounts of oxygen and hydrogen

Table 4.1. Reported Results for Radiolytic Species in the HFIR Moderator at a Reactor Power of 100 Mw

Date	Reported Concentration (M)			Concentration of Excess Oxidant, ^a
	H ₂	O ₂	H ₂ O ₂	α (M)
	$\times 10^{-4}$	$\times 10^{-4}$	$\times 10^{-4}$	$\times 10^{-4}$
5-12-67 ^b	9.5	7.5	2.4	7.9
6-28-67 ^b	8.3	6.6	3.1	8.0
9-14-67 ^c	10.1	7.2	2.4	6.7

^aConcentration of excess oxidant found from material balance equation:



^bR. V. McCord and B. L. Corbett, *HFIR Quarterly Progress Report for April, May, and June of 1967*, ORNL-TM-2017 (Sept. 27, 1967).

^cB. L. Corbett, private communication.

⁵J. W. Boyle, private communication.

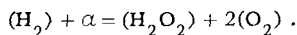
⁶Sampling was done by G. H. Jenks, J. W. Boyle, and A. L. Sutton.

Table 4.2. Reported Results for Radiolytic Species in the HFIR Moderator^a at a Reactor Power of 100 Mw

Date		Reported Concentration (M)			Concentration of Excess Oxidant, ^b
Sampling	Analysis	H ₂	O ₂	H ₂ O ₂	α (M)
		$\times 10^{-4}$	$\times 10^{-4}$	$\times 10^{-4}$	$\times 10^{-4}$
3-3-67	3-10-67 ^c	4.9	2.9	0.35	1.3
3-10-67	3-14-67 ^d			3.5	

^aReported by J. W. Boyle, private communication.

^bConcentration of excess oxidant found from material balance equation:



^cStainless steel autoclave.

^dPolyethylene flask.

Table 4.3. Observed and Predicted Values for Concentration of Hydrogen in the HFIR

Observed Excess Oxidant, ^a α (M)	Hydrogen Concentration (M)				
	Observed ^a	Predicted ^b for R = 1		Predicted ^b for R = 0.48	
		60°C	65°C	60°C	65°C
$\times 10^{-4}$	$\times 10^{-4}$	$\times 10^{-4}$	$\times 10^{-4}$	$\times 10^{-4}$	$\times 10^{-4}$
7.9	9.5	10.0	8.6	6.9	5.8
8.0	8.3	10.0	8.7	6.9	5.8
6.7	10.1	9.9	8.1	6.6	5.5
1.3	4.9	7.6	6.0	5.1	4.1

^aSee Tables 4.1 and 4.2.

^bValues obtained by interpolation of previously calculated values at 50, 60, and 75°C with α values of 10^{-4} and 10^{-3} M at each temperature.

peroxide in the reactor water are considered uncertain.

Observed and predicted values for hydrogen are listed in Table 4.3. The latter include those which would be expected with effective temperatures of 60 and 65°C, with R equal to 1 and 0.48, and with α equal to the value observed at the time the hydrogen was observed. Comparisons between values in Table 4.3 show near agreement for observed and predicted hydrogen if it is assumed that the effective temperature is between 60 and 65°C and if the value of R is 1. As mentioned above, these values for temperature and for R are entirely consistent with the estimates of these parameters made prior to reactor startup.

In connection with the evaluation of R , it is interesting to note that Boyle's results (Table 4.2) also indicate a value of about 1 for this factor if it is assumed that concentrations of hydrogen peroxide in his second sample corresponded to those true concentrations in the reactor and in his stainless steel autoclave sample. In this event, the ratio $(O_2)/(H_2O_2)$ in the reactor was 0.37, while the predicted values of this ratio at 60 or 65°C, with α equal to 1.3×10^{-4} M, are 0.34 for R equal to 1 and 0.55 for R equal to 0.48.

It is tentatively concluded that the radiolysis of moderator in the HFIR is near that expected from prior analyses of available radiation chemistry information. Additional work including, especially, analyses of the ratio of oxygen to hydrogen peroxide in the reactor would be required for all-around verification of our understanding of the radiolysis.

ANODIC FILM GROWTH ON METALS AT ELEVATED TEMPERATURES

A. L. Bacarella H. S. Gadiyar
A. L. Sutton

We have previously reported the results of electrochemical studies on zirconium. We have continued these studies and in addition have performed some measurements on titanium and niobium.⁷⁻⁹

Here we present another interpretation of the results which have been obtained. The classical theory of ionic conduction at high field strengths (10^6 – 10^7 v/cm) predicts that the relation between the ionic current density I and the field strength E should be $I = I_0 \exp(-W(E)/(kT))$, where the activation energy $W(E)$ equals $W_0 - qaE$; q is the charge on the ions, a is the half distance between successive sites occupied by the ions, and I_0 is a constant. Deviations from this relation have been reported in various forms.¹⁰⁻¹² Our more recent interpretation, which provides a fit of the results as satisfactory as that previously reported,¹⁰⁻¹²

⁷H. S. Gadiyar, ORNL-TM-1834 (April 1967).

⁸H. S. Gadiyar, ORNL-TM-1882 (June 1967).

⁹H. S. Gadiyar, A. L. Bacarella, and A. L. Sutton, ORNL-TM-1883 (June 1967).

¹⁰A. L. Bacarella and A. L. Sutton, *Reactor Chem. Div. Ann. Progr. Rept. Jan. 31, 1965*, ORNL-3789, pp. 135–38.

¹¹A. L. Bacarella and A. L. Sutton, *J. Electrochem. Technol.* 4, 117 (1966).

¹²A. L. Bacarella, H. S. Gadiyar, and A. L. Sutton, *Reactor Chem. Div. Ann. Progr. Rept. Dec. 31, 1966*, ORNL-4076, pp. 58–61.

assumes that the activation energy is nonlinear in the field strength E , so that^{13,14}

$$W(E) = W_0 - qa\left(1 - \frac{B}{a}E\right)E.$$

It should be emphasized, however, that in all these interpretations, dielectric polarization¹¹ of the oxide leads to an effective field E causing ion migration which is greater than the average applied field \bar{E} . The Mosotti-Lorentz derivation gives

$$E = \frac{\epsilon + 2}{3} \bar{E},$$

where ϵ is the dielectric constant of the oxide. In a previous discussion¹⁵ of the rate law relating film growth to time t , we referred to Charlesby's¹⁶ analysis of the classical field-dependent rate expression

$$I = I_0 \exp\left(-\frac{W_0}{kT}\right) \exp\frac{qaE}{kT}.$$

He has shown that the particular rate law relating film thickness to time will depend on the portion of the range (t) studied. He has further shown that for values of $z = (qaE/kT) > 3$, the growth should be an approximately logarithmic function of time; for z about equal to 1, the growth should be approximately cubic; and for $z < 1$, the growth approaches a parabolic rate law. For zirconium it was found that the cubic rate law fitted the data adequately, and the value of z was near 1 and consistent with the above analysis.

Results for Titanium

A value of $z > 3$ was expected for titanium since the reported¹⁷ value for the dielectric constant of TiO_2 at 25°C is much greater than the dielectric

¹³L. Young, *Anodic Oxide Films*, pp. 90-101, Academic, New York, 1961.

¹⁴L. Young and F. G. R. Zobel, *J. Electrochem. Soc.* 113, 277 (1966).

¹⁵A. L. Bacarella and A. L. Sutton, *J. Electrochem. Soc.* 112, 546 (1965).

¹⁶A. Charlesby, *Proc. Phys. Soc. (London)* B66, 317 (1953).

¹⁷A. R. Von Hippel (Ed.), *Dielectric Materials and Applications*, p. 302, The Technology Press of M.I.T. and Wiley, New York, 1954.

constant of ZrO_2 :

$$\epsilon_{\text{ZrO}_2}^{25^\circ\text{C}} = 28,$$

$$\epsilon_{\text{TiO}_2}^{25^\circ\text{C}} = 86$$

perpendicular to the optical axis,

$$\epsilon_{\text{TiO}_2}^{25^\circ\text{C}} = 200$$

parallel to the optical axis. Since the effective field E is proportional to the dielectric constant ϵ ,

$$E = \frac{\epsilon + 2}{3} \bar{E},$$

the value of $z = qaE/kT$ would be greater for titanium than for zirconium. From these considerations it was expected that the film growth would follow an approximate logarithmic rate law. We have obtained measurements of the anodic film growth current for titanium in oxygenated 0.05 m K_2SO_4 at constant anodic potential at temperatures to 257°C, and the results are consistent with the above considerations. A logarithmic rate law was obeyed throughout exposures at 200, 240, and 257°C with 9000 to 11,000 min per exposure. We have also obtained simultaneous measurements of the capacitance as a function of film thickness for experiments at 240 and 257°C. From these measurements the calculated dielectric constant of the titanium film (TiO_2) is

$$\epsilon_{\text{TiO}_2}^{240^\circ\text{C}} = 411,$$

$$\epsilon_{\text{TiO}_2}^{257^\circ\text{C}} = 457.$$

For ZrO_2 film the dielectric constant is

$$\epsilon_{\text{ZrO}_2}^{250^\circ\text{C}} = 49.$$

Results for Niobium

Exposure of niobium to oxygenated 0.05 m K_2SO_4 at constant anodic potential at 200°C results in an initial rapid decrease in rate followed by a leveling off to an approximately steady-state rate after only 100 min. The thickness estimated from

the interference color of the film is much less than the thickness calculated from the integrated current-time data. These observations suggest either dissolution of the oxide film or transformation to nonprotective oxide. Exposure to oxygenated $0.05\text{ }m\text{ H}_2\text{SO}_4$ resulted in the formation of nonprotective white oxide. However, in both environments, ac impedance measurements indicated that an oxide having good dielectric properties (nonporous) was present. Plots of $1/C_s$ vs $\log f$ and R_s vs $1/f$ were linear, and the ratio of the slopes was 9.4 (close to the theoretically predicted value of 9.2 for anodic oxide films). Similar results were obtained for the ac impedance measurements on titanium and zirconium.¹⁸

CORROSION SUPPORT FOR THE HIGH-FLUX ISOTOPE REACTOR

P. D. Neumann J. C. Griess

Recent failures in some of the High-Flux Isotope Reactor (HFIR) target rods resulted in the distribution of radioactive contamination (principally ^{244}Cm) throughout the primary system. Methods considered for removing all or part of the contamination from the interior surfaces of the reactor included circulation of either a chelating agent such as the sodium salt of diethylene triamine pentaacetic acid or nitric acid solutions more concentrated than the $10^{-5}\text{ }M$ solution normally used as coolant. Since no data existed on the corrosiveness of such solutions to the permanent aluminum and beryllium parts of the reactor, short-term corrosion tests were conducted.

Specimens of 6061 aluminum and QMV beryllium both separately and in contact with each other and stainless steel were exposed to 10^{-3} and $10^{-4}\text{ }M\text{ HNO}_3$ at 50°C . These tests were conducted in a stainless steel pump loop with the solution flowing past the specimens at 44 fps. With the more concentrated solution the test lasted 258 hr; in the $10^{-4}\text{ }M$ solution the test was continued for 191 hr.

In $10^{-3}\text{ }M\text{ HNO}_3$, attack of both aluminum and beryllium was severe. Aluminum corroded at rates of 100 to 200 mils/year with no evidence of

pitting. On the other hand, beryllium suffered severe localized corrosion in the form of intergranular attack over large areas of the surface. Penetrations as deep as 15 mils developed during the 258-hr test. The effect of coupling stainless steel to either beryllium or aluminum was negligible, as was the attack on stainless steel itself.

In $10^{-4}\text{ }M\text{ HNO}_3$, both aluminum and beryllium showed much less attack than in the more concentrated acid. No localized corrosion was observed on either material. Average corrosion rates were 4 and 50 mils/year for beryllium and aluminum respectively.

Specimens of beryllium and aluminum were exposed to $10^{-3}\text{ }M$ solutions of the sodium salt of diethylene triamine pentaacetic acid ($\text{pH} = 7.2$) in glass equipment for 165 hr at 50°C . Beryllium was completely resistant to this solution, but aluminum corroded uniformly at an average rate of 29 mils/year.

Even with the relatively high corrosion rates observed in the $10^{-4}\text{ }M\text{ HNO}_3$ and the chelating solution, either could be used for short periods in the HFIR without disastrous results. However, acid concentrations greater than $10^{-4}\text{ }M$ should not be allowed in the reactor system.

Actually, the primary system of the HFIR was adequately decontaminated using either 10^{-5} or $10^{-4}\text{ }M\text{ HNO}_3$ to which 1 ppm lanthanum [as $\text{La}(\text{NO}_3)_3 \cdot 6\text{H}_2\text{O}$] was added.¹⁹

The results of tests conducted to determine the effect of heat flux on the corrosion of aluminum were reported previously.²⁰ Based on the results it was concluded that 6061 aluminum had sufficient corrosion resistance to be used as cladding for the HFIR fuel elements. The soundness of this conclusion is attested to by the fact that to this time 17 complete fuel elements have been used without evidence of a cladding failure.

Although the fuel elements have not been a source of trouble, the manufacturing specifications could be relaxed, and the cost of fuel elements would be significantly less, if corrosion could be reduced. Recently, it was shown that certain

¹⁹R. V. McCord and B. L. Corbett, *High Flux Isotope Reactor Quarterly Report, July, August, and September, 1967*, ORNL-TM-2028 (to be issued).

²⁰J. C. Griess, H. C. Savage, and J. L. English, *Effect of Heat Flux on the Corrosion of Aluminum by Water. Part IV. Tests Relative to the Advanced Test Reactor and Correlation with Previous Results*, ORNL-3541 (February 1964).

¹⁸G. H. Jenks et al., *Reactor Chem. Div. Ann. Progr. Rept. Dec. 31, 1966*, ORNL-4076, pp. 61-63.

colloids reduce the corrosion of aluminum in isothermal high-temperature systems.²¹ Based on this report, two brief tests were conducted to see if colloidal silica would have an effect on the corrosion of aluminum under heat-transfer conditions. For these tests the procedure was the same as previously described.²⁰ For both tests the coolant was deionized water flowing at 45 fps and the heat flux was 1.5×10^6 Btu hr⁻¹ ft⁻². The average temperature at the water-specimen interface was 325°F. The first test was started with pure water to establish that the corrosion rate was the same as that predicted by a previously established correlation.²⁰ Once this was established, enough SiO₂ was added to the system to bring the concentration of the coolant to about 20 ppm SiO₂, and by a continuous feed and letdown system, SiO₂-containing solution was continuously fed into the loop to maintain that level. The SiO₂ was added as Syton, a 20% colloidal dispersion of SiO₂ manufactured by Monsanto Chemical Company. The presence of SiO₂ was without effect in this test. The second test was conducted exactly as the first, except the 20 ppm SiO₂ was in the solution from the start. Within experimental error the two results were the same and agreed with those predicted from the previous correlation. Thus, the presence of colloidal SiO₂ in the coolant appears to be of no value as an inhibitor.

CORROSION OF TITANIUM IN SALINE WATERS

E. G. Bohlmann	F. A. Posey
J. C. Griess	J. F. Winesette

Crevice Corrosion of Titanium

Studies concerning the crevice corrosion of titanium were continued. Based on the results presented last year,²² it was predicted that titanium alloyed with sufficient amounts of nickel, palladium, or molybdenum should be more resistant to crevice attack than commercially pure titanium and most commercial alloys. Since that time, actual crevice corrosion tests have been conducted in air-saturated 4.5 M NaCl at 150 to 250°C with

the following alloys: Ti-0.2% Pd, Ti-0.2% Ni, Ti-0.5% Ni, Ti-1% Ni, Ti-1% Ni-1% Mo, and Ti-2% Ni. The alloys containing 0.2% Pd, 2% Ni, and 1% Ni plus 1% Mo showed no evidence of significant attack. In all cases the crevice region was much darker than the outside areas and contained a thin uniform layer of titanium dioxide. The alloys containing 0.2 to 1% Ni also showed relatively little attack in the crevice region, but in these cases there were a few isolated areas within the crevice where localized attack had occurred, as evidenced by relatively heavy local white deposits of titanium dioxide. However, even with the lowest nickel content the extent of attack was much less than was observed with commercially pure titanium exposed under the same conditions. Although actual corrosion tests with molybdenum alloys were not carried out, the results of the above tests generally indicate the validity of the predictions made last year.

Experience has indicated that the reproducibility of titanium crevice corrosion in 1 M NaCl solutions at temperatures of 150°C and higher is poor; usually only about half of the specimens exposed are attacked. Recent tests have shown that in oxygen-containing 4.5 M NaCl essentially all specimens undergo heavy attack during only a few days exposure. Solution samples removed from the crevices of specimens corroding in 1 M NaCl had pH values of about 1; similar solutions from specimens corroding in 4.5 M NaCl had pH values as low as 0.2. The lower pH in the more concentrated solution, which is attributable to the higher activity coefficient of hydrochloric acid in the more concentrated solution, appears to account for the greater corrosion.

The importance of oxygen in crevice corrosion of titanium was demonstrated as follows. A titanium crevice specimen from which solution could be withdrawn was exposed to thoroughly degassed 4.5 M NaCl at 150°C for three days. Several aliquots of solution withdrawn from the crevice at different times during the exposure had pH values between 5 and 6. Examination of the specimen showed no evidence of crevice attack. The experiment was then repeated; and, after an 18-hr exposure, the pH of the solution was again 5 to 6. While at temperature, about 10 psi oxygen was added to the autoclave. After an hour, similar samples had pH values as low as 0.2. The test continued for about 5 hr after the addition of oxygen. Examination of the specimen showed

²¹J. E. Draley and W. E. Ruther, *Corrosion of Aluminum Alloys by Flowing High Temperature Water*, ANL-7227 (January 1967).

²²E. G. Bohlmann et al., *Reactor Chem. Div. Ann. Progr. Rept. Dec. 31, 1966*, ORNL-4076, pp. 121-23.

relatively heavy localized attack in the crevice. Other similar tests yielded the same result.

These results clearly show the essential part played by oxygen in crevice corrosion. When a titanium crevice is immersed in an aqueous salt solution containing dissolved oxygen, the initial concentration of oxygen is the same in the crevice as in the bulk solution. At room temperature and even somewhat higher, the corrosion rate of titanium is low enough so that the consumption of oxygen in the small volume of solution in the crevice is balanced by diffusion of oxygen from the bulk solution into the crevice. As the temperature increases, the corrosion rate of titanium increases at a faster rate than the diffusion process, and ultimately the solution within the crevice becomes depleted in oxygen. Depletion of oxygen within the crevice causes the potential of titanium in the crevice to decrease, a condition necessary for the establishment of a macrocell. To preserve electroneutrality, the small amount of corrosion initially occurring in the crevice must be balanced by migration of chloride ions into, and sodium ions out of, the crevice. Hydrolysis of titanium ions produces acid and a higher corrosion rate, so that the process is autocatalytic if the alloy corrodes appreciably in the initially developed acid solution. In a given corroding crevice, a steady-state acid concentration is reached which represents a balance between migration of chloride ions into

the crevice and diffusion of acid produced by hydrolysis from the crevice. However, the nature of the crevice changes as corrosion proceeds because the volume of the corrosion product (TiO_2) is greater than the volume of metal corroded.

The above analysis indicates that the crevice corrosion of titanium in desalination plants can be eliminated by alloying titanium with sufficient palladium or nickel (and probably molybdenum) or by ensuring the complete absence of oxidizing agents from the brine. The most practical approach appears to be the use of a 2% Ni alloy. Investigations by titanium manufacturers indicate such an alloy has satisfactory metallurgical properties.

Pitting Potentials

Studies of the effects of temperature and alloy composition on titanium pitting potentials have continued.²² Results obtained for a number of commercial and experimental alloys are given in Table 4.4. A paper summarizing the studies on the effect of temperature on pitting potentials of titanium and some of its alloys has been accepted for publication in *Desalination*.²³

²³F. A. Posey and E. G. Bohlmann, *Desalination* (in press).

Table 4.4. Pitting Potentials vs Temperature for Various Titanium Alloys in 1 M NaCl

Temperature (°C)	Pitting Potential (v vs S.C.E.)												
	Ti- 2 Ni	Ti- 0.5 Nb	Ti- 1 Mo	Ti- 5 Mo	Ti- 10 Mo	Ti- 30 Mo	Ti- 6 Al- 4 V	Ti- 2 Nb- 1 Ta- 8 Al	Ti- 4 Mn- 4 Al	Ti- 5 Al- 2.5 Sn	Ti- 1 Al	Ti- 1 Sn	Commercially Pure Ti
25	11.9	10.0	10.0 ^a	7.8	9.0	7.1	2.7	1.9	2.9	1.9	12.9	12.5	9.5
50	10.5	8.3	7.9	6.0	6.3	5.9	2.1	1.8	2.1	1.6 ^a	12.2	12.1	8.3
75	8.0	7.2	6.7	4.1	5.1	4.9	1.8	2.0	1.8	1.4	9.0	10.0	7.5
100	6.5	6.0	5.7	3.8	4.8	4.6	1.7	1.3	1.7	1.3	3.4	7.1	5.9
125	3.3	4.9	4.6	3.4	4.1	4.3	1.1	0.9	0.9	0.7	3.4	3.8	4.5
150	1.9	3.8	4.5	3.4	3.6	4.1	1.2	0.7	1.0	0.5	2.2	1.4	2.2
175	1.6		4.1	3.8	3.8	4.0	1.2	0.7	0.9	0.5	1.7	1.1	0.9
200	1.9	2.1	3.1	4.1	4.3	4.0				0.5	1.8	1.1 ^a	1.0
220		2.2	3.5		5.2					0.5			0.0

^aEstimated.

It was hoped that the results of these measurements would provide information on the mechanistic nature of the effect of added constituents on the pitting potential of titanium. No such conclusions can be drawn on the basis of the measurements made so far; however, some general observations can be made. Although the pitting potentials of the molybdenum alloys are lower at lower temperatures (below 125°C) than the pitting potential of pure titanium, the molybdenum alloys exhibit much higher pitting potentials at elevated temperatures (125 to 220°C). This observation is consistent with the generally enhanced resistance of the molybdenum alloys to all forms of catastrophic attack at elevated temperatures compared with pure titanium and is also consistent with the increased resistance to pitting of stainless steels containing molybdenum. Alloys with appreciable

percentages of aluminum (4 to 8%) all have low pitting potentials. No significant effect of additional additives is apparent. These alloys can be expected to be far more subject to pitting attack than the molybdenum alloys. Alloys with relatively small percentages of alloying elements (1% Sn, 2% Ni) and even the 1% Al alloy show somewhat higher pitting potentials than commercial titanium at lower temperatures (below 100°C), but no particular effect of these additions can be seen at more elevated temperatures. The pitting potential of the 0.5% Nb alloy is similar to that of pure titanium below 100°C but is somewhat higher at higher temperatures.

The apparent substantial effect of aluminum alloy additions on titanium pitting behavior and the frequent use of aluminum in commercial titanium alloys suggested a more detailed study of the

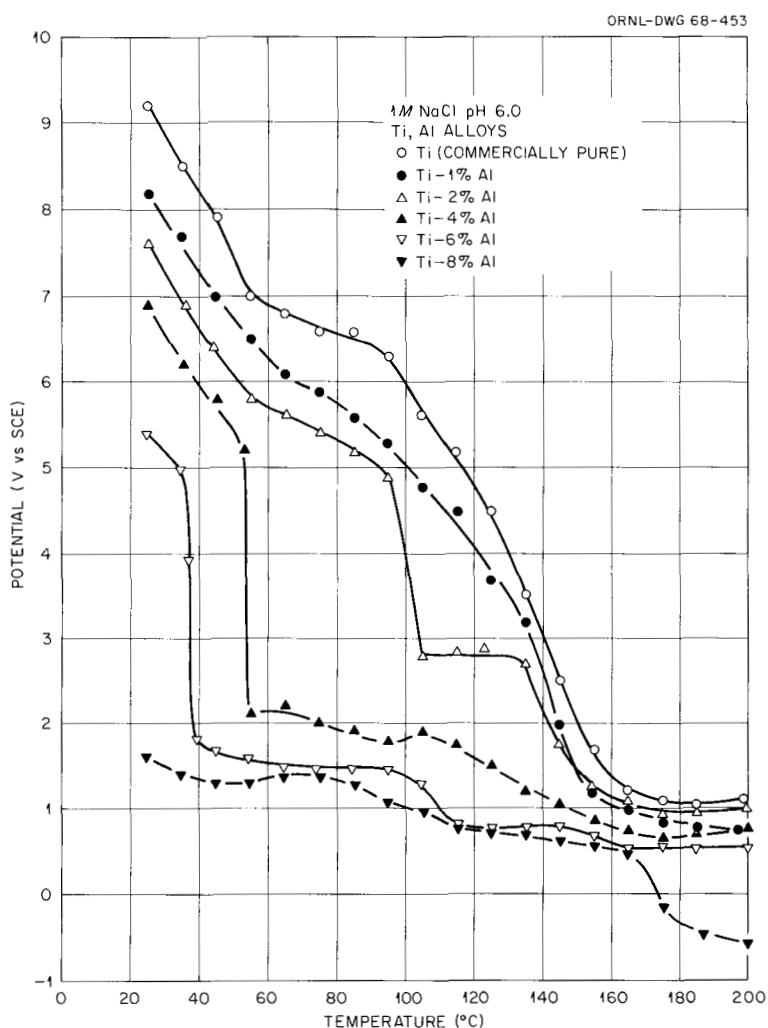


Fig. 4.1. Effect of Temperature on Pitting Potentials of Titanium-Aluminum Alloys in 1 M NaCl.

titanium-aluminum system in the absence of other additives. The Metals and Ceramics Division recently prepared a series of binary alloys containing 1, 2, 4, 6, and 8% aluminum. The effect of temperature on the pitting potentials has been determined and is shown in Fig. 4.1. The pitting potentials show a regular decline with aluminum concentration increase at low temperatures but comparatively little effect at the higher temperatures. The temperature at which a sharp break in the pitting potential occurs is also dependent on the aluminum concentration.

EFFECT OF SULFIDE ON CORROSION IN SALINE WATERS

E. G. Bohlmann J. C. Griess

The presence of sulfide-containing contaminants in seawater can adversely affect the corrosion resistance of materials used in desalination plants. Although a number of studies have been conducted concerning the effect of sulfide on such alloys, they have largely been carried out at ambient temperatures. As part of the corrosion program conducted for the Office of Saline Water, the corrosion behavior of several alloys is being investigated in sodium chloride solutions containing low levels of sodium sulfide. The investigation consists of two parts: the exposure of a large number of specimens²⁴ in a 100-gpm titanium pump loop, and the exposure of single specimens in a smaller pump loop in which electrochemical polarization studies can be carried out. The latter studies are made at temperature and with solution flowing past the specimen.

Specimens of Admiralty brass, Monel, Inconel, both 90-10 and 70-30 cupronickels, Hastelloy C, and three titanium-nickel alloys (0.49% Ni, 2% Ni, and 1% Ni with 1% Mo) have been exposed in the larger loop constructed totally of titanium. In the tests to date the solution has been deaerated 1 M NaCl containing a nominal 10 ppm S (as Na₂S) at 125°C. The sulfide level is maintained essentially constant by continuously pumping fresh sulfide-containing sodium chloride solution into

the loop and removing the same volume through a letdown valve. The sulfide concentration of the letdown stream is frequently verified with an Orion sulfide ion electrode (model 94-16). Flow rates past the specimens have been 3 to 25 fps, and exposure times have been 200 to 1500 hr.

Observations made to date include the following. A more or less uniform black coating formed on all specimens. On specimens which showed little or no attack, the coating was easily removed, whereas on the more heavily corroded specimens prolonged periods of cathodic descaling were required.

The films formed on the 90-10 cupronickel specimens offered only limited protection at flow rates of 15 and 25 fps. Constant corrosion rates of 20 and 32 mils/year, respectively, were observed. At 3 and 7 fps, rates of 3 to 4 mils/year were found after an initial somewhat higher rate. At all flow rates, isolated large pits formed. The 70-30 cupronickel specimens corroded at constant rates of 15, 23, and 27 mils/year at 7, 15, and 25 fps respectively. At 3 fps a continuing rate of 7 to 8 mils/year was observed. In all cases the surfaces were roughened as a result of the attack, but pits were usually absent.

Both Monel and Admiralty brass were considerably more resistant than either of the cupronickels. Localized attack was absent, and during 1500-hr tests, corrosion rates were about 1 mil/year at flow rates up to and including 15 fps. At 25 fps Admiralty brass corroded at 4 mils/year, but Monel corroded at less than 1 mil/year.

Attack on Hastelloy C and the three titanium-nickel alloys was essentially nil. The same was true for Inconel, except crevice attack occurred where the specimens were held in insulating O-rings in the holders.

Based on a comparison run made in the absence of sulfide, the average rate of attack on the cupronickel alloys was a factor of 4 to 7 less in the absence of sulfide than in its presence. Also, without sulfide, pitting of the 90-10 alloy did not occur. With the other alloys the corrosion rates were the same with or without sulfide.

A somewhat surprising observation has been that the presence of corroding carbon steel specimens in the loop results in appreciable inhibition of the attack on copper alloys by sulfide-containing saline water. It has long been known that the presence of ferrous iron effectively inhibits localized attack on copper-base alloys by flowing

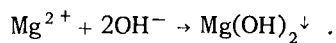
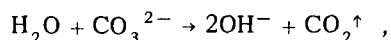
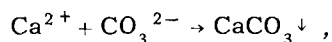
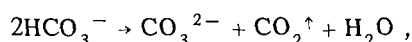
²⁴E. G. Bohlmann and J. C. Griess, *Reactor Chem. Div. Ann. Progr. Rept. Jan. 31, 1965*, ORNL-3789, p. 297.

seawater,^{25,26} but that the inhibitory action persists in the presence of sulfide and elevated temperatures is of considerable interest.

CARBON DIOXIDE SCALE SUPPRESSION STUDIES

S. A. Reed D. M. Eissenberg
C. C. Littlefield

In seawater at ambient temperature under equilibrium conditions, all dissolved CO₂ is primarily in the form of bicarbonate ion, HCO₃⁻. Molecular CO₂ and CO₃²⁻ exist only in trace amounts. When the water is heated, the bicarbonate ion breaks down, and alkaline scales – calcium carbonate and magnesium hydroxide – can form as a result of the following reactions:



To prevent alkaline scale formation in seawater distillation equipment, conventional practice is to add sufficient acid to neutralize the bicarbonate alkalinity and then to degas the seawater to remove the CO₂. Usually sulfuric acid is used, because it is the cheapest acid which is commercially available in most areas of the world.

In present-day distillation plants which produce 1 to 2 million gallons of potable water per day, the cost of acid treatment is in excess of 3¢ per 1000 gal of distillate. For the 150 million gal/day plant which will be operated by the Metropolitan Water District in Southern California, the cost of acid is estimated to be 2.6¢ per 1000 gal of product – about 10% of the total production cost of water.²⁷ In the past four years world demand

for sulfur has exceeded supply, and the price of sulfur has increased nearly 50%. Consequently, it appears unlikely that the incremental cost of acid feed treatment can be reduced below this value, even by on-site production of acid, which has been postulated for larger water plants which may be constructed in the future.

There is a strong incentive then for developing a substitute feed treatment to prevent alkaline scales which would not entail the use of acid or other purchased chemicals.

It is apparent from the above equations that, if CO₂ were added to a pressurized system containing seawater, the equilibrium would shift to the left and more bicarbonate would be formed. Then the alkaline scales would not precipitate. It is known that, if as little as 25 ppm CO₂ (by weight) is added, seawater can be heated under pressure to 325°F without formation of scale.²⁸

In the multistage flash-evaporation process for producing potable water from seawater, it would not be difficult to keep the brine under a pressure above the decomposition pressure of the bicarbonate ion all the way through the brine heater. After passing through the brine heater, where seawater is heated to the maximum process temperature, the water is flashed and the CO₂ will be evolved. When seawater of normal alkalinity (i.e., 120 ppm as CaCO₃) is flashed, approximately 60 ppm of CO₂ is evolved; therefore, a self-sustaining feed treatment cycle utilizing only the carbon dioxide which occurs naturally in seawater appears possible. We are currently investigating the feasibility of such a process.

The investigation is sponsored by the Office of Saline Water and is being carried out at their test station at Wrightsville Beach, North Carolina.

A test program is being conducted using the small flashing device shown schematically in Fig. 4.2. The maximum brine temperature, the flashing temperature drop, and the residence time in the flash chamber correspond to conditions occurring in a large flash evaporator. The program has four major objectives: (1) to demonstrate that CO₂ injected into seawater will effectively prevent alkaline scale formation in the brine heater at temperatures to 300°F, (2) to determine the minimum concentration of CO₂ which is required

²⁵J. W. Bostwick, *Corrosion* 17, 12 (August 1961).

²⁶*Ferrous Sulfate Treatment to Prevent Corrosion of Condenser and Heat Exchanger Tubes*, Technical Information Sheet T.I.S./7,0463, Yorkshire Imperial Metals Limited, Leeds.

²⁷*Engineering and Economic Feasibility Study, Phases I and II, for a Combination Nuclear Power and Desalting Plant*, Bechtel Corp., TID-22330 (vol. I), pp. 9–21 (December 1965).

²⁸B. A. Axelrod et al., *Heating of Saline Water and Mining of Sulfur Therewith*, U.S. Pat. 2,756,035, July 24, 1956.

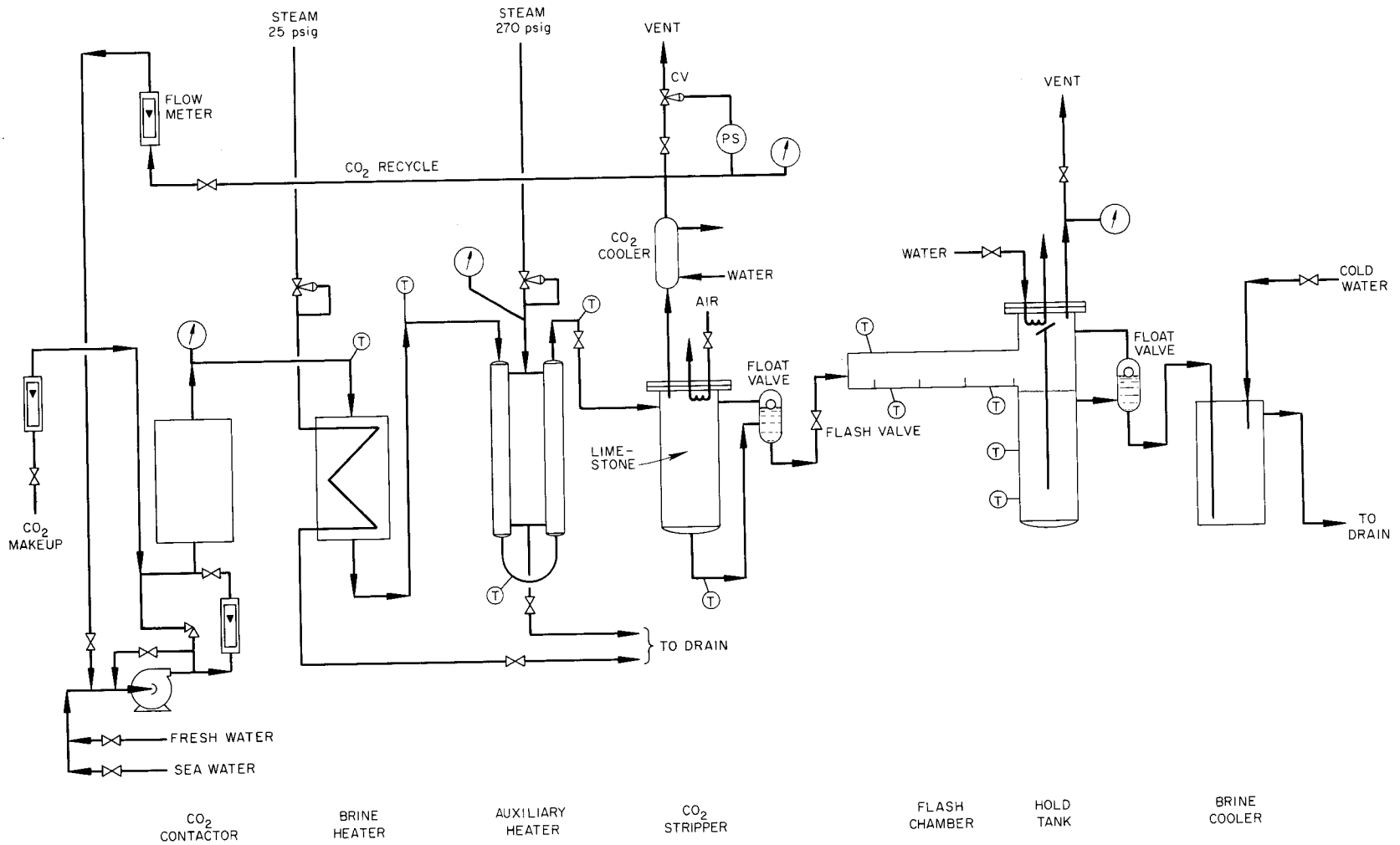


Fig. 4.2. CO₂ Scale Suppression Test Rig.

to prevent scale formation at various temperatures, (3) to observe the deposition behavior of alkaline precipitates which form downstream of a flashing orifice as a result of stripping dissolved CO_2 from the seawater, and (4) to develop a flowsheet and equipment to construct a pilot plant that can be operated to establish the dependability and economics of the process.

Three 4-hr exploratory tests have been conducted, which resulted in the following observations. Injection of 20 ppm (by weight) of CO_2 into the cold seawater feed to the apparatus prevented scale formation in the brine heater at temperatures to 293°F . Solids precipitated immediately when CO_2 was evolved and extracted from the flashing brine in the CO_2 stripper. The solids consisted entirely of CaCO_3 ; that is, no $\text{Mg}(\text{OH})_2$ precipitated. A portion of the CaCO_3 which was formed adhered to the surfaces of the steel flash chamber and to the cupronickel and copper test specimens immersed in the water flowing through the flash chamber; however, no material adhered to companion specimens of Teflon.

Because a portion of the freshly precipitated CaCO_3 adhered to the metal walls of the flash chamber, a seedbed consisting of $\frac{1}{4}$ -in.-mesh anhydrous calcium sulfate particles was installed in the CO_2 stripper. The intended purpose of the bed was to provide nucleation sites where freshly formed CaCO_3 could precipitate and adhere to the seed particles rather than form scale in other parts of the equipment. Calcium sulfate seeds were used instead of CaCO_3 to permit subsequent analytical chemical determination of the quantity of CaCO_3 which was formed in the bed. Two 4-hr tests were then conducted at essentially the same temperature and flow conditions:

Maximum seawater temperature, $^\circ\text{F}$	293
Temperature of seawater entering primary flashing orifice, $^\circ\text{F}$	284
Temperature of seawater in flash chamber, $^\circ\text{F}$	273
Seawater flow rate, gpm	1
CO_2 added, ppm	20

Samples withdrawn from the flash chamber during the tests were clear, and the room-temperature pH measurements of samples taken at various

locations indicated that most of the alkalinity was being removed.

Following the runs the seedbed contactor was disassembled, and a sample of the seeds was submitted for CaCO_3 and $\text{Mg}(\text{OH})_2$ determinations. The analyses showed that the bed contained 8 wt % CaCO_3 and no $\text{Mg}(\text{OH})_2$. This was equivalent to a total of 200 g of CaCO_3 in the bed. Based on the flow rate and the alkalinity of the seawater of 118 ppm (as CaCO_3) determined by chemical analysis, a total of 215 g of CaCO_3 was available for deposition in the bed.

No scale was detected by chemical analysis on the brass and copper specimens which were exposed in the water flowing through the flash chamber.

Currently, the apparatus is being modified preparatory to conducting similar tests of longer duration (up to 100 hr) at higher temperatures using a bed of CaCO_3 seeds and recycling the CO_2 .

OSW MATERIALS INFORMATION CENTER

J. L. English S. A. Reed

Early in 1967, Oak Ridge National Laboratory was requested by the Distillation Division of the Office of Saline Water (OSW) to assist in the establishment of a Materials Information Center. The function of the Center, which will be located temporarily at Oak Ridge, will be to collect, index, abstract, and disseminate information to OSW contractors and other interested parties relative to the corrosion behavior of materials of construction used in distillation processes for the desalination of seawater. The initial objective of the Center, which will become operative early in 1968, is to process all pertinent OSW research and development reports and the bibliographic references contained therein. The Center will maintain a permanent inventory of all processed materials.

As conceived originally, the Center will utilize a manual system for storage and retrieval of information. However, a thesaurus of descriptive key words has been prepared to facilitate transition to a computerized system when and if the situation warrants.

5. Chemistry of High-Temperature Aqueous Solutions

SOLUBILITY OF Fe_3O_4 AT ELEVATED TEMPERATURES

F. H. Sweeton R. W. Ray
C. F. Baes, Jr.

The previously reported¹ study of the solubility of Fe_3O_4 in dilute acid solutions containing dissolved H_2 has been continued with measurements in pure H_2O and extended to dilute alkaline solutions and to lower temperatures.

The experimental method has been essentially the same as before. The dilute solution saturated at 25°C with H_2 at atmospheric pressure was pumped slowly through a heated column containing a specially prepared sample of Fe_3O_4 . A small stream of HCl solution (0.001 to 0.1 *N*) was pumped into the hot stream of solution leaving the Fe_3O_4 column to prevent precipitation of iron in the otherwise neutral or alkaline solution on cooling to room temperature. The iron was then stripped from the flowing solution by a cation exchanger and, after elution, was analyzed with a spectrophotometer as the *o*-phenanthroline complex.

In order to inject HCl solution into the hot solution flowing out of the Fe_3O_4 column, a small part of the stream was diverted to a mercury reservoir. The mercury flowed by gravity through a capillary tube into a lower reservoir containing the HCl solution, which was in turn forced back into the main solution stream. The flow of HCl was monitored by following the weight increase of the lower reservoir. Periodically samples of the HCl were collected at the flow rates used for injection. The iron concentration found in these samples, which was in the order of 4 μm , was used

to correct for iron contributed to the main solubility samples by the injected HCl.

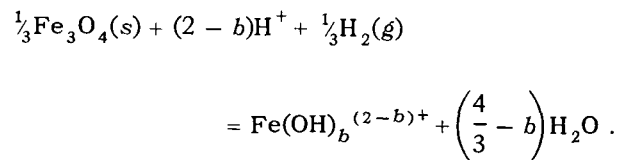
The ion exchanger used to collect the dissolved iron was held in two columns in series. The fraction of iron found on the second column was normally below 20% of that on the first, showing that the columns were working satisfactorily.

Several consecutive runs were normally made at one combination of temperature and solution composition in order to check on the reproducibility of the iron concentration and to see if the concentration varied with flow rate. Within the reproducibility of the data, no consistent effect of flow rate was seen, and thus we believe our flow rate was low enough to allow the solution to equilibrate with the Fe_3O_4 .

During the course of the measurements the composition of the Fe_3O_4 did not change detectably, but its specific surface area increased from 0.14 m^2/g to 0.33 m^2/g as measured by krypton adsorption. The simultaneous etching of the grain boundaries as seen in electron micrographs probably accounts for this effect.

The observed solubilities are plotted in Fig. 5.1 as a function of temperature and the composition of the solution before contact with the Fe_3O_4 . The points with vertical bars represent averages of several runs; the bars show the standard deviations of the associated runs.

In order to analyze the data in terms of the existence of various species of ferrous ions we have used equilibria of the type:



¹F. H. Sweeton, R. W. Ray, and C. F. Baes, Jr., *Reactor Chem. Div. Ann. Progr. Rept. Dec. 31, 1966*, ORNL-4076, pp. 70-72.

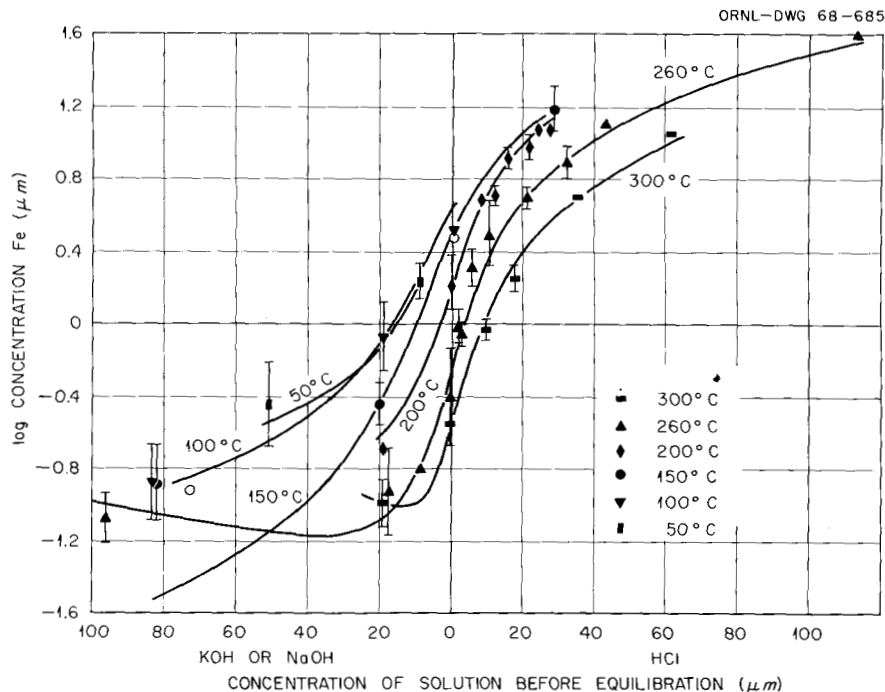


Fig. 5.1. Solubility of Fe_3O_4 in Dilute Acidic and Basic Solutions Saturated at Room Temperature with 1 atm H_2 .

The associated solubility products are

$$K_b = \frac{[\text{Fe}(\text{OH})_b^{(2-b)+}]}{[\text{H}^+]^{(2-b)} P_{\text{H}_2}^{1/3}}$$

We have tried fitting the data assuming the existence of the complexes Fe^{2+} , FeOH^+ , $\text{Fe}(\text{OH})_3^-$, or $\text{Fe}(\text{OH})_4^{2-}$, or various combinations of them. To do this we assumed values for the appropriate solubility products and calculated² by iteration the concentrations of H^+ , OH^- , and the ions $\text{Fe}(\text{OH})_b^{(2-b)+}$ which were necessary to give overall charge neutrality for each solution. Then by a least-squares procedure the logarithms of the calculated and observed iron concentrations were compared, and the solubility products were readjusted accordingly. The whole process was repeated until the solubility products, K_b , could not be improved further. The effective hydrogen pressures at the six temperatures between 50 and 300°C were, respectively, 1.05, 0.95, 0.71, 0.48,

²The values of the dissociation constant of water which were used were 0.0547, 0.616, 2.24, 5.01, 6.76, and 6.54×10^{-12} at 50, 100, 150, 200, 260, and 300°C, respectively; these molal values are based on the data of A. A. Noyes, Yogoro Kato, and R. B. Sosman in *J. Am. Chem. Soc.* **32**, 159 (1910).

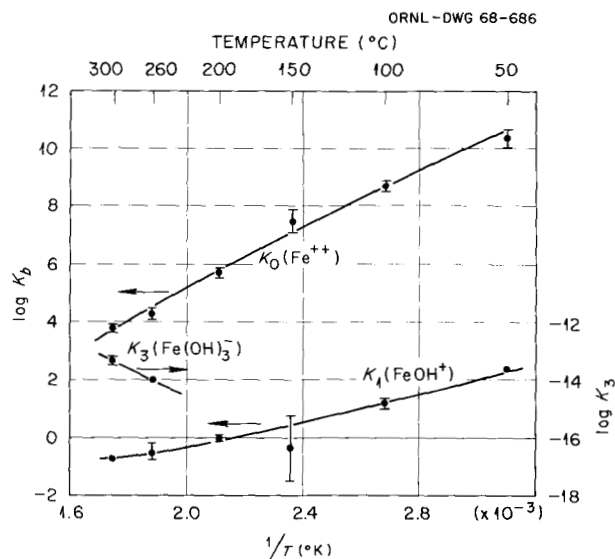


Fig. 5.2. Calculated Solubility Products for the Indicated Ferrous Complexes.

0.26, and 0.16 atm when calculated as before¹ from available solubility data.

We have fitted the data with the complexes Fe^{2+} , FeOH^+ , and $\text{Fe}(\text{OH})_3^-$; the corresponding K_b values, shown in Fig. 5.2, have been used to calculate the smooth curves in Fig. 5.1. At 260 and

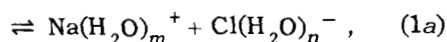
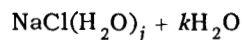
300°C all three complexes were necessary, although $\text{Fe}(\text{OH})_4^{2-}$ explained the data about as well as $\text{Fe}(\text{OH})_3^-$. At 200° three species were not required – Fe^{2+} paired with FeOH^+ , $\text{Fe}(\text{OH})_3^-$, or $\text{Fe}(\text{OH})_4^{2-}$ was sufficient. At the three lower temperatures Fe^{2+} with $\text{Fe}(\text{OH})^+$ gave a slightly better fit than the other pairs; as a consequence, they have been used to fit all the data at 200°C and below. This choice results in a difference of approximately 8.3 units in the logs of the K_b values for Fe^{2+} and FeOH^+ when extrapolated to 25°C; this is in reasonable agreement with the 9.5 units expected from the hydrolysis constant of Fe^{2+} determined at 25°C by Hedström.³

These data will be combined with thermodynamic data for Fe^{2+} , H_2O , H_2 , and H^+ to reevaluate the free energy of formation of Fe_3O_4 .

THE INDEPENDENCE OF ISOTHERMAL EQUILIBRIA IN ELECTROLYTE SOLUTIONS ON CHANGES IN DIELECTRIC CONSTANT

W. L. Marshall A. S. Quist⁴

During the past year it became apparent to us that if the molar concentration of water were included in electrolyte dissociation equilibria as Franck and others had done earlier,⁵ for example,



$$K^\circ = \frac{a_{\text{NaCl}(\text{H}_2\text{O})_m}^+ a_{\text{Cl}(\text{H}_2\text{O})_n}^-}{a_{\text{NaCl}(\text{H}_2\text{O})_j} a_{\text{H}_2\text{O}}^k}, \quad (1b)$$

$$\log K = \log K^\circ + k \log a_{\text{H}_2\text{O}}, \quad (1c)$$

where a is the activity in moles per liter of each reactant, K is a conventional constant, K° is the complete constant, and k is also a constant, then the complete constant K° would be independent of isothermal changes in dielectric constant (D). This behavior is in sharp contrast with previous theory that $\log K$ should be a linear function of

³Bengt O. A. Hedström, *Arkiv Kemi* 5, 457 (1953).

⁴On assignment, Institut für Physikalische und Elektrochemie, Karlsruhe, Germany.

⁵E. U. Franck, *Z. Physik. Chem. (Frankfurt)* 8, 107, 192 (1956).

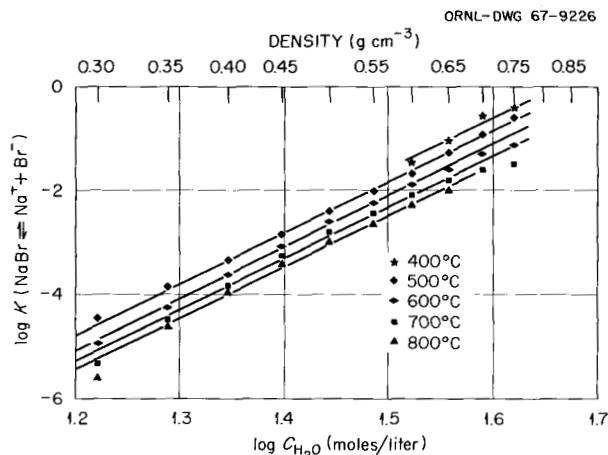


Fig. 5.3. Log K (molar units) for the Equilibrium $\text{NaBr} \rightleftharpoons \text{Na}^+ + \text{Br}^-$ as a Function of the Logarithm of the Molar Concentration of Water at Temperatures from 400 to 800°C.

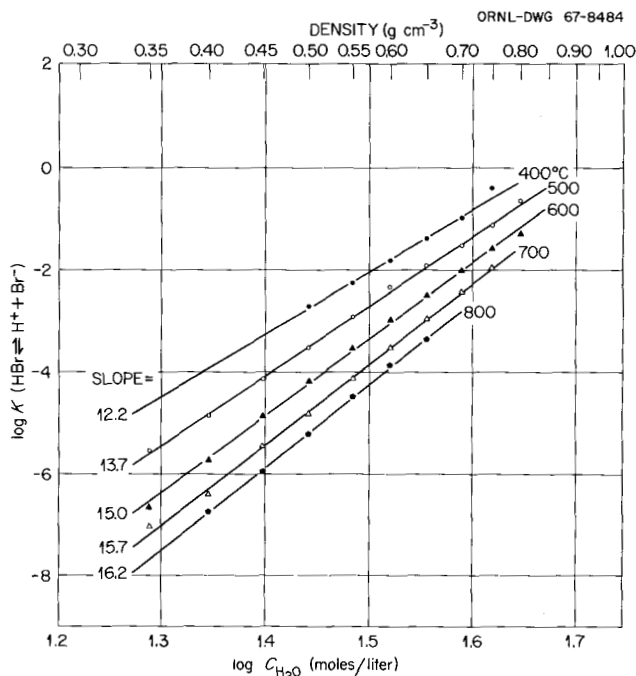


Fig. 5.4. Log K (molar units) for the Equilibrium $\text{HBr} \rightleftharpoons \text{H}^+ + \text{Br}^-$ as a Function of the Logarithm of the Molar Concentration of Water at Temperatures from 400 to 800°C.

$1/D$.⁶ Precise values of $\log K$ do not follow this previous theory. Examples of the linear behavior of $\log K$ (dissociation) vs $\log C_{\text{H}_2\text{O}}$ (where $a_{\text{H}_2\text{O}}$ is replaced by $C_{\text{H}_2\text{O}}$) according to Eq. (1c) for

⁶R. M. Fuoss, *J. Am. Chem. Soc.* 80, 5059 (1958).

sodium bromide and for hydrobromic acid (experimental evaluations of these K 's are discussed in the next subsection) are shown in Figs. 5.3 and 5.4. Examples for sodium chloride were given previously.⁷ For all three cases, the slope of $\log K$ vs $\log C_{\text{H}_2\text{O}}$ (or \log density H_2O) represents the net change in waters of solvation. A paper on these observations and deductions has been published recently.⁸ An abstract of another paper in press⁹ presenting extensive examples of the be-

havior cited above is given below, but with specific explanation of the figures included in this report:

"The importance of including the molar concentration of the solvent as a variable in the equilibrium constant (K°) is discussed. When the solvent is considered to participate actively in the equilibrium, isothermal values of K° are found to be independent of changes in dielectric constant of the solvent mixtures. Extensive examples are given in support of this general principle. The new principle contrasts with existing theory that considers $\log K$ (the conventional constant not containing solvent species as concentration variables) to be a linear function of $1/D$. It is shown to apply to electrolyte behavior in water, water-organic, and organic-organic solvent systems over a wide range of temperature and pressure. For example, in water-dioxane solvent mixtures where

⁷A. S. Quist, W. L. Marshall, and W. Jennings, Jr., *Reactor Chem. Div. Ann. Progr. Rept. Dec. 31, 1966*, ORNL-4076, pp. 65-66.

⁸W. L. Marshall and A. S. Quist, *Proc. Natl. Acad. Sci. U.S.* **58**, 901 (1967).

⁹A. S. Quist and W. L. Marshall, "The Independence of Isothermal Equilibria in Electrolyte Solutions on Changes in Dielectric Constant," *J. Phys. Chem.* (1967), in press.

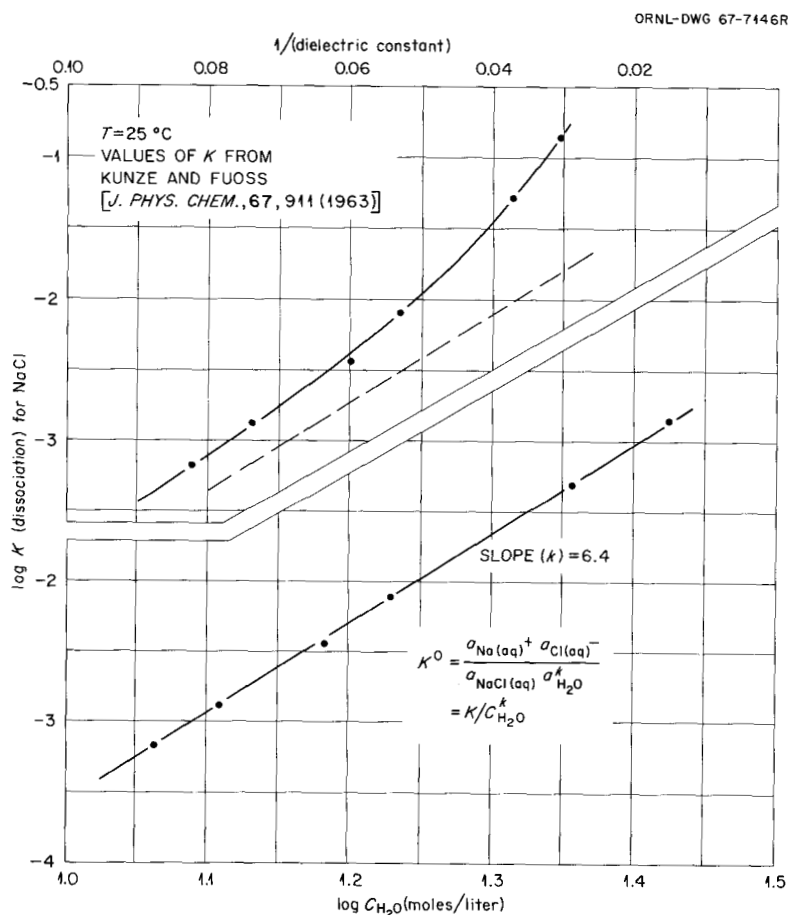


Fig. 5.5. Log K (dissociation) of Sodium Chloride vs $C_{\text{H}_2\text{O}}$ (moles/liter) in Dioxane-Water Mixtures; Also Compared vs $1/(\text{Dielectric Constant}, D)$.

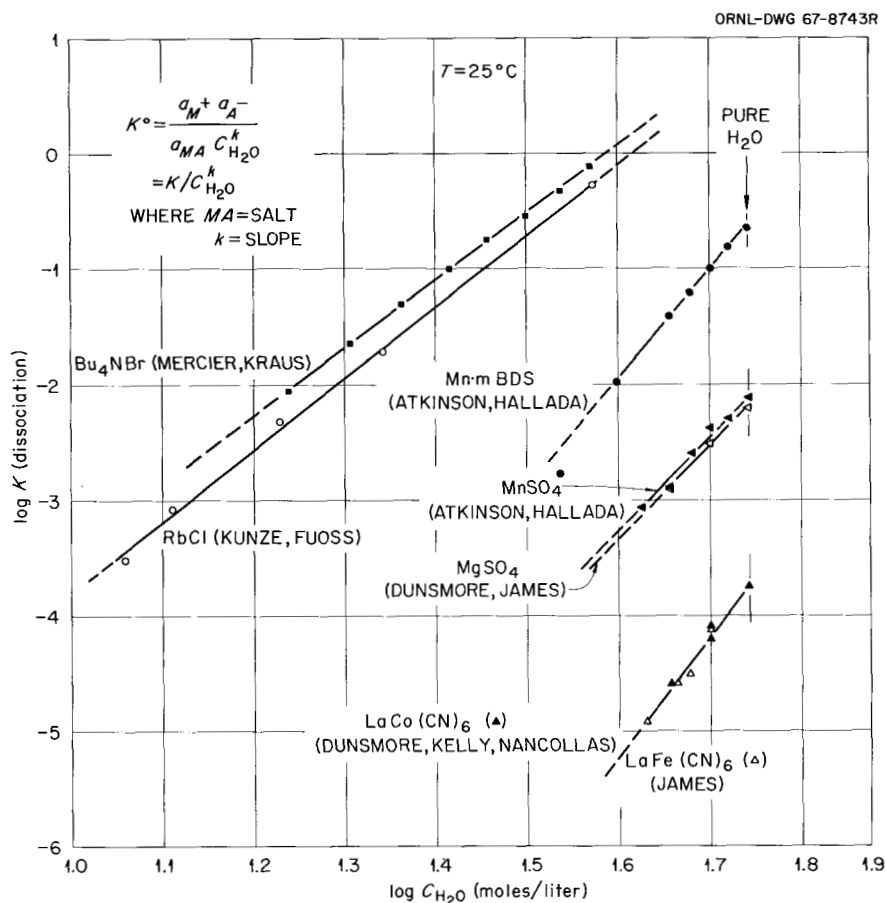


Fig. 5.6. Logarithm of the Conventional Equilibrium Constant K for Several Salts vs C_{H_2O} (moles/liter) in Dioxane-Water Mixtures; $t = 25^\circ\text{C}$.

electrolytes (ions and polar molecules) are preferentially solvated by water molecules, a plot of $\log K$ (dissociation) vs $\log C_{H_2O}$ in moles/liter yields a straight line of intercept K° and slope representing the net change in waters of solvation between equilibrium reactants and products." Examples of this type of plot are shown in Figs. 5.5 and 5.6.

ELECTRICAL CONDUCTANCES OF AQUEOUS ELECTROLYTE SOLUTIONS FROM 0 TO 800°C AND TO 4000 BARS

A. S. Quist⁴ W. Jennings, Jr.
W. L. Marshall

Extensive conductance measurements have been made on several representative electrolytes at temperatures to 800°C and pressures to 4000 bars.

In this high-temperature, high-pressure region, it is desirable that we investigate completely several systems to look for general behavior applicable to all electrolyte systems. With this goal, studies of sodium chloride, sodium bromide, hydrobromic acid, and ammonia in water solution have been completed, and papers are in press.¹⁰⁻¹³ The

¹⁰ A. S. Quist and W. L. Marshall, "Electrical Conductances of Aqueous Sodium Chloride Solutions from 0 to 800°C and at Pressures to 4000 Bars," *J. Phys. Chem.* (1967), in press.

¹¹ A. S. Quist and W. L. Marshall, "Electrical Conductance of Aqueous Sodium Bromide Solutions from 0 to 800°C and at Pressures to 4000 Bars," *J. Phys. Chem.* (1967), in press.

¹² A. S. Quist and W. L. Marshall, "Electrical Conductances of Aqueous Hydrogen Bromide Solutions from 0 to 800°C and at Pressures to 4000 Bars," *J. Phys. Chem.* (1967), in press.

¹³ A. S. Quist and W. L. Marshall, "Ionization Equilibria in Ammonia-Water Solutions to 700°C and to 4000 Bars Pressure," *J. Phys. Chem.* (1967), in press.

following subsections summarize the results and conclusions from these particular studies.

Conductance of Sodium Chloride

The conductance behavior of sodium chloride solutions was reported in some detail in the 1966 Reactor Chemistry Division annual report.⁷ The final experimental portion and interpretation of results was completed during this year (1967), and a paper is in press.¹⁰ The following abstract from the paper summarizes this work:

The electrical conductances of aqueous sodium chloride solutions (0.001 to 0.1 *m*) have been measured to temperatures of 800°C and at pressures to 4000 bars. Limiting equivalent conductances for NaCl were calculated at integral temperatures and densities, and they were found to be a linear function of density (at constant temperature). Moreover, above 400°C at constant density, $\Lambda_0(\text{NaCl})$ was essentially independent of temperature. Conventional ionization constants for the equilibrium $\text{NaCl} \rightleftharpoons \text{Na}^+ + \text{Cl}^-$ were obtained above 400°C at solution densities below 0.8 g cm⁻³. Sodium chloride behaves as a weaker electrolyte as temperature increases (at constant solution density) and as solution density decreases (at constant temperature). From the conventional ionization constants (constant only at constant density) the complete constants that include the concentration of water as a reactant were obtained. These complete constants (K°) are truly independent of solvent density or pressure, and depend only on temperature.^{8,9}

Conductance of Sodium Bromide

In order to investigate extensively another 1-1 electrolyte for comparison with sodium chloride, the conductances of sodium bromide solutions were measured to 800°C and 4000 bars. The abstract of the paper in press¹¹ is given as follows but with some added explanation for the included figures:

The electrical conductances of dilute (0.002 to 0.015 *m*) NaBr solutions were measured from 0 to 800°C and to 4000 bars pressure. Isothermal limiting equivalent conductances were calculated from these measurements and were found to be linear functions of the solvent density. At temperatures of 400°C and above, at constant solvent

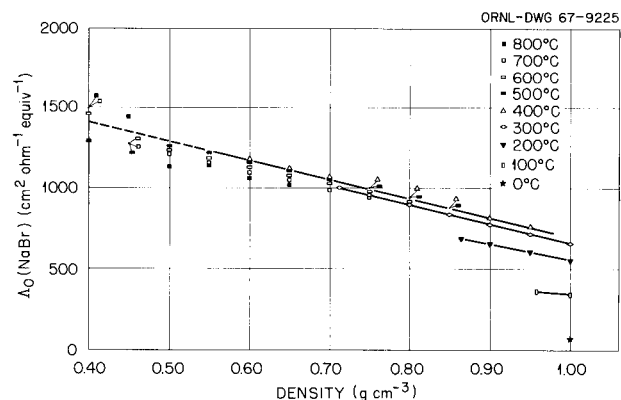


Fig. 5.7. Limiting Equivalent Conductance of NaBr as a Function of Density at Temperatures to 800°C.

density, $\Lambda_0(\text{NaBr})$ was essentially independent of the temperature; moreover, the value of the limiting equivalent conductance extrapolated to zero solvent density (1880 cm² ohm⁻¹ equivalent⁻¹), as indicated in Fig. 5.7, was very close to those obtained previously for other 1:1 electrolytes, signifying that perhaps all 1-1 electrolytes may have nearly the same value of limiting equivalent conductance under these conditions. Equilibrium constants (K) for the ionization of NaBr were calculated from the data at high temperatures where NaBr behaves as a weak electrolyte. The logarithm of K is plotted against the logarithm of the molar concentration of water (C) in Fig. 5.3, where the value of the slope represents the net change in waters of hydration. By considering hydration to be an essential part of the dissociation process, isothermal equilibrium constants were obtained that were independent of solvent density.^{8,9}

Conductance of Hydrobromic Acid

The conductances of aqueous hydrobromic acid were obtained for several concentrations to the extremes of temperature and pressure. This acid was chosen for its relative thermal stability and its common anion, Br⁻, with sodium bromide studied previously. An abstract of the paper currently in press¹² is given as follows:

The electrical conductances of dilute (0.002 to 0.015 *m*) aqueous hydrogen bromide solutions have been measured at temperatures to 800°C and at

pressures to 4000 bars. Limiting equivalent conductances for HBr were calculated at integral temperatures and densities under conditions where it behaved as a strong or moderately strong electrolyte. Hydrobromic acid becomes progressively a weaker electrolyte as the temperature increases and the solution density decreases. Conventional equilibrium constants for the ionization of HBr were calculated from the conductance measurements at temperatures of 400°C and above, and at densities below 0.85 g cm⁻³. By considering hydration to be an essential part of the ionization process, values of the isothermal, complete equilibrium constant (K°) were obtained that were independent of density, as evidenced by the linear relationships of $\log K$ vs $\log C_{\text{H}_2\text{O}}$ shown in Fig. 5.4. The slope at each temperature represents the net change in waters of hydration in a reaction equilibrium described by K° .^{8,9}

Conductance of Ammonia-Water Solutions

Conductances of ammonia solutions were measured to 800°C because of its importance as a base, and to answer the question concerning its basicity at very high temperatures relative to a strong base such as sodium hydroxide. Some measurements were obtained also on sodium hydroxide solutions. An abstract of the paper in press¹³ is given below, with additional explanation on the figure included in this report:

The electrical conductances of 0.0100 and 0.0501 *m* aqueous ammonia solutions were measured to 800°C and 4000 bars. The set of curves of equiv-

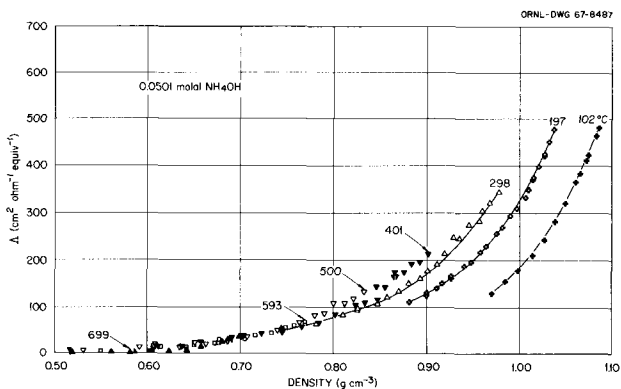


Fig. 5.8. Equivalent Conductances of 0.0501 *m* NH₄OH Solutions as a Function of Density at Several Temperatures.

alent conductance vs density for 0.0501 *m* solutions are shown in Fig. 5.8. Measurements are also reported for 0.0098 *m* NaOH solutions to 300°C, together with estimates of $\Lambda_0(\text{NaOH})$ over the same temperature range. From the measurements on the ammonia solutions, and estimates of the limiting equivalent conductances of ammonium hydroxide, conventional equilibrium constants for the hydrolysis of ammonia were calculated. From these values and their isothermal variation with the concentration of water, the complete constants, K° , were obtained that are independent of changes in dielectric constant or of density.^{8,9}

EFFECT OF ADDED ELECTROLYTES ON THE CRITICAL TEMPERATURE OF WATER

E. V. Jones¹⁴ W. L. Marshall

Very few measurements exist on the effect of electrolytes on the critical temperature of water, an extremely important phenomenon in phase equilibria both as an observation and for interpretation. This lack of information probably arises from the relative difficulty in obtaining results. The values either must be obtained by making extensive *PVT* measurements, where the critical temperature (T_c) is obtained indirectly by determining the point on a *PVT* diagram where $dV/dP \rightarrow \infty$, or by direct sampling and analysis both of liquid and vapor phases until identity of compositions is reached.¹⁵ A simpler method, and the one that we use, involves the direct, visual determination of the disappearance with temperature of the meniscus between the liquid and vapor phases. In order to distinguish a true T_c from an apparent T'_c , the observation must be made where the liquid volume is equal to the vapor volume. For each electrolyte concentration, therefore, measurements of T'_c must be made at several apparent liquid-volume to vapor-volume fillings (R) and these values of T'_c then plotted vs R to obtain T_c at $R = \text{unity}$.¹⁶ In this program, with the use of apparatus and visual techniques developed previously,¹⁷ exten-

¹⁴Consultant.

¹⁵S. Sourirajan and G. C. Kennedy, *Am. J. Sci.* **260**, 115 (1962).

¹⁶W. L. Marshall and E. V. Jones, *J. Inorg. Nucl. Chem.* **25**, 1021 (1963).

¹⁷C. J. Barton, G. M. Hebert, and W. L. Marshall, *J. Inorg. Nucl. Chem.* **21**, 141 (1961).

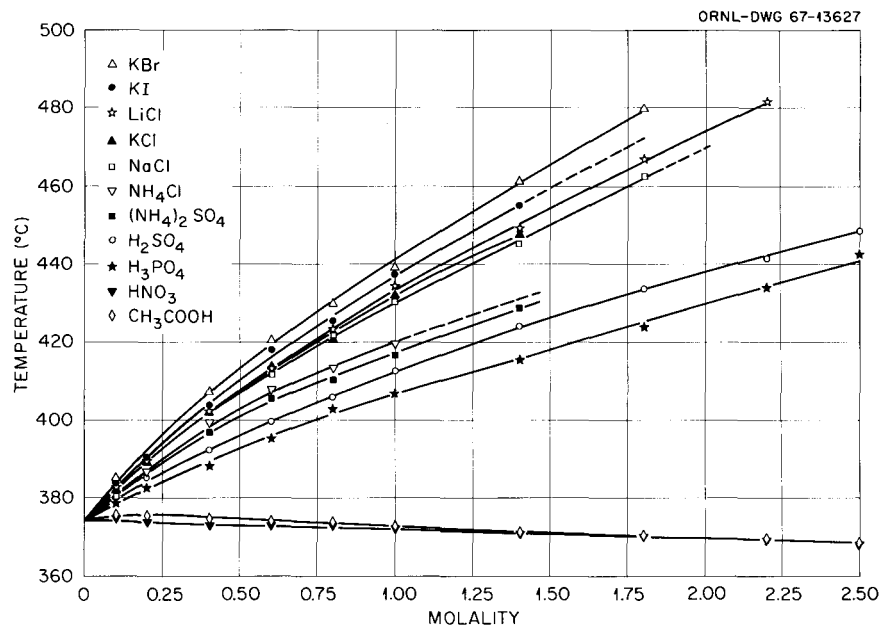


Fig. 5.9. The Effect of Added Electrolytes on the Critical Temperature of Water; Set I.

sive determinations of T_c for many aqueous electrolytes have been obtained as a function of molality to 1.5–2.5 *m*. Comparisons with a few previously published values on 1-1 electrolytes,^{18–20} for the most part at low molalities, and on H_2SO_4 ²¹ show reasonably good agreement. The calculated values of Secoy²¹ also agree reasonably well. The electrolytes studied in this program were as follows:

KBr	KHSO ₄	NH ₄ Cl	CH ₃ COOH
KI	CsNO ₃	(NH ₄) ₂ SO ₄	HNO ₃
KCl	CaCl ₂	H ₂ SO ₄	HCl
LiCl	(NH ₄) ₂ CO ₃	H ₃ PO ₄	HClO ₄ ^a
NaCl	NH ₄ HCO ₃		H ₃ BO ₃

^aDecomposes to HCl.

The effect of these added electrolytes on the critical temperature of water ($T_c = 374^\circ$ for pure water) is shown in Figs. 5.9 and 5.10, where each separate value for each molality is the critical temperature T_c obtained by interpolation of T'_c to

$R = 1$. The (apparent) behavior of $HClO_4$, however, represents the behavior of HCl, since $HClO_4$ decomposed rapidly at temperatures above $300^\circ C$ to release oxygen. By inserting a silica capillary tube containing $HClO_4$ into our molten-salt bath¹⁷ at an initial temperature just below T'_c , a very approximate value of T'_c for $HClO_4$, in the vicinity of those for other 1-1 electrolytes, could be obtained before the complete, rapid decomposition to HCl.

The overall results show some systematic behavior in that the 1-1 salts all produce about the same effect on T_c , and a 1-2 acid (H_2SO_4) shows a smaller effect, although at these high temperatures H_2SO_4 behaves predominantly as a 1-1 acid. The 1-1 acids (HCl and HNO_3) show a very small effect, probably reflecting the large amount of association at high temperature.

The very large increase in critical temperature (about $75^\circ C$ for a 1 *m* salt solution such as $KHSO_4$) is to be noted. Contrast this behavior with the approximately $0.5^\circ C$ rise in boiling point (at 1 atm pressure) for a 1 *m* salt solution. The results presented herein might be used for calculating other properties of the respective electrolyte systems, such as those performed by Bien.²² Additional interpretation is planned.

¹⁸E. Schroer, *Z. Physik. Chem.* **129**, 79 (1927).

¹⁹A. Ölander and H. L. Liander, *Acta Chem. Scand.* **4**, 1437 (1950).

²⁰J. E. Stuckey and C. H. Secoy, *J. Chem. Eng. Data* **8**, 386 (1963).

²¹C. H. Secoy, *J. Phys. Colloid Chem.* **54**, 1337 (1950).

²²P. B. Bien, *J. Phys. Chem.* **71**, 2731 (1967).

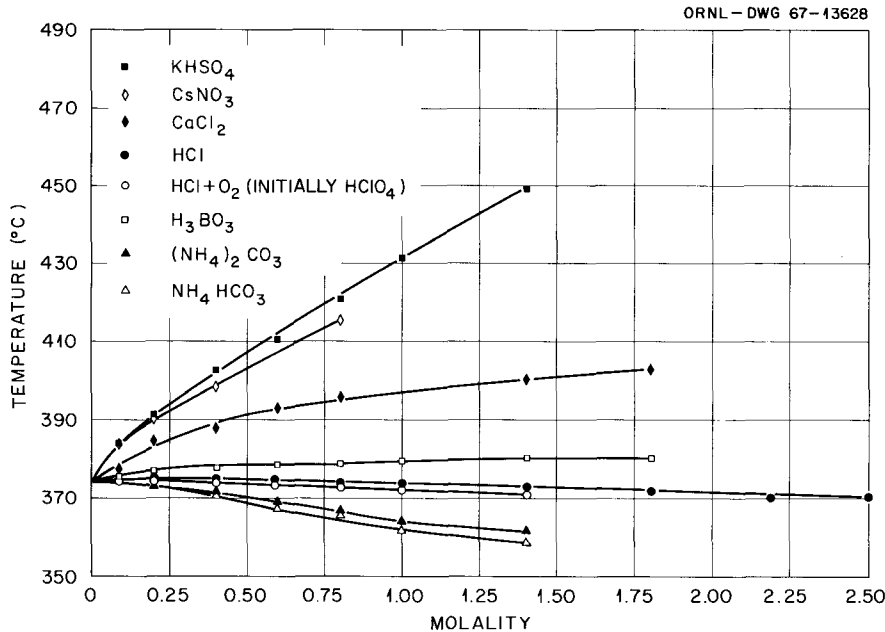
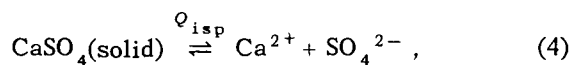
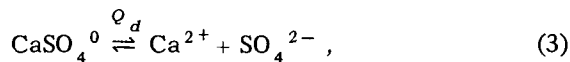
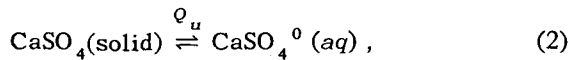


Fig. 5.10. The Effect of Added Electrolytes on the Critical Temperature of Water; Set II.

ACTIVITY COEFFICIENTS, ASSOCIATION BEHAVIOR, AND THERMODYNAMIC FUNCTIONS OF CALCIUM SULFATE IN AN AQUEOUS MIXED ELECTROLYTE TO 350°C²³

L. B. Yeatts W. L. Marshall

The first experimental results and interpretations of the solubility of calcium sulfate in the mixed electrolyte system sodium nitrate-sodium sulfate have been reported.²⁴ At each ionic strength the complete solubility equilibria could be represented by a combination of two of the following equilibria:



²³Jointly sponsored by the USAEC and the Office of Saline Water, U.S. Dept. of Interior.

²⁴L. B. Yeatts and W. L. Marshall, *Reactor Chem. Div. Ann. Progr. Rept. Dec. 31, 1966, ORNL-4076*, pp. 68-70.

where Q_u , Q_d , and Q_{isp} are equilibrium quotients and Q_u equals also the molality of CaSO_4^0 . Since

$$s = [\text{CaSO}_4^0] + [\text{Ca}^{2+}] \quad (5)$$

$$= Q_u + Q_{isp}/(\text{total sulfate} - Q_u) \quad (6)$$

$$= Q_u + Q_{isp}/[\text{SO}_4^{2-}], \quad (7)$$

where s = analytical molality of total calcium, a plot of s vs $1/[\text{SO}_4^{2-}]$ yielded a slope Q_{isp} and intercept Q_u , as discussed in detail previously.²⁴ The experimental results have indeed shown that for this system and with this model the activity coefficients of the ions and of the ion pair at constant ionic strength are independent of the composition of supporting electrolyte, NaNO_3 - Na_2SO_4 .

Many additional data have now been obtained that allow further interpretation of the behavior of activity coefficients as a function of I not only for the ions, Ca^{2+} and SO_4^{2-} , but for the neutral ion pair, CaSO_4^0 . The activity coefficient behavior of this latter species (CaSO_4^0) is of very great importance since, to our knowledge, it represents the first experimentally determined example for a neutral, but polar, species in ionic solutions. In most applications in ionic media, the logarithm of the activity coefficient of the

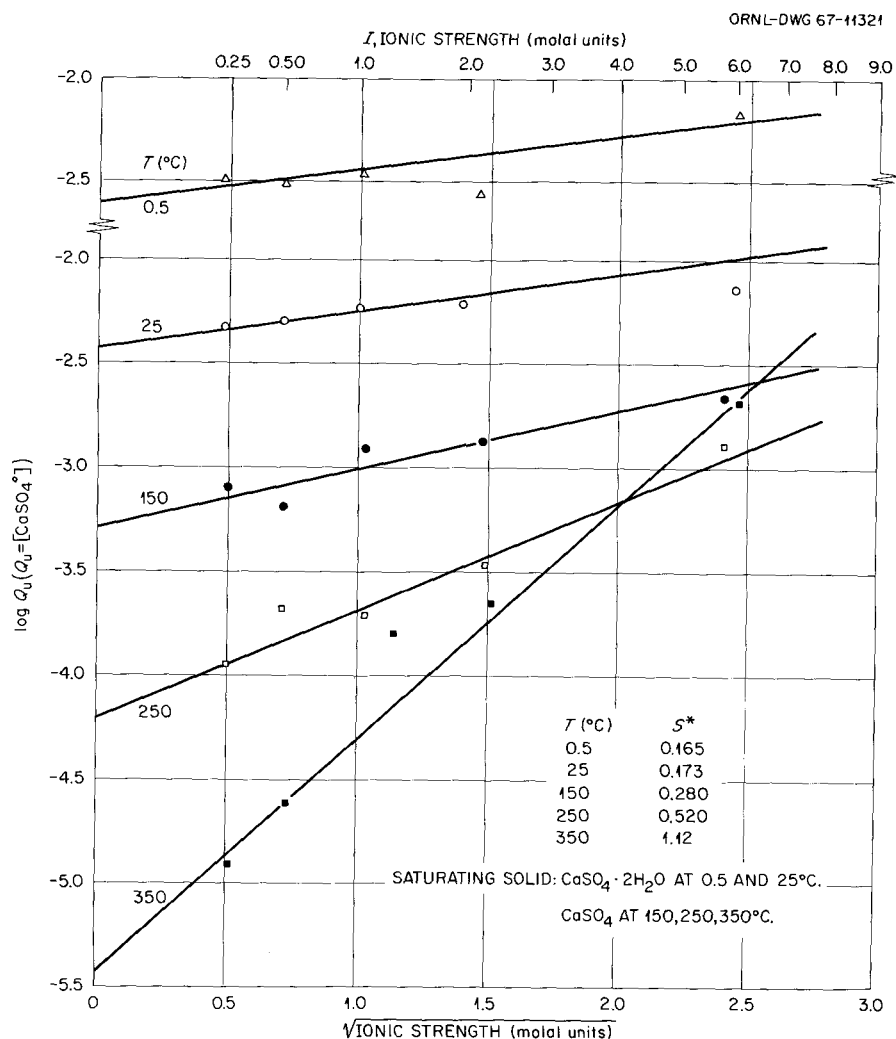


Fig. 5.11. Relationship Between Ionic Strength and Molality of Associated CaSO_4 from 0.5 to 350 $^{\circ}\text{C}$.

neutral species is assumed to be independent of ionic strength (I) or, for lack of experimental information, is estimated to be a linear function of I according to one theory. The variation of the saturation molality of the neutral species CaSO_4^0 with ionic strength as determined by the methods presented previously²⁴ is shown in Fig. 5.11 at temperatures from 0 to 350 $^{\circ}\text{C}$. The slopes that are drawn correspond to the best least-squares determination from the data shown. In actuality, the solubility values first were fitted to an expression

$$\log Q_u = \log K_u + S^* \sqrt{I} / (1 + A^* \sqrt{I}), \quad (8)$$

where S^* and A^* are adjustable parameters and K_u represents the solubility concentration of

CaSO_4^0 at zero ionic strength, the selected reference state for all solute species. With this approach, the least-squares values of A^* were found to be approximately zero, within the precision of the values of Q_u , from 0 to 350 $^{\circ}\text{C}$; therefore the term $A^* \sqrt{I}$ was considered unnecessary (Fig. 5.11). The significance of the parameter S^* is believed to be attributed to a polar characteristic of CaSO_4^0 . Although Eq. (8) would correspond to that for extended Debye-Hückel theory if S^* were the theoretical Debye-Hückel limiting slope S , the values of S^* are approximately one-half of S for a 1+ ion. Since the calculated limiting slope S varies inversely with the three-halves power of dielectric constant (D) times T ($^{\circ}\text{K}$), it was of interest to compare the variation of S^* with DT . Figure 5.12 shows a plot of $\log S$ and of \log

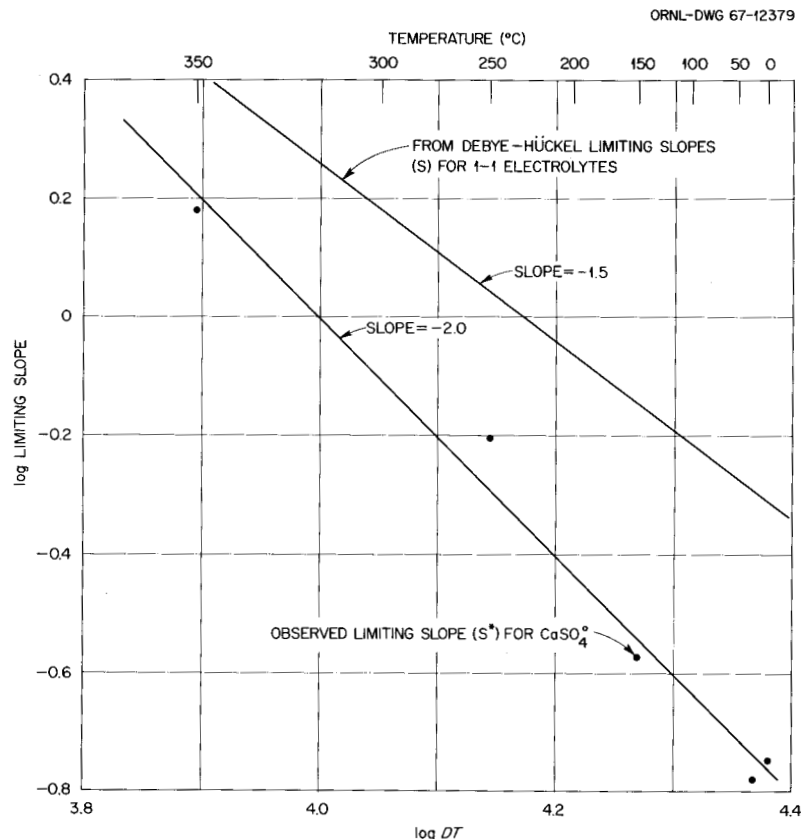


Fig. 5.12. Dependence of the Limiting Slope for CaSO_4^0 upon the Product of Dielectric Constant and Temperature.

S^* vs $\log(DT)$ where the exponent of (DT) is equal to the slope. The slope for $\log S$ vs $\log(DT)$ must be $-\frac{3}{2}$ by calculation; the interesting observation is that the slope for $\log S^*$ vs $\log(DT)$ is -2 . This proportionality of S^* with $(DT)^{-2}$ is in agreement with theory²⁵ and may therefore have significance in calculating limiting slopes for neutral species in ionic solutions where the polar (or charge interaction) characteristic of neutral species is considered.

From all measurements and the subsequent extrapolations to infinite dilution of electrolyte, the dissociation constant (K_d), ionic solubility product (K_{isp}), and neutral species constant (K_u) were obtained at the several temperatures (0 to 350°C). These values are plotted vs $1/T$ in Fig. 5.13. Some representative thermodynamic functions for the dissociation of $\text{CaSO}_4(aq)$, calculated from the temperature variation of K_d , are given in Table 5.1.

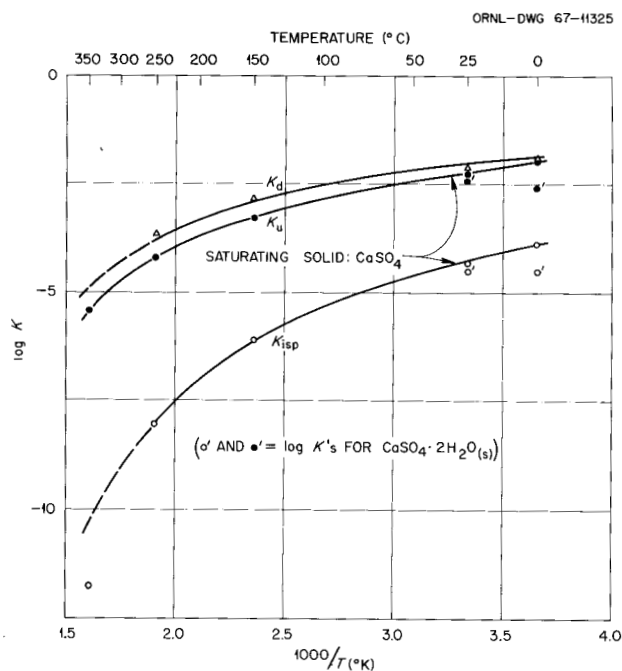


Fig. 5.13. Equilibrium Constants and Ionic Solubility Product Constants for CaSO_4 from 0.5 to 350°C.

²⁵J. G. Kirkwood, *Chem. Rev.* 24, 233 (1939).

Table 5.1. Thermodynamic Functions for the Dissociation Equilibrium $\text{CaSO}_4^0(aq) \rightleftharpoons \text{Ca}^{2+}(aq) + \text{SO}_4^{2-}(aq)$

T (°C)	K_d	ΔG° (kcal/mole)	ΔH° (kcal/mole)	ΔS° (cal mole ⁻¹ deg ⁻¹)
0.5	1.17×10^{-2}	2.41	-1.11	-12.9
25	9.29×10^{-3}	2.77	-1.93	-15.8
50	6.83×10^{-3}	3.20	-2.81	-18.6
100	3.13×10^{-3}	4.27	-4.80	-24.3
150	1.23×10^{-3}	5.63	-7.07	-30.0
200	4.35×10^{-4}	7.28	-9.63	-35.7
250	1.42×10^{-4}	9.21	-12.5	-41.5
300	4.40×10^{-5}	11.4	-15.6	-47.2
350	1.30×10^{-5}	13.9	-19.0	-52.9

THE LANTHANUM FLUORIDE ELECTRODE RESPONSE IN AQUEOUS CHLORIDE MEDIA

R. E. Mesmer

With the recent introduction of solid-state electrodes, very sensitive analytical tools have become available for several anions. The best characterized of these is the lanthanum fluoride electrode doped with Eu^{2+} .²⁶⁻²⁸ The sensitivity of this fluoride electrode is at least 1000-fold for fluoride over chloride.^{26,28} Because equilibrium studies in aqueous solutions are commonly conducted in the presence of a relatively high concentration of "inert electrolyte" to control the ionic strength of the medium, the magnitude of the electrode interference from the medium could be a limiting factor. As a result of our interest in the use of chloride media at this Laboratory we have examined in detail the chloride interference at 25°C.

A Teflon cell was employed with a reference H_2 electrode and with a fluoride electrode (Orion model 94 09) and a second H_2 electrode in the titration compartment. For experiments designed to observe any interference of chloride, 1.00 *m* chloride solutions were prepared from three different sources of purified chloride: NaCl (Baker and Adamson Reagent Grade) recrystallized once from water (I); NaCl prepared from Fisher Certified

NaOH and Baker Analyzed Reagent HCl (II); and KCl prepared as a large single crystal of very high purity at Oak Ridge National Laboratory (III).

The pH of 1.00 *m* solutions of chlorides I, II, and III was adjusted to 6-7, and dilute fluoride solutions in 1 *m* chloride were added incrementally to obtain the data in Fig. 5.14.

Several possible causes for the deviation from Nernst behavior at low fluoride concentrations can be eliminated without difficulty, but chloride interference and a fluoride impurity in the purified chloride cannot be distinguished by a single experiment. If the experimental data in Fig. 5.14 are corrected for an assumed fluoride impurity in the chloride, then Nernst behavior is obtained down to about 8×10^{-6} *m* fluoride. The corrections which give straight lines with the Nernst slope require 6.5×10^{-5} *m*, 1.5×10^{-5} *m*, and 6.0×10^{-6} *m* fluoride concentrations, respectively, for solutions I, II, and III. Because these concentrations are different for the three 1.00 *m* chloride solutions, the effect clearly cannot be due to chloride alone. Chloride interference must depend on the chloride concentration (which was constant in these three experiments).

The cause of the deviation was unequivocally identified as fluoride impurity by determination of the HF dissociation constant in one of these solutions by adding acid and then measuring $[\text{H}^+]$ with the hydrogen electrode and $[\text{F}^-]$ with the fluoride electrode. The dissociation constant obtained, $(1.29 \pm 0.07) \times 10^{-3}$, is in precise agreement with carefully determined values of the HF dissociation constant measured at higher concentrations of fluoride in 1 *m* NaCl. From the data

²⁶M. S. Frant and J. W. Ross, Jr., *Science* **154**, 1553 (1966).

²⁷J. J. Lingane, *Anal. Chem.* **39**, 881 (1967).

²⁸G. A. Rechnitz, *Chem. Eng. News*, 147 (1967).

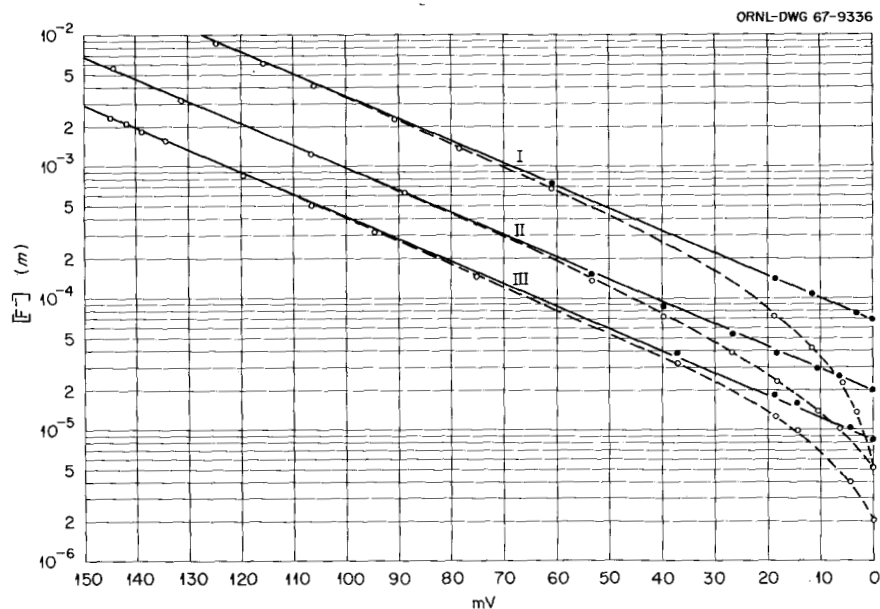


Fig. 5.14. Potential of the Fluoride Electrode vs Fluoride Concentration in 1.00 *m* Chloride Solutions Prepared from Three Sources of Chloride. The reference cell solution composition was different in each experiment. Open circles – experimental data; closed circles – data corrected for assumed fluoride impurities of 6.5×10^{-5} *m* (I), 1.5×10^{-5} *m* (II), and 6.0×10^{-6} *m* (III); solid curves – calculated Nernst plots.

on the dissociation constant the selectivity of the electrode for fluoride over chloride can be set at $>5 \times 10^7$. With the wide range of Nernst behavior (to $<2 \times 10^{-7}$ *m*) and the absence of significant chloride interference, this electrode appears to be useful for measurement of fluoride impurities to <1 ppm in chlorides and for complexing studies in chloride or other media involving metal ions which complex fluoride strongly giving rise to very low levels of free fluoride.

BERYLLIUM FLUORIDE COMPLEXES IN AQUEOUS CHLORIDE AND PERCHLORATE MEDIA

R. E. Mesmer C. F. Baes, Jr.

The stability and composition of beryllium fluoride complexes in aqueous media have not been well defined, although some attempts have been reported.²⁹⁻³¹ The lack of reversible electrodes

for either beryllium or fluoride has contributed to the difficulty of these studies. With the newly developed lanthanum fluoride electrode discussed in the previous section, this and other similar systems can now be examined with much greater ease and reliability.

With the Teflon cell described in the previous section, measurements of H^+ and F^- concentrations have been obtained at 25°C in 1 *m* NaCl and in 1 *m* NaClO₄ for analysis of the hydrogen fluoride and beryllium fluoride equilibria. In the absence of beryllium, the data are consistent with equilibria involving F^- , HF, and HF_2^- species. Results obtained for beryllium complexing under widely varying conditions in 1 *m* NaCl are shown in Fig. 5.15. The variation of component concentrations is summarized as follows: total beryllium concentration, 4×10^{-4} to 2×10^{-2} *m*; total fluoride concentration, 6×10^{-4} to 4×10^{-2} *m*; free acidity, 2×10^{-2} to 1×10^{-2} *m*; and free fluoride, 2×10^{-6} to 4×10^{-2} *m*. All these data fall on a single curve for a plot of \bar{n} (average number of fluoride ions bound per beryllium in solution) vs $-\log$ free fluoride concentration (*f*). This indicates the absence of polynuclear complexes as well as complexes containing either H^+ ions or OH^- ions. The most sensitive measure of the

²⁹L. M. Yates, Thesis, State College, Wash., 1955, Univ. Microfilms 15662.

³⁰C. J. Hardy, B. F. Greenfield, and D. Scargill, *J. Chem. Soc.* 174 (1961).

³¹K. E. Kleiner, *Zh. Obshch. Khim.* 21, 18 (1951).

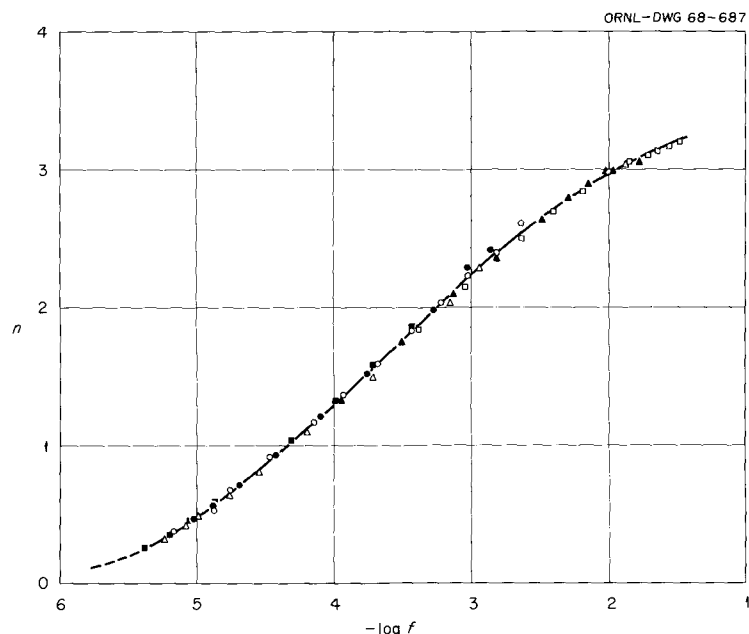


Fig. 5.15. Average Number of Fluorides Bound per Beryllium in Solution vs Free Fluoride Concentration as the Total Beryllium, Total Fluoride, and Free Acidity Were Varied Widely in Several Experiments in 1 *m* NaCl at 25°C.

level of existence of the latter was obtained from titrations of BeCl_2 solutions (without excess acid) into neutral NaF solutions. The very small pH change proves that the hydroxide complexed is less than 0.5% of the beryllium at $n \geq 1.5$.

The overall formation constants for complexes, and their standard errors, were computed by means of a nonlinear least-squares program with the use of data from both hydrogen and fluoride electrodes. Results are summarized in Table 5.2. (A refinement in the small liquid junction correction resulting from the consideration of contributions of the complexes themselves will be made.) The small difference in the constants in 1.00 *m* NaCl and in 1.00 *m* NaClO_4 is accountable as an activity coefficient effect, so that the assumption of a species such as BeCl^+ is not warranted by these data. Also, the significance of the larger increment for the constant for the last stepwise formation reaction has not yet been explained, although it seems unlikely that simple considerations of statistical or electrostatic factors will account for the behavior. A steric effect is being considered, since in the BeF_4^{2-} ion the anions are in close contact based on Pauling's ionic radii. Equilibrium data will also be obtained at 60°C to determine whether this effect is reflected in the entropy and/or enthalpy of the reaction.

Table 5.2. Log *K* for Beryllium Fluoride Equilibria at 25°C^a

<i>x</i>	Log <i>K</i> in —		
	1.00 <i>m</i> NaCl	1.00 <i>m</i> NaClO_4	0.5 <i>m</i> NaClO_4 ^b
Overall Formation Reactions:			
$\text{Be}^{2+} + x\text{F}^- = \text{BeF}_x^{(2-x)+}$			
1	4.901 ± 0.013	4.985 ± 0.015	5.08
2	8.673 ± 0.016	8.769 ± 0.016	8.88
3	11.439 ± 0.016	11.548 ± 0.017	11.9
4	12.472 ± 0.028	12.604 ± 0.032	
Stepwise Formation Reactions:			
$\text{BeF}_{x-1}^{(3-x)+} + \text{F}^- = \text{BeF}_x^{(2-x)+}$			
1	4.901 ± 0.013	4.985 ± 0.015	
2	3.772 ± 0.021	3.784 ± 0.022	
3	2.766 ± 0.023	2.779 ± 0.024	
4	1.033 ± 0.032	1.056 ± 0.036	

^aRefinements will be made in the liquid junction corrections used for these data.

^bL. M. Yates, Thesis, State College, Washington, 1955, Univ. Microfilms 15662.

The maximum amounts of the species formed, expressed as percent of the beryllium, in 1 *m* NaCl at 25° are: BeF^+ , 65%; BeF_2 , 60%; BeF_3^- , 79%; and BeF_4^{2-} , 100%. The amount of BeF_4^{2-} is not greater than 95% until the concentration of

free fluoride exceeds 2 *m*. These results explain ^{19}F n.m.r. results reported by Kotz *et al.* within the last year.³²

The Raman spectrum³³ of a 3 *m* $(\text{NH}_4)_2\text{BeF}_4$ solution in 2.6 *m* NH_4F exhibits low-intensity peaks assigned to BeF_4^{2-} at 544 cm^{-1} (ν_1) and 800 cm^{-1} (ν_3), which is consistent with a tetrahedral structure having highly ionic bonding. The low-intensity peaks expected between 300 and 500 cm^{-1} are masked by broad peaks in the background in this region.

THE HYDROLYSIS OF BERYLLIUM(II) IN 1 *m* NaCl ³⁴

R. E. Mesmer C. F. Baes, Jr.

The investigation of the hydrolysis behavior of beryllium(II), described previously,³⁵ has now been completed. Of the previous work the most authoritative is that of Kakihana and Sillén in 1956.³⁶ They proposed a scheme of three species to explain potentiometric data in 3 *M* NaClO_4 media, that is, $\text{Be}_2(\text{OH})^{3+}$, $\text{Be}_3(\text{OH})^{3+}$, and $\text{Be}(\text{OH})_2$. Several arguments have been raised³⁴ challenging the existence of the neutral $\text{Be}(\text{OH})_2$ species at the levels predicted on the basis of the results of Kakihana and Sillén, and for this reason a thorough investigation of the hydrolysis behavior of Be(II) was undertaken.

Potentiometric measurements were made in 1 *m* chloride with hydrogen electrodes at 0 and 60°C and with a quinhydrone electrode at 25°C. Liquid-junction corrections were made by means of the Henderson equation. Beryllium concentrations between 0.022 and 0.05 *m* and pH values between 2 and 7 were covered.

Results were analyzed by techniques previously employed at ORNL. Conclusions are based on the view that the best fit is that given by the simplest scheme – the one consisting of the fewest species – which fits the data within the experi-

mental error. Consideration of the nature of plots of \bar{n} (ligand number) vs $\log h$ (free acidity) and $\log \bar{n}$ vs $\log h$ shows that one species cannot account for all data. After placing the necessary restrictions and testing a large number of possible two-species schemes it was apparent that only data below an \bar{n} of 0.5 could be fitted. The composition of the required third species was determined by allowing x and y to vary in the formula $\text{Be}_x(\text{OH})_y^{(2x-y)+}$. The best three-species fit based on several criteria was given by the scheme $\text{Be}_2\text{OH}^{3+}$, $\text{Be}_3(\text{OH})_3^{3+}$, and $\text{Be}_5(\text{OH})_7^{3+}$, although the effect of replacing the third species by $\text{Be}_6(\text{OH})_8^{4+}$ is not great. A detailed analysis of the experimental errors shows that inclusion of additional species beyond three is unwarranted. Figure 5.16 shows plots of the data at the three temperatures and compares the presently proposed three-species scheme with the scheme of Kakihana and Sillén.

The thermodynamic quantities for the formation of these hydrolysis products are tabulated in Table 5.3 along with those for several metal ions for which temperature coefficient data are available. The average ΔH° per hydroxide, $\Delta H^\circ/y$, is found to be surprisingly constant in all cases, 7.6 ± 1.6 kcal per hydroxide. A correlation of this nature was pointed out originally by Baes *et al.* for the UO_2^{2+} and Th^{4+} systems.^{37,38} This value is slightly more than half the value for the neutralization of a strong acid, a somewhat analogous reaction involving the hydrogen ion. The average $\Delta S^\circ/y$ (hypothetical mole fraction unity standard state) shows more variation, 36 ± 10 e.u. However, a correlation with z^2 , the charge on the unhydrolyzed metal ion squared, gives the relationship

$$\Delta S^\circ/y = 28 + 1.0z^2,$$

with an average deviation of 3.0 e.u. and a maximum deviation of 5.6 e.u. This correlation probably indicates a real dependence of ΔS° on y and z , which is believed to be related largely to the change in hydration of the unhydrolyzed ion compared with that of the hydrolyzed species. More data of this type are needed to test the generality of this correlation.

³²J. C. Kotz, R. Schaeffer, and A. Clouse, *Inorg. Chem.* **6**, 620 (1967).

³³Spectra recently obtained by G. M. Begun of Chemistry Division.

³⁴R. E. Mesmer and C. F. Baes, Jr., *Inorg. Chem.* **6**, 1951 (1967).

³⁵*Reactor Chem. Div. Ann. Progr. Rept. Dec. 31, 1966, ORNL-4076, p. 72.*

³⁶H. Kakihana and L. G. Sillén, *Acta Chem. Scand.* **10**, 985 (1956).

³⁷C. F. Baes, Jr., N. J. Meyer, and C. F. Roberts, *Inorg. Chem.* **4**, 518 (1965).

³⁸C. F. Baes, Jr., and N. J. Meyer, *Inorg. Chem.* **1**, 780 (1962).

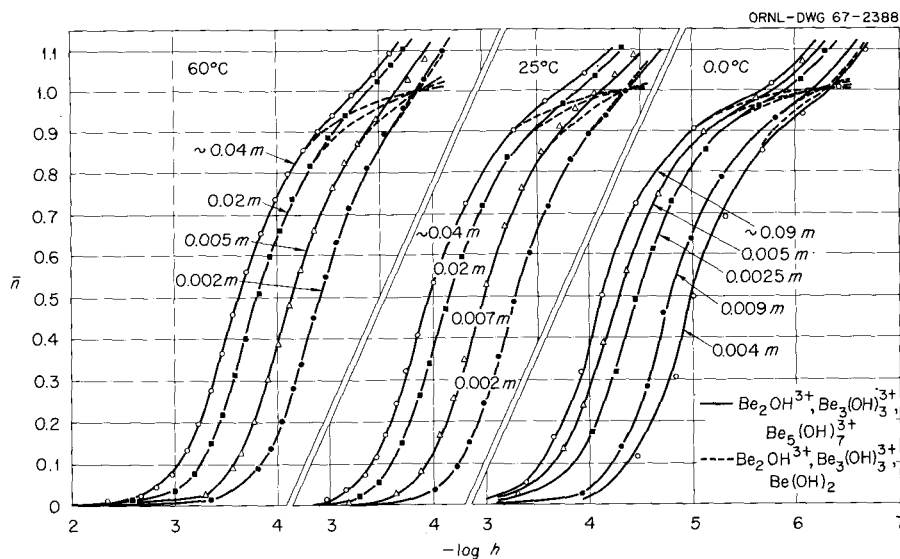


Fig. 5.16. Hydrolysis Data for Be^{2+} in 1 m NaCl from 0 to 60°C; Hydrogen Electrode Data at 0 and 60° and Quinhydrone Data at 25°. The numbers refer to total beryllium concentration which decreases with increasing \bar{n} as a result of dilution.

Table 5.3. Summary of Thermodynamic Data at 25° for Polynuclear Hydrolysis Products of the Formation Reaction $x\text{M}^{n+} + y\text{OH}^- = \text{M}_x(\text{OH})_y^{(nx-y)+}$

Species	ΔH°	ΔS°	$\frac{\Delta H^\circ}{y}$	$\frac{\Delta S^\circ}{y}$	Medium	Reference
$\text{Fe}_2(\text{OH})_2^{4+}$	-18.4	76.4	-9.2	38.2	3 M (Na)ClO ₄	<i>a</i>
$\text{Fe}_3(\text{OH})_4^{5+}$	-36.0	161.1	-9.0	40.3	3 M (Na)ClO ₄	<i>a</i>
$\text{In}_2(\text{OH})_2^{4+}$	-16.6	70.9	-8.3	35.5	3 M (Na)ClO ₄	<i>a</i>
$\text{Pb}_4(\text{OH})_4^{4+}$	-33.5	108.5	-8.4	27.1	3 M (Na)ClO ₄	<i>a</i>
$\text{Pb}_3(\text{OH})_4^{2+}$	-27.1	105.3	-6.8	26.3	3 M (Na)ClO ₄	<i>a</i>
$\text{Pb}_6(\text{OH})_8^{4+}$	-57.8	222.6	-7.2	27.8	3 M (Na)ClO ₄	<i>a</i>
$\text{Be}_2(\text{OH})_3^{3+}$	-8.4	36.7	-8.4	36.7	1 m (Na)Cl	<i>b</i>
$\text{Be}_3(\text{OH})_3^{3+}$	-24.2	113.2	-8.1	37.7	1 m (Na)Cl	<i>b</i>
$\text{Be}_5(\text{OH})_7^{3+}$	-48.5	258.2	-6.9	36.9	1 m (Na)Cl	<i>b</i>
$\text{Th}_2(\text{OH})_2^{6+}$	-12.0	91.0	-6.0	45.5	1 m (Na)ClO ₄	<i>c</i>
$\text{Th}_4(\text{OH})_8^{8+}$	-49.5	348.8	-6.2	43.6	1 m (Na)ClO ₄	<i>c</i>
$\text{Th}_6(\text{OH})_{15}^{9+}$	-89.5	644.7	-6.0	43.0	1 m (Na)ClO ₄	<i>c</i>
$(\text{UO}_2)_2(\text{OH})_2^{2+}$	-16.8	69.6	-8.4	34.8	0.5 m (K)NO ₃	<i>d</i>
$(\text{UO}_2)_3(\text{OH})_5^+$	-42.0	162.2	-8.4	32.4	0.5 m (K)NO ₃	<i>d</i>

^aL. G. Sillén and A. E. Martell, *Stability Constants of Metal-Ion Complexes*, pp. 39–84, The Chemical Society, London, 1964.

^bR. E. Mesmer and C. F. Baes, Jr., *Inorg. Chem.* **6**, 1951 (1967).

^cC. F. Baes, Jr., N. J. Meyer, and C. F. Roberts, *Inorg. Chem.* **4**, 518 (1965).

^dC. F. Baes, Jr., and N. J. Meyer, *Inorg. Chem.* **1**, 780 (1962).

APPARATUS FOR HYDROLYTIC EQUILIBRIA STUDIES UP TO ABOUT 300°C

R. E. Mesmer C. F. Baes, Jr.

Apparatus for the measurement of hydrolytic equilibria by titration experiments has been designed and constructed. The measurements of hydrogen ion concentration by means of the hydrogen electrode at temperatures above 100°C thus far have been limited in both number and accuracy. The need for the information such measurements could provide is clearly present for those cases such as Al^{3+} ion for which equilibrium is slowly attained at ordinary temperatures and in general since ΔC_p behavior for complex equilibria is not yet theoretically predictable with good accuracy.

The approach chosen for this purpose utilizes a hydrogen concentration cell with liquid junction. A pressure vessel for this purpose has been constructed of Hastelloy B with a wall thickness of 2.7 cm and an internal diameter of 4.8 cm. Solutions are contained in concentric Teflon cylindrical cups (85 and 35 ml volumes) connected by a porous Teflon liquid junction with very low leak rate. The leak rate of the junction, an important factor in limiting errors from the mixing of the solutions, has been adjusted to 0.001 to 0.0002 g per centimeter head of water per hour. The resulting liquid-junction potentials are accurately expressed by the Henderson equation. During an experiment, titrant is injected into the outer compartment by means of a calibrated pressure generator.

Each compartment contains a Chromel-Alumel thermocouple encased in a 0.040-in. platinum sheath and insulated from the sheath with MgO. The platinized sheaths act as electrodes. Both compartments are stirred with Teflon-coated stirring bars. For temperature control the entire assembly is submerged in an oil bath, but to curtail distillation between compartments during the heat-up period, the temperature differential between compartments can be controlled by means of a heater placed in the inner compartment.

Since the choice of electrodes for measurement of the hydrogen ion concentration under these extreme conditions is limited to the hydrogen electrode, the media which can be chosen for controlling ionic strength are limited to the alkali metal halides. The apparatus will be useful for

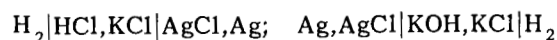
the study of protolytic equilibria of any type, provided the species involved are stable in the hydrogen atmosphere.

APPARATUS FOR DETERMINING THE DISSOCIATION CONSTANT OF WATER AT ELEVATED TEMPERATURES

F. H. Sweeton R. W. Ray

Apparatus for determining the dissociation constant of water at elevated temperatures is essentially complete. This dissociation constant, while important in the field of high-temperature chemistry, has been studied to only a limited extent. The chief work is that of Noyes *et al.*,³⁹ who more than 50 years ago used electrolytic conductivity methods to determine the hydrolysis of ammonium acetate and from this calculated the dissociation constant of H_2O up to 306°C.

At temperatures up to 60°C, Harned *et al.*⁴⁰ have used the cell pair



to obtain the best available values of K_w , the dissociation constant. However, at elevated temperatures the AgCl of the reference electrode is more soluble⁴¹ and reacts with the H_2 , changing the emf and releasing HCl to the solution. For our studies we are therefore combining the two cells by bringing the two solutions into direct contact, thereby eliminating the Ag, AgCl electrodes. In order to keep the emf correction for the resulting liquid junction low, we will always keep the KCl concentration much higher than that of the HCl and KOH.

The cell is shown schematically in Fig. 5.17. The pressure vessel is constructed of INOR-8. The inside machined pieces, which form the cell proper, are made of Teflon. The incoming solutions are equilibrated with H_2 before entering the cell, thus avoiding the inconvenience and uncertainties involved in equilibrating the solution with a vapor phase at high temperature and pressure.

³⁹A. A. Noyes, Yogoro Kato, and R. B. Sosman, *J. Am. Chem. Soc.* **32**, 159-78 (1910).

⁴⁰Herbert S. Harned and Benton B. Owen, *The Physical Chemistry of Electrolytic Solutions*, 3d ed., p. 638, Reinhold Publishing Co., New York, 1958.

⁴¹Richard S. Greeley *et al.*, *J. Phys. Chem.* **64**, 652 (1960).

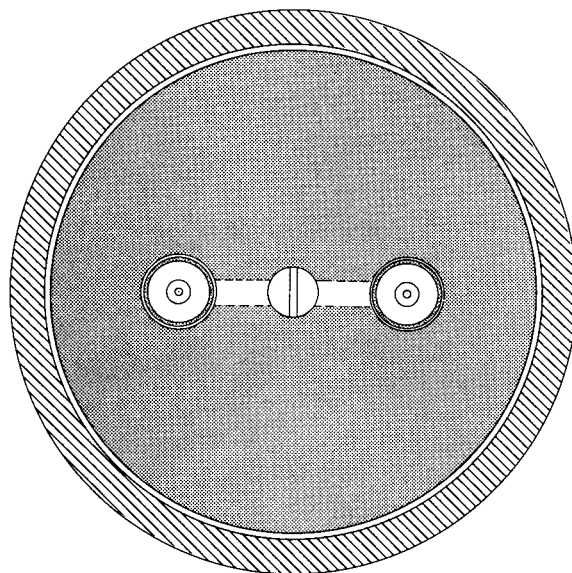
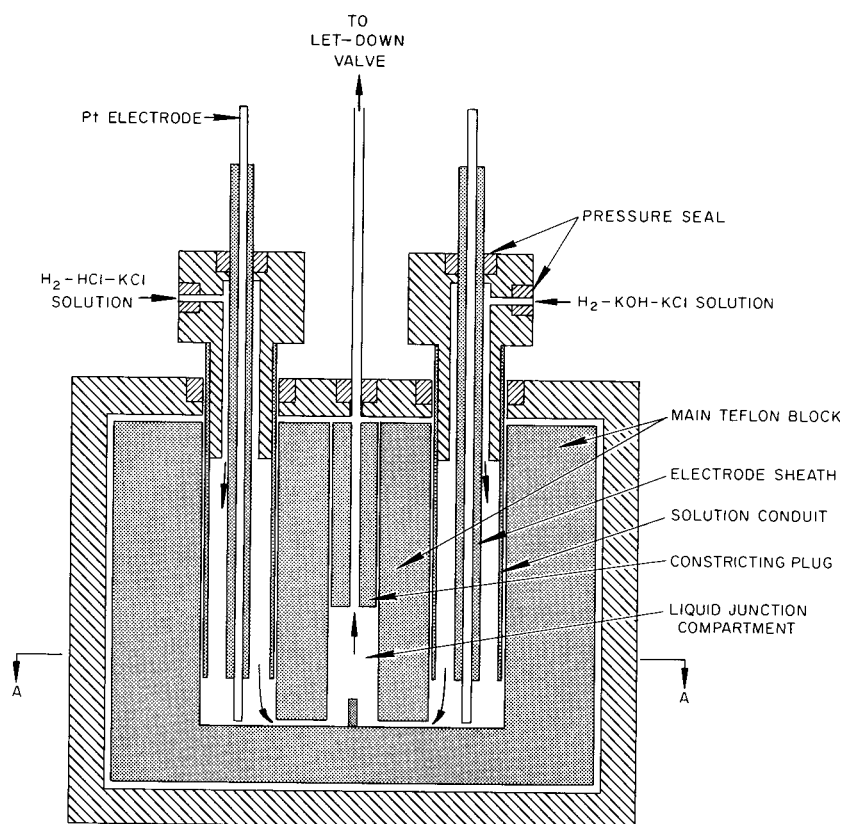


Fig. 5.17. Schematic Sketch of EMF Cell for Determining Dissociation Constant of Water.

The cell configuration has the additional advantage that fresh solution can be introduced at will to control the probable increase in pickup of impurities with time at elevated temperatures. The chief design problem of the cell arises from the fact that we want to go up to 300°C, where Teflon tends to flow when used as a packing in high-pressure seals. Because of this we have constructed the packing rings out of a flow-resistant Teflon material containing a solid additive and are employing disk springs to maintain a relatively low pressure on the packing rings at all temperatures.

The cell is now being tested, and the necessary associated equipment such as thermostat, high-pressure displacement pumps, letdown valve, and apparatus for preparation of solutions is on hand.

HIGH-TEMPERATURE ISOPIESTIC STUDIES

Design and Construction of an Improved High-Temperature Isopiestic Unit

H. F. McDuffie P. B. Bien

The desire to study mixed electrolytes with the high-temperature isopiestic unit made it imperative to improve the system of apparatus for better precision. The original pressure vessel,⁴² after many years of operation with chloride-containing solutions, was inspected by our test engineers and found to be unsafe for projected operations at 200°C and 15.6 bars (~235 psia) pressure. A new vessel, using a standard stainless steel pipe cap and flange, was designed and fabricated. The design followed closely that of the original vessel with minor modifications – the original stainless steel bellows was replaced by a Viton O-ring assembly which would permit the required up and down motions, and the thrust bearing, which had corroded, was replaced by a Stellite ball bearing. To protect the system from corrosion, the inside of the vessel was plated with silver.

The new vessel, which stood a hydrostatic pressure test at 1350 psig, has been installed. The period required for the whole assembly to come into thermal equilibrium has been studied. Due to the larger size and heavier material the thermal lag in the new vessel was larger. A steady state

⁴²B. A. Soldano *et al.*, "A High-Temperature Isopiestic Unit," pp. 224–35 in *The Structure of Electrolytic Solutions*, ed. by W. J. Hamer, Wiley, New York, 1959.

could be reached within 4 hr. After a revision of the air bath heating system, the thermal control of the air bath was extremely steady with a stability of $\pm 0.05^\circ\text{C}$ over a period of several days. We have not yet measured accurately the temperature variation inside the pressure vessel, but we anticipate that it will be $\sim 0.001^\circ\text{C}$.

After prolonged testing of the original weighing device it was decided that the precision and the reproducibility could not meet the tolerance limits set by the projected experiments. A "top-loading" balance, incorporating three vertical struts to provide a parallelogram suspension, was designed and fabricated. The original principle of electromagnetic levitation was retained, but a new coil of silver wire was made with 1300 turns in order to reduce the internal heating during the balancing operation. A photograph of the finished balance is shown in Fig. 5.18. Preliminary tests of the balance gave a sensitivity of a few micrograms per second of arc at a load of 10 g. Distortions due to noncentral placement of weights on the balance pans were reduced to the level of that of a good analytical balance.

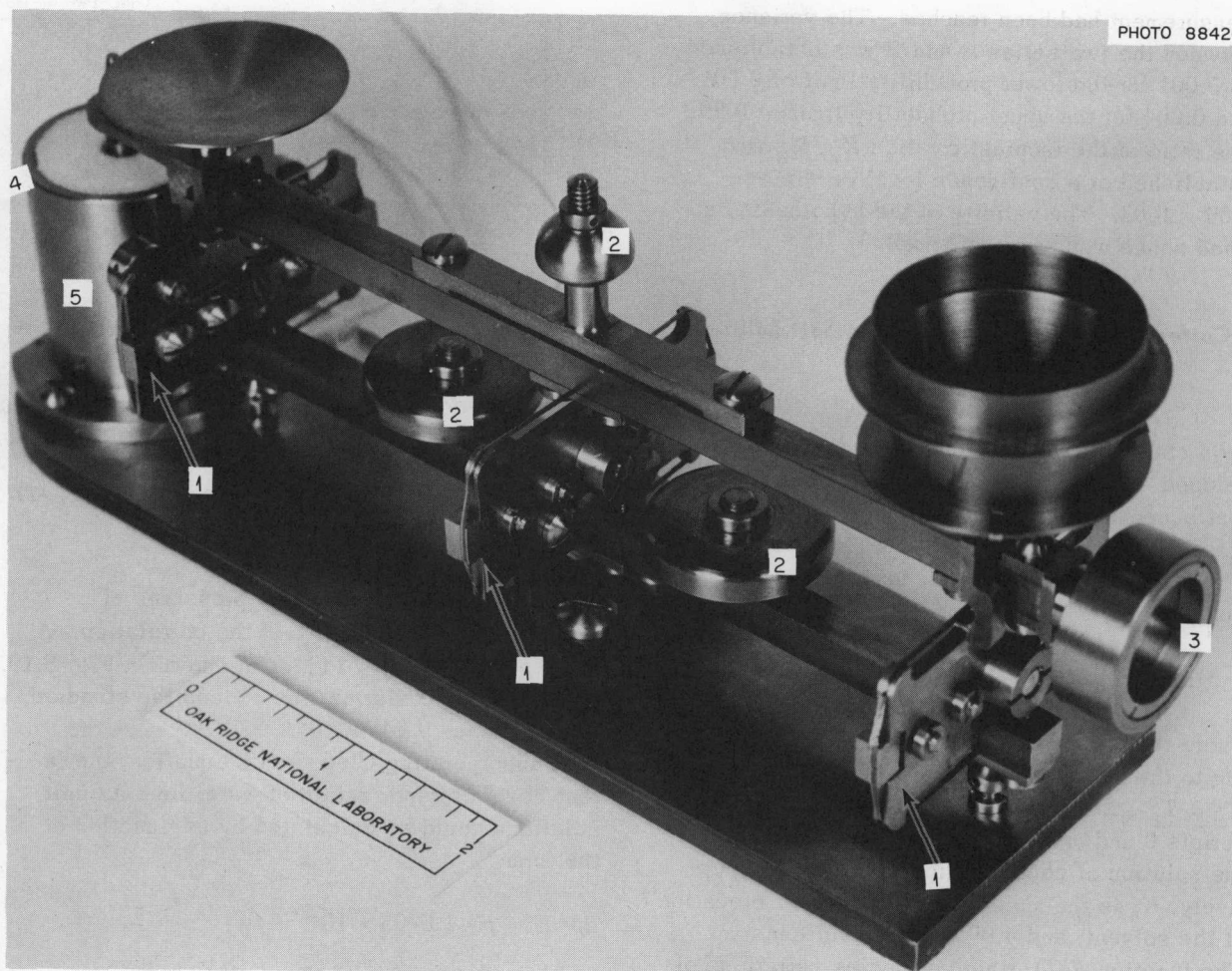
In order to reduce the time required for routine weighings during an experimental run, an electronic servo circuit was added. This circuit has demonstrated its ability to bring the balance from a displaced position back to the null position within 3 to 4 sec. There remain some long-time-constant drifts in the readout circuit, which are believed to result from slight heating or residual magnetic effects after the balance is left energized for periods up to 1 hr. The balance is now being installed in the pressure vessel to see whether these drifts can be reduced or eliminated by operation at temperatures of 100°C and higher. In any case, the use of internal standards of weight should minimize the effects of any such slow drifts.

The "Total Ion" Concept and Isopiestic Behavior of Simulated Sea Salt Solutions

P. B. Bien

It has been suggested that isopiestic data of most electrolyte solutions can be faithfully represented by considering the molal concentrations of the ions alone (as if they are molecular species without the electrical charges).⁴³ This concept

⁴³Dr. George Scatchard, private communication.



1. STRUTS 2. CENTER OF GRAVITY BOBS 3. STELLITE MIRROR
4. ALNICO 5. PERMANENT MAGNET 5. SOLENOIDAL ELECTROMAGENT

Fig. 5.18. Top-Loading Electromagnetic Balance for Isopiestic Studies.

is a departure from the conventional ionic strength treatment of electrolyte solutions. Scatchard called it the "total ion concept," or "osmolality" because it is specially adept in treating osmotic data. The most important implication of this concept is that two different solutions of mixed electrolytes at the same total ion concentration should have the same isopiestic ratio. They should have the same osmotic coefficient vs concentration curves at any particular temperature, unless chemical reactions or solubility limits induce stoichiometric disproportionation. It can be further adduced that the point of stoichiometric disproportionation, either through chemical reactions or solubility limits, can be located graphically either by plotting ϕ vs t or ϕ vs m , extending the usefulness of the isopiestic technique.

The data on the isopiestic behavior of simulated sea salt solutions⁴⁴ were used to test this hypothesis. Solutions A and B, which contained no ions which would precipitate salts whose solubility limits were exceeded at the temperature and concentrations, gave almost identical isopiestic ratios to the common standard, $\text{NaCl}(aq)$, when their total ion concentrations were used. The data for solution C were not consistent with those for solutions A and B when compared on a total ion concentration basis; this is consistent with the conclusion⁴⁵ that substantial amounts of CaSO_4 had precipitated by the time the temperature of

⁴⁴P. B. Bien and B. A. Soldano, *Reactor Chem. Div. Ann. Progr. Rept. Dec. 31, 1965*, ORNL-3913, p. 115.

⁴⁵W. L. Marshall, private communication.

measurement had been reached. The variance between the two series A and B was established as 0.001 for the lower probability limit of 0.001, and 0.004 for the upper probability limit of 0.99. The ratio of the isopiestic ratios R_A/R_B was established at a confidence level of 99% as 1.00 ± 0.03 . The validity of the hypothesis outlined above was amply affirmed.

Corresponding States of Aqueous Salt Solutions

P. B. Bien

An extension of the "total ion concept" was developed⁴⁶ to give a correlation based on the notion that aqueous salt solutions can be in corresponding states with themselves and with the pure solvent. A reduced equation of state was written, after Guggenheim,⁴⁷ in the form

$$\ln(p/p_c) = F(T)(1 - T_c/T), \quad (1)$$

where the critical constants were defined, according to the "total ion concept," by the relations $T_c^m = T_c^0 + 2mK_b$ and $p_c^m = p_c^0 - 4.09m$. The superscripts 0 and m refer to the pure solvent and to the solution at concentration m (molal), respectively, K_b is the molecular boiling point elevation of the solvent, and 4.09 a statistical constant. The function $F(T)$, which embodies variations of both the enthalpy changes and volume variations, took the form

$$F(T) = 9.7548 - 1.0795 \times 10^{-2}T + 1.1499 \times 10^{-5}T^2. \quad (2)$$

⁴⁶P. B. Bien, *J. Phys. Chem.* **71**, 2731 (1967).

⁴⁷E. A. Guggenheim, *Thermodynamics, an Advanced Treatment for Chemists and Physicists*, 4th ed., North-Holland Publishing Co., Amsterdam, 1959.

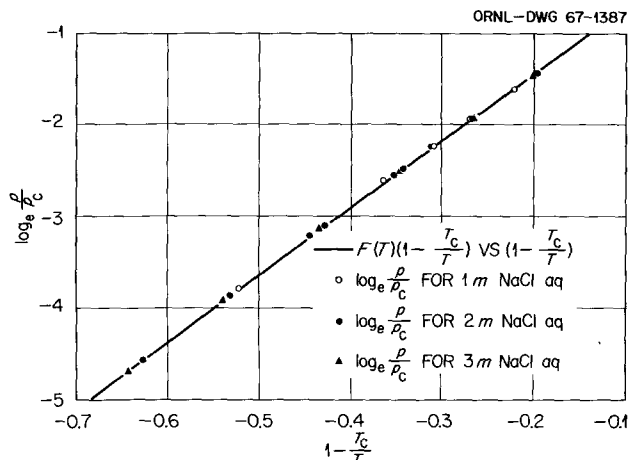


Fig. 5.19. Plot of $\ln p/p_c$ as a Function of $(1 - T_c/T)$.

The British data on the vapor pressures of $\text{NaCl}(aq)$ ⁴⁸ were used to test the correlation. A $\ln(p/p_c)$ vs $(1 - T_c/T)$ plot is shown in Fig. 5.19. The maximum deviation was 1% and the standard deviation was 0.246%.

By incorporating Clapeyron's equation, the latent heats of vaporization of water from its salt solutions could be calculated by an equation of the form

$$\begin{aligned} dp/dT &= p(-1.0795 \times 10^{-2}T_c \\ &\quad - 2.2998 \times 10^5 T + 9.7548T_c/T^2) \\ &= \Delta h/T(v_g - v_l). \quad (3) \end{aligned}$$

There are very few data to test the calculations, but the trend of the heats of vaporization with increases in concentration is downward, as is true for the equation.

⁴⁸E. R. Gardner, P. J. Jones, and H. J. deNordwall, *Trans. Faraday Soc.* **59**, 1994 (1963).

6. Interaction of Water with Particulate Solids

SURFACE CHEMISTRY OF THORIA

Heats of Immersion and Adsorption

H. F. Holmes E. L. Fuller, Jr.
R. B. Gammage

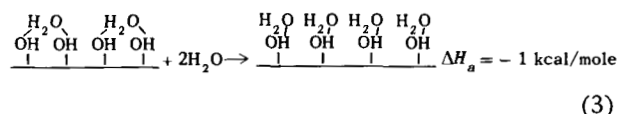
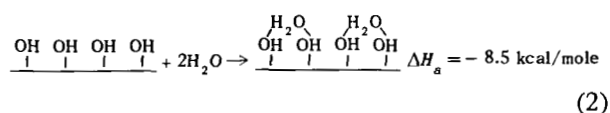
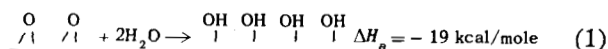
Net differential heats of adsorption for water on thoria were obtained from the integral heats of immersion of samples containing known amounts of presorbed water. The apparatus and associated techniques have been adequately described.^{1,2} The three thoria samples used in the present study were prepared by the thermal decomposition of thorium oxalate and were carefully characterized as to purity, calcining temperature, particle size, and crystallite size. Specific surface areas, as determined by nitrogen adsorption, were 2.96, 6.60, and 14.5 m²/g for samples I, H, and G respectively.

Initial net differential heats of adsorption at low surface coverages ranged from -15 to -40 kcal/mole. The results can be explained in terms of dissociative chemisorption to form surface hydroxyl groups, with additional contributions from hydrogen bonding involving surface hydroxyl groups and irreversibly adsorbed water molecules. Samples G and H gave results which are typical of heterogeneous surfaces. In contrast, results from sample I exhibited three regions in which the net differential heat of adsorption was independent of surface coverage. This same type of result was obtained² for a thoria sample (E) having a specific surface area of 1.24 m²/g. Net differential heats of adsorption were approximately equal for samples E and I. These results can be attributed to the formation of successive homogeneous, immobile monolayers. Combination of the results from

¹H. F. Holmes and C. H. Secoy, *J. Phys. Chem.* **69**, 151 (1965).

²H. F. Holmes, E. L. Fuller, Jr., and C. H. Secoy, *J. Phys. Chem.* **70**, 436 (1966).

samples E and I makes it possible for one to give semiquantitative enthalpy values for the idealized surface reactions of hydroxylation and subsequent associative adsorption by means of hydration of the surface hydroxyl groups. These reactions are depicted schematically in Eqs. (1), (2), and (3).



A significant fraction of the immersional heat for samples G and H was released over a relatively long period of time. No slow heat release was ever observed with sample I. This slow heat of immersion can be associated with the known^{3,4} pore structure of thoria samples calcined at 1000°C or lower. At high coverages, sample I gave a heat of immersion of -120 ± 3 ergs/cm² based on the nitrogen area. This is essentially a Harkins-Jura⁵ absolute surface area determination which agrees remarkably well with the area obtained from nitrogen adsorption. Sample E of the previous study showed the same behavior. Due to complications from capillary condensation, this type of result is not obtained with samples of high specific

³E. L. Fuller, Jr., H. F. Holmes, and C. H. Secoy, *J. Phys. Chem.* **70**, 1633 (1966).

⁴H. F. Holmes, E. L. Fuller, Jr., and C. H. Secoy, submitted for publication to the *Journal of Physical Chemistry*.

⁵W. D. Harkins and G. Jura, *J. Am. Chem. Soc.* **66**, 1362 (1944).

surface area. The present results, in their entirety, reinforce the idea⁶ that high calcining temperatures ($>1000^{\circ}\text{C}$) are required to produce a relatively low-specific-surface-area material that is indicative of an ideal planar surface.

The Effect of Irreversibly Adsorbed Water on the Character of Thoria Surfaces

R. B. Gammage H. F. Holmes
E. L. Fuller, Jr.

Past gravimetric^{3,4} and calorimetric^{1,2,7} measurements were directed towards explaining the complex interaction of H_2O with the thoria surface. Some success was achieved in the description of adsorption on the clean surface as a primary dissociative chemisorption event to form a hydroxylated surface with additionally adsorbed H_2O molecules slowly converting from a reversibly physisorbed state to an irreversibly adsorbed condition involving strong hydrogen bonding to underlying OH groups. This picture has been extended to involve a more detailed description of such irreversibly bound H_2O on both (100) and (111) type faces, as is shown schematically in Figs. 6.1 and 6.2. Completion of the slow binding process leads to the equivalent of one water molecule being bound to each hydroxyl group. It will be demonstrated that the surface offered by such an ordered water structure is particularly significant with respect to its effects on additional physically adsorbed water and also on adsorbed nitrogen and argon.

In constructing models of the completely hydrated 100 and 111 faces, prime consideration was given to formation of the maximum number of hydrogen bonds. An additional restraint on the model is that the hydrogen bond distances and angles should be consistent with, but not necessarily equal to, those observed in other systems.⁸ For the purpose of clarity, the positions of the oxygen and thorium ions, but not their sizes, have been drawn to scale. On the hydrated 100 surface, hydroxyl groups occupy the same positions as oxygen ions in a normal 100 plane. Hydrate

⁶E. L. Fuller, Jr., H. F. Holmes, C. H. Secoy, and J. E. Stuckey, *J. Phys. Chem.*, in press, February 1968.

⁷H. F. Holmes, E. L. Fuller, Jr., and C. H. Secoy, submitted for publication to the *Journal of Physical Chemistry*.

⁸G. C. Pimentel and A. L. McClellan, *The Hydrogen Bond*, p. 283, W. H. Freeman and Co., San Francisco, 1960.

water molecules lie in a plane above the surface hydroxyl groups. It can be seen that each hydrate water molecule forms four hydrogen bonds involving two different types designated *a* and *b*. A most salient feature of the special water structure is that the hydrogen bonding capacity of each water molecule is completely satisfied. Any further adsorption onto this structure *cannot* occur by means of hydrogen bonding to the sub-

ORNL-DWG 67-6008

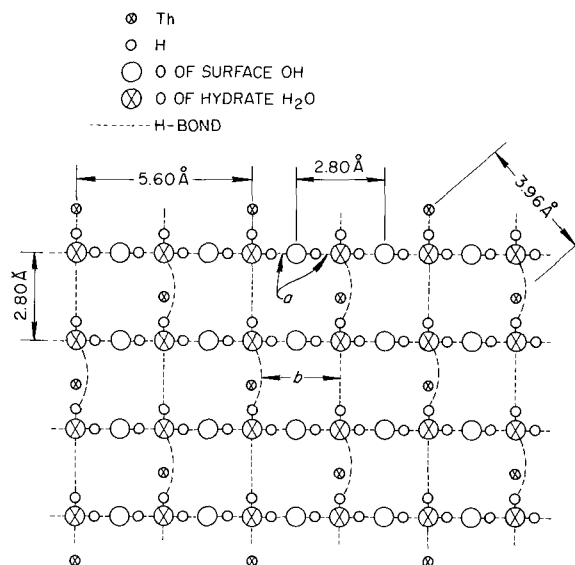


Fig. 6.1. Model of Hydrated 100 Surface of ThO_2 .

ORNL-DWG 67-6009

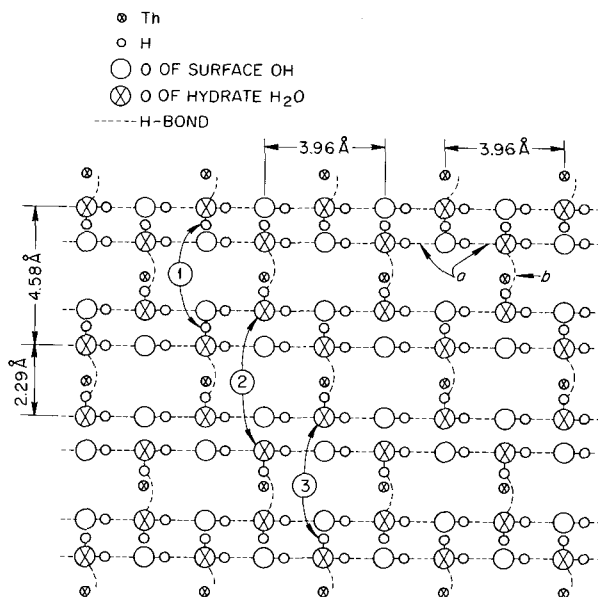


Fig. 6.2. Model of Hydrated 111 Surface of ThO_2 .

strate. Another description is to say that the associatively bound water has reduced the polarity of the exposed surface. The proposed model for the fully hydrated 111 surface does not completely take care of the hydrogen bonding capacity of the special water structure. In the model, each surface hydroxyl again forms two hydrogen bonds with adjacent hydrate water molecules. This time, however, each water molecule forms only three hydrogen bonds; two of these are with underlying surface hydroxyl groups and one is with an adjacent water molecule. Again two types of hydrogen bond (*a* and *b*) are involved, differing in length and linearity.

The unsatisfied hydrogen bonding potential would be expected to have effect on further adsorption, particularly of water vapor. The hydrate water molecules shown in Fig. 6.2 make up a hexagonal network, each hexagon having an area 13.6 \AA^2 . Adsorption sites with unsatisfied hydrogen bonding are offered across opposing corners of the hexagon. Depending on the orientation of the water molecules at the opposite corners, the adsorption sites are divisible into three types designated 1, 2, and 3. This orientation is expected to occur in a random manner so that there will be 25% each of type 1 and 2 sites and 50% of type 3. Considering hydrogen bond formation as an electrostatic phenomenon, one is led to believe that an adsorbing water molecule will interact preferentially with a type 3 site. Here the two points of attachment are a hydrogen atom and a lone pair of electrons. In forming two hydrogen bonds, electron charge will be shifted both to and away from the adsorbing molecule. In attachment to sites of type 1 or 2, hydrogen bonding will involve shift of charge either wholly away from or toward the adsorbate molecule. The resulting species will be "charged up," less stable and less strongly adsorbed than one attached to a type 3 site.

From the proposed surface molecular structures, the adsorptive capacity of each for water can easily be estimated. Comparison with experimental monolayer capacities will then allow an evaluation of the models. A water molecule adsorbed at the 100 hydrated surface is expected to be close-packed at monolayer completion and to have a cross-sectional area of 10.6 \AA^2 (true physical adsorption). On the hydrated 111 surface, the filling of type 3 sites only would give each water molecule an effective area of 27.2 \AA^2 . For occupancy of all the type 1, 2, and 3 adsorption sites, the corresponding area would be halved to 13.6 \AA^2 .

Water adsorption at 25°C was measured on a series of thoria samples which were first hydrated and then outgassed at 25°C . The specific surface areas were also determined by nitrogen adsorption at -195°C for comparative purposes. For this purpose, samples were outgassed at 500°C . The apparent surface areas were determined and are recorded in Table 6.1. For the correlation of the data with the proposed models, the reduced surface area (the ratio of water to nitrogen surface area) is of particular importance. For physisorbed water (10.6 \AA^2) on 100 type faces, the expected ratio is 1.00. With adsorption on 111 faces, the ratio is 0.78 for attachment of water to type 1, 2, and 3 sites and only 0.39 if the monolayer capacity corresponds to the filling of type 3 sites only.

Electron diffraction patterns from coarse particles of thoria have indicated that they are single crystal in nature with a predominance of exposed 111 faces. The reduced surface areas for the coarser samples D, I, and S would indicate preference for a model of adsorption at type 3 sites on 111 faces. As an example, the reduced area of 0.55 obtained with sample I could be accounted for by an admixture of 111 and 100 surfaces in the ratio 70:30. Turning to the finely porous thoria, samples B and C, the reduced surface areas of 0.75 and 0.98 would suggest adsorption is taking place on surfaces predominantly of the 100 type. The agreement between model and experiment is not perfect but yet is sufficiently close to be gratifying.

The results of the adsorption of nitrogen and argon on cleaned and water-saturated thoria surfaces support in a general way the proposed models for the hydrated surface. It has been stressed that the development of the associative, bound water structures leads to a reduced surface polar character, compared with the bare or hydroxyl-covered surface. It can thus be argued that a molecule such as nitrogen, with its quadrupole moment, will be less strongly adsorbed at the hydrated surface. This difference should reflect in the *C* values obtained from BET treatment, which are directly related to the heat of adsorption. In contrast, the interaction of argon with all surfaces is nonpolar, involving only dispersion forces. One would expect the extent of hydration to have a lesser effect on the character of argon adsorption. The data included in Table 6.2 indicates that nitrogen indeed adsorbs less strongly at the hydrated surface. Surprisingly, the same trend is noted for argon, which is puzzling. Measurements on sample B show a pronounced reduc-

Table 6.1. Summary of Surface Areas

Sample	N ₂ Surface Area ^a (m ² /g)	H ₂ O Surface Area ^b (m ² /g)	$\frac{\text{H}_2\text{O Surface Area}}{\text{N}_2 \text{ Surface Area}}$
D ^c	1.43	0.55	0.38
I ^c	2.96	1.64	0.55
S ^c	5.96	2.94	0.49
B ^d	11.90	11.65	0.98
C ^d	5.50	4.13	0.75

^aAssuming that an adsorbed nitrogen molecule occupies 16.2 Å² on the surface outgassed at 500°C.

^bComputed on the basis of 10.6 Å² per adsorbed water molecule for the surface outgassed at 25°C.

^cNonporous or coarsely porous (>50 Å).

^dFinely porous.

Table 6.2. BET Data for ThO₂

Sample	Outgassing Temperature (°C)	$\Sigma (\text{N}_2)$ (m ² /g)	C (N ₂)	$\Sigma (\text{Ar})$ (m ² /g)	C (Ar)	$\Sigma (\text{N}_2)/\Sigma (\text{Ar})$
B	25	9.42	74	6.88	52	1.37
B	500	11.90	975	8.76	475	1.36
I	25	2.68	23.9	2.02	16.3	1.33

$\sigma(\text{N}_2) = 16.2 \text{ \AA}^2/\text{molecule}$

$\sigma(\text{Ar}) = 13.8 \text{ \AA}^2/\text{molecule}$

tion in apparent specific surface area (20%) brought about by hydration. The same magnitude of area reduction is noted for both nitrogen and argon adsorbates. Sample I behaves in like manner for nitrogen adsorption. This sample is nonporous, which precludes any explanation of the diminution as an area loss brought about by hydrate molecules blocking off fine pores. Instead it seems more likely that occupancy areas of the nitrogen and argon molecules are affected by the degree of hydration. The magnitude of such an effect would seem to be the same for nitrogen and argon. Evidence is provided by the constancy of the ratio of apparent areas with change in state of hydration.

Infrared Spectra of Adsorbed Species on Thoria

E. L. Fuller, Jr. R. B. Gammage
H. F. Holmes

A high-resolution infrared spectrophotometer has been modified to accept sample chambers that will allow the attainment of the stringent conditions required to remove the adsorbed species from thoria. A standard spectrophotometer (Beckman IR 12) was lengthened to provide the space for these operations. Preliminary studies have shown that high-resolution transmission spectra can be obtained in situ for temperatures up to 450°C. A photoconductive (PbS) detector has been found

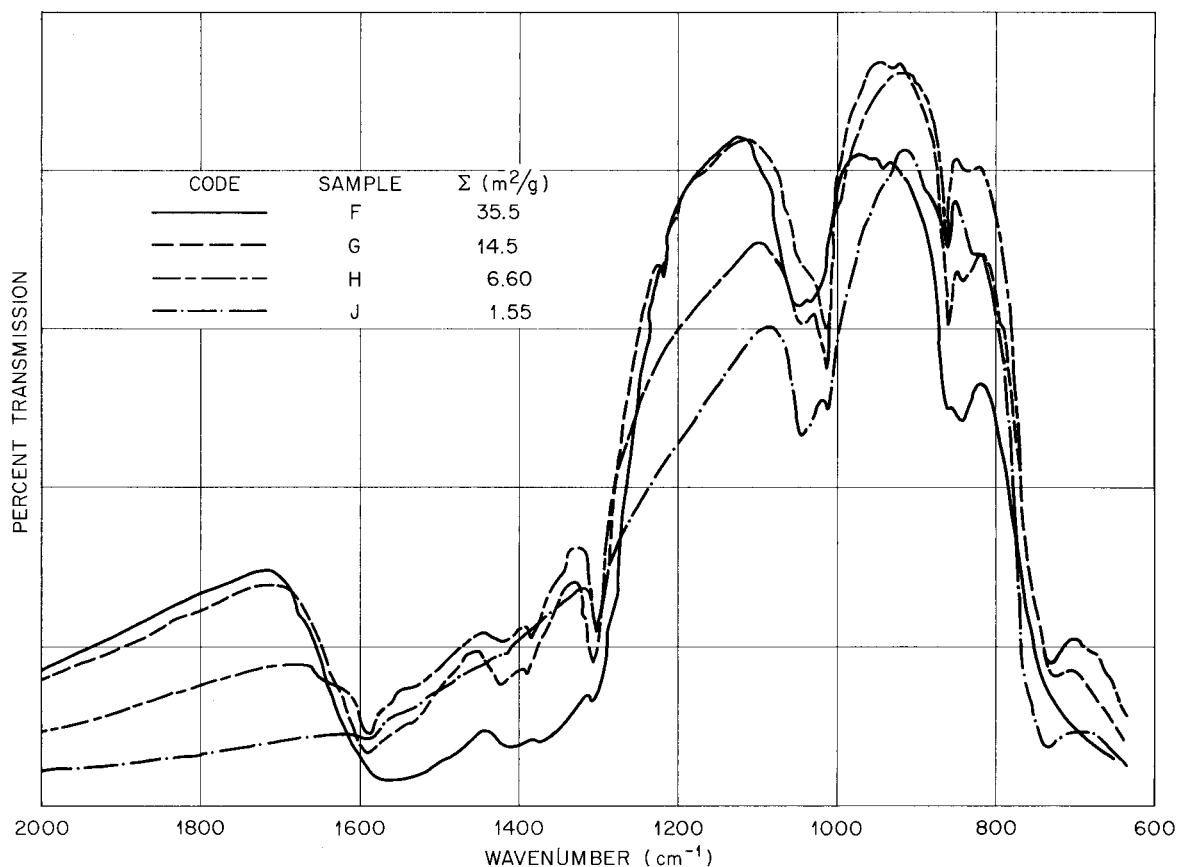


Fig. 6.3. Infrared Spectra of Thoria of Varied Specific Surface Area.

to perform excellently in the range of 2400 to 4000 cm^{-1} for spectral evaluation in the presence of the inherent particulate scattering. The detector is approximately 200 times as sensitive as a standard thermocouple and allows investigation of the surface hydroxyl region of the spectra (heretofore deemed impossible for samples of low specific surface area^{9,10}).

Preliminary studies with the powdered thoria samples between KBr plates in the purge atmosphere (4 ppm H_2O) of the instrument gave the spectra shown in Fig. 6.3. The range covered here is 600 to 2000 cm^{-1} and shows the marked variation with specific surface area of the material (surface area was diminished by higher temperature calcinations of F). The amount of thoria in the light

beam was approximately the same. In all cases a broad, single band at 1060 cm^{-1} changed with exposure to the purge to give the spectra noted, and the region between 1300 and 1600 cm^{-1} also became more detailed. Heating the sample at 120°C accomplished in 1 hr spectral changes that required days in the purge; however, continued heating had no additional effect on the spectra.

These spectra show that there are at least two effects predominating in addition to the structural effects: (1) marked scattering of light by the sample particles as noted by the curved continuum background (1000 to 2000 cm^{-1}), and (2) the transmission cutoff normally associated with ionic crystals (200 to 800 cm^{-1}). Reliable band assignment cannot be made without the aid of controlled atmospheric conditions and in situ spectral studies. However, it is noteworthy that the 1200 to 1700 cm^{-1} bands diminish considerably as the amount of surface decreases, whereas the 900 to 1100 cm^{-1} band remains relatively

⁹A. C. Zettlemoyer, R. D. Iyengar, and P. Scheidt, *J. Colloid Interface Sci.* **22**, 172 (1966).

¹⁰W. H. Wade and N. Hackerman, *Advan. Chem. Ser.* **43**, 222 (1964).

constant. This would indicate that the former are due to surface species, whereas the latter are probably associated with the bulk of the thoria.

PROCESSING OF SOL-GEL UO_2 MICROSPHERES

C. F. Weaver D. N. Hess
H. F. McDuffie

The previously reported¹¹ successful processing scheme for UO_2 microspheres was further studied with emphasis on monitoring the removal of carbonaceous material, shortening the time, reducing the maximum temperature, and simplifying the sequence. A detailed report¹² of this work is in preparation.

A Beckman hydrocarbon analyzer was employed to monitor the removal of carbonaceous material. It was found that this instrument was particularly useful in determining the minimum time required for the removal of organic materials. Details of the pattern of hydrocarbon generation varied from run to run even though the samples were selected from the same batch of microspheres, but, generally, bursts of hydrocarbon evolution occurred near 250, 350, 450, and 550° with a maximum at 450° and none above 550°.

Densification was accomplished at temperatures as low as 850°C, consistent with the claim in the literature¹³ that sintering of UO_2 in steam begins

¹¹D. N. Hess *et al.*, *Reactor Chem. Div. Ann. Progr. Rept. Dec. 31, 1966*, ORNL-4076, pp. 78-79.

¹²C. F. Weaver *et al.*, *The Processing of ThO_2 and UO_2 Sol-Gel Materials*, ORNL-TM-1809 (in preparation).

¹³W. E. Bailey *et al.*, *Am. Ceram. Soc. Bull.* 41, 768 (1962).

as low as 750°. A 2-hr period at 850° was sufficiently long for the sintering step, but a shorter time may be satisfactory.

The reduction of the oxygen-to-uranium ratio to nearly 2.000 (see Table 6.3) was accomplished with H_2 at 850° in 2 hr. This time can be reduced at least to 1 hr and probably less.

These results lead to a considerably shortened and simplified processing scheme at lower maximum temperature:

Time (hr)	Temperature (°C)	Atmosphere
1.5	100-550	Ar + H_2O
2	550	Ar + H_2O
0.75	550-850	Ar + H_2O
2	850	Ar + H_2O
2	850	H_2

A variety of batches of UO_2 microspheres were treated in this way. The results are shown in Table 6.3.

Several processing attempts were unintentionally terminated by equipment failure. Analysis of such samples provides information on the characteristics of the UO_{2+x} microspheres at different stages of the processing scheme. Table 6.4 gives typical ranges for these results. Numbers for which no range is given represent one datum only. Table 6.5 represents the best results which were obtained regularly, but not routinely, during the studies.

Our experience suggests that the hydrocarbon analyzer should be most useful in monitoring and controlling the operations in a full-scale processing

Table 6.3. Properties of Processed Batches

Properties	P-6-12-1153	P-6-19-1408	P-6-16-1545	P-6-14-1550
O/U	2.001	2.007	<2.002	2.005
C, %	0.012	<0.001	0.018	0.002
Surface area, m^2/g	0.013	0.033	0.006	0.011
D_{Hg} at 210 psi	10.5	10.36	10.78	10.52
N_2 , %	0.001			

Table 6.4. Properties at Various Stages of Processing

	O/U	C (%)	Density (g/cm ³)	Nitrogen (%)	Surface Area (m ² /g)
Starting material	2.25–2.49	1.8–8.0	4.70	0.09–0.19	50.8
End stripping, 550°C	2.11–2.21	0.012–0.017	8.78		
End sintering, 850°C	2.092	0.002	10.8		
End reduction, 850°C	2.000–2.009	<0.001–0.013	10.5–10.9	<0.001	0.006–0.033

plant. This is especially so since the individual sol-gel batches vary somewhat from average values, and no fixed set of processing conditions can handle them all without wasting time on batches that are relatively easy to process.

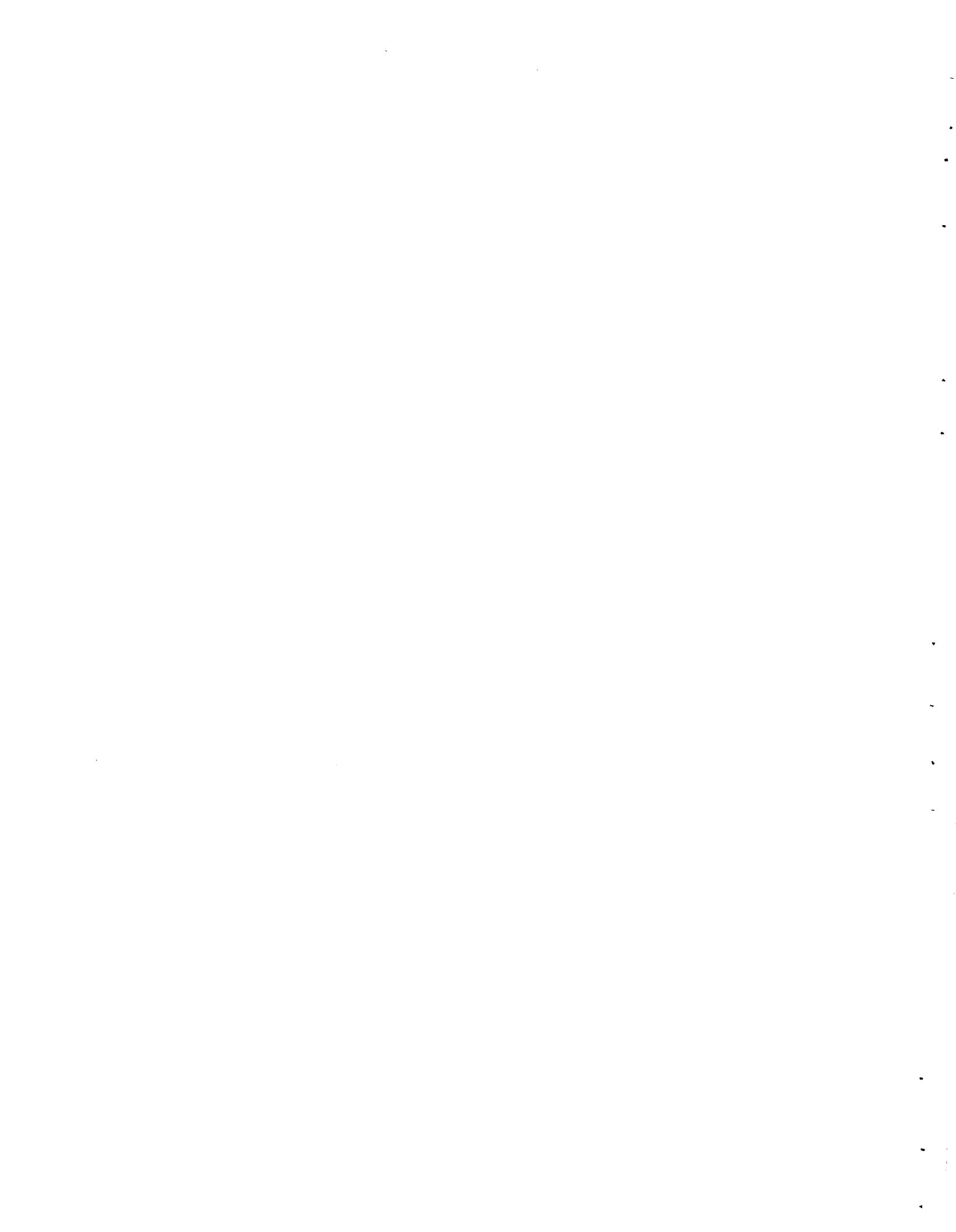
Although this work was brought to a close September 1, 1967, because of budget cuts, it is obvious that additional studies along these lines could very well lead to significant improvement in the processing techniques.

Table 6.5. Best Results Obtained

O/U	2.000
C, %	<0.001
N ₂ , %	<0.001
D _{Hg} at 210 psi	10.9
Surface area, m ² /g	0.006



Part III
Gas-Cooled Reactors



7. Diffusion Processes

TRANSPORT PROPERTIES OF GASES

Diffusion Studies in Noble Gas Systems

A. P. Malinauskas M. D. Silverman
J. Q. Searcy¹

Interest in the phenomenon of binary mutual diffusion in gases, in addition to practical applications such as fission product migration, arises from the dependence of the diffusion process on molecular interactions. In this regard the phenomenon is particularly attractive, since the interaction dependence is almost totally governed by unlike-molecule, in contrast to like-molecule, collisions. Moreover, only the transport of mass is involved, and this quantity is strictly conserved in a collision. Complications due to inelastic collisions among the molecules can therefore be safely ignored.

In practice, however, it is difficult to glean unambiguous information regarding intermolecular forces from diffusion data unless the latter span a wide range of temperatures or have been determined to a high degree of accuracy. Unfortunately, neither requirement can be readily realized with the present experimental techniques. As a result, the potential utility of the phenomenon and, consequently, the motivation for research in this field have been blunted somewhat.

Ironically, virtually an opposite situation is encountered in studies of the viscosity characteristics of binary gas mixtures; both accuracy and temperature range requirements can be met reasonably well, but the phenomenon is complicated by an equally significant dependence on like- and upon unlike-molecule interactions. The problem does not arise, of course, in the case of a pure gas; thus viscosity measurements have served as a most

useful tool in the investigation of elastic collisions among identical molecules. For unlike-molecule interactions, however, the information derived from viscosity measurements proves to be about as ambiguous as that obtained from diffusion data.

Several years ago a scheme had been proposed whereby diffusion coefficient data which were determined over a restricted temperature range might be supplemented with values outside this range by utilizing these data in connection with viscosity measurements on the corresponding binary gas mixtures as a function of composition.² The gaseous diffusion studies which were undertaken at this laboratory have been oriented to a considerable degree in an effort to test the proposal and to resolve some of the discrepancies between viscosity and diffusion which were noted previously.²

The first series of experiments were conducted over the temperature range 0 to 120°C with the systems He-Ar, Ar-Xe, and He-Xe. Perhaps the most significant aspect of this work has been a demonstration of the compatibility between viscosity and diffusion in the case of the lattermost system.³ These data have since been shown to be consistent with thermal diffusion and thermal conductivity data as well.⁴

In the second series of experiments, the systems He-Kr, Ar-Kr, and Kr-Xe were investigated over the same temperature range as in the previous case. The Kr-Xe data represent virtually the only diffusion information which is currently available. Moreover, the utility of the proposal to supplement diffusion data with viscosity-derived coefficients was once again affirmed.⁵

¹Summer participant, Purdue University.

²S. Weissman and E. A. Mason, *J. Chem. Phys.* **37**, 1289 (1962).

³A. P. Malinauskas, *J. Chem. Phys.* **42**, 156 (1965).

⁴S. Weissman, *J. Chem. Phys.* **44**, 428 (1966).

⁵A. P. Malinauskas, *J. Chem. Phys.* **45**, 4074 (1966).

A study of the systems He-Ne, Ar-Ne, Ne-Kr, and Ne-Xe constitutes the third part of this research. Although a major part of the experimental work has been completed, the data are not yet in a form which is suitable for presentation.

Thermal Transpiration

A. P. Malinauskas

Thermal transpiration is properly defined as the phenomenon in which a *net* transport of gas molecules is made to occur between two regions in space as the result of a thermal gradient. In current usage, however, the term has been applied to the steady-state condition which results in a closed system when such a thermally induced transport is counterbalanced by transport due to a resultant pressure gradient.

The phenomenon in a sense owes its existence to gas-surface collisions, and for this reason it proved difficult to describe in a mathematically rigorous manner. In fact, the most successful attempt at a formulation of the problem has come only recently, and even this is couched in awkward terminology.^{6,7} However, the treatment does describe the experimental data satisfactorily; moreover, it has also revealed a hitherto unknown dependence of the transpiration effect on inelastic collisions. This dependence has since been exploited to obtain values of the rotational collision number for a number of molecules.⁸⁻¹⁰

Current studies of the thermal transpiration phenomenon in this laboratory are being conducted with a twofold purpose: to clarify some discrepancies between theory and experiment which still persist, and to utilize the effect in an investigation of inelastic collision processes. With respect to the former, the most disquieting defect in the theory is its apparent failure to correctly account for the low-pressure limit observed in capillaries, a trait it holds in common with all previous attempts to describe the phenomenon.

⁶E. A. Mason, R. B. Evans III, and G. M. Watson, *J. Chem. Phys.* **38**, 1808 (1963).

⁷E. A. Mason, A. P. Malinauskas, and R. B. Evans III, *J. Chem. Phys.* **46**, 3199 (1967).

⁸E. A. Mason, *J. Chem. Phys.* **39**, 522 (1963).

⁹A. P. Malinauskas, *J. Chem. Phys.* **44**, 1196 (1966).

¹⁰A. Tip, J. Los, and A. E. de Vries, *Physica* **35**, 489 (1967).

Theoretically, the low-pressure limit is given by

$$R \equiv \frac{p_1}{p_2} = \left(\frac{T_1}{T_2} \right)^{1/2}, \quad (1)$$

where p_1 and p_2 denote the steady-state values of the pressures in the regions at temperatures T_1 and T_2 respectively. The high-pressure limit, on the other hand, is given by

$$R = 1. \quad (2)$$

That significant deviations from Eq. (1) do occur is clearly demonstrated by the data displayed in Fig. 7.1, in which R is plotted as a function of the pressure p_2 in the warmer region. These data were obtained with nitrogen in an apparatus consisting of ten 0.2-mm-ID Pyrex glass capillaries arranged in parallel. The transpiration effect was generated by maintaining the ends of each of the capillaries at 335.6°K and 569.8°K respectively. The solid line which appears in the figure has been constructed from a modified version of the recently developed theory, the modification being simply that the low-pressure limit be determined by experiment. Whether or not this alteration is sufficient, and the geometrical and gas property dependence of the low-pressure limit, await further experimental study for clarification. Such studies are currently in progress.

RECOIL OF FISSION PRODUCTS IN HETEROGENEOUS CARBON STRUCTURES

R. B. Evans III J. L. Rutherford
R. B. Perez

A previously reported investigation of the recoil behavior of "light" and "heavy" fission fragments in a uniform pyrocarbon structure (GE PyC)¹¹ has been extended to include five additional structures, shown in Fig. 7.2, with porosities ranging from 5 to 23 vol %. As before, fragments were induced to penetrate target structures as nearly monoenergetic beams with random r -space directions. Data were collected and arranged to produce plots of fractional activities remaining at various grinding levels

¹¹R. B. Evans III, J. L. Rutherford, and R. B. Perez, *J. Appl. Phys.* **38**(8), 3127-34 (1967).

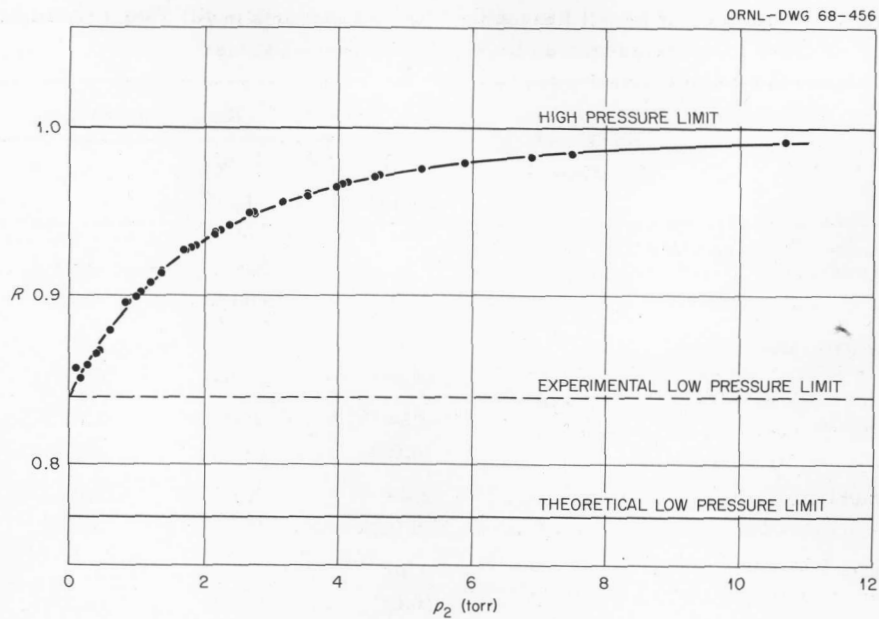


Fig. 7.1. Variation of the Thermal Transpiration Pressure Ratio R for Nitrogen as a Function of Pressure in 0.2 mm Capillaries.

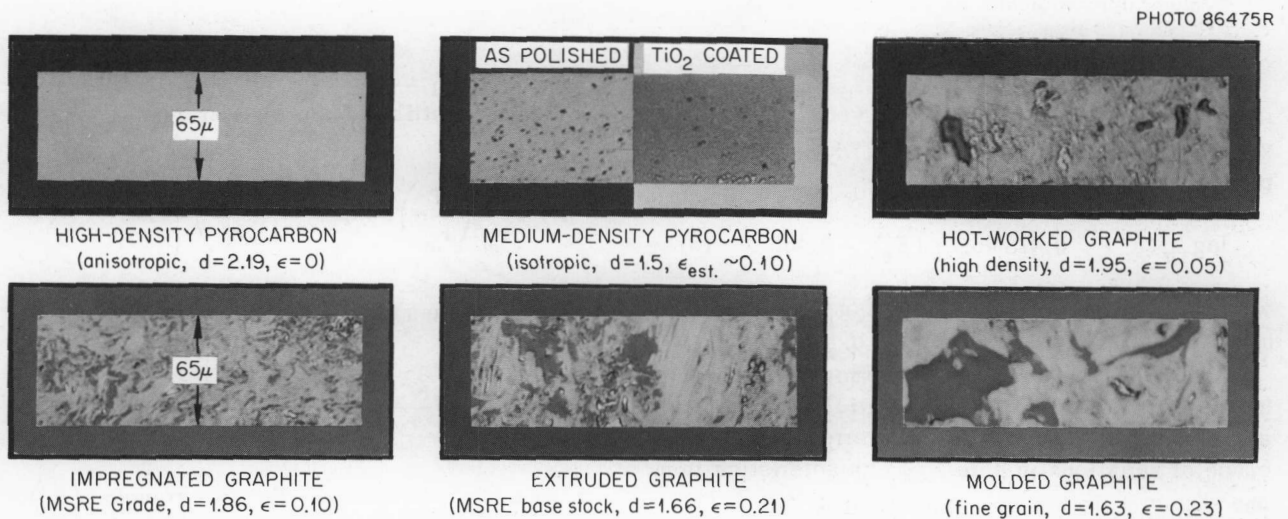


Fig. 7.2. Montage Showing Plastic-Mounted Thin Sections of All Carbon Structures Investigated. Photographs were obtained at relatively low magnifications to permit comparisons of macrostructure and large-pore sizes. With the exception of the medium-density pyrocarbon, dark regions indicate the presence of plastic.

along the z coordinate normal to thin (neutron-activated) ^{235}U source planes. Such plots are integrated forms of the z -space probability-density functions (called distribution functions); these, in turn, are specified by associated r -space functions. An important facet of these studies was the de-

velopment of integrated z -space equations that would exhibit good agreement with data for porous structures. Selection of realistic r -space functions was therefore mandatory. Application of the proper integrated equations permitted evaluation of several sets of range values that were nearly identical and

Table 7.1. Summary of Recoil Ranges for Fission Fragments in All Target Materials Investigated (Averaged Experimental Values)

Target Material	Number of Experiments	Range (mg/cm ²)			
		¹⁴¹ Xe (Ce) ^a	¹⁴⁰ Xe (La) ^a	¹⁰³ Ru ^a	⁹⁵ Y (Zr) ^a
High-density pyrocarbon	6	2.54 (0.09) ^b	2.50 (0.08)	2.94 (0.10)	3.01 (0.11)
Medium-density pyrocarbon	3	2.55 (0.06)	2.53 (0.03)	2.97 (0.03)	3.02 (0.03)
Hot-worked graphite	3	2.54 (0.05)	2.53 (0.02)	3.02 (0.02)	3.14 (0.05)
Impregnated graphite	6	2.49 (0.05)	2.51 (0.06)	3.04 (0.05)	3.07 (0.09)
Extruded graphite	3	2.46 (0.04)	2.51 (0.03)	3.11 (0.05)	3.15 (0.05)
Molded graphite	4	2.58 (0.01)	2.58 (0.08)	2.94 (0.06)	2.99 (0.08)

^aSpecies counted.

^bValues in parentheses are average deviations.

independent of the structures involved. These values are presented in Table 7.1. A compact expression for all results is:

$$\log_{10} (R')_i = 0.478 \log_{10} (E_0)_i - 0.465, \quad (3)$$

where R' (mg/cm²) is the range of any i th fragment with an initial fission energy E_0 (Mev).

Although the range values for homogeneous and heterogeneous materials are essentially the same, applicable distribution functions varied in form because of variations in pore-size characteristics from one structure to the next. As shown in Fig. 7.2, some of the pore sizes encountered were equal to or greater than the range. This resulted in large straggling effects and asymmetric r -space distributions; furthermore, the R' in the above expression corresponds to the most probable distance of r -space travel. Range results for only two of the six structures investigated (the pyrocarbons) were correlated on the basis of a normal (or Gaussian) r -space distribution, where the average and most probable range are synonymous. Results for all other structures were correlated by using general forms of the Maxwell distribution. For r -space

travel, these distributions are given by

$$f(r) = \frac{c_\gamma}{r_m} \left(\frac{r}{r_m} \right)^\gamma \exp \left[-\frac{\gamma}{2} \left(\frac{r}{r_m} \right)^2 \right], \quad (4)$$

where c_γ is a normalization constant of the form

$$c_\gamma = \frac{2}{\Gamma[(1/2)(\gamma + 1)]} \left(\frac{\gamma}{2} \right)^{(\gamma + 1)/2}. \quad (5)$$

In these cases, the average distance traveled $\langle R' \rangle$ is always greater than R' – to an extent depending on the skewness of the distribution function selected for data correlation.

The degree of skewness, which related also to pore-induced straggling effects, is determined by the value of γ used to correlate results for various structures. For the hot-pressed graphite $\gamma = 3$; for the extruded and impregnated graphites, $\gamma = 2$; for the molded graphite $\gamma = 1$. A value of $\gamma = 2$ appears to be most appropriate for the majority of cases one might encounter in practical applications of results given by Eqs. (3)–(5).

8. Oxidation of Carbonaceous Materials by Water Vapor

L. G. Overholser

REACTION OF BONDED COATED-PARTICLE FUEL COMPACTS WITH STEAM

C. M. Blood G. M. Hebert

Proposed fuel element designs include a type in which pyrolytic-carbon-coated fuel particles are bonded by residual binder material and this bonded bed of particles is enclosed in graphite. The coated fuel particles would be protected to some degree against oxidation by steam entering the coolant circuit by both the graphite and residual binder. The steam in diffusing through the graphite would react, at least in part, with the graphite, resulting in a reduced partial pressure of steam and a buildup of reaction products in the gas reaching the bonded bed of coated particles. The residual binder also could be protective if it is more reactive with steam than the coated particles.

Experimental studies of the oxidation of bonded fuel compacts were made at 1000, 1100, and 1200°C using a partial pressure of steam of 20 or 150 torrs. The bonded fuel compact, prepared by Gulf General Atomic, has a graphite container 0.75 in. in diameter and 1 in. long enclosing a bonded bed of coated fuel particles 0.45 in. in diameter and 0.65 in. long.¹ Rates of reaction of this type of fuel compact were determined from weight changes and analyses of effluent gases. Microscopic examinations of the oxidized fuel compacts were performed to establish the extent of damage to the fuel compacts.

¹C. M. Blood, G. M. Hebert, and L. G. Overholser, *GCR Program Semiann. Progr. Rept. Mar. 31, 1967*, ORNL-4133, pp. 108-9.

Reaction rates obtained for fuel compact FC-5 are given in Fig. 8.1 along with rates for solid graphite cylinders. Reaction rates given for the latter agree well with those shown for the fuel compacts, suggesting that oxidation of the fuel compact was largely limited to the graphite container, although a similar effect would be observed if a significant partial pressure of steam reached the bonded bed and reaction rates for the graphite and residual binder were comparable. Postoxidation examination indicates that most of the oxidation occurred in the graphite container. There was no evidence of any attack of the coatings on the fuel particles and no detectable oxidation of the bonding material.

Fuel compact FC-11 was oxidized at 1100°C to a burnoff of 6 wt % using a partial pressure of steam of 150 torrs. The general appearance of the

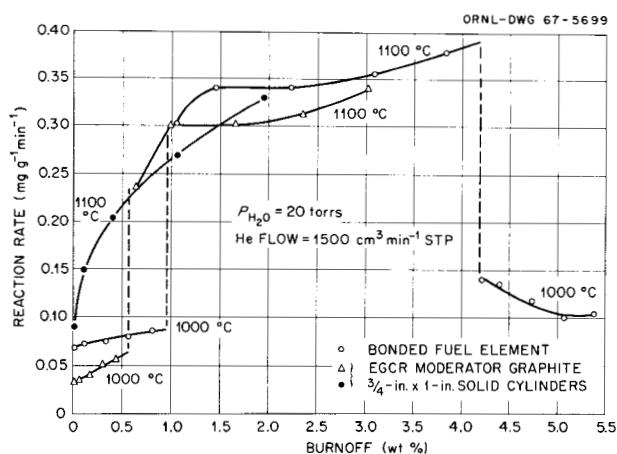


Fig. 8.1. Rates of Reaction of Fuel Compacts and Graphite Cylinders with Steam at Various Temperatures.



Fig. 8.2. Damaged Fuel Compact FC-8 After Oxidation to 50 wt % Burnoff by 25-hr Exposure to Steam Pressure of 20 torrs at 1100°C.

oxidized fuel compact after cleavage was very similar to that of an unoxidized fuel compact, indicating that no visually detectable oxidation of the graphite container, bonding material, or coatings on the fuel particles occurred at this burnoff.

Fuel compact FC-8 was oxidized to a burnoff of ~50 wt % by exposure to a partial pressure of steam of 20 torrs for 25 hr at 1100°C. This severe oxidation was performed to damage the coatings on the fuel particles. The graphite container essentially retained its original shape but lost most of its strength. Figure 8.2 shows a view of the compact after part of the graphite container had been scraped

away. The particles were loose, indicating that most of the bonding material had been oxidized. The coatings showed evidence of attack, but an acid leach revealed that only 0.2% of the coatings had failed despite the extensive oxidation of the fuel compact. Results from earlier studies^{2,3} of the oxidation of loose coated particles showed

²R. D. Burnette, J. M. Dixon, D. R. Lofing, and L. R. Zumwalt, *Experiments on the Reaction of High-Temperature Steam with Pyrolytic-Carbon-Coated (Th,U)C₂ Particles*, GA-7005 (March 1966).

³C. M. Blood and L. G. Overholser, *Compatibility of Pyrolytic-Carbon Coated Fuel Particles with Water Vapor*, ORNL-4014 (November 1966).

more damage to the coatings at similar temperatures and partial pressures of steam.

These results show that the graphite container and probably the bonding material were quite effective in protecting the coatings. It seems probable that at least 20 wt % burnoff of this type of fuel compact under these conditions of temperatures and steam pressures could occur without significant damage to the coated fuel particles. Serious damage to the graphite container and bonding material probably would occur, however.

REACTION OF PYROLYTIC-CARBON-COATED FUEL PARTICLES WITH WATER VAPOR

J. E. Baker

Gaseous fission products would be expected to be retained within the fuel particle until the coating fails even at high burnup. Nonvolatile fission products (Ba, Sr, and Cs) may diffuse slowly through the coatings during prolonged operation at high temperatures. Failure of the coatings due to oxidation following inleakage of steam into the coolant would cause a release of the gaseous fission products and might result in a transport of the nonvolatile fission products by the coolant. Fuel elements having bonded beds of coated particles surrounded by graphite would afford some protection to the coatings, due to partial depletion of steam as it diffuses into the fuel body. As a result, only low partial pressures of steam might be available for oxidation of the coatings.

Earlier studies⁴ of the oxidation of coated fuel particles were performed at temperatures of 1000 to 1400°C and utilized concentrations of water vapor in helium of 250 to 1000 ppm by volume. Additional studies have been made under similar experimental conditions using mainly a series of batches of coated fuel particles prepared for irradiation testing in sweep-capsule experiment A9-9.⁵ Reaction rates were obtained from weight changes given by a continuously recording semi-micro balance and from effluent gas analyses per-

formed by a sensitive gas chromatograph. The percentage of coating failures was obtained from microscopic examination and acid leach of the oxidized coated fuel particles.

Reaction rates obtained for various batches of coated fuel particles, along with some coating properties, are given in Table 8.1. The rates obtained at 1100°C vary by more than an order of magnitude, with OR-789C particles giving the highest rate. In agreement with past experiences, it has not been possible to correlate satisfactorily these differences in rates with properties of the coatings. In general, the reaction rates decrease with increasing coating density, but the high rate found for OR-789C particles is a notable exception. Oxidation rates obtained for coatings prepared from CH₄ and C₃H₆ indicate that the hydrocarbon used for deposition of the coatings has no consistent effect on oxidation rates. The degree of contamination of the coatings may be important, but it is very difficult to establish the type and level of contamination.

Plots of weight losses as a function of time at 1200°C given in Fig. 8.3 for OR-789C, OR-813R, OR-814R, and OR-815 particles show the marked differences in rates of carbon removal. The weight losses are very nearly linear with time except for OR-789C particles. Reaction rates, however, calculated on the basis of pyrolytic carbon present at any particular time, increase with time or burnoff for all of these materials.

Data are included in Table 8.1 which show the percentage of coatings that failed during exposure of the various batches of coated particles to water vapor. In some instances, the long exposure times combined with high oxidation rates caused extensive oxidation of the coatings, and, as might be expected, large percentages of coatings failed. Substantial percentages of failures also occurred at fairly low burnoffs in a number of cases. It appears that burnoffs of 10 wt % may be experienced by Isotropic 6, OR-689C, and OR-790C particles with less than 1% of coatings failing, whereas coating failures in excess of 1% would be expected for OR-813R and OR-814R particles at burnoffs of ~5 wt %. The type of oxidation that the coating undergoes could be responsible for these differences. A localized attack would produce failures at low burnoff, whereas a more general type of oxidation would give fewer failures even at larger burnoffs. Microscopic examinations failed to show any pronounced differences in the oxidized coatings, however.

⁴J. E. Baker and L. G. Overholser, *GCR Program Semiann. Progr. Rept. Mar. 31, 1967*, ORNL-4133, pp. 95-100.

⁵J. H. Coobs and H. Beutler, *GCR Program Semiann. Progr. Rept. Mar. 31, 1967*, ORNL-4133, pp. 25-27.

Table 8.1. Rates of Reaction of Pyrolytic-Carbon-Coated Fuel Particles with Water Vapor^a

Batch Designation	Deposition Temperature (°C)	Hydrocarbon Decomposed	Coating Density (g/cm ³)	Oxidation Temperature (°C)	Percent of Coating Oxidized (by weight)	Reaction Rate ^b (mg g ⁻¹ hr ⁻¹)	Coating Failures ^c (%)
OR-788 ^d	2000	CH ₄	2.0	1100	4.9	1.6	2.1
OR-789C ^d	1250	C ₃ H ₆	2.0	1100	40	11	21
OR-789C ^d	1250	C ₃ H ₆	2.0	1200	64	25	31
OR-790C ^d	1600	CH ₄	1.6	1100	16	7.5	0.3
OR-813R ^d	2000	CH ₄	1.75	1100	3.2	2.0	4.0
OR-813R ^d	2000	CH ₄	1.75	1200	15	7.0	13
OR-814R ^d	1250	C ₃ H ₆	1.98	1100	5.1	2.9	5.4
OR-814R ^d	1250	C ₃ H ₆	1.98	1200	13	5.5	8.6
OR-815 ^d	1600	CH ₄	1.54	1100	15	6.0	3.1
OR-815 ^d	1600	CH ₄	1.54	1200	43	19	16
Isotropic 6 ^e	2000	CH ₄	2.00	1100	0.8	0.3	<0.1
Isotropic 6 ^e	2000	CH ₄	2.00	1200	3.7	0.8	<0.1
OR-689 ^d	1250	C ₃ H ₆	1.9	1100	7	3.5	0.8
OR-689 ^d	1250	C ₃ H ₆	1.9	1200	19	7.2	0.8

^a100 mg sample exposed for approximately 24 hr to helium containing 1000 ppm by volume of water vapor at flow rate of 200 cm³ STP/min.

^bReaction rates based on weight of pyrolytic carbon coating; rates given for less than 5 wt % burnoff.

^cCalculated from quantity of uranium (thorium) in acid leach solution and total quantity of uranium (thorium) originally present in 100 mg of coated particles.

^dSupplied by Metals and Ceramics Division, Oak Ridge National Laboratory. Further details in ref. 5.

^eSupplied by General Atomic Division, General Dynamics Corp. Further details given by J. C. Bokros and R. J. Price, *Carbon* 4, 441 (1966).

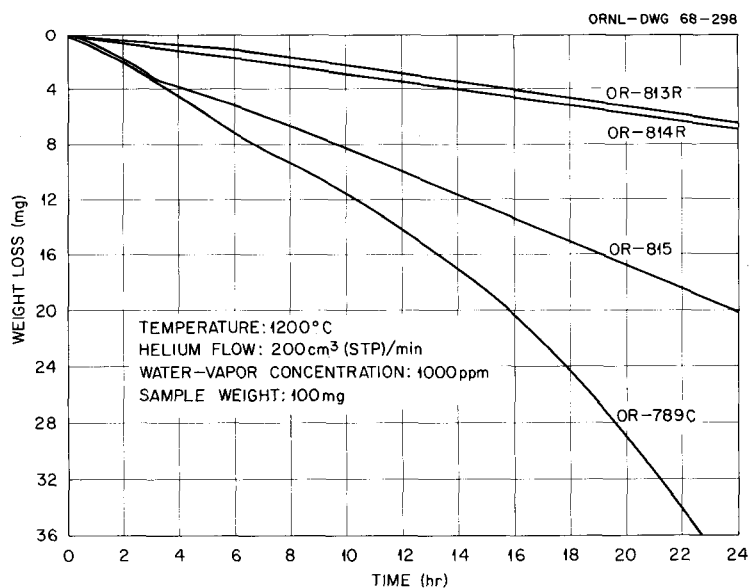


Fig. 8.3. Time Dependence of the Oxidation of Various Batches of Coated Fuel Particles by Water Vapor.

REACTION OF NEEDLE-COKE GRAPHITE WITH STEAM

C. M. Blood G. M. Hebert

Experimental results were reported earlier⁶ for the oxidation of various length hollow cylinders of ATJ graphite. These studies utilized hollow cylinders of both virgin graphite and graphite impregnated with barium. The effects of burnoff, of cylinder length, and of barium on the reaction rates were studied, and, in addition, any transport of barium by the gas stream was established by use of a deposition tube.

More recently a needle-coke graphite (EGCR moderator graphite), similar to that used for the bonded fuel compacts, has been used in the oxidation studies. Hollow and solid cylinders of dimensions similar to those of the fuel compacts were reacted at 1100 and 1200°C with a steam-

helium mixture having a steam pressure of ~20 torrs and a total pressure of 1 atm. Hollow graphite cylinders which had been impregnated with barium also were oxidized under similar experimental conditions.

Reaction rates obtained at 1100°C from effluent gas analyses and based on either the weights or geometric surface areas of the various specimens are given in Fig. 8.4. The lack of agreement between rates based on weights for the 1-in. hollow and solid cylinders indicates that a substantial portion of the solid cylinder was not effectively oxidized due to depletion of steam as it diffused inward. Although a better agreement results when rates are compared on the basis of geometric surface areas, the oxidation was not strictly an outer surface attack. BET surface areas of the specimens were increased by oxidation, indicating attack within the pore structure to some unknown depth. Rates of oxidation obtained at 1200°C and BET surface areas of the oxidized specimens indicate that the reaction also was controlled by in-pore diffusion of water vapor at this higher temperature.

⁶C. M. Blood, G. M. Hebert, and L. G. Overholser, *GCR Program Semiann. Progr. Rept. Mar. 31, 1967*, ORNL-4133, pp. 100-108.

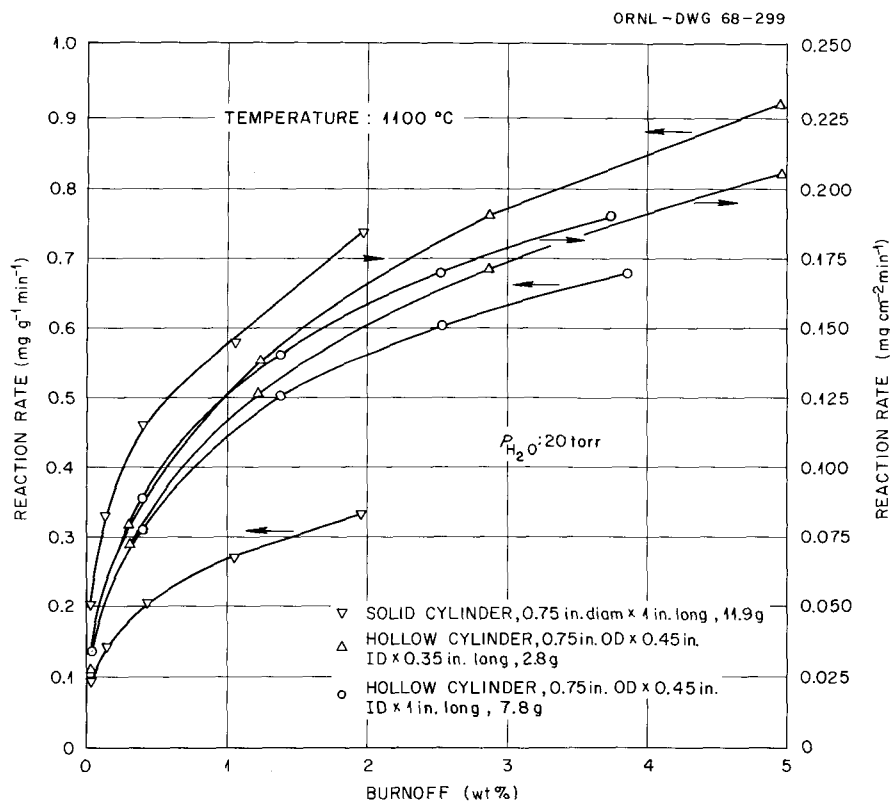


Fig. 8.4. Rates of Reaction of Various Needle-Coke Graphite Cylinders with Steam.

Reaction rates given in Fig. 8.4 indicate that the effect of water vapor depletion and buildup of hydrogen along the length of the hollow cylinders (0.33 and 1.0 in. long) was small. Sectioning of the 1-in.-long hollow cylinder and examination of the influent and effluent sections showed that the removal of carbon per unit length and BET surface areas were only slightly different for the sections. This suggests that only a small axial oxidation gradient was developed in the 1-in.-long hollow cylinder.

Hollow graphite cylinders which had been impregnated with barium containing tracer quantities of ^{133}Ba were heat treated in dry helium at 1200 or 1400°C prior to being oxidized at these temperatures by wet helium having a steam pressure of 20 torrs. The oxidation rates obtained are higher than those measured for unimpregnated graphite, indicating that the reaction is catalyzed by barium. The appearance of the oxidized specimens suggested that oxidation occurred primarily on the geometric surface. A small increase in BET surface area upon oxidation confirmed this observation. The reaction rate at 1200°C was sufficiently

high to make mass transport of steam through the surface film the rate-controlling process.

An alumina sample holder and deposition tube were employed in both the heat treatment and oxidation of the impregnated graphite specimens. Examination of the deposition tubes showed that very little, if any, barium was transported to the deposition tube by dry helium at 1200°C or at either 1200 or 1400°C by wet helium. A significant quantity was transported by dry helium at 1400°C, giving a band of barium in the region where the temperature of the deposition tube was about 1200 to 1300°C. Earlier studies⁷ found a transport of barium in dry helium at 1000°C. The fact that $\text{Ba}(\text{OH})_2$ was used as impregnant in the earlier work, whereas $\text{Ba}(\text{NO}_3)_2$ was used in the more recent work, may account for the differences in transport behavior. If so, the method of impregnation can play an important role in the subsequent behavior of barium.

⁷C. M. Blood, *Reactor Chem. Div. Ann. Progr. Rept.* Dec. 31, 1966, ORNL-4076, pp. 93-95.

9. Irradiation Behavior of High-Temperature Fuel Materials

O. Sisman

J. G. Morgan

IN-PILE TESTS ON PYROLYTIC-CARBON-COATED FUEL PARTICLES

P. E. Reagan E. L. Long, Jr.¹
J. G. Morgan J. W. Gooch

We are studying the irradiation effects on pyrolytic-carbon-coated fuel particles by measuring the fission-gas release rates during irradiation at high temperature and by postirradiation examination. Pyrolytic-carbon-coated fuel particles are presently in use in the AVR, Peach Bottom, and Dragon Reactors. We have compared the fission-gas release from fuel particles coated from three hydrocarbon gases applied at various temperatures and deposition rates.²⁻⁴ Several coating structure combinations have been studied, and this study has revealed that a successful coating must (1) withstand internal pressure exerted by the fission gas and fuel expansion, (2) resist reaction between the fuel material and the pyrolytic carbon coating, and (3) be economically competitive in manufacturing costs.

The first pyrolytic-carbon-coated uranium oxide particles to perform well in irradiation tests were coated with a porous carbon buffer inner layer deposited from acetylene at 1150°C and a dense isotropic outer layer deposited at 1800°C from methane. Investigation of coatings from other

hydrocarbons revealed that dense isotropic outer coatings could be deposited at lower temperature and higher deposition rates, which would result in lower fuel contamination in the pyrolytic carbon and in a large reduction in coating costs.⁵ Subsequently, particles coated from butadiene and propylene deposited at 1250°C and at 6 to 12 μ /min deposition rates were studied during irradiation at high temperature. The irradiation test results, including fractional ⁸⁸Kr release, are summarized in Table 9.1.

The OR-354 coated particles, irradiated as experiment B9-26, were coated from methane. In general, these particles performed well during irradiation. The fission-gas release was low and remained about constant throughout the test. Post-irradiation metallography revealed only very minor structural changes as a result of irradiation.

The OR-767 coated particles, irradiated in experiment B9-33, were coated at 1250°C from butadiene. During irradiation these coated particles did not perform as well as those deposited from methane. The fission-gas release increased during the test, and an abrupt burst of fission gas, released after about 5% uranium burnup, indicated that at least one of the coatings had failed, although postirradiation examination revealed no appreciable microstructural changes as a result of irradiation.

The OR-653 and -654 coated particles, irradiated in capsules A9-8 and A9-12, were also coated at 1250°C, but with propylene as the hydrocarbon

¹Metals and Ceramics Division.

²P. E. Reagan *et al.*, *GCR Program Semiann. Progr. Rept. Sept. 30, 1966*, ORNL-4036, pp. 92-107.

³O. Sisman *et al.*, *GCR Program Semiann. Progr. Rept. Mar. 31, 1967*, ORNL-4133, pp. 33-47.

⁴J. H. Coobs and H. Beutler, *GCR Program Semiann. Progr. Rept. Mar. 31, 1967*, ORNL-4133, pp. 25-33.

⁵R. L. Beatty *et al.*, *GCR Program Semiann. Progr. Rept. Sept. 30, 1966*, ORNL-4036, pp. 1-7.

Table 9.1. Fission-Gas Release from Pyrolytic-Carbon-Coated Fuel Particles

Experiment Number	Batch	Fuel	Coating Gas, ^a Isotropic Layer	Coating Temperature (°C)	Deposition Rate (μ/min)	Burnup ^b (% H.M.)	Irradiation Temperature (°C)	Fractional Fission-Gas Release, R/B, ^c for ⁸⁸ Kr During Last Week of Test
B9-26	OR-354	UO ₂	Methane	1800	3.2	12	1350	4 × 10 ⁻⁶
A9-8	OR-653 OR-654	UO ₂	Propylene	1250	6.6 7.4	17	1400	2 × 10 ⁻⁸
A9-12	OR-654	UO ₂	Propylene	1250	7.4	12	1550– 1650	1 × 10 ^{-3^d}
B9-33	OR-767	UO ₂	Butadiene	1250	12.3	6	1250	3 × 10 ⁻⁵

^aBuffer layer deposited from acetylene at 1150°C and 30 to 33 μ/min.

^bBased on a thermal flux by argon activation.

^cR/B = release rate/birth rate.

^dEstimated value based on xenon release.

supply. These were the best coated particles, based on the extremely low fission-gas release rates and the structural stability, when irradiated to high burnup at 1400°C. However, in the 1550 to 1650°C irradiation temperature range the fission-gas release increased rapidly. Several bursts of fission gas were released, indicating that about 1% of the coatings had failed.⁶ Postirradiation examination revealed that several particles had failed by the formation of a small hole in the coating. Metallographic examination indicated that these holes resulted from reaction between the uranium oxide fuel and the coating. Three irradiated particles, showing different degrees of damage, are compared with an unirradiated particle in Fig. 9.1.

It appears that experiment A9-12 operated at too high a temperature for the power density. It should be noted that these experiments are accelerated burnup tests. In a typical HTGR application,⁷ the fuel has a lifetime of three years and a burnup rate of the fissile particles of 0.5% per month. Experiment A9-12 was irradiated at a

burnup rate of 6% per month, a much more severe test than under actual HTGR conditions.

IN-PILE TESTS ON SILICON-CARBIDE-COATED FUEL PARTICLES

P. E. Reagan
J. G. Morgan

E. L. Long, Jr.¹
T. W. Fulton

We are studying the effects of irradiation at high temperature on pyrolytic-carbon-coated fuel particles that contain a silicon carbide layer. It has already been shown that dense isotropic pyrolytic-carbon-coated fuel particles will retain fission gases within present gas-cooled reactor design criteria,^{7,8} but, at high temperature, fission solids (notably Sr, Ba, and Cs) will diffuse through the pyrolytic carbon.⁹ Therefore, a silicon carbide layer was added as a diffusion barrier. Both the DRAGON Reactor and the AVR incorporate this layer in their reference fissile particles.

The four irradiation experiments are listed in Table 9.2. All particles had an inner porous pyrocarbon layer. This was followed by an outer SiC

⁶P. E. Reagan *et al.*, "Evaluation of Coated Fuel Particles Irradiated in ORR Positions A9 and B9," *GCR Program Semiann. Progr. Rept. Sept. 30, 1967* (in press).

⁷P. E. Reagan, *Fission-Gas Release and Irradiation Damage to AVR Pyrolytic Carbon Coated Thorium-Uranium Carbide Particles*, ORNL-4053 (January 1967).

⁸P. E. Reagan, R. L. Beatty, and E. L. Long, Jr., *Nucl. Sci. Eng.* **28**, 34–41 (1967).

⁹O. Sisman, J. G. Morgan, and M. T. Morgan, "Fission-Product Release from High-Burnup Coated Fuel Particles by Postirradiation Annealing," *GCR Program Semiann. Progr. Rept. Sept. 30, 1967* (in press).

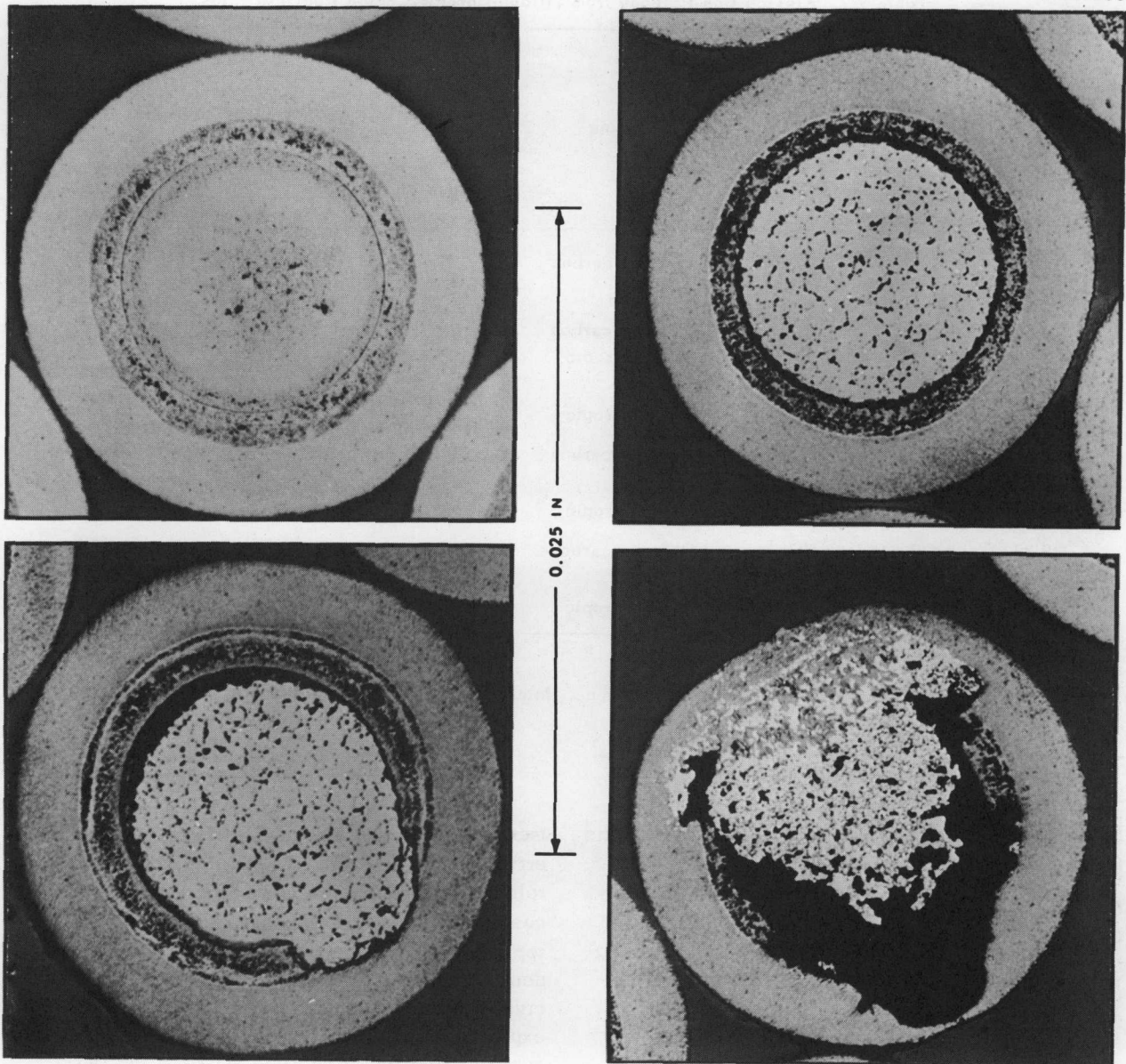


Fig. 9.1. Pyrolytic-Carbon-Coated Uranium Oxide Particles from Batch OR-654; (Upper Left) Unirradiated, (Upper Right and Lower) Irradiated to 12.3 at. % Burnup at 1550 to 1650°C in Capsule A9-12.

layer in experiment B9-34. At 1250°C the fission-gas release (R/B = release rate/birth rate) increased from 1×10^{-5} to 3×10^{-4} during the irradiation to 7% heavy-metal burnup. This increase was due to a small fraction (<2%) of failed coatings.

In the next test, A9-7, the coating had four layers. The inner porous pyrocarbon layer was followed by a dense isotropic layer deposited from propylene. The SiC layer was next, with a very thin (5μ) outer layer of isotropic carbon. These

particles had a very low gas release at 1300°C, which remained constant throughout the test. The outer pyrocarbon also prevented the particles from sticking together, as had occurred in the previous test.

The three-layer coating arrangement in batch OR-818 particles had the SiC between the buffer and isotropic pyrocarbon layers. At 1250°C the fission-gas release was very low and remained so during the irradiation. When these same particles were irradiated at 1700°C, however, the gas re-

Table 9.2. Fission-Gas Release from Silicon-Carbide-Coated Fuel Particles

Experiment Number	Batch	Fuel ^a	Coating ^b	Burnup ^c (% H.M.)	Irradiation Temperature (°C)	Fractional Fission-Gas Release, R/B, for ⁸⁸ Kr During Last Week of Test
B9-34	GA-331	UC ₂	porous carbon + SiC	7	1250	3 × 10 ⁻⁴
A9-7	GA-327	(U,Th)C ₂	porous carbon + isotropic + SiC + isotropic	3	1300	6 × 10 ⁻⁸
B9-35	OR-818	UO ₂	porous carbon + SiC + isotropic	11	1250	2 × 10 ⁻⁸
B9-37	OR-818	UO ₂	porous carbon + SiC + isotropic	8	1700	3 × 10 ⁻⁴

^aFuel particle diameters averaged 200 μ.

^bBuffer layer averaged 40 μ, deposited from acetylene. Isotropic layer averaged 40 μ. SiC layer averaged 24 μ, deposited from methyltrichlorosilane.

^cBased on a thermal flux by argon activation.

lease was high and coating failures occurred. This failure was caused by the high burnup rate, 0.5% per month, which had also caused failures in an all-pyrocarbon coating. A particle severely damaged by irradiation at 1700°C is compared with an unirradiated particle in Fig. 9.2. Severe damage to all three coating layers can be seen as the result of the fuel migration.

FISSION PRODUCT RELEASE BY POSTIRRADIATION ANNEALING OF COATED PARTICLES

M. T. Morgan R. L. Towns

To study the retention of fission products by coated fuel particles at high temperatures, two capsules (each containing eight different batches of coated particles) were irradiated to burnups of 15 and 5% uranium metal respectively. The purpose of these postirradiation annealing experi-

ments was to evaluate the effects of coating properties on coating stability and fission product release and to compare coated UO₂ particles with coated UC₂ particles. The outer coating anisotropy factors, σ_{oz}/σ_{ox} , varied from 1 to 1.5, the density varied from 1.44 to 2.01 g/cm³, and the crystallite size varied from 25 to 130 Å in these experiments. The outer coatings were deposited over identical inner coatings on UC₂ and UO₂ particles.

After irradiation the coated particles were separated into samples of ten particles each. Samples of each type of coated particle were annealed at 1700°C, and duplicate samples were annealed at 2000°C. The experimental procedure has been described.¹⁰ The anneals were carried out in steps of 6 or 6½ hr for a total of 19½ hr for the

¹⁰M. T. Morgan, D. C. Evans, and R. M. Martin, *GCR Program Semiann. Progr. Rept. Mar. 31, 1963*, ORNL-3445, pp. 103-6; M. T. Morgan *et al.*, *GCR Program Semiann. Progr. Rept. Sept. 30, 1963*, ORNL-3523, pp. 149-52.

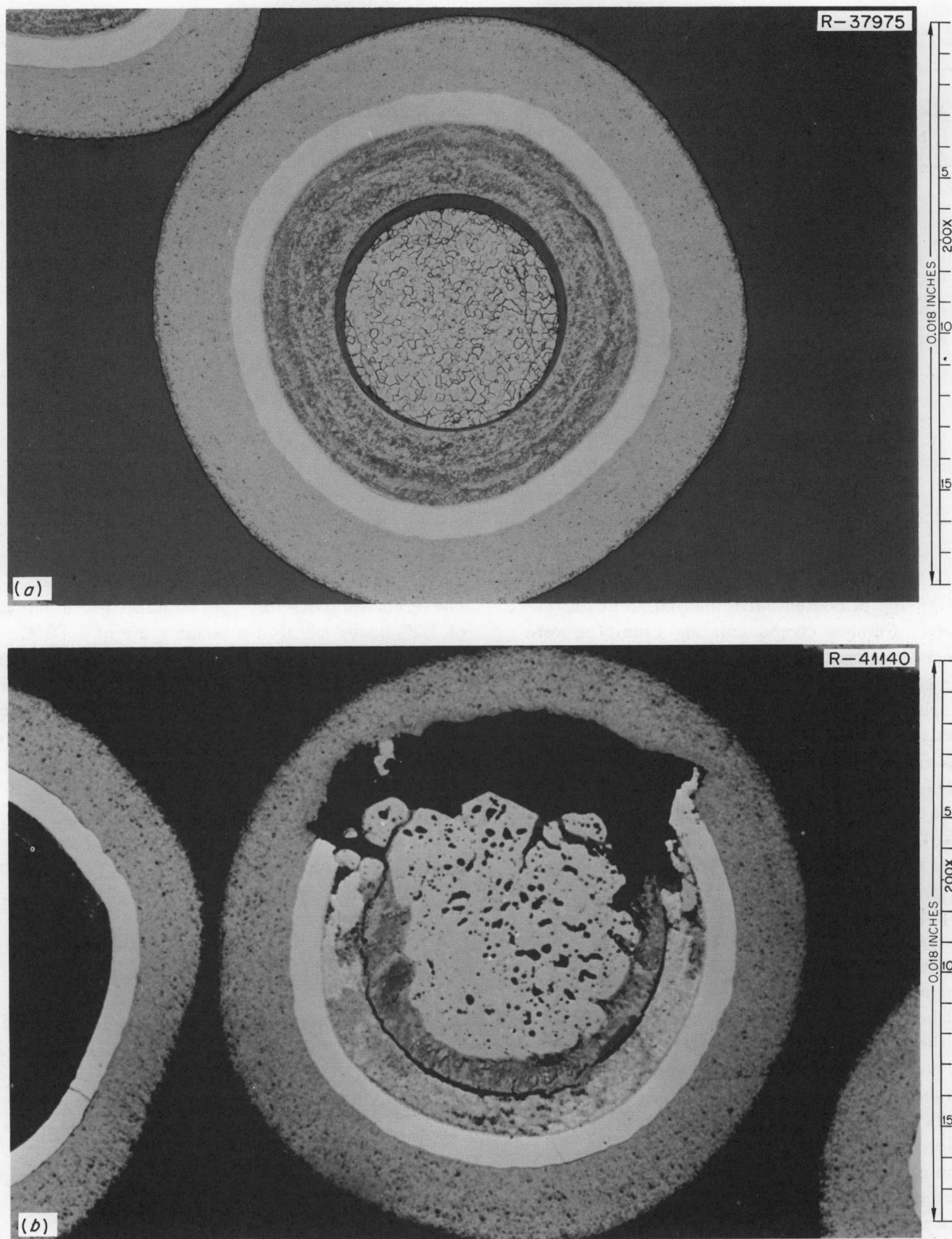


Fig. 9.2. Pyrolytic-Carbon- and Silicon-Carbide-Coated Uranium Oxide Particles from Batch OR-818. (a) Unirradiated. (b) Irradiated to 7.7% burnup at 1700°C maximum in capsule B9-37. 200X.

Table 9.3. Fractional Release of Fission Products During Anneals of Pyrolytic-Carbon-Coated Fuel Particles

Experiment Number	Number of Samples	Fuel Material	Percent of Fission Products Released			
			^{89}Sr	^{137}Cs	^{144}Ce	^{91}Y
At 1700°C						
A9-4	4	UO ₂	11	3.4	0.012	
A9-9	3	UO ₂	8.5	2.6	0.019	0.036
A9-4	2	UC ₂	11	1.2	5.4	
A9-9	3	UC ₂	6.4	1.7	3.9	3.9
At 2000°C						
A9-4	4	UO ₂	38	36	0.18	
A9-9	4	UO ₂	37	38	0.18	<0.15
A9-4	1	UC ₂	67	16	39	
A9-9	3	UC ₂	58	14	54	88

first groups of coated particles and 12 hr for the second. Furnace components and crucibles were removed and analyzed for solid fission products after each step. Fuel migration studies by metallography and microradiography were reported previously.¹¹

No difference in fission product releases was observed that could be ascribed to coating variables in the pyrolytic carbon coatings. Consistent differences were observed, however, between the fission product release from coated UO₂ particles and that from coated UC₂ particles. In Table 9.3 the analytical results of 13-hr anneals in the A9-4 experiment were averaged to compare with the averages of 12-hr anneals on the A9-9 experiment. These averages show good agreement between the two experiments and indicate that the ^{137}Cs release is higher in the coated UO₂ particles, while the ^{144}Ce and ^{91}Y release is higher in the coated UC₂ particles. These results are also in agreement with some of our earlier experiments.

One postirradiation annealing study was completed on pyrolytic-carbon-coated (Th,U)C₂ particles with a silicon barrier layer in the coating.

These coated particles were irradiated to a burnup of 3.2% heavy metal at a temperature of 1300°C. A sample of the irradiated particles was separated into three groups of 50 particles each for annealing at temperatures of 1300, 1700, and 2000°C respectively. The 1300 and 1700°C groups were annealed for 6½ hr each. The 2000°C group was annealed in steps of 6½ hr for a total of 32 hr.

Fission product release was negligible at 1300 and at 1700°C during the 6½-hr anneals, except for ^{137}Cs . The release of ^{89}Sr , ^{91}Y , ^{95}Zr , ^{103}Ru , ^{140}Ba , and ^{144}Ce was less than 25 ppm for each. The ^{137}Cs release was 0.2% at 1300°C and 3.2% at 1700°C. The results of the 2000°C anneal are shown in Fig. 9.3. The release of most of the fission products was low during the first 6-hr anneal but increased rapidly over the 32-hr period.

MECHANISM OF FISSION-GAS RELEASE FROM FUELED PYROCARBON-COATED MICROSPHERES

C. D. Baumann P. E. Reagan

Two experiments have been carried out in the A-9 fuels irradiation facility in the ORR to learn more about the mechanism of fission-gas release

¹¹M. T. Morgan, C. D. Baumann, and R. L. Towns, *Reactor Chem. Div. Ann. Progr. Rept. Dec. 31, 1966*, ORNL-4076, pp. 101-2.

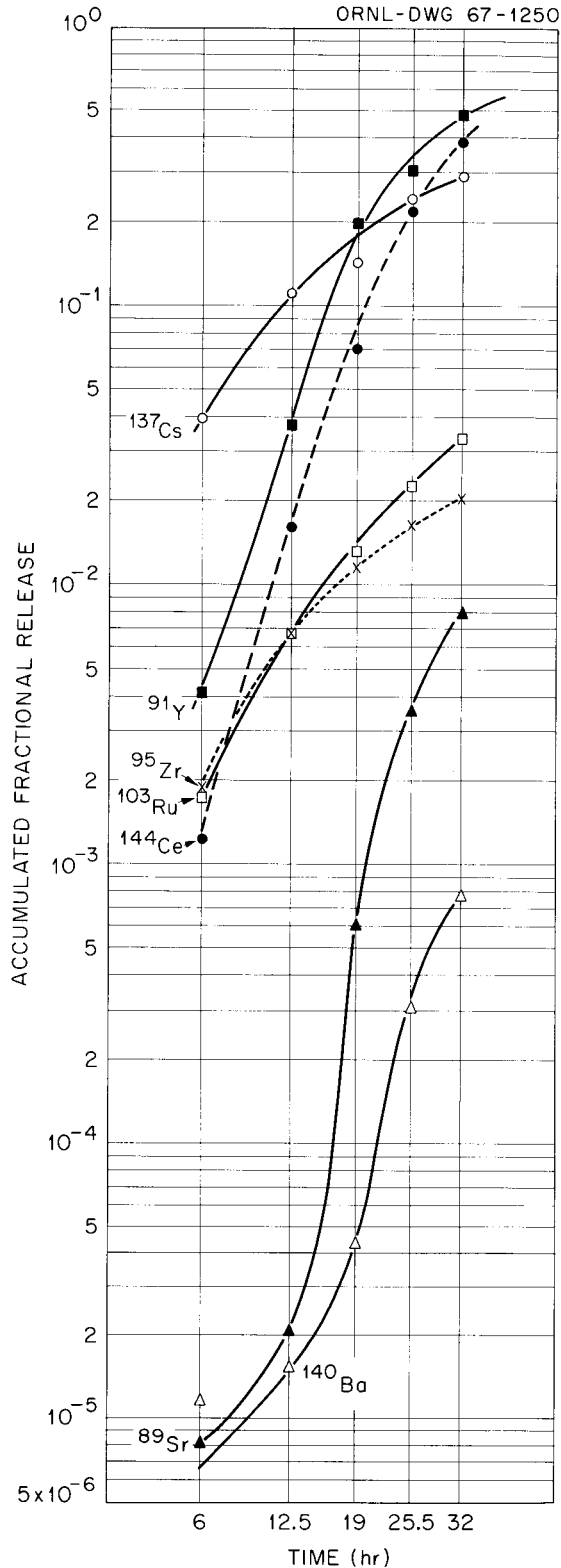


Fig. 9.3. Fission Product Release During Postirradiation Anneals of Pyrolytic-Carbon-Coated (Th,U) C_2 Particles with Silicon Carbide Barrier Layer.

from pyrolytic-carbon-coated fueled particles. To evaluate the experimental results, mathematical models for five different idealized modes of release were developed. The models are as follows:

1. All release is due to fission products born in intact uranium-contaminated coatings. The modes of release from the surface of the coating are by

a) Direct recoil only. The fractional release of all fission products having the same recoil range is identical.

b) Fickian solid-state diffusion only. For low fractional release, the fractional release $\approx \frac{1}{\sqrt{\lambda}}$ for fission products having the same diffusion coefficient.

c) Simultaneous direct recoil and diffusion:

$$(f_1 - f_2) / \left(\frac{1}{\sqrt{\lambda_1}} - \frac{1}{\sqrt{\lambda_2}} \right)$$

is a constant, where f_1 and f_2 are fractional releases of two isotopes having the same diffusion coefficient and the same recoil range.

2. The coating is barren; all fission products originate in the fueled kernel and migrate through the intact coating via

a) Fickian solid-state diffusion:

$$\left(\ln \frac{\lambda_1 f_1}{\lambda_2 f_2} \right) / (\sqrt{\lambda_2} - \sqrt{\lambda_1}) \approx e \Delta E / 2RT,$$

where ΔE is the activation energy of diffusion and T ($^{\circ}\text{K}$) is the characteristic irradiation temperature.

b) Knudsen flow through pores in the coating:

$$\left(\ln \frac{\lambda_1 f_1}{\lambda_2 f_2} \right) / (\sqrt{\lambda_2} - \sqrt{\lambda_1}) \approx T^{-1/4}.$$

In applying the tests of the various models to the low fractional releases (order of 10^{-8} at 1550°C) in the first experiment, it was found that the criteria for diffusive flow from contaminated

coatings fitted the data better than any other; that is, $\sqrt{\lambda} f$ for ^{85m}Kr , ^{87}Kr , and ^{88}Kr agreed within approximately 10%.

The release rates from the second experiment, A9-11, were one to two orders of magnitude greater than A9-10, probably because of a higher level of uranium contamination in the coating. These data are now being analyzed.

RELEASE OF IODINE FROM BROKEN COATED PARTICLES (IN PILE AND OUT OF PILE)

M. T. Morgan P. E. Reagan
O. Sisman R. L. Towns

One of the current problems in nuclear safety for the HTGR is the determination of the possible magnitude of fission product iodine release during an accidental reactor excursion. It has already been determined that pyrolytic-carbon-coated particle fuels retain practically all of the fission product iodine as long as the coatings remain intact, but it was desired to know how much iodine would escape if the coatings were fractured. Some answers to this problem have been obtained by (1) postirradiation heating experiments, (2) analysis of iodine remaining in fuel particles, and (3) measuring the release rate of the xenon daughter during irradiation.

Fractional Release of ^{131}I During Postirradiation Anneals of Cracked Coated UO_2 Particles

Pyrolytic-carbon-coated UO_2 particles irradiated to a burnup of 16% U were reirradiated to an additional burnup of 1% at a low temperature to produce fresh fission product iodine for the postirradiation experiments on iodine release. The coatings were cracked after irradiation to simulate coating failures, and the particles were annealed for 1 hr to determine ^{131}I release. Anneals were performed on one particle at a time, and ^{131}I analyses were made on the coated particles before heating and on the furnace components after the anneal to determine the amount released. The analyses are accurate to $\pm 10\%$ and the temperatures within $\pm 30^\circ\text{C}$. Analyses have been made

Table 9.4. Fractional ^{131}I Release During 1-hr Anneals of Pyrolytic-Carbon-Coated UO_2 Particles with Coatings Cracked to Simulate Failures

Temperature ($^\circ\text{C}$)	Release (% of total)
1100	0.6
1300	2
1350	6
1400	10

at several temperatures to determine the iodine release as a function of temperature. These results are given in Table 9.4. These studies are continuing, but the initial data are indicating that the release rate will be quite low in the temperature range of interest for the HTGR, between 900 and 1200°C . Future studies of the release rate vs time are expected to correct the low-temperature release rate downward because of the initial burst release during heatup.

Fractional Release of ^{131}I from Bare UO_2 Cores During Irradiation

SiC-coated UC_2 particles were irradiated to a burnup of 25.6 at. % uranium at an estimated particle core temperature of 1700°C . After irradiation some of the intact coated particles were cracked and the coatings separated from the cores. Analyses of the coatings and cores showed that 55% of the ^{131}I was retained in the cores, while 45% had transferred to the coating. We calculated the release rate from the cores by the relation

$$R = \lambda \frac{F}{1 - F},$$

where

R = release rate (fraction/hr),

λ = ^{131}I decay constant,

F = fraction released to coating.

The calculated release rate of ^{131}I from bare cores during irradiation was 0.3%/hr.

Iodine Release from UC_2 and UO_2 Particles During Irradiation

The release of ^{133}I and ^{135}I was measured on bare UC_2 and UO_2 particles during irradiation by measuring the release rate of the xenon daughters. The fuel was held at a constant temperature until equilibrium was established. It was then quickly withdrawn from the reactor while continuing to measure the xenon release. At this low temperature the xenon comes only from iodine which was released during irradiation and deposited outside the fuel. The total ^{135}Xe release rate and that released as iodine are shown in Fig. 9.4 for the bare UC_2 particles over the temperature range from 700 to 1200°C.

About half of the ^{135}Xe was released from the UC_2 fuel as ^{135}I . At 1200°C this release rate corresponds to about 0.5%/hr of the equilibrium amount of iodine in the fuel particles. For comparable-size UO_2 particles operating under comparable conditions, the release rate of ^{135}I was lower than for the UC_2 particles by a factor of 20.

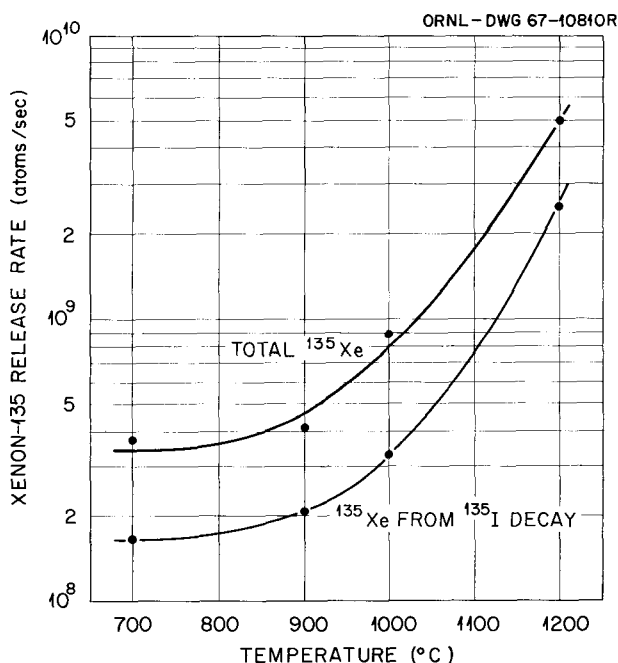


Fig. 9.4. Total ^{135}Xe Release Rates During Irradiation Compared with ^{135}Xe Release Rates from ^{135}I Decay Following In-Pile Capsule Withdrawal.

POSTIRRADIATION STUDIES OF HIGH-BURNUP COATED PARTICLES

D. R. Cuneo
J. A. Conlin¹²

E. L. Long, Jr.¹
H. E. Robertson

A series of experiments has been designed by the Reactor Division in support of the high-temperature gas-cooled reactor fuel program to evaluate the overall stability of coated particles to burnups of 50% heavy metal at coated particle surface temperatures between 1100 and 1400°C. The capsule design and details of operation along with detailed postirradiation findings for two of the experiments have been reported previously.¹³⁻¹⁸ The following will summarize postirradiation evaluations of the first experiment and the second to the present extent of completion.

The first experiment, designated as F-9-1, contained monolayers of two batches of coated particles in separate graphite fuel holders: HB-23 particles (triplex coated UO_2) in the upper holder and GA-320 (biso coated UC_2) in the lower holder. The assembly was operated to 44.4% heavy-metal burnup in the upper holder and 49.0% in the lower. The fission-gas release rate increased by 2 orders of magnitude between the estimated burnups of 6 and 14%. The rates then stayed constant to the end of irradiation. The sharp increase is surprising, as metallographic examination of the fuel particles showed no failures. No potential failures were observed in either batch of coated particles, but in about 5% of the GA-320's localized attack had occurred at the inner surface of the buffer coating and extended into the isotropic layer. No crystalline detail could be resolved in

¹²Reactor Division.

¹³A. W. Longest and J. A. Conlin, *GCR Program Semiann. Progr. Rept. Mar. 31, 1965*, ORNL-3807, pp. 53-65.

¹⁴A. W. Longest, J. A. Conlin, and V. A. DeCarlo, *GCR Program Semiann. Progr. Rept. Sept. 30, 1965*, ORNL-3885, pp. 78-82.

¹⁵A. W. Longest and J. A. Conlin, *Design of an Irradiation Experiment to Test Coated-Particle Fuels to High Burnup*, ORNL-TM-1427.

¹⁶A. W. Longest et al., *GCR Program Semiann. Progr. Rept. Sept. 30, 1966*, ORNL-4036, pp. 72-78.

¹⁷J. A. Conlin et al., *GCR Program Semiann. Progr. Rept. Mar. 31, 1966*, ORNL-4133, pp. 60-76.

¹⁸J. A. Conlin et al., *GCR Program Semiann. Progr. Rept. Sept. 30, 1967*, ORNL-4200.

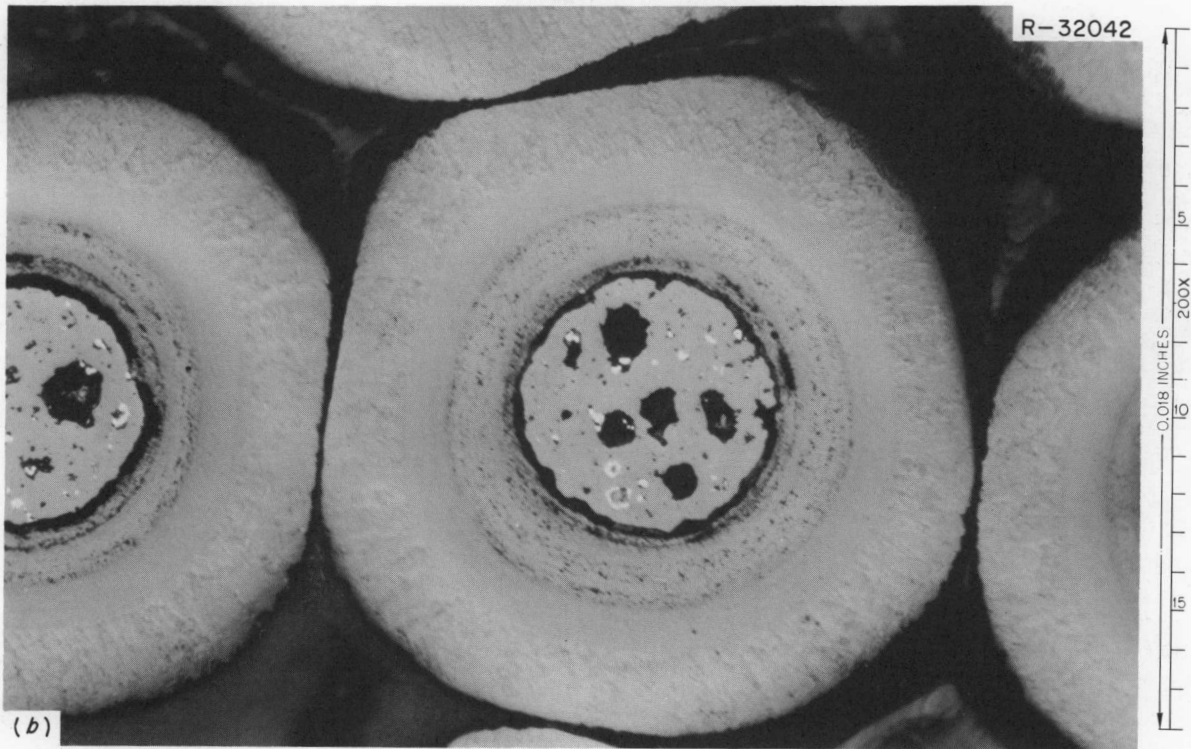
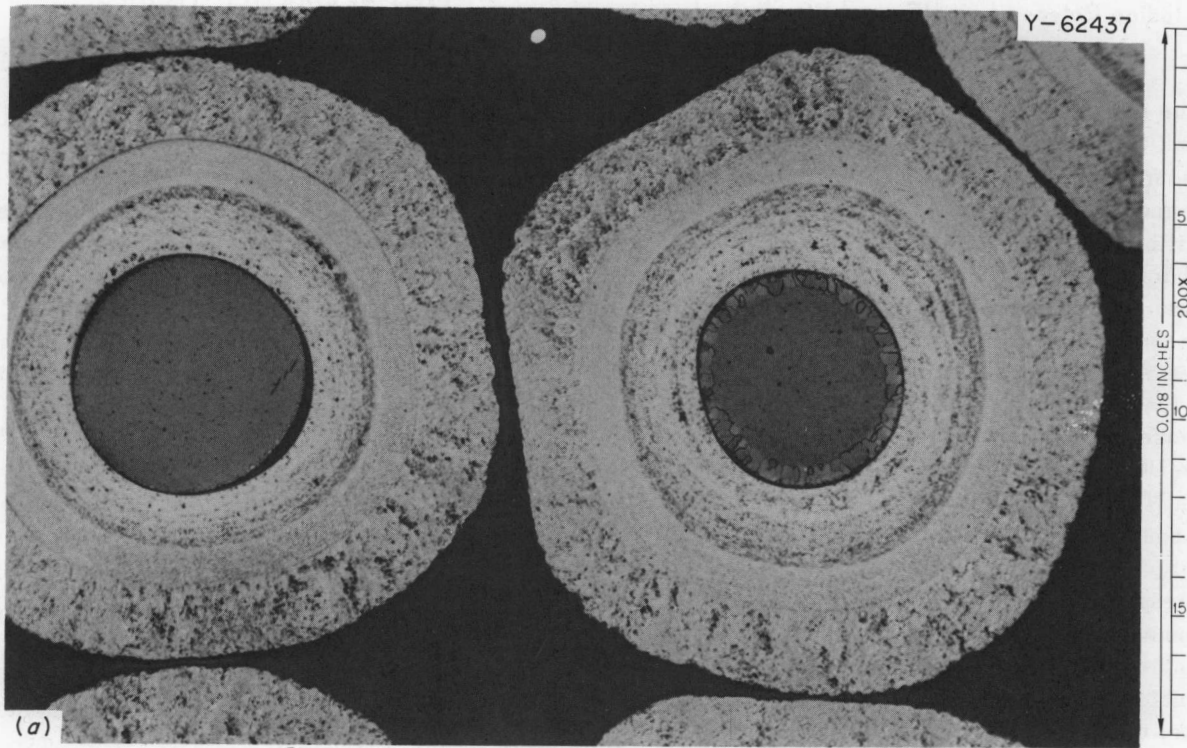


Fig. 9.5. Typical Pyrolytic-Carbon-Coated Sol-Gel UO_2 Particles from Batch OR-HB-23. (a) Unirradiated. (b) Irradiated.

the fuel cores of either batch after irradiation because of the high burnup. The fuel surface temperature is believed to have been 1400°C maximum. Figure 9.5 shows an irradiated HB-23 particle as well as an unirradiated control.

The second experiment in the series, F-9-2, was of similar overall design to the first except that nine different batches of particles were irradiated. Four of these batches were designed according to a mathematical model¹⁹ to withstand about 50% burnup, while two other batches were designed to fail between 30 and 45% burnup. In addition, two batches of particles had barrier-type coatings of SiC (deposited from CH_3SiCl_3), which are of interest for retention of metallic fission products.

Initial fission-gas release rates for this experimental assembly were normal; however, they increased rapidly until at termination of the experiment they were of the order of 1% for ^{135}Xe and 10% for ^{133}Xe . These large values and the pattern of achieving them indicated gross particle coating failures, and the experiment was terminated.

Disassembly of the experiment revealed that essentially 100% of the GA-331 coated particles had failed. The other SiC batch, GA-330, was mixed with pyrolytic-carbon-coated GA-329 particles. These SiC-coated particles also failed, but not as badly as the GA-331's. From preliminary metallographic examinations we believe that the particles ran in excess of the design temperature of 1250 to 1300°C. Preliminary burnup calculations show a value of about 20% heavy-metal burnup.

RADIATION DAMAGE IN FAST GAS-COOLED REACTOR FUELS

D. R. Cuneo E. L. Long, Jr.¹
H. E. Robertson J. A. Conlin¹²

Evaluations of irradiated experimental fuel assemblies of interest to the fast gas-cooled reactor program have continued. This is a cooperative program with Gulf General Atomic Company. Details of test conditions and procedures were de-

termined by the ORNL Reactor Division in cooperation with GA, and the fuel specimens are supplied by GA. This series of tests is designed to investigate the effects of irradiation, thermal cycling, external pressure, and fuel-cladding interactions on the integrity and behavior of metal-clad UO_2 and $(\text{Pu,U})\text{O}_2$ fuel elements having design features that approximate those for the General Atomic fast gas-cooled reactor design. During the past year we have completed examinations of three capsules containing a total of seven fuel elements. Six of the seven were of the fuel-cladding interacting type in which the cladding is designed to collapse onto the fuel pellets at the outset of pressure and temperature. The other fuel element was of the free-standing fuel or "flexcan" type. This type has a deformed section of cladding above the fueled region that is capable of flexing with pressure changes, and the internal void is filled with sodium. Four of the fuel elements contained UO_2 ; three contained $(\text{Pu,U})\text{O}_2$.

The design and operation of these experimental assemblies, earlier ones in the series, and details of postirradiation findings have been previously reported in detail.²⁰⁻²⁵ Operating conditions and metallographic observations are given in Table 9.5. Figure 9.6 shows, at high magnification, the shiny metallic crystals found along the grain boundaries of the fuel in GA-8. Figure 9.7 shows the dimpled and cracked region of the cladding in GA-14, as well as the microstructural changes observed in the fuel.

¹⁹J. W. Prados and J. L. Scott, *Nucl. Appl.* 2(5), 402-14 (October 1966).

²⁰F. R. McQuilkin *et al.*, *GCR Program Semiann. Progr. Rept. Sept. 30, 1965*, ORNL-3885, pp. 244-50.

²¹F. R. McQuilkin *et al.*, *GCR Program Semiann. Progr. Rept. Mar. 31, 1966*, ORNL-3951, pp. 169-79.

²²D. R. Cuneo *et al.*, *GCR Program Semiann. Progr. Rept. Mar. 31, 1966*, ORNL-3951, pp. 179-80.

²³D. R. Cuneo *et al.*, *GCR Program Semiann. Progr. Rept. Sept. 30, 1966*, ORNL-4036.

²⁴J. A. Conlin *et al.*, *GCR Program Semiann. Progr. Rept. Mar. 31, 1967*, ORNL-4133, pp. 139-65.

²⁵J. A. Conlin *et al.*, "Capsule Irradiations to Study Interactions of Fuel and Cladding," *GCR Program Semiann. Progr. Rept. Sept. 30, 1967*, ORNL-4200 (in press).

Table 9.5. Operating Conditions and Metallographic Observations
for Experimental Fast Gas-Cooled Reactor Fuel Elements

Experiment and Fuel Element	Fuel	Burnup (% H.M.)	Cladding Material	Maximum Cladding Temperature (°C)	Operating Pressure (psi)		Metallographic Observations
					Internal	External	
P4B4							
GA-8	UO ₂ (21.58% 235)	0.86	304 SS	720	(Flexcan type)		Slight equiaxed grain growth, with slight loss in grain boundary integrity noted in central region of fuel, where shiny metallic crystals were found along with a non-metallic phase in the grain boundaries. See Fig. 9.6.
GA-9	UO ₂ (30.2% 235)	0.90	Hastelloy X	670	1000	500	UO ₂ pellet near top of fuel stack underwent columnar grain growth. Pellet near midlength showed only equiaxed growth.
O4-P5							
GA-10	UO ₂ (29.3% 235)	1.02	Hastelloy X	815	1000	70	Subsurface voids to maximum depth of 1.5 mils in cladding. Equiaxed grain growth started 35 mils from the outer fuel surface and continued to 85 mils from surface; columnar grain growth from this region to the inner surface. Central hole in the fuel now elliptical (diameter, 30 and 50 mils).
GA-11	UO ₂ (29.5% 235)	1.32	Hastelloy X	710	1000	500	Subsurface voids in cladding to a depth of 4 mils at pellet interfaces, which had begun to sinter together 30 mils from their outer surface. Equiaxed and columnar grain growth noted at 15 and 50 mils, respectively, from outer fuel surface.
O4-P6							
GA-12	UO ₂ , 88 wt % (6% 235); PuO ₂ , 12 wt %	0.40	Hastelloy X	816	1000	300	No evidence of damage to cladding; no reaction observed at fuel-cladding interfaces. Equiaxed grain growth starting 35 to 50 mils from fuel surface — extended to 75 mils, where columnar grain growth with lenticular voids started and continued to inner surface.
GA-13	Same	0.48	Hastelloy X	816	1000	70	Cladding partially collapsed near midlength. Central void in fuel became elliptical (diameter, 38 and 73 mils). Equiaxed grain growth started at 10 mils from OD. At 25 mils small columnar grains formed, and starting at 45 mils large columnar grains extended to the central void. No evidence of fuel melting. Fuel-cladding reaction product (metallic) about 10 μ thick on fuel.
GA-14	Same	0.48	Hastelloy X	816	1000	700	Deep (80 mils) dimple ($\frac{1}{8}$ in. diam) in cladding $\frac{13}{16}$ in. from top end; longitudinal crack $\frac{7}{8}$ in. long starting at dimple (see Fig. 9.7). Central void in fuel closed in this region, but no evidence of melting. Equiaxed grain growth in fuel within 0.5 mil of outer surface adjacent to failed cladding. Large columnar grains started at 45 to 60 mils and continued to inner surface. Distinct circumferential separation visible at juncture of equiaxed and columnar grains; partial bridging indicated this did not result from last cooldown.

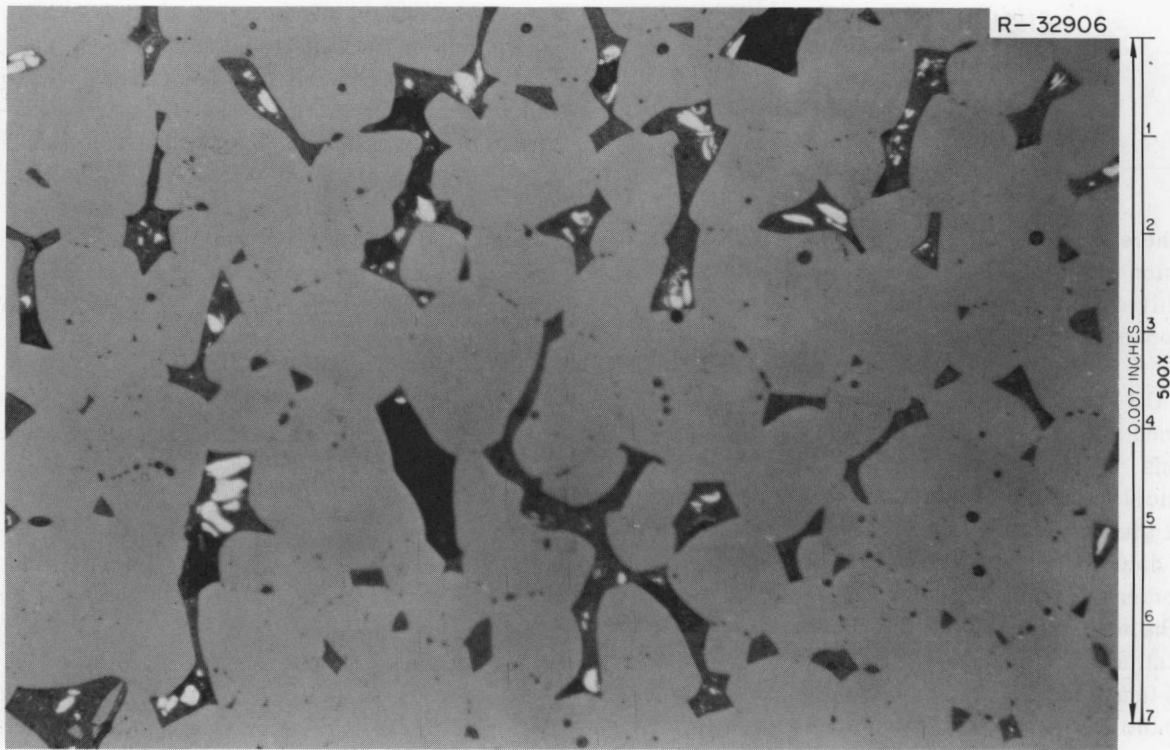


Fig. 9.6. Appearance of Central Region of UO_2 in GA-8, Showing Shiny Metallic Crystals in Grain Boundaries.

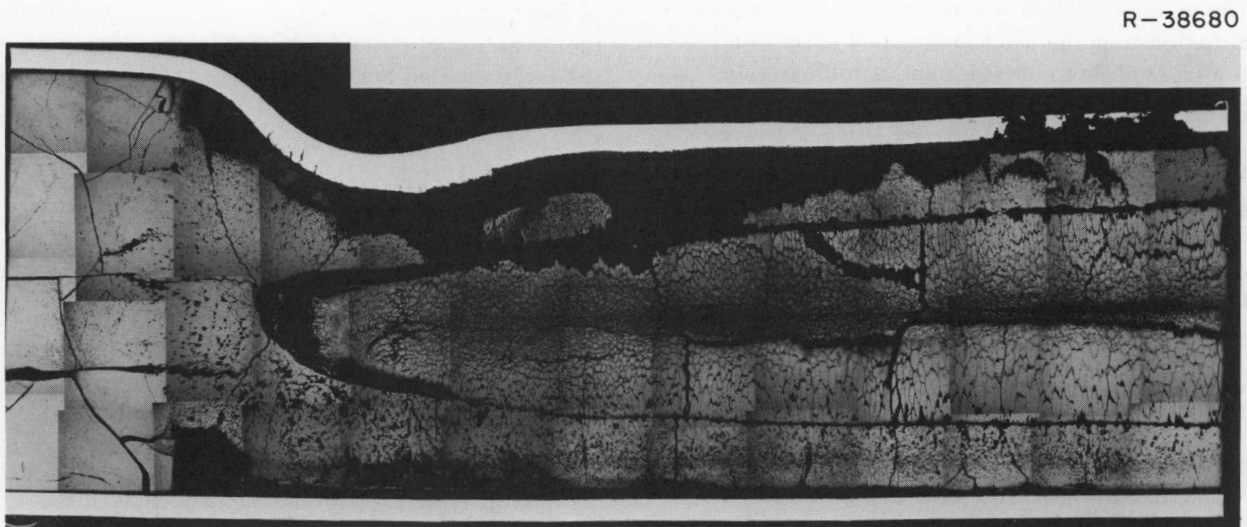


Fig. 9.7. Appearance of Longitudinal Section from the Upper End of GA-14 Showing Dimpled and Cracked Region of Cladding and Grain Growth in the $(Pu,U)O_2$ Fuel.

FISSION-GAS RELEASE DURING FISSIONING OF UO_2

R. M. Carroll R. B. Perez
G. M. Watson O. Sisman
T. W. Fulton

There are many interacting factors controlling fission-gas behavior in UO_2 .²⁶ Using data from highly controlled in-pile experiments we have proposed a defect-trap model of fission-gas escape.²⁷ This theory postulates that defects in the UO_2 crystal structure, whether natural or formed by irradiation, will trap migrating gas atoms.²⁸ The model has been placed in mathematical form, and earlier calculations have shown that steady-state measurements cannot produce the data necessary to solve the equations.²⁹ In order to obtain an additional degree of freedom in the analysis,³⁰ dynamic experiments are being constructed wherein oscillations of fission rate and temperature are imposed on the fuel specimen, and the resulting oscillations in fission-gas release are measured.

The mathematical model has been coded by the Mathematics Division to allow computer fitting of the data.³¹ This computer code yields the release rate of fission gas as a function of time, and the transfer function as a function of frequency. The present studies include analysis of several diffusion-trapping mechanisms and parameter search studies to obtain a set of release rate parameters for engineering calculations.

In evaluating the dynamic experiment it was necessary to calculate the dispersion of fission gas within the helium sweep gas. The dispersion was measured experimentally in a bench test, and a flow model was developed which had excellent agreement with the theoretical results.³² This

flow model should prove useful to other experimenters doing sweep-gas experiments.

As now formulated, the mathematical model applies only to temperatures where clusters of defects do not migrate, for UO_2 below about 1100°C. To obtain information at higher temperatures, single-crystal³³ and fine-grain specimens³⁴ were irradiated at temperatures ranging to 1700°C. Both types of specimens showed gas release which was characteristic of small cluster migration in the temperature range 1100 to 1600°C. The fine-grain specimen showed increased gas release at 1700°C, which is interpreted as caused by grain growth.³⁴ The activation energy for gas release from the single-crystal UO_2 did not change, up to 1700°C.

At temperatures of 1600°C and above, short bursts of gas were released by both specimens during steady-state operation. When the fine-grain specimen was cooled by removing it from the neutron flux a large burst of gas resulted (see Fig. 9.8). Iodine was also released in this burst, so that more ^{135}Xe was being released after withdrawal than just before (because of iodine decay into xenon). We think the spontaneous bursts are caused by the collection of gas into large defect traps near the specimen surface, where enough pressure is eventually generated to cause microcracks in the specimen surface. A temperature of about 1600°C appears to be necessary to allow the formation of these large traps, resulting in the large cooling burst. After the initial cooling burst, following the 1600 to 1700°C irradiation, a second spontaneous burst was observed (see Fig. 9.8). This was likely caused by the decay of trapped iodine into xenon, the increased pressure causing a microcrack.

IN-PILE THERMAL CONDUCTIVITY OF URANIUM DIOXIDE

R. B. Perez O. Sisman
R. M. Carroll J. G. Morgan

Feasibility studies on the measurement of the thermal conductivity of specimens of UO_2 under irradiation have continued for the past year.

²⁶R. M. Carroll, *Nucl. Safety* 8(4), 345-53 (1967).

²⁷R. M. Carroll and O. Sisman, *Nucl. Sci. Eng.* 21(2), 147-58 (1965).

²⁸R. M. Carroll and O. Sisman, *J. Nucl. Mater.* 17(4), 305-12 (1965).

²⁹R. M. Carroll, R. B. Perez, and O. Sisman, *J. Am. Ceram. Soc.* 48(2), 55-59 (1965).

³⁰R. M. Carroll and O. Sisman, *Nucl. Appl.* 2(2), 142-50 (1966).

³¹Paul Nelson, Jr., and V. A. Singletary, *A Package of Programs for Calculating the Release Rate of Fission Gases by the Defect-Trap Model*, ORNL-CF-67-8-57 (August, 1967).

³²R. M. Carroll, R. B. Perez, and O. Sisman, *Am. Nucl. Soc. Trans.* 10(2), 657 (1967).

³³R. M. Carroll et al., *Fuels and Materials Development Program Quart. Progr. Rept. June 30, 1967*, ORNL-TM-1941, pp. 81-93.

³⁴R. M. Carroll et al., *ibid.*, Sept. 30, 1967 (in press).

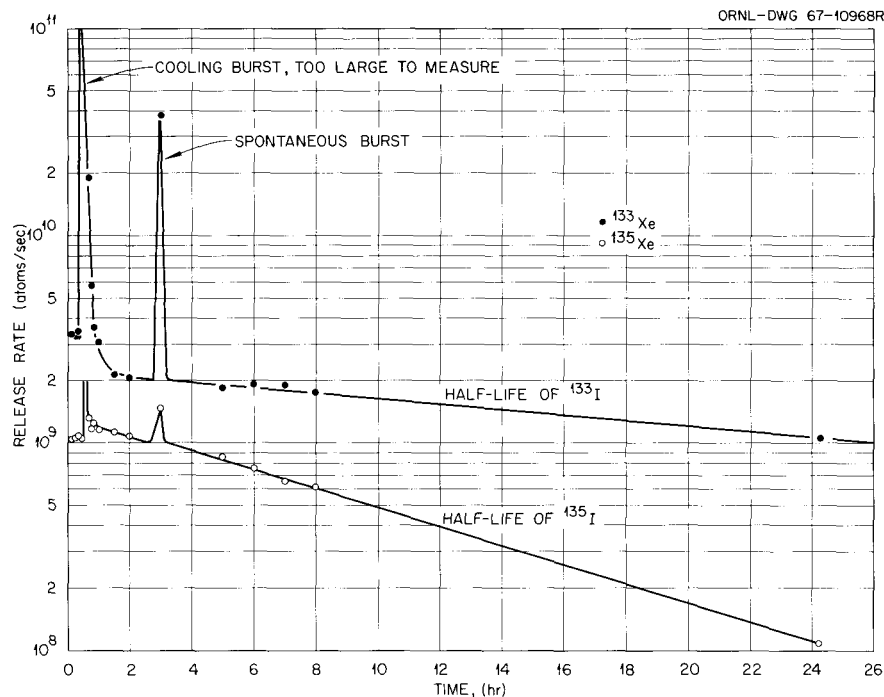


Fig. 9.8. ^{133}Xe and ^{135}Xe Release when Fine-Grain Specimen (C1-20) Was Withdrawn from Neutron Flux After 5 Days Irradiation at 1700°C ($\phi = 6.0 \times 10^{13}$).

Briefly, the technique is based on changing the heat input of the specimen in a stepwise fashion by moving it into a higher flux region in the reactor. Specimen temperature and the surrounding temperature are measured both at the initial position and as a function of time after the flux change. The experimental details have been reported elsewhere.^{35,36} The theory and some preliminary results are summarized below.

Call T_{10} and T_{20} , respectively, the initial temperatures of the center of the specimen and of the specimen surroundings.³⁷ Defining $\Delta T_{1\infty}$ and $\Delta T_{2\infty}$ as the deviations from the above initial points (after equilibrium has been reached at the end of the step) one has

$$\Delta_0 \equiv T_{10} - T_{20} = \frac{1}{2} \left(\frac{P_0}{\rho c} \right) \left(\frac{R^2}{k} \right), \quad (1)$$

³⁵R. M. Carroll and J. G. Morgan, *Fuels and Materials Development Program Quart. Progr. Rept. June 1966*, ORNL-TM-1570, pp. 85-95.

³⁶R. M. Carroll et al., *ibid.*, June 1967, ORNL-TM-1941, pp. 81-93.

³⁷R. M. Carroll et al., *ibid.*, December 1966, ORNL-TM-1720, pp. 91-96.

$$\Delta_\infty \equiv \Delta T_{1\infty} - \frac{B_2}{B_1} \Delta T_{2\infty} = \left(\frac{R^2}{k} \right) \left(\frac{M_0}{x^2} \right) \left(\frac{\Delta P_0}{\rho c} \right), \quad (2)$$

with

$$x J_1(x) - B_2 J_0(x) = 0, \quad (3)$$

$$B_2 = B_0 [1 + 4\epsilon(T_{20} + 273)], \quad (4)$$

$$B_1 = B_0 [1 + 4\epsilon(T_{10} + 273)], \quad (5)$$

$$B_0 = \frac{HR}{K} \quad (\text{Biot number}), \quad (6)$$

where

$$M_0 = f(x),$$

$$x = \alpha_0 R \quad (\text{dimensionless}),$$

$$R = \text{radius of the sample (cm)},$$

$$k = K/\rho c = \text{thermal diffusivity, cm}^2/\text{sec},$$

$$P_0 = \text{power input corresponding to the initial position, cal cm}^{-3} \text{ sec}^{-1},$$

$$K = \text{thermal conductivity, cal cm}^{-1} \text{ sec}^{-1} (\text{ }^\circ\text{C})^{-1},$$

ΔP = increment of power from the initial to final conditions, $\text{cal cm}^{-3} \text{sec}^{-1}$,

ρ = density, g/cm^3 ,

c = specific heat, $\text{cal g}^{-1} (\text{°C})^{-1}$,

$J_0(x), J_1(x)$ = Bessel functions,

$\epsilon = \sigma E/H$, $(\text{°K})^{-3}$,

σ = Stefan's constant = $1.365 \times 10^{-12} \text{ cal cm}^{-2} \text{ sec}^{-1} (\text{°K})^{-4}$,

E = emissivity (dimensionless),

H = conductance of the gap, $\text{cal cm}^{-2} \text{ sec}^{-1} (\text{°K})^{-1}$.

The dimensionless magnitudes B_2 and B_1 are generalized Biot numbers, reducing to B_0 for $H \gg 1$ and low temperatures, that is, when conduction and convection prevail over radiation.

In this case, Eqs. (1), (2), and (3) become

$$T_{10} - T_{20} = \frac{1}{2} \left(\frac{P_0}{\rho c} \right) \left(\frac{R^2}{k} \right) \left(\frac{1}{B_0} + \frac{1}{2} \right), \quad (7)$$

$$\Delta_{\infty c} = \Delta T_{1\infty} - \Delta T_{2\infty} = \left(\frac{R^2}{k} \right) \left(\frac{M_0}{x^2} \right) \frac{\Delta P(0)}{\rho c}, \quad (8)$$

and

$$x J_1(x) - B_0 J_0(x) = 0, \quad (9)$$

where (M_0/x^2) is now a function of B_0 only. For the other extreme case, in which heat loss is only by radiation ($H \cong 0$), one obtains

$$\Delta_0 = \frac{1}{2} \left(\frac{P_0}{\rho c} \right) \left(\frac{R^2}{k} \right) \left(\frac{1}{B_R} + \frac{1}{2} \right), \quad (10)$$

$$\Delta_{\infty R} = \Delta T_{1\infty} - \left(\frac{T_{01}}{T_{02}} \right)^3 \Delta T_{2\infty} = \frac{R^2}{k} \left(\frac{M_0}{x^2} \right) \frac{\Delta P(0)}{\rho c},$$

where $B_R = (4\sigma E/K) T_{02}^3$ is the Biot number for the radiation case, which satisfies the equation

$$x J_1(x) - B_R J_0(x) = 0. \quad (11)$$

It is immediately apparent from the previous results that the mixed case, in which both conduc-

tion and radiation processes are important, is difficult to handle. We have therefore taken the position of performing low-temperature runs to minimize radiation and, conversely, high-temperature runs with a vacuum established in the gap. For both the conduction and radiation cases there are relations which must be satisfied by the data, that is,

$$2 \left(\frac{\Delta_0}{\Delta_{\infty}} \right) \frac{\Delta P(0)/\rho c}{P/\rho c} = \frac{x^2/M_0}{f(B)} = 2, \quad (12)$$

$$(\Delta_0/\Delta_{\infty})_1 / (\Delta_0/\Delta_{\infty})_2 = 1, \quad (13)$$

where

$$M_0 = \frac{2}{x J_1(x) \{1 + [J_0(x)/J_1(x)]^2\}}, \quad (14)$$

$$F(B) = \frac{1}{B} + \frac{1}{2} \quad (B \text{ equal to either } B_0 \text{ or } B_R). \quad (15)$$

Relation (12) arises from the remarkable fact that for any value of B , the value of x^2/M_0 is equal to 2.0, within a large range of Biot numbers. As a corollary of (12), the ratio Δ_0/Δ_{∞} for two different runs at the same flux level should be the same (13). Two temperature runs were analyzed (see Table 9.6) which satisfied requirement (13). The value of $P/\rho c$ had to be adjusted from 17.0 (°C/sec) to 22.2 (°C/sec) to satisfy condition (12). This change is within our experimental error of the absolute value of the specimen heating.

Table 9.6. In-Pile Thermal Conductivity of Fine-Grain UO_2

Run	T (°C)	Δ_0 (°C)	Δ_{∞} (°C)	B_0	$K^{a,b}$ [$\text{cal cm}^{-1} \text{sec}^{-1} (\text{°C})^{-1}$]
					$\times 10^{-3}$
1	714.5	218.0	15.5	0.90	6.1 ± 0.2
2	764.5	204.1	14.9	0.99	6.0 ± 0.2

^aReference 38 reports $K = 8.1 \times 10^{-3} \text{ cal cm}^{-1} \text{sec}^{-1} (\text{°C})^{-1}$ [$3.4 \times 10^{-2} \text{ watt cm}^{-1} (\text{°C})^{-1}$] at $T = 800\text{°C}$.

^b $\rho c = 0.8116$.

Fortunately, $\Delta P(0)/\rho c$ depends only upon the difference in thermal flux at the two extreme positions of the sample movement. The computation of the thermal diffusivity, k , was accomplished by iteration between Eqs. (1), (8), (9), which can be done with a desk computer. The results are shown in Table 9.6. The values obtained for the thermal conductivity of UO_2 are somewhat lower than some of the results reported in the literature.³⁸ This

can be due either to different structure and composition of the samples or to the fact that the irradiation of the sample produces "heat traps" which lower the bulk conductivity. A definite answer will have to wait until data at various flux levels have been analyzed.

³⁸J. Belle, ed., *Uranium Dioxide: Properties and Nuclear Applications*, pp. 180-181, U.S. Government Printing Office, Washington, 1961.

10. Behavior of Nonfissile Materials Under Irradiation

EFFECTS OF LARGE DOSES OF FAST NEUTRONS ON THE MONOCARBIDES OF TITANIUM, ZIRCONIUM, TANTALUM, NIOBIUM, AND TUNGSTEN

G. W. Keilholtz R. E. Moore

Because the monocarbides of the refractory metals (e.g., Ti, Zr, Ta, Nb, and W) have melting points that are among the highest known of any materials, they are considered potentially useful as components of high-temperature nuclear reactors and thermionic converters. We are investigating the changes in properties of carbides during neutron irradiation to resolve questions concerning radiation stability. The specimens under investigation are $\frac{1}{2}$ -by $\frac{1}{2}$ -in. solid cylinders of each of the five carbides made by three processes: (1) hot pressing, (2) slip casting and sintering, and (3) explosion pressing and sintering.

Results of low-temperature (300–700°C) irradiations of specimens made by all three processes were reported previously.^{1,2} Data from a high-temperature (~1000°C) irradiation assembly containing hot-pressed and slip-cast carbides from the same batches are now available. The fast (>1 Mev) neutron doses received by the specimens in this assembly ranged from 1.5 to 4.8×10^{21} neutrons/cm².

There was virtually no gross damage to the specimens irradiated at high temperature. In previous irradiations at low temperature, the

carbides of zirconium, tantalum, and niobium sustained minor to severe fracturing after receiving doses greater than $\sim 2 \times 10^{21}$ neutrons/cm². The volume expansion was much less in the high-temperature irradiations. In fact, a shrinkage to values less than the values before irradiation

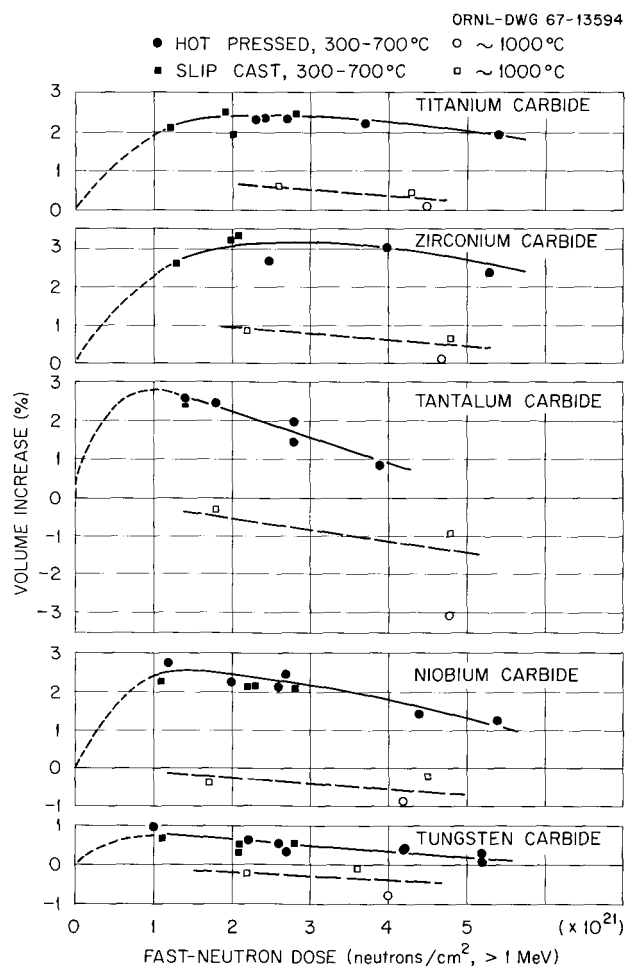


Fig. 10.1. Gross Volume Increase of Monocarbides of Ti, Zr, Ta, Nb, and W as a Function of the Fast-Neutron Dose.

¹G. W. Keilholtz, R. E. Moore, and M. F. Osborne, *Reactor Chem. Div. Ann. Progr. Rept. Dec. 31, 1966*, ORNL-4076, pp. 114–15.

²G. W. Keilholtz, R. E. Moore, and M. F. Osborne, "Effects of Large Doses of Fast Neutrons on the Monocarbides of Titanium, Zirconium, Tantalum, Niobium, and Tungsten," *Nuclear Applications* (for publication in May 1968 issue).

occurred at high neutron doses in the carbides of tantalum, niobium, and tungsten. In the low-temperature (300–700°C) experiments, these three carbides expanded initially up to a dose of 1 to 2×10^{21} neutrons/cm² and then shrank at higher doses, but they did not shrink below their pre-irradiation volumes. Volume expansions at both low temperature and high temperature are plotted as a function of the fast-neutron dose in Fig. 10.1. The very large shrinkage of tantalum carbide may be a consequence of the transmutation of tantalum to tungsten by slow neutrons.

Despite the fact that the irradiation temperature ($\sim 1000^\circ\text{C}$) was relatively low as compared with the melting points of the carbides, there was unquestionably an in-reactor annealing effect on gross damage and dimensional changes. Rapid diffusion within the specimens, as indicated by bonding together of adjoining specimens in some cases, would anneal out some of the point defects as they were being produced by fast-neutron irradiation. Shrinkage during irradiation has also been observed in graphite. It may be possible to explain this phenomenon in the carbides in a similar manner when x-ray diffraction data are obtained.

**IRRADIATION DAMAGE
TO REFRACTORY-METAL NITRIDES
EXPOSED TO FAST-NEUTRON DOSES
FROM 0.7 TO 4.9×10^{21} neutrons/cm²
AT 150°C**

G. W. Keilholtz R. E. Moore

Nitrides of Zr, Ti, Ta, and Nb were irradiated at $\sim 150^\circ\text{C}$ to fast (> 1 Mev) neutron doses ranging from 0.7 to 4.9×10^{21} neutrons/cm². The specimens were solid cylinders nominally $\frac{1}{2}$ by $\frac{1}{2}$ in. There were 10 specimens each of the nitrides of tantalum and niobium and 11 specimens each of the nitrides of titanium and zirconium, distributed evenly over the flux profile of the irradiation assembly.

Dimensional changes of the nitrides did not show a dependence on the neutron dose. The specimens of titanium nitride and niobium nitride expanded in volume by 2 to 3%. The few specimens of zirconium nitride which could be measured had expanded by 3%.

The nitrides of titanium and niobium generally withstood the fast-neutron irradiation without

fracturing up to doses of $\sim 3.8 \times 10^{21}$ neutrons/cm². Severe fracturing occurred in most of the specimens of these nitrides at higher doses. All the nitride specimens of tantalum and zirconium fractured during irradiation.

Titanium nitride and niobium nitride show promise as radiation-resistant high-temperature materials. The current effort is aimed at elucidating the mechanisms of damage in nitrides. An experiment is now in progress to determine whether improvements in stability can be obtained through in-reactor annealing at high temperatures. The impetus in the nitride program stems from the interest in uranium nitride fuel in the Liquid Metal Fast Breeder Reactor Program. In this connection, experiments in which depleted uranium nitride will be irradiated at high temperatures are planned.

**IRRADIATION DAMAGE
TO REFRACTORY-METAL DISILICIDES
EXPOSED TO FAST-NEUTRON DOSES
FROM 0.4 TO 2.7×10^{21} neutrons/cm²
AT 150°C**

G. W. Keilholtz R. E. Moore

Disilicides of Zr, Ti, Ta, and W were irradiated in the form of $\frac{1}{2}$ - by $\frac{1}{2}$ -in. solid cylinders at approximately 150°C. The estimated fast (> 1 Mev) neutron dose range of the experiment was 0.4 to 2.7×10^{21} neutrons/cm². The assembly contained 18 specimens of each disilicide evenly distributed over the flux profile of the ETR J-12 irradiation facility.

Dimensional changes were much smaller than had been observed in corresponding monocarbides. Zirconium disilicide expanded in volume by $\sim 0.7\%$ over the entire neutron dose range of the experiment. The expansion of titanium disilicide was $\sim 0.8\%$ at low neutron doses, but above 1.5×10^{21} neutrons/cm² the expansion was not as great. The specimens receiving fast-neutron doses of 2.6×10^{21} neutrons/cm² expanded by only 0.3%. The specimens of tantalum disilicide expanded in volume by approximately 1% over the dose range of the experiment.

The disilicides of zirconium and titanium were generally undamaged up to a neutron dose of approximately 2×10^{21} neutrons/cm², but nearly all specimens receiving higher doses were severely fractured. Tantalum disilicide was somewhat less

resistant to fast neutrons; the breakpoint was $\sim 1.5 \times 10^{21}$ neutrons/cm² in that case. Tungsten disilicide was found to be especially vulnerable to neutron damage. Only one WSi₂ specimen out of the 18 did not suffer severe fracturing during the irradiation.

The same types of silicides are being irradiated at high temperature ($\sim 1000^\circ\text{C}$) to determine whether in-reactor annealing processes can improve their radiation resistance.

FAST-NEUTRON EFFECTS ON ELECTRICAL INSULATORS

Irradiation Damage to Aluminum Oxide Exposed to 5×10^{21} Fast Neutrons/cm²

G. W. Keilholtz R. E. Moore

A nuclear thermionic fuel element must have electrical insulators as seals between the electron emitters and collectors and as structural components. Alumina is the most widely used thermionic insulator, because it can withstand the high temperatures required and because its fabrication is well developed. We are investigating the changes in its properties resulting from exposure to large fast-neutron doses of the order of magnitude that it would be required to withstand in realistic application. The effort has concentrated upon commercially available high-density alumina.³ The cylindrical specimens currently being investigated are 99.8% of theoretical density with an average grain size of 25 μm .

The results at relatively low irradiation temperatures (300 to 600°C) have been reported previously.^{4,5} At these low temperatures, grain boundary separation begins to occur at a fast (> 1 Mev) neutron dose of approximately 2.3×10^{21} neutrons/cm², and it becomes progressively worse with increasing neutron dose. Extensive fracture was observed in specimens exposed to doses above 3×10^{21} neutrons/cm². It was suggested that grain boundary separation, which causes the fracturing, is produced by an anisotropic

³Lucalox, trade name of a proprietary product of General Electric Company, Cleveland, Ohio.

⁴G. W. Keilholtz and R. E. Moore, *Reactor Chem. Div. Ann. Progr. Rept. Dec. 31, 1966*, ORNL-4076, pp. 113-14.

⁵G. W. Keilholtz and R. E. Moore, *Nucl. Appl.* 3(11), 686-91 (1967).

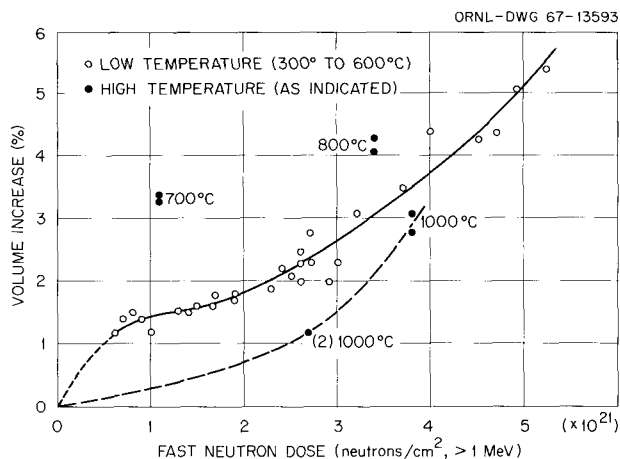


Fig. 10.2. Volume Increase of Irradiated Specimens of Translucent $\alpha\text{-Al}_2\text{O}_3$ (99.8% of Theoretical Density) as a Function of the Fast-Neutron Dose.

expansion of the crystals produced by defect agglomerates which are too large to affect the lattice parameter measurements.

The irradiation of a high-temperature (700 to 1000°C) assembly containing similar specimens was carried out to determine whether in-reactor annealing would extend the useful life of alumina as a thermionic insulator beyond a fast-neutron dose of 2 to 3×10^{21} neutrons/cm². The results were encouraging, as can be seen from the gross damage data for the high-temperature specimens summarized in Table 10.1. The low-temperature data are included for comparison. The volume increases are plotted in Fig. 10.2. Volume expansions at $\sim 1000^\circ\text{C}$ are considerably less than at low temperature (300 to 600°C), but values at 700 and 800°C fall above the low-temperature curve.

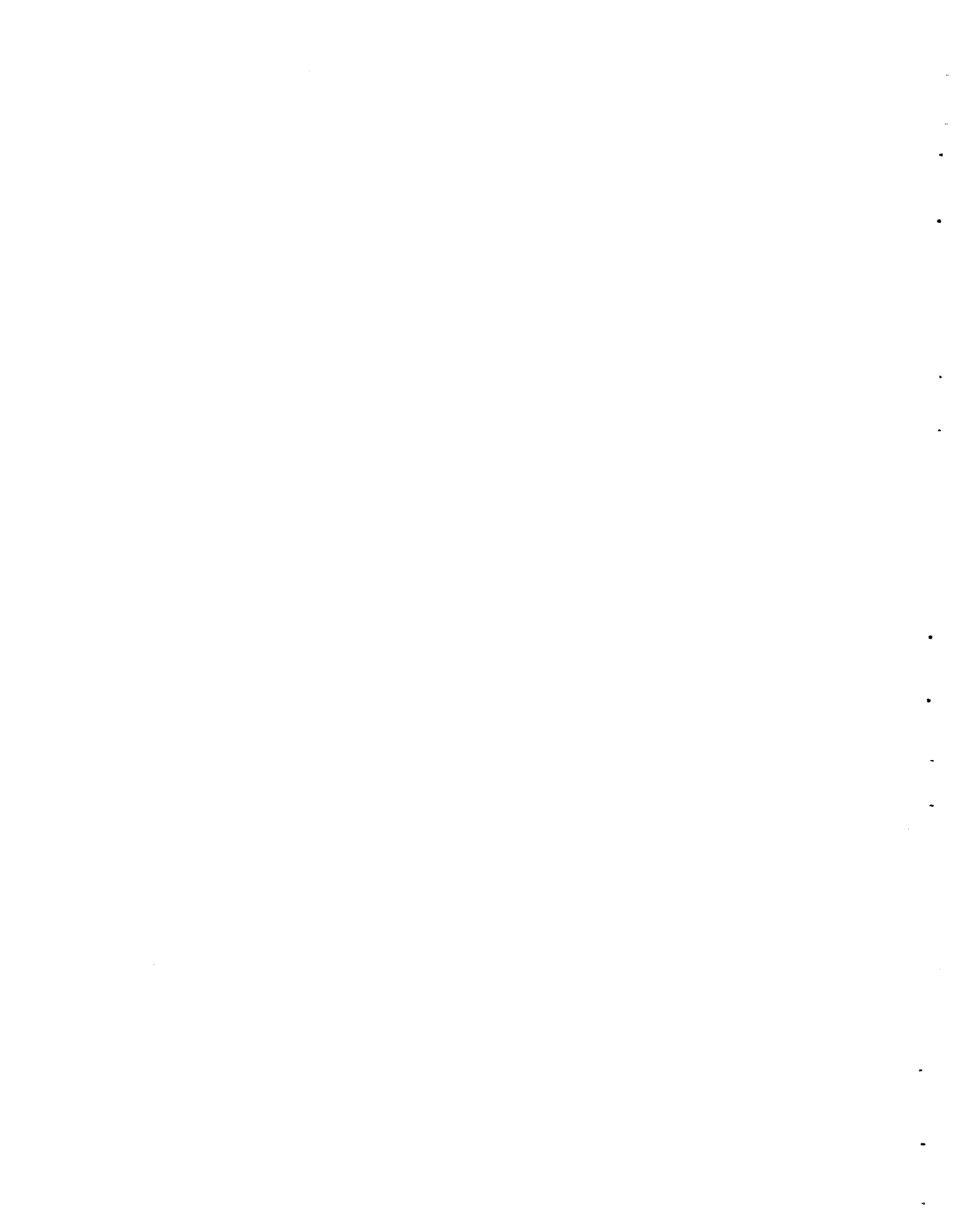
High-temperature experiments are now being carried out in which there are larger numbers of specimens than in the previous experiments. The specimens are maintained at three different temperatures: 600, 800, and 1100°C . The results are expected to provide better statistical information on gross damage effects and to resolve the question as to whether volume expansion passes through a maximum between 600 and 900°C , as the data of Fig. 10.2 imply. This question is particularly pertinent for the design of thermionic converters. Alumina of smaller grain size is also included in the current experiments in order to minimize grain boundary separation, which promotes gross fracturing of specimens.

Table 10.1. Gross Damage to Irradiated Translucent α -Alumina of 99.8% of Theoretical Density

Fast-Neutron Dose (neutrons/cm ² , > 1 Mev)	Temperature (°C)	Number of Specimens	Number of Specimens Damaged to Degree Indicated		
			No Damage	Minor Damage ^a	Severe Fracturing ^b
$\times 10^{21}$					
0.6 to 1.8	300-600	11	10	1	0
1.8 to 2.8	300-600	10	3	6	1
2.8 to 5.2	300-600	12	0	3	9
1.1	700	2	2	0	0
3.4	800	2	1	0	1
2.7	1000	2	0	2	0
3.8	1000	2	1	0	1

^aShort fractures not traversing entire specimen.

^bFractures traversing entire specimen.



Part IV
Nuclear Safety



11. Experiments in Major Facilities

FISSION PRODUCT BEHAVIOR DURING IN-PILE MELTING OF REACTOR FUELS

S. H. Freid B. F. Roberts
 C. E. Miller, Jr.¹ O. W. Thomas
 W. H. Montgomery

The in-pile facility at ORNL is one of several major installations in which one can study the effects of fission product release and transport from miniature ($\frac{1}{4}$ -in.-diam by 1-in.-long) Zircaloy-clad UO_2 fuel elements which were melted under realistic conditions of nuclear self-heating and high radiation fields. Previously we have reported iodine release rates for several experiments,² discussed an analytical model for predicting the fractional release of a given fission product,³ and detailed² the addition of an aging chamber to the in-pile facility. We have completed two experiments using this chamber and are in the process of verifying in-pile the Containment Systems Experiment (CSE) method of generating fission product simulants.

In these in-pile experiments there was a moist air atmosphere in the furnace area and dry air in the aging chamber. In the first experiment, the chamber was maintained at the reactor pool temperature, 35°C, and in the second, it was maintained at 103°C. These temperatures were kept constant during the meltdown and sampling periods. Aerosol sampling in the chamber was performed using May packs and bulk gas samplers.

In the first experiment the moist air was passed over the molten puddle for 5 min, and the flow was continued for 15 min after the furnace was retracted

from the reactor core. In the second experiment, however (due to a rapid rise in pressure in the aging chamber), the experiment was retracted after 3.25 min, and the flow of moist air was halted. Postirradiation examination showed that in both cases the fuel was completely melted. In addition, the behavior of cesium in the aging chamber was identical, indicating no apparent gross changes in the aerosols produced.

Table 11.1 lists the percentages of ^{131}I and ^{137}Cs found in various segments of the facility. In both experiments there was 1% or less release from the furnace area for ^{95}Zr , ^{140}Ba , ^{141}Ce , and ^{144}Ce . Figures 11.1 and 11.2 show the relative concentrations of the iodine species in the chamber as a function of time for the two experiments. Although the total amount of iodine species reaching the chamber was different in these two cases, the extrapolated amount of organic iodine initially produced was approximately the same, 2.8% from the first experiment and 3.4% from the second experiment. Figure 11.2 also indicates that considerable desorption from the hot (103°C) chamber walls and conversion to a more penetrating iodine form occurred. Gas chromatographic analysis of the bulk gas samples gave retention times for the

Table 11.1. Percent of Fission Products Retained

	Percent of Fission Products Retained			
	Experiment 1		Experiment 2	
	^{131}I	^{137}Cs	^{131}I	^{137}Cs
Furnace area	46.5	45.5	12.9	40.6
Transfer lines	22.5	1.3	14.8	18.0
Aging chamber	31.0	53.2	71.3	41.3

¹Argonne National Laboratory, Argonne, Ill.

²C. E. Miller, Jr., et al., *Nucl. Safety Program Semi-ann. Progr. Rept. Dec. 31, 1966*, ORNL-4071, p. 3.

³C. E. Miller, Jr., *The Light Bulb Model of Fission Product Release from Reactor Fuels*, ORNL-4060 (April 1967).

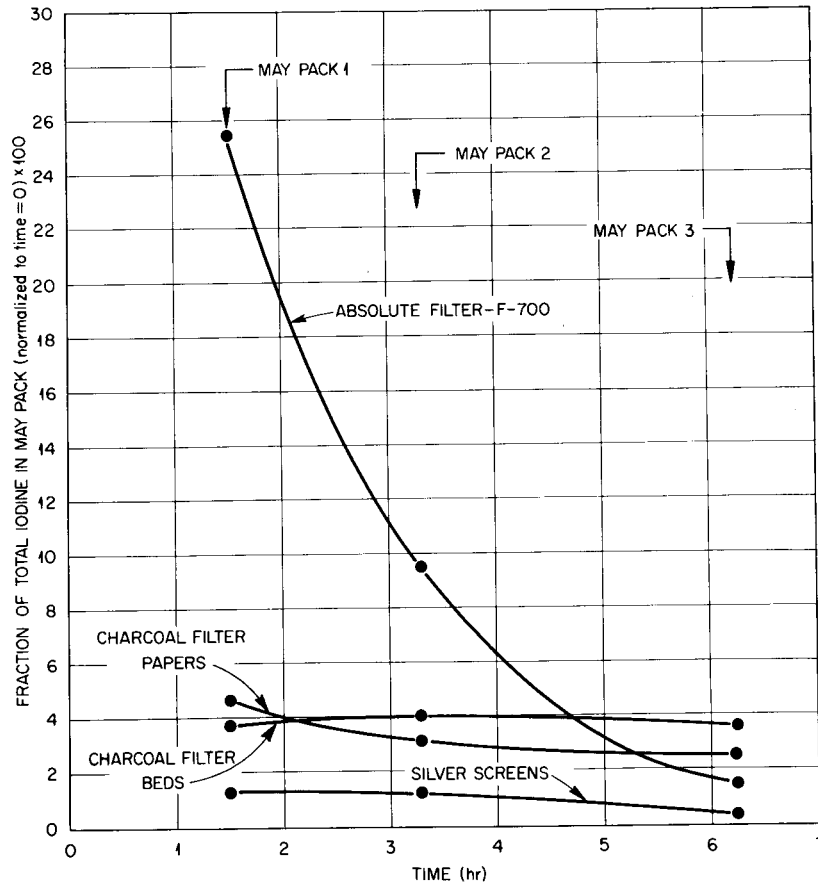


Fig. 11.1. Relative Concentrations of Iodine Species as a Function of Time in the Aging Chamber at 35°C.

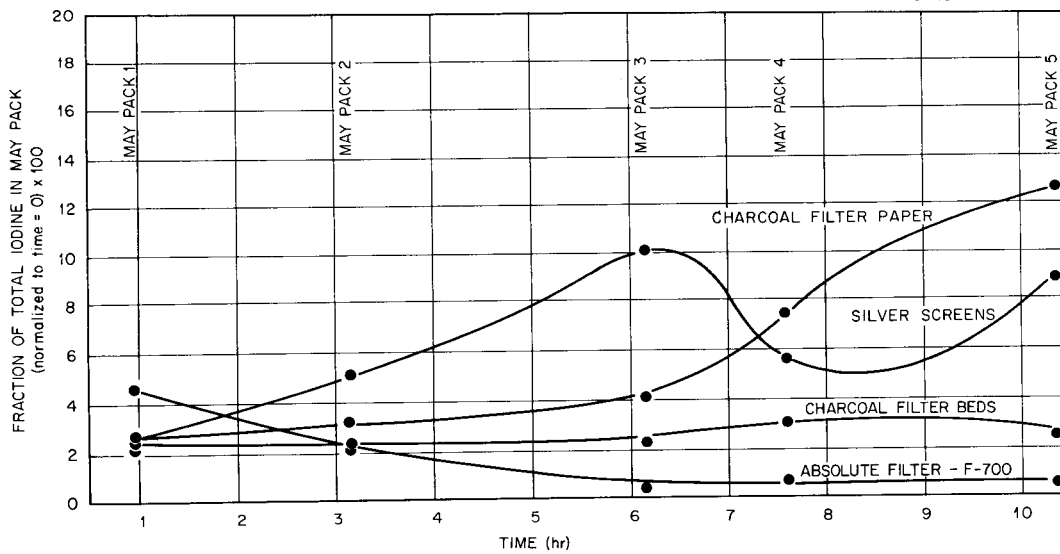


Fig. 11.2. Relative Concentrations of Iodine Species as a Function of Time in the Aging Chamber at 103°C.

organic iodine species that were identical with ethyl and methyl iodide retention times, with ethyl iodide indicated as being the predominant species.

We conclude from these two experiments that (1) relatively large amounts of cesium and iodine were released, (2) approximately 3% of the total iodine released was in an organic form, and (3) iodine was desorbed from the hot chamber walls and was converted to an organic iodide.

IN-PILE BEHAVIOR OF HTGR FUEL ELEMENTS IN MIXTURES OF STEAM AND HELIUM

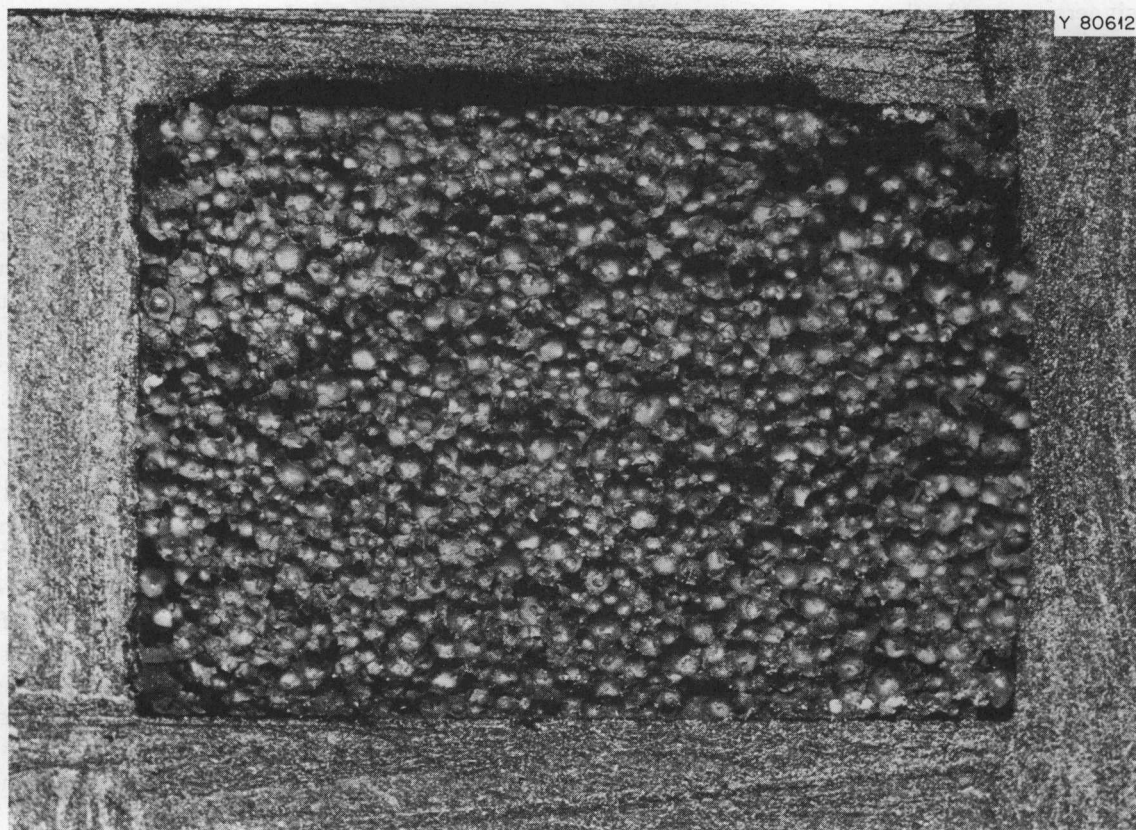
H. J. deNordwall	S. H. Freid
B. F. Roberts	O. Sisman
O. W. Thomas	W. H. Montgomery

The apparatus used⁴ for evaluating the behavior of metal-clad UO_2 fuel elements under meltdown

conditions is being adapted to investigate the behavior of HTGR fuel elements during accidents in which steam enters the core chamber. The new apparatus will permit rates of reaction between steam and model fuel elements (see Fig. 11.3) to be measured at surface temperatures of 700 to 1300°C, as functions of burn-off, water concentration, fission product concentration, irradiation field, and radial temperature gradient. The mechanical state of the fuel coating will be continuously monitored by measuring ^{88}Kr release. The distribution of long-lived fission products will be determined after each experiment, if any are released.

This facility will be used to establish that a model of the behavior of an HTGR element in he-

⁴W. E. Browning, Jr., et al., *Nucl. Safety Program Semiann. Progr. Rept. June 30, 1965*, ORNL-3843, p. 156.



0.5 in.

Fig. 11.3. Section Through Model HTGR Fuel Element.

Table 11.2. Percentages of Isotopes Found^a

	⁹⁵ Zr	¹⁰³ Ru	¹²⁹ Te	¹³¹ I	¹³⁷ Cs	¹⁴⁰ Ba	¹⁴¹ Ce	¹⁴⁴ Ce
Percent of fission products found in:								
Fuel	96.6	100	80.2	81.9	75.8	92.0	83.3	83.7
ThO ₂ insulator	3.0	0.0	10.6	5.7	18.5	7.3	15.7	16.7
ZrO ₂ insulator	0.3	0.0	0.1	6.6	4.7	0.5	0.6	0.4
Hot wall	0.1	0.0	5.9	1.5	0.5	0.1	0.4	0.2
Percent of fission products released from high-temperature zone								
	0.0	0.0	3.2	4.3	0.5	0.1	0.0	0.0

^a ¹²⁹Te, ¹⁴¹Ce, ¹⁴⁴Ce observed total fissions are low by a factor between 2.5 and 4. Calculated total fissions = 1.61×10^{18} ; average observed fissions = 1.58×10^{18} based on ⁹⁵Zr, ¹⁰³Ru, ¹³¹I, ¹³⁷Cs, and ¹⁴⁰Ba. No carbon analysis was performed.

lium and steam can be made that will enable reactor designers to assess the number of boiler tube failures that an HTGR core can tolerate before the fuel element either becomes locally too weak or loses its particle binder or begins to emit fission products.

It has proved desirable to demonstrate initially the protection offered to HTGR fuels by their coatings of carbon-pyroc carbon binder and fuel element structural graphite. A model fuel element operated with a surface temperature between 1050 and 1150°C was exposed to steam of 3 mole % concentration for 52.5 hr over a period of a week. Seventy percent of the carbon was oxidized. Reaction rates, measured from 700 to 1150°C, suggest that no enhancement of rate of attack over that observed⁵ out of pile had occurred.

The coated particles were loose in the debris of the graphite case, which had almost vanished. Broken and pitted coatings were seen. A gas release rate of $>5 \times 10^{-3}$ (R/B) was estimated. In spite of this, only 4% of the ¹³¹I left the hot zone (>700°C) of the apparatus — it was found within 6 in. Table 11.2 shows the distribution of fission products found. The fuel particles in this model HTGR element have been shown to be well protected against oxidation by steam at ~1100°C by their binder and surrounding structural carbon.

⁵C. M. Blood, G. M. Hebert, and L. G. Overholser, personal communication.

FISSION PRODUCTS FROM FUELS UNDER REACTOR-TRANSIENT CONDITIONS

G. W. Parker

R. A. Lorenz

The series of underwater transient-melting experiments with 32-g UO₂ fuel specimens has been extended to include studies of the effect of pressure during melting. Two experiments, 11Z and 12Z, which are described in more detail elsewhere,⁶ more realistically simulated a transient accident in a water reactor by including a sealed primary vessel around the fuel and water. A preliminary report on these experiments was given in the previous progress report.⁷ In both experiments the UO₂ fuel specimens were clad with Zircaloy-2 and were submerged in water in sealed primary vessels with small expansion space. Rupture disks of 300 psi (experiment 11Z) and 2500 psi (experiment 12Z) on the primary vessels released the steam pressure when approximately 15% of the total specimen fission heat (510 cal per gram of UO₂) transferred to the water. More expansion space was available in previous experiments, so that the maximum pressure was 180 to 300 psi. Pressure release was effected by an explosive valve that opened imme-

⁶G. W. Parker and R. A. Lorenz, *Nucl. Safety Program Semiann. Progr. Rept. Dec. 31, 1967*, ORNL-4228.

⁷G. W. Parker, R. A. Lorenz, and J. G. Wilhelm, *Reactor Chem. Div. Ann. Progr. Rept. Dec. 31, 1966*, ORNL-4076, p. 152.

diately after the transient. We modified the apparatus to explore the effect of higher pressures during transient melting, expecting reduction of fission product release if high pressure persisted as long as the UO_2 was molten.

In each experiment, most of the melted UO_2 and cladding flowed into a collecting cup and solidified in a dense solid mass. Some small particles adhered to the inside of the primary vessel. As expected, about 45% of the zirconium cladding reacted with water to form hydrogen. Fission product release and distribution were nearly identical in the two experiments. Compared with the four previous experiments, in which the fuel was under water before melting, the transport of fission products out of the fuel autoclave was much lower. The amount of volatile fission products (tellurium, cesium, and iodine) that was carried out of the fuel autoclave in experiments 11Z and 12Z ranged from 0.4 to 2.2% of the total. In previous experiments the range was 2.2 to 19%. The transport of the nonvolatile materials (ruthenium, cerium, zirconium, and UO_2) was lower by more than a factor of 10 compared with previous experiments.

Two effects that may have contributed to the lower release and distribution of fission products in the latest experiments are that (1) the rupture disks allowed high pressure to build up, which may have inhibited release from the fuel, and (2) fission product release may have lagged behind the fast release of steam in experiments 11Z and 12Z even though $\frac{1}{16}$ -in.-ID tubing was used to restrict steam release from the primary vessels. Metal-water reaction was not affected by the change in steam release. Further experimentation and analysis are needed to clarify the above mechanisms and to relate them to probable full-scale reactor transient accidents.

No additional underwater melting experiments are planned for the immediate future. Instead, the prompt-release phase of loss-of-coolant accidents, discussed in the following section, will be investigated in TREAT.

Investigation of the Prompt-Release Phase of Loss-of-Coolant Accidents

Assemblies are being designed for use in TREAT to study the prompt release of fission products during loss-of-coolant accidents. "Prompt release" refers to the immediate escape of volatile and gaseous fission products from the void spaces of fuel

rods when cladding is ruptured following a loss-of-coolant blowdown accident. In these experiments, TREAT will be operated at steady power, so that fissioning in the test fuel rods will heat the cladding to failure in a steam-helium atmosphere in about 30 sec.

A batch of fuel rods built to Dresden I specifications will be used initially in the experiment. These rods contain 94%-dense, 1.5%-enriched UO_2 pellets clad with 0.568-in.-OD Zircaloy-2. The fueled length is about 27 in., and the rods contain a void volume of about 5 cc. A cluster of seven rods will be used. The center rod will be irradiated for one 18-day cycle in the MTR to build up fission products under conditions similar to that of the peak rod in modern water reactors. A linear heat rating of 15.2 kw/ft will duplicate the fission gas release rate expected in the peak rod of the Browns Ferry Reactor. The burnup will be 810 Mwd/ton, and the ^{133}Xe release to the voids is expected to be about 5%.

A hot cell at Idaho will be used to place the irradiated rod in the experiment assembly as soon as possible, so that the prompt release may be performed in TREAT; the subsequent radiochemical analysis will be performed at Oak Ridge before too much of the ^{131}I has decayed. The outer circle of six unirradiated rods will be monitored with thermocouples attached to the cladding. Some of these unirradiated rods will be pressurized with helium, so that the pressure threshold of rupture can be determined. The ruptures in the unirradiated rods will be compared with that of the irradiated rod. If extra irradiated rods are available, they may be placed in the outer circle of six.

To perform the "prompt release" phase of the experiment in TREAT, the fuel rod cluster will be heated to about 280° using external electric heaters. A gas flow of 22 liters/min consisting of equal parts of helium and water will pass upward through the cluster and into a fission product collection train. This train consists of a heated fiber glass filter pack, a radiation monitor on the gas outlet tube, a condenser, warm charcoal bed, freeze trap, and a cold charcoal bed. The TREAT reactor will then be quickly brought to a steady power level such that fission energy in the test fuel rods will heat the UO_2 and cladding to rupture temperature in about 30 sec. Shortly after rupture the gas flow will be switched to a second collection train, so that the delayed fission product release can be determined.

At ORNL the fuel rods will be examined, and fission product release from the rods will be determined. The release of ^{129}I , ^{131}I , ^{133}Xe , and ^{85}Kr will be compared. An effort will be made to determine ^{131}I retained in the void spaces by using a technique involving the flushing of $^{131\text{m}}\text{Xe}$ and chemical leaching of ^{131}I .

Future experiments will use fuel rods with higher burnup. Fuel rods from the Vallecitos Boiling Water Reactor with burnup of several thousand Mwd/ton are available; if desired, additional irradiation of these rods can be accomplished in the Materials Testing Reactor.

BEHAVIOR OF FISSION PRODUCT SIMULANTS IN THE CONTAINMENT RESEARCH INSTALLATION (CRI) TANK

G. W. Parker W. J. Martin
G. E. Creek N. R. Horton⁸

The method of simulating the aerosol from overheated reactor fuels proposed for use at the Con-

tainment Systems Experiment (CSE) facility at Battelle-Northwest involves the technique of vaporizing the required amount of the fission product elements in small high-temperature furnaces and passing the vaporized material through a furnace containing molten UO_2 . A direct comparison of the behavior of real and simulated fission product aerosols can be carried out most conveniently in a relatively small well-shielded facility such as the Containment Research Installation (CRI) or the smaller Containment Mockup Facility (CMF). Data obtained in these two facilities are compared in Table 11.3 for an irradiation level of 7000 Mwd/ton; we have not yet melted highly irradiated fuel specimens in the CRI, so we cannot yet make a direct comparison for this type of fission product behavior. Cesium and ruthenium behavior in the three experiments was not significantly different. Differences in iodine behavior can be attributed,

⁸Present address, General Electric Co., San Jose, Calif.

Table 11.3. Comparison of Distribution of Real and Simulated Fission Products in the CMF and CRI

	Iodine			Cesium			Ruthenium		
	Run CMF 4-11-66 ^a	Run CMF 1008 ^b	Run CRI 107 ^b	Run CMF 4-11-66 ^a	Run CMF 1008 ^b	Run CRI 107 ^b	Run CMF 4-11-66 ^a	Run CMF 1008 ^b	Run CRI 107 ^b
Time in containment, hr	4.5	4.7	20.6	4.5	4.7	20.6	4.5	4.7	20.6
Activity, %									
Tank washes and deposition coupons	51.6	38.9	84.1	63.8	67.9	61.8	88.0	78.5	95
Condensates	22.6	45.1	14.8	28.7	15.0	26.7	3.5	8.9	
Total	74.2	84.0	98.9	92.5	82.9	88.5	91.5	87.4	95
Airborne activity at end of aging period, %									
Gas samples	0.1	2.1	0.06	0.4	3.1	1.0	0.5	3.0	1.2
Released on venting	9.0	6.0	0.55	1.1	8.4	4.5	1.2	5.2	3.5
Recovery by argon sweep	13.6	7.9	0.43	5.9	5.5	6.0	6.7	4.5	0.3
Recovery by air sweep	3.1			0.1			0.03		
Total	25.8	16.0	1.04	7.5	17.0	11.5	8.4	12.7	5.0

^aZircaloy-clad UO_2 sample irradiated to 7100 Mwd/ton.

^bSimulant designed to mock up Zircaloy-clad UO_2 sample irradiated to 7000 Mwd/ton.

at least in part, to the longer aging period in the CRI.

In one simulant experiment in the CRI (run 108), only radioiodine was added to the Zircaloy-clad UO_2 . The cladding material used in this experiment had been previously highly irradiated and had aged until it contained similar quantities of ^{125}Sb , ^{113}Sn , and ^{60}Co . The specimen was heated about twice as long (12 min) as usual. Visual observation of the melted specimen indicated that extensive vaporization occurred. This was confirmed by analysis of samples of the containment vessel atmosphere removed at intervals during the aging period. The above-mentioned cladding activities

were found to plate out at approximately the same rate, with a half-time of deposition of 200 to 250 min. The airborne iodine concentration showed the usual sharp drop during the first 40 min of the aging period but then remained almost constant during the balance of the 20-hr sampling period. Analytical data are incomplete, but it appears that approximately 25% of the tin content of the Zircaloy-2 cladding vaporized. This work is described in more detail elsewhere.⁹

⁹G. W. Parker *et al.*, *Nucl. Safety Program Semiann. Progr. Rept. Dec. 31, 1967*, ORNL-4228.

12. Development of Devices for the Separation and Measurement of Particles and Fission Products

CLASSIFICATION OF SUBMICRON PARTICLES BY A LOW-PRESSURE IMPACTOR

G. W. Parker H. Buchholz¹
R. J. Davis

Aerosols from serious reactor accidents are expected to be submicron in size. Much of the particulate matter may be 0.1μ or less in diameter. The mechanics of aerosol particles, which invariably depend on particle sizes, commonly determine their first-order properties. It is therefore imperative that devices to determine particle size in the range down to about 0.01μ in diameter be made available. For use in large-scale fission product release experiments, the further specification that such devices be simple and nearly foolproof is important. It is to fill this need that the low-pressure impactor² (as well as the 1-atm impactor described in the following section) was developed.

An inertial impactor is simply a series of jet plates and impactor plates. Aerosol particles are accelerated through holes in the jet plates, and those particles with sufficient inertia (i.e., the larger particles) leave the stream lines of air flow and are deposited on the impactor plate. Successive stages in an impactor use smaller holes, therefore higher velocities, to deposit successively smaller particles. Reasonable design criteria (for hole sizes and air velocity) limit the minimum particle size which can be deposited in an impactor at

atmospheric pressure to about 0.16μ in diameter (the lower limit of the ORNL impactor described in the following section).

In the low-pressure impactor, smaller particles can be deposited. Small particles (i.e., those which are of the order of or smaller than the mean free path of the air molecules) suffer less viscous drag force than predicted by Stokes law because they slip between molecular collisions, and it is the viscous drag force which tends to hold the particle in the air flow stream lines. It follows, therefore, that decreasing the pressure (which increases the mean free path of air molecules) decreases the viscous drag and allows smaller particles to be carried by their inertia to the impactor plate. The minimum particle size which can be separated by this means at a pressure of 40 mm Hg is about 0.01μ in diameter.

Two impactors and the system to provide the required aerosol flow (8 liters/min) at the required pressure (40 mm Hg) were designed and built. One impactor is a modified (commercially available) Andersen sampler. The second (Mark II) impactor was designed to improve simplicity of operation. O-ring seals and spring-loaded pins to keep the throw-away impactor plates in place provide a unit which can quickly be assembled and disassembled. Design specifications are reported elsewhere.²

Loss of material by deposition on the walls or by bouncing off the impactor plates was shown to be slight.

Calculated calibration curves (particle size range vs stage number) shown in Fig. 12.1 for the improved-design Mark II impactor were checked by means of tests with several aerosols having a very narrow size distribution. Good agreement with the calculated calibration curves was achieved.

¹Present address: Hahn-Meitner-Institut für Kernforschung, Berlin, Germany.

²G. W. Parker and H. Buchholz, *Size Classification of Submicron Particles by a Low-Pressure Impactor*, ORNL report in preparation.

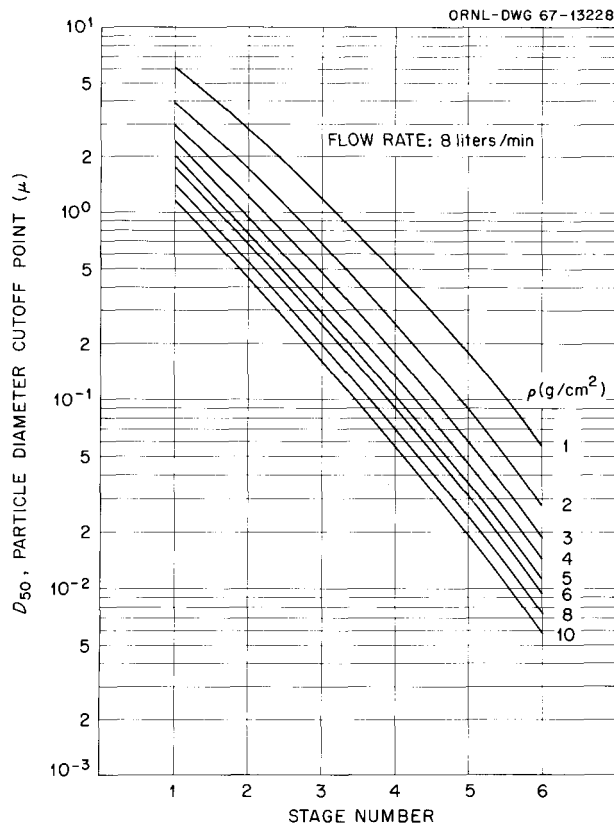


Fig. 12.1. Calculated Particle Size Distribution in the Mark II Impactor.

In summary, a low-pressure impactor has been developed which separates particles into seven size ranges (including a range caught by a final membrane filter) indicated by the following particle diameter cutoff points: 2.0, 0.76, 0.29, 0.11, 0.036, 0.012, and $<0.012 \mu$ (for particles with a density of 5.0). The device is simple and is recommended for use in nuclear safety containment studies.

ATMOSPHERIC PRESSURE SAMPLERS FOR SIZING PARTICULATE AEROSOLS

R. E. Adams

R. J. Davis

There exists a need for a simple, remotely operable aerosol sampling and sizing device which is capable of operating under the environmental conditions of large containment vessel experiments. Both the fibrous filter analyzer and a multistage inertial impactor sampler, of im-

proved design, are being developed concurrently in an attempt to fill this need.³

The fibrous filter analyzer (FFA) is a device which characterizes the aerosol in terms of its response to filtration processes by developing an aerosol distribution as a function of depth in an expanded filter under carefully controlled conditions. In use the FFA samples an aerosol of unknown size, the mass of aerosol collected on each of the several filter mats (in series) is determined, and a graph is constructed relating aerosol mass to filter depth; by analysis of this curve it is possible to deduce information relative to the size of the unknown aerosol. Development and application of this technique was demonstrated by Silverman *et al.*⁴ using an aerosol of ^{65}Zn particles. Complete experimental verification of the filter theory upon which the FFA is based was not possible at ORNL because of the lack of generators for producing monodisperse aerosols of various sizes and the lack of rather sophisticated analytical equipment with which to measure the size and size distribution of these aerosols. Since such equipment was available at the Particle Technology Laboratory of the University of Minnesota, an agreement was reached for further calibrations of the FFA by their laboratory.

The operation and response of the fibrous filter analyzer has been individually tested with aerosols of diameters of 0.07, 0.08, 0.13, 0.23, 0.56, 0.8, 1.0, and 1.3μ , composed of various materials such as dioctylphthalate, glycerin, uranine dye, and polystyrene latex; operating parameters such as gas velocity and humidity of the gas have also been varied.

The data collected so far serve to validate the usefulness of the FFA as a unique tool in the study of aerosol behavior. Additional study with polydisperse aerosols of the type expected in nuclear accident situations will be required before the FFA can be applied as a proven field sampler.

A four-stage inertial impactor sampler was designed by personnel at the University of Minnesota Particle Technology Laboratory, fabricated at ORNL, and calibrated at the Particle Technology

³Much of this study is being conducted under sub-contract by A. R. McFarland and R. B. Husar of the Particle Technology Laboratory of the University of Minnesota.

⁴M. D. Silverman *et al.*, *Characterization of Radioactive Particulate Aerosols by the Fibrous Filter Analyzer*, ORNL-4047 (March 1967).

Laboratory with monosize dye particles.⁵ At a sampling rate of 6.25 liters/min, and with particles of density 4 g/cm³, the cutoff points of the four stages are 2.6, 1.1, 0.4, and 0.16 μ in diameter. Additional calibration tests will be carried out at ORNL utilizing oxide aerosols of uranium and stainless steel.

The ORNL impactor provides improved sharpness of aerosol particle fractionation as compared with commercially available impactors and facilitates possible remote disassembly; each impactor stage consists of only two parts, the jet plate and the impactor plate.

IODINE CHARACTERIZATION SAMPLERS

R. E. Adams R. L. Bennett
W. H. Hinds

A program is being conducted to develop and test analytical samplers for separating and measuring the various forms of iodine present in experiments conducted under simulated accident conditions. To perform satisfactorily these samplers must be capable of operating at elevated temperatures and high humidities and, in addition, must be capable of remote operation. One widely applied iodine sampler (May pack) is composed of a sequence of filters and adsorbents designed to separate iodine forms on the basis of chemical reactivity or adsorption tendency. Considerable testing has been accomplished in an attempt to determine the optimum materials and component arrangements within the sampler for successful application at elevated temperatures and humidities.

The pack arrangement examined first was that which was initially proposed by the LOFT program. The component sequence was: (1) three high-efficiency filters to remove particles, (2) eight silver-plated screens to remove elemental iodine, (3) five charcoal-loaded filter papers for removal of easily adsorbed iodine compounds, (4) two $\frac{3}{4}$ -in.-deep charcoal beds for adsorption of the more penetrating organic iodides such as methyl iodide, and, finally, (5) a high-efficiency filter to remove airborne particles which might be eluted from the charcoal beds. The tests were conducted at 90°C with an air flow rate of 1 liter/min through the

⁵A. R. McFarland and R. B. Husar, *Development of a Multistage Inertial Impactor*, Particle Technology Laboratory Publication 120, University of Minnesota, Minneapolis, October 1967.

packs. Dry air and air at 90% relative humidity were used. Details of the testing facility and procedure have been reported along with results of the distribution of elemental iodine, methyl iodide, and aerosols through the components of the original LOFT sequence.^{6,7}

Although a large variety of high-efficiency filter media was examined, none was found which did not retain significant amounts of elemental iodine. The pack was modified by reversing the filter and silver screen sections so that the latter became the inlet section. However, testing this arrangement with aerosols generated by arc melting an irradiated stainless steel tube with a UO₂ insert revealed that the screens trapped unacceptably large fractions of the particles.

The unsatisfactory high sorption of elemental iodine on the first filter of the original LOFT May-pack sequence and the high retention of aerosol on the initial screen section of the alternative arrangement led to the development of a new iodine sampler design featuring a silver honeycomb as the first section.⁷ The use of a silver honeycomb as a separation device for molecular iodine and larger aerosol particles is based on the much larger diffusivity of the former. Deposition on the hexagonal honeycomb walls may be approximated by the equation for deposition from cylindrical channels:⁸

$$\Delta \log n_s / \Delta Z = 5.00D/Q,$$

where

- n_s = number of particles deposited per unit length,
- Z = distance from the diffusion channel entrance,
- D = diffusion coefficient of particles in the carrier gas,
- Q = volumetric flow rate through the honeycomb channels.

The honeycomb offers an ideal geometry for deposition of iodine molecules, since it divides a

⁶R. E. Adams *et al.*, *Nucl. Safety Program Ann. Progr. Rept. Dec. 31, 1966*, ORNL-4071, pp. 173-89.

⁷R. L. Bennett, W. Hinds, and R. E. Adams, *Development of Iodine Characterization Sampler for Application in Humid Environments*, ORNL-TM-2071 (to be issued).

⁸W. E. Browning, Jr., and R. D. Ackley, *Nucl. Safety Program Semiann. Progr. Rept. June 30, 1964*, ORNL-3691, p. 55.

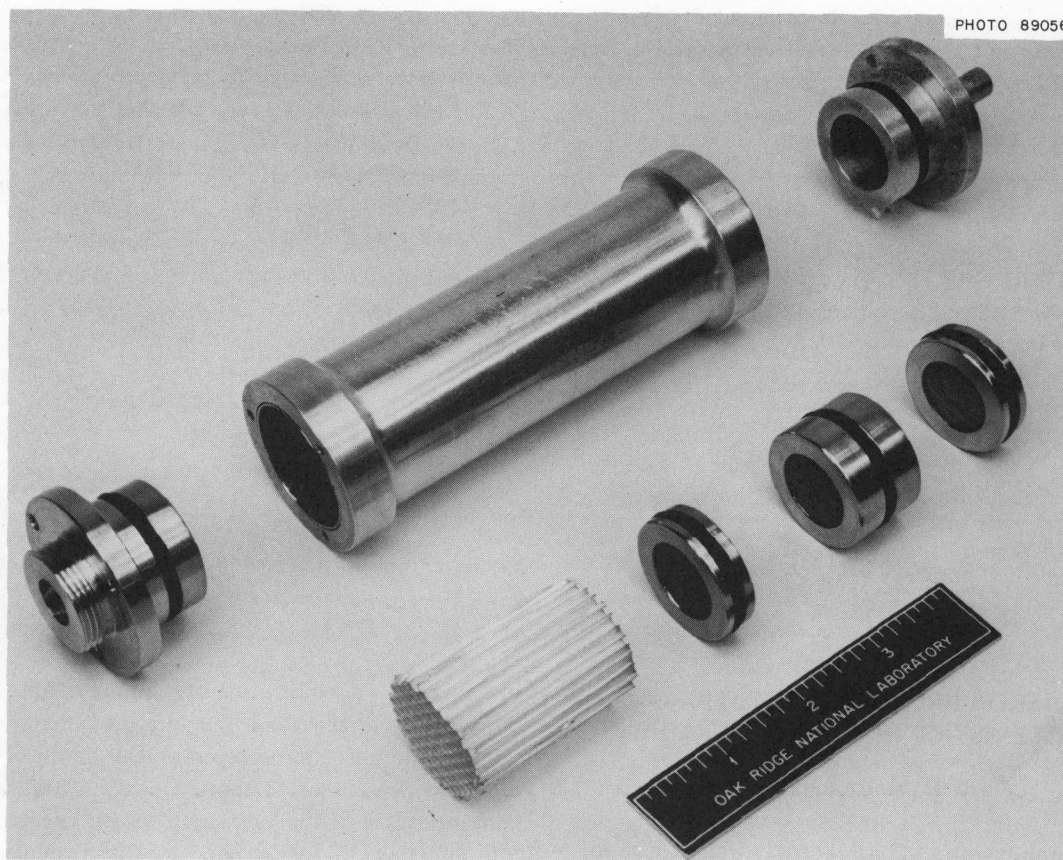


Fig. 12.2. Silver Honeycomb Iodine Characterization Pack.

large total volumetric flow into smaller parallel flows. At the same time it presents a minimal solid cross section so that particle collection by other mechanisms such as interception and inertial impaction is small. The proposed honeycomb characterization pack, shown in Fig. 12.2, consists of (1) a 5-cm silver-plated honeycomb with $\frac{1}{8}$ -in. hexagonal channels followed by (2) a high-efficiency filter section for aerosol removal, (3) an impregnated charcoal bed for methyl iodide adsorption, and (4) a final high-efficiency filter for removal of any airborne particles eluted from the charcoal bed. This honeycomb has been tested with elemental iodine, methyl iodide, and aerosols, individually.

Results of these separate tests, given in Table 12.1, demonstrate the capability of the honeycomb to retain iodine and not remove methyl iodide and particles. In the elemental-iodine tests the lower efficiency of test T was due to a lack of dispersion of the air flow entering the pack into all of the hexagonal channels of the honeycomb. It was

observed by visual examination and radioactivity counting that most of the iodine flowed down the center third of the honeycomb. By increasing the inlet diameter and tapering the section opening to the diameter of the honeycomb, the air distribution was improved, and the higher efficiency observed in test U was obtained. Retention of methyl iodide on the silver honeycomb is acceptably small ($\sim 1\%$), although it is larger than retention on an eight-silver-screen section. The very low collection of aerosol on the honeycomb appears to offer an excellent solution to the elemental iodine-aerosol separation problems. As an additional test, a mixture of elemental iodine (^{131}I) and irradiated stainless steel- UO_2 aerosol (^{51}Cr) was introduced into a 0.1-m^3 tank and then passed through two parallel honeycomb packs. The resulting distributions confirmed the excellent separation observed in the individual tests; thus, the honeycomb sampler appears to be far superior to all other May-pack arrangements examined.

Table 12.1. Retention of Elemental Iodine and Penetration of Methyl Iodide and Stainless Steel Aerosol in Separate Tests with Silver Honeycomb

Species	Test	Pack No.	Load (μg)	Percent Relative Humidity	Percent Retention on Honeycomb
I_2	T	MP1	386	90	97.68
		MP2	397	90	97.79
	U ^a	MP1	340	90	99.81
		MP2	306	90	99.61
CH_3I	V	MP1	13.1	90	0.92
		MP2	12.5	90	1.34
Aerosol	HC1			~15	2.27
	HC2			~91	0.71
	HC3			~95	0.73

^aInlet hardware modified between tests U and T to provide more uniform distribution of air flow through honeycomb.

FISSION PRODUCT DEPOSITION CHARACTERISTICS IN THERMAL GRADIENTS

A. P. Malinauskas

Considerable interest has recently been focused upon the possible employment of thermal gradient tubes in studies related to the identification and characterization of gaseous fission product species. The method, first advanced by Castleman,⁹ takes advantage of vapor pressure differences to effect separation of a multicomponent gas mixture by passing the mixture down a tube along which a temperature gradient is maintained.

In a typical case the experimental procedure entails passing a carrier gas over a solid sample in such a manner that either the gas is not saturated with the vapor in equilibrium with the sample, or that equilibrium between the vapor and solid is not attained. As a result, the vapor carried by the gas is characteristic of the equilibrium vapor pressure of the solid at a temperature T_d which is less than that at its origin. If the mixture is passed down a tube in which the temperature is gradually decreased, deposition of the vapor will begin only when the temperature of the tube is T_d .

In a mixture of vapors, all of which emanate from their solids at the same temperature, one can therefore achieve separation on the basis of the different deposition temperatures T_d which are characteristic of the individual components.

In addition, the deposition profile displayed by a particular component under a given set of temperature and flow conditions is governed by both its transport and thermodynamic characteristics, so that an examination of such profiles can, in principle, yield thermodynamic and transport property data as well.

Our current activities in this area primarily involve the examination of mathematical models, some of which have already been developed,⁹ which describe the processes involved; the purpose of the work is to provide theoretical support for experimental studies in this area which will commence shortly.

The essential features of data obtained from the thermal gradient method can be most easily presented from the consideration of a model in which only the thermodynamic aspects are taken into account. In this model it is assumed that thermodynamic equilibrium prevails throughout, except that the vapor carried away by the sweep gas at a temperature T_0 is not in equilibrium with its solid phase (this can be accomplished, for example, by separating the solid and the sweep gas with a porous barrier). If supersaturation of the carrier with vapor prior to deposition of the latter can be

⁹A. W. Castleman, Jr., I. N. Tang, and H. R. Munkelwitz, *Proceedings of the International Symposium on Fission Product Release and Transport Under Accident Conditions, Oak Ridge, Tennessee, April 5-7, 1965*, CONF-65407, pp. 325-43.

neglected, and deposition is simply a condensation mechanism, then the deposit first appears at that temperature T_d at which the molecular density begins to obey the Clapeyron equation

$$n = n^0(T_d/T) \exp [-\Delta H(T_d - T)/RT_d T], \quad (1)$$

where n^0 represents the molecular density at the temperature T_0 , R is the gas constant, and ΔH is the heat of sublimation of the condensing species.

In this particular case, thermodynamic equilibrium throughout implies steady-state conditions as well, and f , the fraction of material deposited per unit length of tube, measured relative to the amount of material entering the tube, is given by

$$f = (x/x^0) (\Delta H/RT^2) (1 - x) (-dT/dz), \quad (2)$$

in which $(-dT/dz)$ is the thermal gradient along the tube, and x^0 and x denote the mole fractions of vapor at the point of origin (i.e., at T_0) and at temperature T along the tube respectively. Equa-

tion (2) can be further simplified if the depositing species is present in trace amounts ($x \ll 1$) and variations in total pressure are negligible; thus

$$f = (T_d/T_0) (\Delta H/RT^2) (-dT/dz) \exp \times [-\Delta H(T_d - T)/RT_d T]. \quad (3)$$

Aside from the abrupt onset of deposition which is observed experimentally, this simplified description likewise correctly predicts the exponential character of the deposition profile.

The thermodynamic treatment assumes a virtually infinitely rapid rate of diffusion of the condensing species in the radial direction (in the case of circular tubes), so that diffusion can be expected to lessen the exponential decay by decreasing f at the onset of deposition and increasing its value further downstream. The degree to which these effects can be detected experimentally, however, awaits further work.

13. Supporting Laboratory and Theoretical Studies

MECHANISMS OF SORPTION OF MOLECULAR IODINE

R. J. Davis

This work has been reported in detail¹ and will only be outlined here. The objectives were to: (1) classify the surface chemistry of molecular iodine in a reactor containment, (2) suggest the important parameters which control each class of reaction, (3) illustrate the way in which the surface chemistry can be incorporated with equations for mass transfer to the surface, and (4) suggest specific research to provide needed information.

A detailed study of selected literature and a consideration of possible conditions for surface reactions in a reactor containment suggested the following classes of reactions: (1) chemisorption on bare metals, (2) monolayer adsorption with dissociation on dry oxides, (3) diffusion-controlled reaction with oxide-coated metals, (4) adsorption into water or aqueous solutions, (5) adsorption on a rapidly forming corrosion film, and (6) sorption from a damp atmosphere.

Each class of reaction was considered, and data from various sources were used to substantiate mechanisms. For each class of reaction, an equation was developed which shows the iodine concentration in a containment as a function of time as a result of iodine removal by that reaction. In the case of one reaction (adsorption on dry oxides), the equation was demonstrated to fit data from Containment Mockup Facility and Nuclear Safety Pilot Plant containment experiments.

Research recommended includes the study of iodine sorption on several dry oxides from dry and moist atmospheres.

¹R. J. Davis, *Mechanisms of Sorption of Molecular Iodine*, ORNL-4126 (August 1967).

UPTAKE OF METHYL IODIDE FROM WIND TUNNEL GASES BY A SUSPENDED DROP OF WATER

B. A. Soldano

W. T. Ward

A study of the transport of methyl iodide gas into a water drop suspended in a wind tunnel has been directed toward an examination of the effect of solution additives on this process. More detailed reports are given elsewhere.²

The concentration of CH₃I in the tunnel gases is kept constant, about 10⁻⁵ millimole/cc. The water drop under study remains suspended in the wind tunnel through the upward thrust of the flowing gas mixture. The penetration of CH₃I into the water drop between $t \approx 1$ sec and the time of complete saturation can be represented as follows:

$$\log F = C_i + (\text{slope})t, \quad (1)$$

where F is the fraction of steady-state concentration of iodide ion in the water phase at time t , and $C_i \approx 0.35$ is an empirical constant which is independent of such chemical variables as additive type, concentration, pH, etc.

The work of Garner³ *et al.* has shown that the rate of drop saturation can be approximately represented by a diffusion-based error function equation as follows:

$$\log(1 - x) \sim -\frac{4\pi^2Dt}{d^2}, \quad (2)$$

²Nucl. Safety Program Semiann. Progr. Rept. Dec. 31, 1967, ORNL-4228 (to be published); ORNL Nuclear Safety Research and Development Program Bimonthly Reports; paper presented at the American Nuclear Society Winter Meeting, Nov. 5-9, 1967, Chicago, Illinois.

³F. H. Garner and J. J. Lane, *Trans. Inst. Chem. Engrs. (London)* 37, 151-72 (1959).

where the logarithm of the fractional degree of saturation $(1 - x)$ is a function of the diffusion coefficient (D) and the square of the diameter (d) of the drop.

If one assumes that the Marshall-Ranz correlation holds, then Griffith⁴ has shown that the mass transfer coefficient and the diffusion coefficient can be related as follows:

$$v_L = \frac{2}{3} \frac{\pi^2 D}{d}, \quad (3)$$

where v_L is the mass transfer coefficient. Substituting for D in Eq. (2), one obtains an expression [Eq. (4)] analogous in form to that of Eq. (1). This suggests that the slope of Eq. (1) is related to the mass transfer coefficient v_L :

$$\ln F = \text{constant} + \frac{a_1 v_L t}{d}, \quad (4)$$

where a is a numerical factor.

One finds that keeping all conditions constant and simply altering the drop radius, the slope of Eq. (1) obeys the following equation:

$$\text{slope} = a - br^2. \quad (5)$$

This slope dependency indicates that the mass transfer coefficient as represented by Eqs. (1) and (4) is proportional to at least two terms, one of which is dependent on the surface area of the drop (r^2) and the other on the interior of the drop. The surface term is not unexpected in mass transfer of gases into liquids. The second term is consistent with our premise that factors such as natural circulation affect the mass transfer process inside the liquid bulk.

Since the problem of relating single-drop performance to that of a distribution of drops found in sprays might well pose unforeseen complications, we have chosen to free the present study from any theoretical ambiguity by examining the behavior of an empirical mass transfer coefficient (v_L) as reflected in the behavior of the slope in Eq. (1) at a fixed drop radius of 0.21 cm. Our objective will be to determine the role of additives and other system variables on the empirical mass transfer coefficient.

At low concentrations (~ 0.2 wt %) such diverse additives as $\text{NH}_2\text{-NH}_2$, NaOH , $(\text{NH}_4)_2\text{S}$, and

$\text{Na}_2\text{S}_2\text{O}_3$ all affect the mass transport of CH_3I in a similar manner. The common line extrapolates to a lower or limiting mass transport coefficient value for CH_3I into pure water at 25°C equal to 3.25×10^{-3} cm/sec. Conversely, the differences in the specific effectiveness of additives in enhancing the mass transport of CH_3I become apparent at higher additive concentrations with values ranging as high as $\sim 4 \times 10^{-2}$ cm/sec.

On the acidic side, for water and solutions containing 1 wt % $\text{Na}_2\text{S}_2\text{O}_3$, the mass transfer rate is lower ($\sim 5 \times 10^{-3}$ cm/sec at 25°C) than at a pH of 7 or higher (3.6×10^{-2} cm/sec), and the mass transfer coefficient is temperature dependent with an activation energy of 10,000 cal/mole. At higher pH the mass transfer coefficient is temperature independent.

The relative insensitivity to temperature of the mass transport coefficients on the basic side coupled with 100% reduction in the rate of CH_3I pickup in the absence of light would indicate that the surface photolysis of CH_3I , that is, $\text{CH}_3\text{I} + \text{H}_2\text{O} + \gamma \rightarrow \text{CH}_3\text{OH} + \text{H} + \text{I}^0$, plays a role in the primary step of the mass transport process. From the basic-range pH dependency of the v_L values, one can conclude that the reduction of the I^0 by $\text{Na}_2\text{S}_2\text{O}_3$ in the interior of the drop constitutes the final mass transfer step.

REMOVAL OF MOLECULAR FORMS OF RADIO- IODINE FROM MOIST AIR SYSTEMS

R. E. Adams R. D. Ackley
Zell Combs

In addition to elemental iodine, methyl iodide constitutes a recognized species of airborne radioiodine; therefore, for an air cleaning system to be an acceptable safeguard against all forms of fission product iodine that might be accidentally released into a reactor containment vessel, the system must include the capability of trapping radioactive methyl iodide. The trapping problem, in the case of a water-cooled reactor experiencing a loss-of-coolant accident, may be made more difficult by production of steam with attendant elevation of air temperature, pressure, and humidity.

⁴V. Griffiths, *Nucl. Safety* 6(2), 186 (1965).

Removal of Radioactive Methyl Iodide by Iodized Charcoals

Methyl iodide is more difficult to trap, for example, by the usual types of activated charcoal, than is elemental iodine. However, results presented previously have shown that certain specially impregnated (iodized) charcoals are effective under a variety of conditions, for trapping the ^{131}I of $\text{CH}_3^{131}\text{I}$, via an isotopic exchange reaction.⁵ During the past year, additional types of iodized charcoal have been developed, and this work has been continued to evaluate their capabilities for trapping $\text{CH}_3^{131}\text{I}$. A more detailed description of this work has been reported.^{6,7}

Two distinct sets of test conditions have been employed in determining the efficiencies of impregnated charcoals for removing radioactive methyl iodide from moist air streams. One set of conditions, used mainly for screening purposes, includes 77°F, 14.5 psia, 65 to 70% relative humidity, and air sweep at 40 fpm. The other set includes (typically) 270°F, 60 psia, steam-air sweep at 40 fpm, and relative humidities which were varied over the range 70 to 100%. A selection of the results from the steam-air tests is presented in Fig. 13.1. A usable $\text{CH}_3^{131}\text{I}$ removal efficiency is attainable with a 2-in. depth of iodized charcoal provided the prevailing relative humidity does not greatly exceed 90%.³ These results were obtained in a single-pass system; for a recirculatory system, particularly at the higher relative humidities, the situation would be considerably more favorable. The tests at 77°F encompassed a greater variety of charcoal types; the results indicated that most were highly effective under the test conditions involved.⁶

Removal of Elemental Radioiodine by Iodized Charcoal

Because iodized charcoal is impregnated during manufacture with one or more iodine-containing substances, the question arose as to whether or

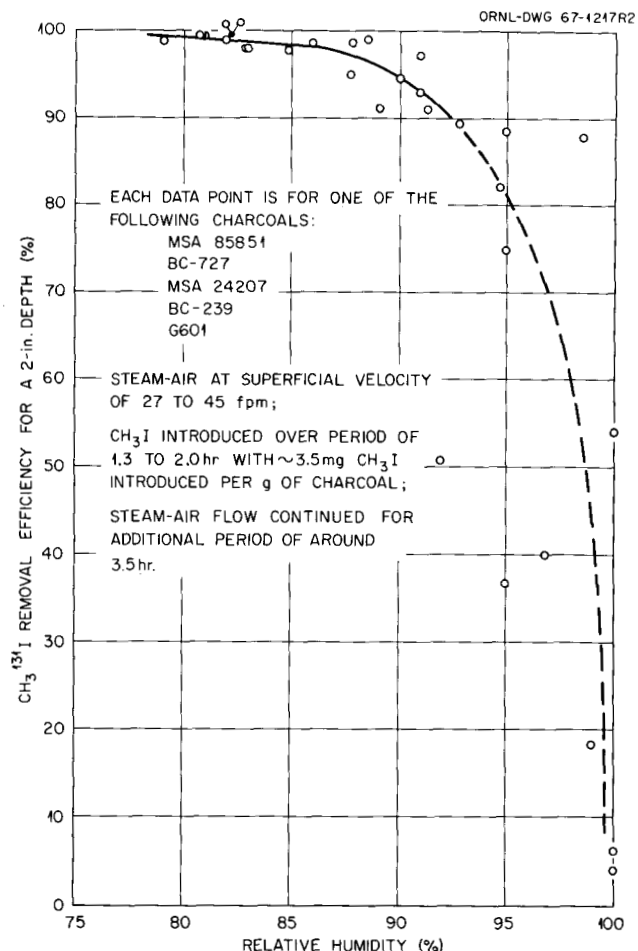


Fig. 13.1. Effect of Relative Humidity on the Removal of Radioactive Methyl Iodide from Flowing Steam-Air by Iodized Charcoals at Temperatures and Pressures Around 270°F and 60 psia.

not the capacity of such charcoal for elemental iodine (I_2) had been reduced to an unacceptably low level. This question has been investigated for room temperature, and, again, the detailed results are reported elsewhere.⁸ High to extremely high I_2 loadings on the charcoal and high relative humidities (98 and 100%) were used in this work. In the case of the 100% relative humidity condition, the charcoal contained bulk phase liquid water; that is, it was waterlogged. A sampling of the results obtained is given in Table 13.1.

⁵R. E. Adams *et al.*, *Nucl. Safety Program Ann. Progr. Rept. Dec. 31, 1966*, ORNL-4071, pp. 127-40.

⁶R. E. Adams, R. D. Ackley, and Zell Combs, *Nucl. Safety Program Ann. Progr. Rept. Dec. 31, 1967*, ORNL-4228 (to be published).

⁷R. D. Ackley and R. E. Adams, *Removal of Radioactive Methyl Iodide from Steam-Air Systems (Test Series II)*, ORNL-4180 (October 1967).

⁸R. E. Adams and R. D. Ackley, *Removal of Elemental Radioiodine from Flowing Humid Air by Iodized Charcoals*, ORNL-TM-2040 (November 2, 1967).

Table 13.1. Efficiency of Iodized Charcoals for Removing Elemental Radioiodine at High I_2 Loading and High Relative Humidity from Flowing Air (40 fpm) at 20 to 25°C

Charcoal Under Test	Relative Humidity (%)	I_2 Loading for 2-in. Depth of Charcoal (mg/g)	I_2 Removal Efficiency (%)	
			For 1-in. Depth	For 2-in. Depth
MSA 85851	98	66	99.90	99.92
BC-727	98	64	99.94	99.960
BC-272	98	60	99.965	99.976
BC-727	98	16	99.957	99.979
BC-727	100	10	99.33	99.970
BC-727	100	5	98.43	99.90
BC-117	98	6	99.995	99.998
BC-117	100	6	98.64	99.967
BC-117	100	4	95.96	99.91

The high efficiencies observed for the highest loadings (which are much higher than any postulated for a full-scale charcoal adsorber system) show that the capacities of these charcoals for I_2 are adequate at room temperature. The effect of elevated temperatures on capacity remains to be studied. Considering the other results, particularly those for 100% relative humidity and for a 1-in. depth of charcoal, the trapping performance is seen to be rather erratic. This behavior probably can be ascribed to sweep gas channeling, a process that is somewhat random in nature. Obviously, operational conditions which might result in waterlogging should be avoided if efficient trapping of I_2 is required.

REACTIONS OF IODINE VAPOR IN CONTAINMENT SYSTEMS

R. E. Adams R. L. Bennett
Ruth Slusher

When radioiodine is released into a closed environment, a generally small, but possibly significant, fraction may appear in the form of methyl iodide and other alkyl iodides. These iodides are difficult to remove from humid environments; therefore, it is desirable to identify the primary mechanisms for the production of organic iodides in order to avoid, if possible, conditions or materials conducive to their formation. In an accident situation, organic iodides may be formed in

the containment atmosphere by gas-phase reactions with organic contaminants or on the various types of surfaces within the containment vessel with subsequent desorption into the gas phase.

The reactions of elemental iodine with painted surfaces of interest in the nuclear safety program are being studied. Experiments were performed by aging at a temperature of 100, 150, or 250°C two identically painted reaction vessels, one with added iodine and the other without. Samples of the gases were taken periodically from both vessels and analyzed by gas chromatography utilizing dual electron capture and hydrogen flame ionization detection.

The multilayer paint coatings examined included the Amercoat 66 formulation for steel surfaces, Amercoat 66 formulation for concrete surfaces, and Phenoline 302. Individual experiments with layers of Amercoat 64 primer, Amercoat 66 surfacer, or Amercoat 66 seal gloss were also performed. Detailed descriptions of the reaction products from each of these surfaces have been reported.⁹ In general, all of the above coatings yielded several organic iodides including methyl iodide.

To gain insight into the chemical processes leading to CH_3I formation in the gas phase, a study is being made of calculated equilibrium and

⁹R. E. Adams, R. L. Bennett, and Ruth Slusher, "Reactions of Iodine Vapor in Containment Systems," *Nucl. Safety Program Ann. Progr. Rept. Dec. 31, 1967*, ORNL-4228 (to be published).

nonequilibrium concentration of CH_3I for a range of conditions typical of reactor accidents.¹⁰ In the previously reported studies,¹¹ limited equilibrium calculations of the reaction between CH_4 and I_2 predicted concentrations of methyl iodide consistent with those observed in some experiments, while the more complex homogeneous cases predicted methyl iodide concentrations that were orders of magnitude lower than concentrations found under some experimental situations. The presence of other chemical species which can compete with CH_3I for the available carbon, hydrogen, and oxygen leads to low methyl iodide concentrations. This indicates that in the experimental situation, equilibrium conditions may not prevail and that kinetic factors may be controlling.

The results of homogeneous kinetics calculations based on the simple reaction system involving CH_4 and I_2 show nonequilibrium CH_3I concentrations which are higher than the concentrations attained at equilibrium. The overshoot in the CH_3I concentration can be more than two orders of magnitude greater than the equilibrium values at temperatures of 800 and 1000°K, with the maximum difference being at the higher temperature. The higher-than-equilibrium CH_3I concentrations occur for reaction times between about 1 min and 1 hr. This places the CH_3I peak at a point in time where it could be a factor in many of the experiments where CH_3I concentrations above those expected at equilibrium are observed. Thus CH_3I concentrations at the levels observed experimentally can be reproduced by this simple model, indicating the possibility that the high CH_3I concentration observed experimentally could be nonequilibrium concentrations produced at high temperatures and then frozen in at low temperatures.

As part of this study the levels of trace organic contaminants in various representative atmospheres were determined. Samples were taken within buildings housing reactors and large-scale

reactor experiments at ORNL and at an isolated wooded area. The concentration of identified organic compounds and total unsaturated and saturated hydrocarbons is reported elsewhere.⁹ Generally, the samples contained about the same organic compounds but varied considerably as to individual quantities. The total hydrocarbon concentration ranged from 188 ppb in the wooded area to 10,090 ppb in the building housing the NSPP. Organic materials in these concentrations would be adequate to produce organic iodides in the quantities observed in various experiments.

The influence of nuclear radiation on the formation of CH_3I was also considered.¹⁰ A small experimental study has been initiated to determine the rate of reaction between CH_4 and I_2 in the gas phase and in the presence of ^{60}Co gamma radiation. The results of these measurements can then be factored into the kinetic calculations involving the thermally induced reactions which lead to CH_3I formation.

APPLICATION OF IODIZED CHARCOALS TO AIR CLEANING SYSTEMS

R. E. Adams R. D. Ackley
Zell Combs

Various types of iodized charcoal have been tested and found to be highly effective for trapping radioactive methyl iodide under humid conditions. The practical application of this development has prompted the need for information concerning the ability of these charcoals to withstand both normal and abnormal operating conditions. Consequently, an investigation has been initiated to obtain this information.⁶

Effect of Weathering

Weathering (or exposure to humid air flow), aging, and poisoning may deleteriously affect the $\text{CH}_3^{131}\text{I}$ trapping capability of iodized charcoal, and, while all three of these processes are currently receiving attention, the experimentation currently in progress is most directly concerned with determining the effect of weathering. Two facilities for subjecting iodized charcoal samples to long-term weathering have been put in operation, and samples are periodically withdrawn and tested for $\text{CH}_3^{131}\text{I}$ retention. One facility uses

¹⁰This phase of the study was conducted by Battelle Memorial Institute under contract to ORNL. The information was extracted from the following report: R. H. Barnes *et al.*, *Analytical Studies of Methyl Iodide Formation Under Nuclear-Reactor-Accident Conditions*, BMI-1816 (September 15, 1967).

¹¹R. H. Barnes, J. F. Kircher, and C. W. Townley, *Chemical-Equilibrium Studies of Organic-Iodide Formation Under Nuclear-Reactor-Accident Conditions*, BMI-1781 (August 15, 1966).

Table 13.2. Retention of Radioactivity by ^{131}I -Labeled Iodized Charcoals After Successive Heating Periods at Progressively Higher Temperatures

Duration of each heating period, 4 hr; superficial air velocity, 60, 67, 74, and 80 fpm at 150, 200, 250, and 300°C respectively

Charcoal	Percentage of Initial Radioactivity ^a Retained After Heating Period at Temperature Indicated ^b			
	150°C	200°C	250°C	300°C
MSA 85851	99.9	90.9	65.0	44.1
BC-727	99.6	92.8	62.1	33.0
BC-272	99.7	98.5	79.1	42.9
BC-117	99.7	98.8	94.6	50.6

^aAppropriate allowance has been made for radioactive decay.

^bTemperature is that of the center of the charcoal bed (1 in. in diameter, 2 in. deep).

air from the ORR building, while the other, located in the laboratory, uses cleaned and humidified air. According to the results thus far obtained, which cover a period of about six months, weathering does cause a gradual decline in trapping capability (0.1 to 1.9%). As might be anticipated, the ORR-exposed samples, which are subjected to some degree of poisoning by trace organics in the air, exhibited a somewhat greater rate of decrease in $\text{CH}_3^{131}\text{I}$ removal efficiency as compared with the laboratory samples exposed under rather ideal conditions. In view of these and other observations, it would appear desirable, wherever possible, to avoid subjecting charcoal to air flow except when the actual need to trap molecular radioiodine arises; in those cases where continued air flow is required, an additional upstream charcoal bed to bear the brunt of poisoning due to organic impurities would be helpful. No means for counteracting the slow loss of efficiency through exposure to flow of moist air have been developed; replacement of the adsorber when the efficiency drops is presently the only solution.

Loss of Impregnant at Elevated Temperatures

If iodized charcoal in an air cleaning system is exposed to elevated temperatures, a loss of impregnant may occur, and one or both of two possibly serious consequences may ensue: (1) there may be a loss in effectiveness of the charcoal, and (2) radioactivity may be evolved if the char-

coal has previously been used to trap radioactive methyl iodide and/or elemental iodine. To evaluate this problem and to determine the relative stabilities of various types of impregnated charcoal, a series of laboratory tests is being conducted. In these tests the impregnant on the charcoal is labeled with ^{131}I , the charcoal is heated at progressively higher temperatures, and any ^{131}I radioactivity emitted is collected. The emitted radioactivity is in the form of elemental iodine or an iodine form of similar chemical reactivity.

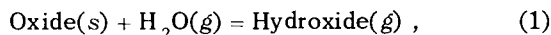
A summary of the results available is given in Table 13.2. According to the data, all of these charcoals are reasonably stable at 150°C. At 200°C two types were still observed to be fairly stable, but at 250°C (and higher) the magnitudes of the radioactivity losses are such as to limit seriously the applicability of even the better of these iodized charcoals if temperatures much in excess of 200°C should be envisaged.

EFFECT OF WATER VAPOR ON THE VOLATILITY OF FISSION PRODUCT OXIDES: TELLURIUM DIOXIDE

A. P. Malinauskas

It has become increasingly evident over the past few years that the presence of water vapor enhances the vapor pressure of a rather broad class of oxides. To date, unfortunately, the underlying mechanism has not been established, although

sufficient evidence has been presented in support of the proposed chemical reaction,



to account for the observed enhancement.

Studies of this type of reaction have been conducted during the past year with tellurium dioxide; in accordance with Eq. (1), this compound should display a volatility enhancement in the presence of water vapor as a result of the chemical reaction



if a one-to-one correspondence is assumed for TeO_2 and H_2O . On the basis of this reaction, the apparent vapor pressure $p_{\text{TeO}_2}^*$ of TeO_2 at a given temperature should vary linearly with water vapor pressure $p_{\text{H}_2\text{O}}$; thus

$$p_{\text{TeO}_2}^* = K_p p_{\text{H}_2\text{O}} + p_{\text{TeO}_2}, \quad (3)$$

where p_{TeO_2} represents the vapor pressure of tellurium dioxide under dry conditions ($p_{\text{H}_2\text{O}} = 0$), and K_p is the equilibrium constant characteristic of Eq. (2).

Although studies involving this system had already been reported in the literature,¹² in which the linear relationship of Eq. (3) had been verified, it appeared worth while to duplicate some of the experiments. Accordingly, the transpiration apparatus sketched in Fig. 13.2 was constructed, and a rather extensive series of experiments were performed at 955°K.

The transpiration or mass transport method of vapor pressure determination involves saturating a carrier gas with the material under investigation in one region of the apparatus, transporting it in this manner to another region where the vaporized species is removed from the carrier, and then determining the amount transported by some suitable means. Oxygen was chosen as the carrier gas in the present investigations. As is illustrated in Fig. 13.2, the gas was first saturated with water vapor at a predetermined vapor pressure and the mixture brought into contact with a loosely compacted bed of TeO_2 in a resistance-heated furnace. The carrier gas was subsequently stripped of its additives by passing it down a quartz tube along which was maintained a temperature gradient

such that the TeO_2 was deposited, and then through a dry-ice-cooled condenser.

The amounts of TeO_2 and H_2O which saturated the carrier gas were determined gravimetrically. These measurements, in addition to the amount of O_2 employed and the total pressure of the system (which is almost equal to atmospheric pressure), are sufficient to calculate both $p_{\text{H}_2\text{O}}$ and $p_{\text{TeO}_2}^*$.

At 955°K the data of Glemser, Haeseler, and Müller¹² indicate that the linear relationship between the apparent vapor pressure and the vapor pressure of water is given by

$$p_{\text{TeO}_2}^* (\text{torr}) = 2.98 \times 10^{-4} p_{\text{H}_2\text{O}} (\text{torr}) + 0.0259; \quad (4a)$$

the present investigations, on the other hand, yield

$$p_{\text{TeO}_2}^* (\text{torr}) = 2.21 \times 10^{-4} p_{\text{H}_2\text{O}} (\text{torr}) + 0.0283. \quad (4b)$$

In both cases the range of water vapor pressure is from 0 to about 1 atm. Although the temperature corrections required to reduce the present data to 955°K had been made in an approximate

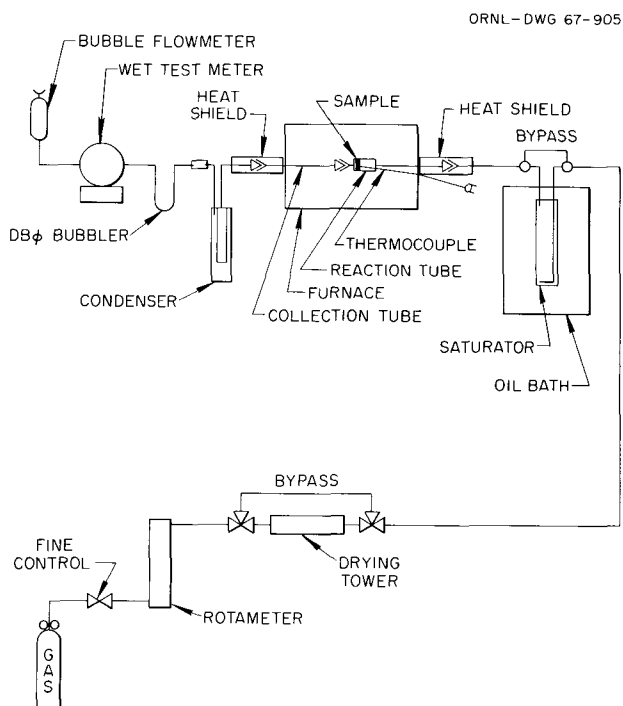


Fig. 13.2. Mass Transport Apparatus.

¹²O. Glemser, R. V. Haeseler, and A. Müller, *Z. anorg. Allgem. Chem.* 329, 51 (1964).

manner and are therefore subject to modification, the magnitudes involved are sufficiently small that Eq. (4b) will not be altered materially by subsequent studies of the temperature dependence of K_p .

It is interesting to note that a recent survey¹³ of vapor pressure measurements of TeO_2 under dry conditions suggests a temperature dependence given by

$$\log_{10} p_{\text{TeO}_2} \text{ (torr)} = -(13.179 \pm 0.079) (10^3/T) + (12.2750 \pm 0.0864), \quad (5)$$

in which the temperature T is given in $^\circ\text{K}$. At 955°K the vapor pressure of TeO_2 , on the basis of Eq. (5), amounts to 0.0299 torr. This value is to be compared with the intercepts of Eqs. (4); in view of the mutual errors involved, all three values are in excellent agreement. The present data does not demonstrate as strong a dependence on water vapor pressure as the previous work, however, and this facet will be explored further at other temperatures.

Fission Product Deposition Characteristics in Thermal Gradients

Considerable interest has recently been focused upon the possible employment of thermal gradient tubes in studies related to the identification and characterization of gaseous fission product species. The method, first advanced by Castleman,¹⁴ takes advantage of vapor pressure differences to effect separation of a multicomponent gas mixture by passing the mixture down a tube along which is maintained a temperature gradient.

As a typical case the experimental procedure entails passing a carrier gas over a solid sample in such a manner that either the gas is not saturated with the vapor in equilibrium with the sample or that equilibrium between the vapor and solid is not attained. As a result the vapor carried by the gas is characteristic of the equilibrium vapor pressure of the solid at a temperature T_d which is less than that at its origin. If the mixture is passed down a tube in which the

temperature is gradually decreased, deposition of the vapor will begin only when the temperature of the tube is T_d . In a mixture of vapors, all of which emanate from their solids at the same temperature, one can therefore achieve separation on the basis of the different deposition temperatures T_d which are characteristic of the individual components.

In addition, the deposition profile displayed by a particular component under a given set of temperature and flow conditions is governed by both its transport and thermodynamic characteristics, so that an examination of such profiles can, in principle, yield thermodynamic and transport property data as well.

Our current activities in this area primarily involve the examination of mathematical models, some of which have already been developed,¹⁴ which describe the processes involved; the purpose of the work is to provide theoretical support for experimental studies in this area which will commence shortly.

The essential features of data obtained from the thermal gradient method can be most easily presented from the consideration of a model in which only the thermodynamic aspects are taken into account. In this model it is assumed that thermodynamic equilibrium prevails throughout, except that the vapor carried away by the sweep gas at a temperature T_0 is not in equilibrium with its solid phase (this can be accomplished, for example, by separating the solid and the sweep gas with a porous barrier). If supersaturation of the carrier with vapor prior to deposition of the latter can be neglected and deposition is simply a condensation mechanism, then the deposit first appears at that temperature T_d at which the molecular density begins to obey the Clapeyron equation

$$n = n^0(T_d/T) \exp[-\Delta H(T_d - T)/RT_d T], \quad (1)$$

where n^0 represents the molecular density at the temperature T_0 , R is the gas constant, and ΔH is the heat of sublimation of the condensing species.

In this particular case, thermodynamic equilibrium throughout implies steady-state conditions as well, and f , the fraction of material deposited per unit length of tube, measured relative to the amount of material entering the tube, is given by

$$f = (x/x^0) (\Delta H/RT^2) (1 - x) (-dT/dz), \quad (2)$$

¹³A. P. Malinauskas, *Vapor Pressure of Tellurium Dioxide*, ORNL topical report (to be issued).

¹⁴A. W. Castleman, Jr., I. N. Tang, and H. R. Munkelwitz, "Chemical Reactions and Transport Behavior of Fission-Product Iodine," pp. 325-43 in *Proceedings of International Symposium on Fission Product Release and Transport Under Accident Conditions*, Oak Ridge, Tennessee, April 5-7, 1965, USAEC report CONF-65407.

in which $-dT/dz$ is the thermal gradient along the tube, and x^0 and x denote the mole fractions of vapor at the point of origin (i.e., at T_0) and at temperature T along the tube respectively. Equation (2) can be further simplified if the depositing species is present in trace amounts ($x \ll 1$) and variations in total pressure are negligible; thus

$$f = (T_d/T_0) (\Delta H/RT^2) (-\partial T/\partial z) \times \exp [-\Delta H(T_d - T)/RT_d T]. \quad (3)$$

Aside from the abrupt onset of deposition observed experimentally, this simplified description likewise correctly predicts the exponential character of the deposition profile.

The thermodynamic treatment assumes a virtually infinitely rapid rate of diffusion of the condensing species in the radial direction (in the case of circular tubes), so that diffusion can be expected to lessen the exponential decay by decreasing f at the onset of deposition and increasing its value further downstream. The degree to which these effects can be detected experimentally, however, awaits further work.

CHEMICAL EQUILIBRIA OF FISSION PRODUCT-FUEL MIXTURES: GAS PHASE COMPOSITION OF THE URANIUM-OXYGEN-STRONTIUM SYSTEM IN THE PRESENCE OF THE CONDENSED PHASE

M. H. Fontana R. E. Bailey¹⁵

The transport of fission products released during a reactor accident depends on their chemical state, which at present is largely unknown. Computation of chemical equilibria in the gas phase is difficult because of the presence of the fuel, a nonstoichiometric condensed phase which may act as a solvent for the fission product. We have

worked out methods of using multicomponent chemical equilibrium computer techniques to treat this problem and have tested them against published Knudsen cell-mass spectrometer data¹⁶ for the U-O system. This served as a base point from which the U-O-Sr system was extended.

It was found that for the U-O systems the gas phase composition (i.e., the partial pressures of U, O₂, UO, UO₂, and UO₃) could be predicted as a function of the O/U ratio in the solid phase, given the equilibrium constants of formation of the compounds of interest and the experimentally determined total pressure and atom ratios in the gas phase. A sample comparison between experimental data and computed results is shown in Fig. 13.3. The total pressure in this case is approximately 10⁻⁷ atm.

The U-O-Sr system was estimated by relating the chemical species in the gas phase (U, O₂, UO, UO₂, UO₃, Sr, and SrO) to a computed equilibrium composition of the same species in the condensed phase. The pressures of the strontium-bearing species were then computed by using estimated Henry's law coefficients. A typical result is shown in Fig. 13.4. The effects of excess oxygen pressure, variation in activity coefficients, and variability in the thermodynamic properties were investigated. We showed that the total amount of strontium in the gas phase is most highly affected by the oxygen-to-uranium ratio in the solid, the equilibrium constant of formation of SrO, and the activity coefficient of strontium. Reducing conditions enhance the total amount of strontium in the gas phase, as confirmed by independent experimental data on fission product release.

¹⁵Purdue University.

¹⁶R. J. Ackerman, E. G. Rauh, and M. S. Chandrasekhariah, *A Thermodynamic Study of the Uranium-Uranium System*, ANL-7048 (1965).

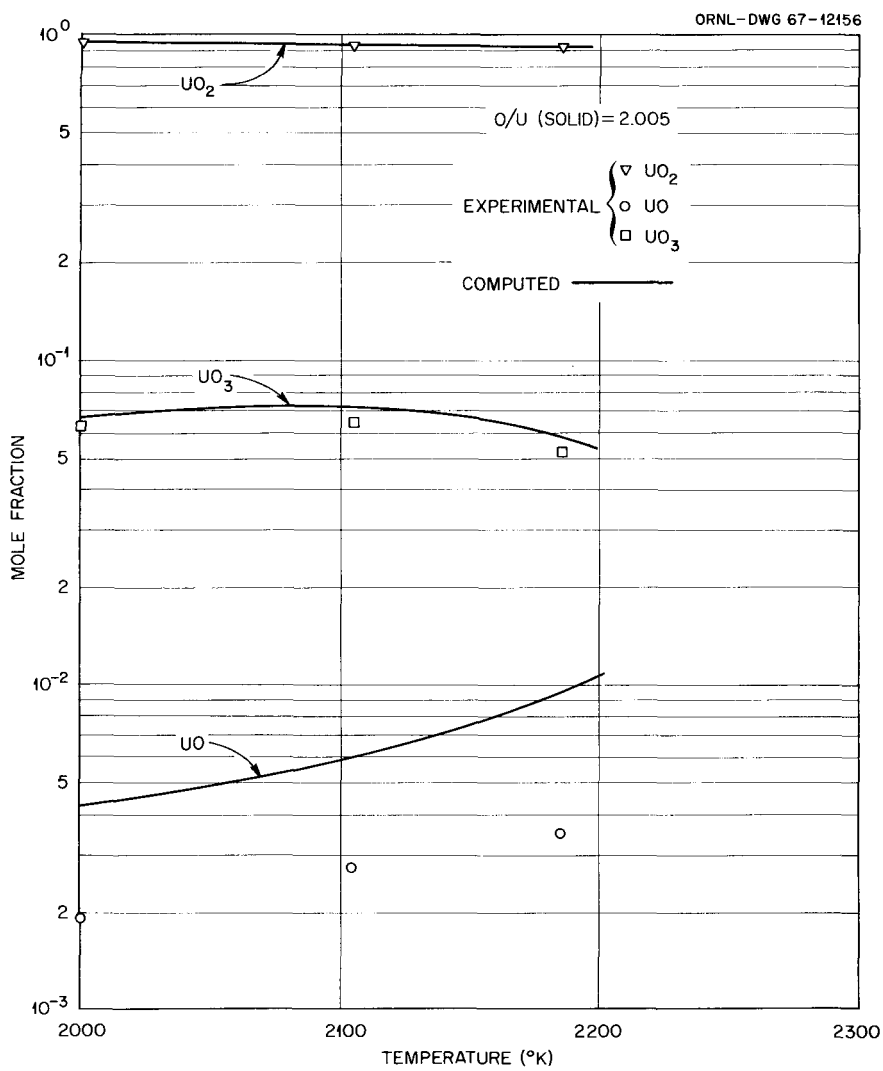


Fig. 13.3. Experimental and Computed Mole Fraction of UO, UO₂, and UO₃ in the Vapor Phase.

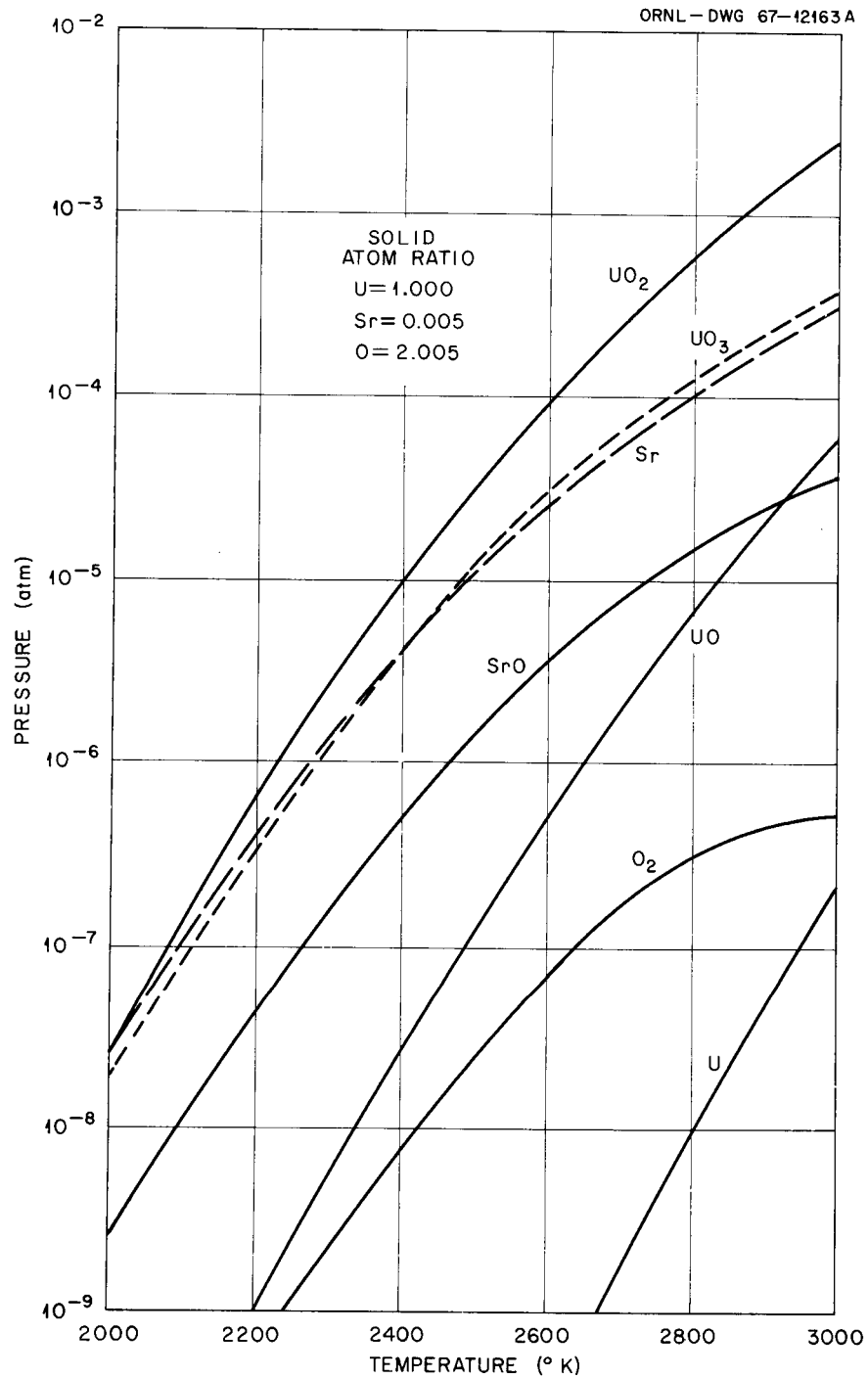


Fig. 13.4. Computed Vapor Pressure of Species Above a U-Sr-O Condensed Phase.

CALCULATION OF THE AMOUNT OF VOLATILE RADIOACTIVITY IN FUEL ROD VOID SPACES – THE D' (EMPIRICAL) METHOD

G. W. Parker R. A. Lorenz

The D' (empirical diffusion) method has been developed to predict the amount of stable and radioactive fission gases in fuel rod void spaces that are available for prompt release. "Prompt release" refers to the immediate escape of volatile and gaseous fission products from void spaces in high-burnup fuel rods when cladding is ruptured following a loss-of-coolant blowdown accident in pressurized-water and boiling-water reactors. Cladding rupture in these accidents is a result of high internal gas pressure and low cladding strength because of high temperature following loss of coolant.

To provide background information about fission gas release for design of experiments and analysis of results, we developed a method of calculating the release of fission gas. In our correlation of the release of radioactive and stable fission gas with UO_2 fuel operating conditions, we made use of the "classical" diffusion release equations developed by Booth and Rymer^{17,18} and also by Beck.¹⁹ These equations, based on Fick's law of volume diffusion, describe the release of both radioactive and stable fission gas. The approximate equations are

$$F = 4 \sqrt{D't/\pi} \quad \text{and} \quad F = \sqrt{D'/\lambda},$$

where $F < 0.2$ for small fractional release of stable and radioactive fission products.

It is now known that fission gas release, especially at high temperature, is dependent on a variety of parameters such as burnup, grain growth, trapping, bubble migration, and possibly temperature cycling. However, we believe that the time dependence and radioactive decay dependence described in the diffusion equation may be valid, and we are therefore examining the use

¹⁷A. H. Booth and G. T. Rymer, *Determination of the Diffusion Constant of Fission Xenon in UO_2 Crystals and Sintered Compacts*, CRDC-720 (August 1958).

¹⁸J. Belle (ed.), p. 486 in *Uranium Dioxide: Properties and Nuclear Applications*, U. S. Government Printing Office, Washington, D.C., 1961.

¹⁹S. D. Beck, *The Diffusion of Radioactive Fission Products from Porous Fuel Elements*, BMI-1433 (April 18, 1960).

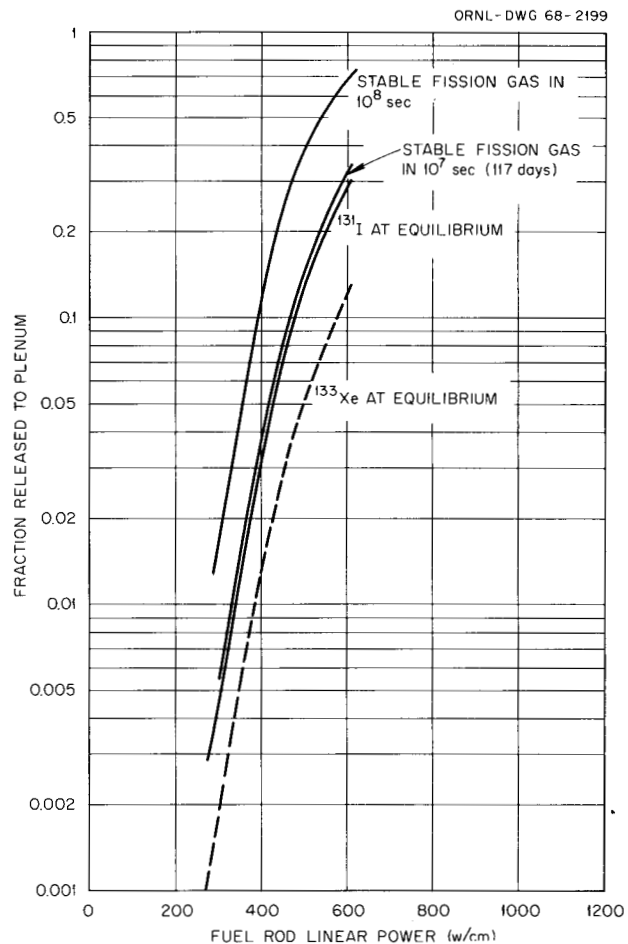


Fig. 13.5. Relative Fractional Release of Stable and Radioactive Fission Gases Calculated by the D' Method.

of a fission gas release parameter, D'_1 , whose temperature dependence is empirically determined.²⁰

The temperature-equivalent parameter that we chose for our correlation is the linear power (watts per cm of length) of a cylindrical fuel rod. Linear power is convenient to use, since all experimental capsule, rod, and reactor rod data may be expressed in these terms, using burnup data and time at power and assuming heat output of 182 Mev/fission. Our investigations show that most of the current generation of metal-clad UO_2 -fueled reactors use fuel of similar composition, density, and manufacture, so that the resulting correlation is suitable for most boiling-water and pressurized-water reactors.

²⁰G. W. Parker and R. A. Lorenz, *Nucl. Safety Program Semiann. Progr. Rept. Dec. 31, 1967*, ORNL-4228 (to be published).

The basis for our determination of D' (empirical) was the release of stable fission gas in capsules and fuel rods as reported by Atomic Energy Canada Limited (AECL). We chose the AECL work because of the large number of carefully conducted and well-reported experiments. The effect of density on thermal conductivity was accounted for by applying a correction factor to the linear power. We used data for burnup of 1000 Mwd/ton or higher, assuming that sintering, grain growth, cracking, and bubble formation in the first 1000 Mwd/ton burnup would minimize the effect of initial structure on fission gas release.

The relative fractional release of stable and radioactive fission gases calculated by this method is shown in Fig. 13.5. The release of stable gas is a function of time, but the release of radioactive gas reaches an equilibrium after a period equal to several half-lives.

The D' method was applied to the Browns Ferry Reactor. The fraction of ^{133}Xe released to the fuel rod void spaces was calculated to be about 0.6%, and the fraction of stable xenon and krypton released to the voids was calculated to be about 6%.

PROMPT RELEASE OF FISSION PRODUCTS FROM HIGHLY RATED ZIRCALOY-CLAD UO_2 FUEL

M. F. Osborne G. W. Parker

The future of economic power reactors is dependent on the development of reliable fuel elements with progressively higher heat output. The inventory of volatile fission products which accumulate in the element void space as a result of high-temperature operation is potentially hazardous in the event of a reactor accident; any cladding failure can release to the coolant a large fraction of such fission products. Consequently, we are studying the behavior of volatile fission products, principally I, Cs, Te, and Ru, under the conditions of a reactor loss-of-coolant accident. The release of krypton and xenon under such conditions is relatively well known.^{21,22}

Irradiated Zircaloy-clad UO_2 fuel capsules will be heated to failure inside a ceramic-lined tungsten-element resistor furnace. A carrier gas of helium or helium-steam will sweep the released fission products through a fractionation train of

absolute filters, silver membranes, and charcoal cartridges, which will separate and collect the fission products for radiochemical analysis.

Iodine Tracer Experiments

A series of preliminary experiments designed to study the behavior of iodine only and to prove the capabilities of the system has been completed. The test specimens were unirradiated fuel capsules containing an implanted vial of short-lived ^{130}I . The results of three such experiments are summarized in Table 13.3. In each experiment the capsule ruptured and released iodine at about 1300°C. Two fractionation trains were used: one to collect the initial release at constant pressure, and the second to collect the release during three pressure reduction cycles (1.0 to 0.1 atm). In the second experiment the carrier gas was pure helium, and the test temperature was extended to the melting point of Zircaloy. Apparently, the heating rate influenced the type of cladding failure; a much larger fracture (and also greater iodine release) occurred in experiment PR-3, which had a higher heating rate ($\sim 100^\circ\text{C}/\text{min}$) than in PR-1 ($\sim 10^\circ\text{C}/\text{min}$).

For reasons not clear, very little of the iodine penetrated the absolute filters, which collected some 40% of the total inventory in each experiment. We plan to investigate the significance of the formation of volatile ZrI_4 by the reaction of released iodine with the Zircaloy cladding.²³ Two possible reasons for the greater iodine release in experiment PR-3 (1400°C) than in PR-2 (1800°C) are (1) the rapid heating rate and large fracture, and (2) the presence of steam in PR-3. Somewhat similar tracer experiments by Collins *et al.*²⁴ yielded much less iodine release ($\sim 5\%$ vs $> 50\%$). However, significant experimental differences such as (1) lower temperature (900°C vs 1400°C), and (2) size of cladding fracture would

²¹G. W. Parker *et al.*, *Out-of-Pile Studies of Fission Product Release from Overheated Reactor Fuels at ORNL, 1955-1965*, ORNL-3981 (July 1967).

²²R. C. Nelson *et al.*, *Fission Gas Release from UO_2 Fuel Rods with Gross Central Melting; I. Pellet Fuel*,² GEAP-4572 (July 1964).

²³H. S. Rosenbaum, J. H. Davies, and J. Q. Pon, *Interaction of Iodine with Zircaloy-2*, GEAP-5100-5 (January 1966).

²⁴R. D. Collins, J. J. Hillary, and J. C. Taylor, *Air Cleaning for Reactors with Vented Containment*, U. K. At. Energy Authority, Reactor Group, TRG Inform. Ser., report 1318(W).

Table 13.3. Release of ^{130}I from Ruptured Fuel Capsules

Experiment and Conditions	Fraction Retained in Fuel Capsule	Fraction of Total Inventory at Sample Location					Totals
		Furnace Tube	Teflon Header	Absolute Filter	Silver Membrane	Hot Charcoal	
PR-1 ^a (1350°C, helium and steam)	0.44	<i>b</i>	<i>b</i>	0.433	0.087	0.039	0.559
(a) 15 min at constant pressure				0.430	0.065	0.007	0.502
(b) 40 min, 3 pressure cycles				0.003	0.022	0.032	0.057
PR-2 ^a (1800°C, helium only)	0.248	0.329	0.0104	0.412	0.0002	<0.0001	0.7516
(a) 40 min at constant pressure				0.368	0.0002	<0.0001	0.3680
(b) 20 min, 2 pressure cycles				0.0440	<0.0001	<0.0001	0.044
PR-3 (1400°C, helium and steam)	0.0789	0.255	0.111	0.4616	0.00050	0.00079	0.8289
(a) 6 min at constant pressure				0.3173	0.00003	0.00001	0.3173
(b) 60 min, 3 pressure cycles				0.1443	0.00047	0.00078	0.1456

^aData for PR-1 inferior because of ^{24}Na interference; pretest inventory not known.

^bNo sample.

indicate more release for our experiments. Collins performed other experiments with irradiated fuel capsules, in which <1% of the iodine was released. Values of 4 and 7% for the release of ^{131}I from defected fuel rods into pressurized water loops during irradiation have been reported by other investigators.^{25,26} Additional experiments should improve our understanding of and ability to predict iodine release.

Highly Rated Fuels Experiments

Twelve fuel capsules have been irradiated at high heat ratings (up to 500,000 Btu hr⁻¹ ft⁻²) by the General Electric Company. These low-burnup irradiations were completed November 5, 1967. Nondestructive examinations – neutron radiography, gamma scans, and dimensional measurements – indicate that design conditions were attained. Central voids were formed in the fuel of seven capsules, and there was evidence of con-

siderable fission product migration. Accordingly, three capsules were selected for destructive examination, and the other nine capsules will be tested in the prompt-release equipment in the near future.

DEVELOPMENT OF FILTRATION TECHNOLOGY

R. E. Adams J. S. Gill
R. J. Davis J. Truitt
W. D. Yuille²⁷

This program is being conducted to investigate the influence that a postaccident environment resulting from a loss-of-coolant accident to a water reactor might have on the behavior of particulate aerosols and also on the filtering characteristics of high-efficiency filters. Results from this program are reported in detail elsewhere.^{28,29}

²⁵G. M. Allison and H. K. Rae, *The Release of Fission Gases and Iodines from Defected UO₂ Fuel Elements of Different Lengths*, AECL-2206 (June 1965).

²⁶B. Weidenbaum *et al.*, "Release of Fission Products from UO₂ Operating at High Power Rating," pp. 885–907 in *Proceedings of the International Symposium on Fission Product Release and Transport Under Accident Conditions*, Oak Ridge, Tenn., April 5–7, 1965, CONF-650407, vol. 2.

²⁷Visiting scientist, UKAEA.

²⁸R. E. Adams *et al.*, "Filtration of Oxide Aerosols of Stainless Steel and Uranium by High-Efficiency Filter Media," *Nucl. Safety Program Ann. Progr. Rept. Dec. 31, 1967*, ORNL-4228 (to be published).

²⁹R. E. Adams *et al.*, "Coagulation of Aerosols," *Nucl. Safety Program Ann. Progr. Rept. Dec. 31, 1967*, ORNL-4228 (to be published).

Efficiency of Commercial Filter Media for Simulated Accident Aerosols

The efficiencies of several commercially available high-efficiency filter media for stainless steel- UO_2 aerosols are being measured as a function of air velocity, humidity of the atmosphere, amount of water contained in the filter media, and other parameters. The aerosol is generated by an electric arc using as the consumable electrode a small irradiated stainless steel tube containing a cylindrical UO_2 insert. The aerosol is generated, diluted with air, and passed into a tank fitted with a recirculation loop containing the filter media under test. The filter efficiencies are calculated as the ratio of radioactivity on the first filter to the total radioactivity on the first and on all the backup filters (and on filter holder parts downstream of the first filter paper).

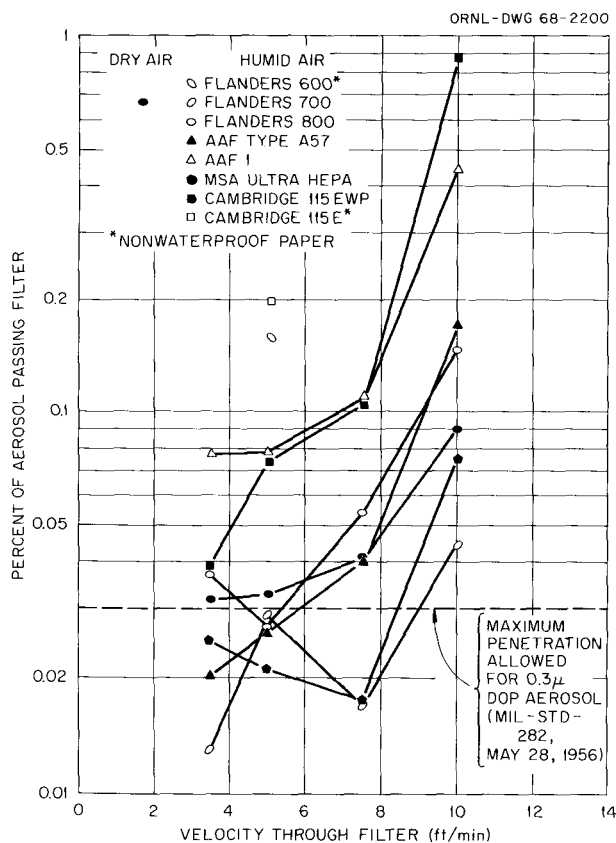


Fig. 13.6. Penetration of Filter Media by Oxide Aerosol of Stainless Steel and Uranium Under Dry and Humid Conditions.

A collection of data from tests with eight types of commercial filter media is presented in Fig. 13.6, a plot of the percent of disperse phase material which passed the filter ($100 - \text{filter efficiency}$) as a function of gas velocity through the filter. The efficiencies do not change much with velocity in the range 3.5 to 7.5 fpm but decrease above 7.5 fpm; the normal velocity for application is 5 fpm. The nonwaterproof media were significantly less efficient than waterproofed papers under humid conditions. Two of the waterproofed papers were significantly less efficient than the others tested.

Contained in Table 13.4 are the results of experiments designed to show the effect of water adsorbed in the filter media on the filter efficiency. The efficiency of filter media has been found to decrease substantially if the media is exposed to a water-saturated atmosphere for long periods or, in the case of a nonwaterproofed medium, if a drop of water is placed on the filter disk just prior to testing.

It is suggested that the deleterious effect of moisture on the filter media is caused by condensation of water between some of the tiny fibers. The result is an apparent increase in fiber diameter which decreases the filter efficiency. This hypothesis has been explored by calculating filter efficiencies based on filter theory.^{30,31} It can be shown that a hypothetical filter composed of 2- and $0.15\text{-}\mu$ fibers under certain conditions will have a minimum efficiency of 98.5% for $0.2\text{-}\mu$ particles; if one assumes then that the $0.15\text{-}\mu$ fibers are increased in size to $0.3\text{-}\mu$ by condensing moisture, the filter efficiency drops to 81%. This result lends some support to the hypothesis put forth.

Behavior of Oxide Aerosols in Humid Atmospheres

Small-scale experiments were made to examine effects of moisture on aerosols produced by arc melting, or by high-frequency spark melting, of

³⁰W. L. Torgeson, *The Theoretical Collection Efficiency of Fibrous Filters Due To the Combined Effects of Inertia, Diffusion, and Interception*, paper No. J-1057, Applied Science Division, Litton Systems, Inc., St. Paul, Minnesota, 1963.

³¹K. T. Whitby, "Calculations of the Clean Fractional Efficiency of Low Media Density Filters," *ASHREA J.* 1965, pp. 56-65.

Table 13.4. Effect of Moisture on Filter Efficiency

	Percent Passing Filter		
	Flanders 800	MSA UltraHepa	Flanders 600
Stored in 100% humidity at room temperature 12-13 days	0.02	0.06	
	0.06	0.07	
	<u>0.54</u>	<u>0.15</u>	
Average	0.21	0.09	
Stored in 100% humidity at room temperature 43-45 days	0.57	0.35	
	0.67	0.59	
	<u>0.83</u>	<u>0.69</u>	
Average	0.69	0.54	
Stored in 100% humidity at 80°C for 24-48 hr	0.21	0.28	
One drop of water put on filter disk			0.63
			1.07
			2.02
			<u>0.73</u>
Average			1.11

simulated reactor fuel in air. The results have been reported in detail elsewhere.³²

The only simulant used was stainless-steel-clad uranium dioxide, and an effect of moisture was obtained either by generating in air at 80 to 90% relative humidity or by bubbling the dry generated aerosol through water.

One aspect of the effect of moisture was demonstrated by comparing the performance of filter packs against wet and dry aerosols. Roughing filters, punched from a loose weave of Dacron fibers, were assembled in series, 8 to 10 such filters comprising a filter pack. Usually 80 to 90% of the mass of dry aerosol was retained on the first stages of the filter pack. In contrast, the wet aerosol was filtered with a marked reduction in efficiency.

These results were explained in terms of a moisture effect on the aerosol particle size. Particle size measurements were made with fibrous filter analyzers³³ and by electron microscope examination of samples taken with thermal precipitators. In air of high relative humidity, a reduction in agglomerate size of one order of magnitude was measured, these agglomerates tending to be compact entities distinct from the

extended chain structures of agglomerates encountered in dry systems. The reduced particle size, to the range 0.1 to 1.0 μ in diameter, accounted for measured losses in filtration efficiency when wet aerosols were passed through filter packs made from Dacron fibers.

The favored mechanism by which water vapor alters particle size and shape is adsorption of water onto particle surfaces. The resulting surface-tension forces of water films could bring about the observed changes in particle size and shape.

Coagulation of Aerosols

Coagulation is one of the more important natural processes which determine the airborne concentration of particulate matter as a function of time. An experimental system is being assembled to study the coagulation of aerosols of interest as

³²W. D. Yuille and R. E. Adams, *Behavior of Oxide Aerosols of Uranium and Stainless Steel in Humid Atmospheres*, ORNL-4198 (January 1968).

³³M. D. Silverman *et al.*, *Characterization of Radioactive Particulate Aerosols by the Fibrous-Filter Analyzer*, ORNL-4047 (March 1967).

a function of turbulence, humidity, and initial concentration of aerosol. As a preliminary to the experimental phase a simple model has been developed for calculating airborne concentration as a function of time. This model makes use of the "self-preserving" size distribution hypothesis advanced by Friedlander.³⁴ The size distribution function is

$$dN/dr = 0.05\phi_0 r^{-4},$$

where N is the number of particles of radius r per unit volume of gas, and ϕ_0 is the fraction of the volume of gas occupied by the aerosol particles. The major steps of the calculation are as follows:

1. Assert a value of the initial volume fraction of the disperse phase, ϕ_0 .
2. Assume that coagulation and other natural processes give the "self-preserving" size distribution.
3. Calculate the number of particles which settle (assuming stirred conditions) from each size range, during the first time increment.
4. Calculate the new volume fraction of disperse phase, ϕ_1 .
5. Reiterate step 2 (i.e., one presumes that coagulation will have proceeded in order to re-establish the "self-preserving" distribution) and also steps 3 and 4. In this way, values of ϕ_2, ϕ_3, ϕ_4 , etc., are calculated.

The results from this calculation are generally in agreement with our semiquantitative experience with the behavior of stainless steel- UO_2 aerosol. The applicability of the calculation will continue to be tested with experimental data generated by future experiments.

IGNITION OF CHARCOAL ADSORBERS

R. E. Adams R. P. Shields
R. J. Davis

Charcoal adsorbers for radioiodine constitute an important part of reactor safety systems for the removal of accident-released fission products from the containment volume either during recirculation of the atmosphere or as it is being exhausted from the containment shell. During operation the charcoal adsorbers would be subject to loading with large quantities of fission products and, consequently, would be heated by decay of the trapped fission products.

Experimental Studies

A program is under way both in the laboratory and in-pile to establish the effects of fission products and of irradiation on the ignition temperature of charcoal adsorbers. Three in-pile experiments have been conducted; the first two utilized Bamebey-Cheney type KE charcoal, and the results have been reported.^{35,36} The third in-pile experiment (IGR-3) testing the effect of fission gases on the ignition temperature of Mine Safety Appliances type 85851 charcoal (an iodized charcoal) has been performed, and analysis of the data is in progress. The experimental system was modified to replace the stainless steel ignition tube with one of quartz to withstand better the severe oxidizing conditions, and by addition of a glass vacuum-insulated adsorber to measure decay heat and fission product distribution. Fission products emanating from the in-pile furnace were alternately routed to the insulated adsorber and to the ignition tube during the course of the experiment.

While the radiochemical analysis is incomplete, some preliminary observations can be made based upon temperatures recorded during the experiment. The initial ignition event for MSA 85851 charcoal in the presence of fission gases from fissioning UO_2 was 35°C lower than the initial ignition temperature of 370°C measured in the same ignition tube in the laboratory. In-pile the succeeding ignition events took place at lower temperatures, following a pattern almost identical to that measured in the laboratory. This behavior of MSA 85851 charcoal (iodized) is quite different from that of KE (noniodized) charcoal in the previous experiments, and the cause for this difference will be delineated by future study employing both in-pile and laboratory tests.

Laboratory experiments have been performed in support of the in-pile ignition program. Ignition tests have been made under a variety of conditions on many charcoals with an apparatus constructed according to a design agreed on by ORNL,

³⁴S. K. Friedlander, "Theory of Self-Preserving Size Distribution in a Coagulated Dispersion," pp. 253-59 in *Radioactive Fallout from Nuclear Weapon Tests*, A. W. Klemet (ed.), CONF-765 (November 1965).

³⁵R. P. Shields and C. E. Miller, Jr., *The Effect of Fission Products on Charcoal Ignition (In-Pile Experiment)*, ORNL-TM-1739 (January 10, 1967).

³⁶C. E. Miller, Jr., and R. P. Shields, *Nucl. Safety Program Ann. Progr. Rept. Dec. 31, 1966*, ORNL-4071, pp. 149-57.

Table 13.5. Ignition Temperature of Various Charcoals Measured with the Standard Ignition Apparatus

Charcoals	Ignition Temperatures ($^{\circ}\text{C}$) at Given Air Velocities (fpm) and a Heating Rate of $10^{\circ}\text{C}/\text{min}$					
	4	8	10	20	40	70
BC-416	315	318	320	325	328	
MSA 85851 ^a	365	358	361	370		373
BC-592	445		455			500
	445				468	487
	447				458	473
BC-117 ^a	455			450		475
				455		456
BC-212 ^a	290					307

^aIodized charcoal.

Savannah River Laboratory, and Barnebey-Cheney; this standard apparatus has been described in a previous report.³⁵

Samples of two new iodized charcoals were recently obtained from Barnebey-Cheney; one, designated BC-272, is very similar to BC-727 except that the level of impregnation is lower; and the second, BC-117, represents a new class of impregnated charcoals designed to have a high ignition temperature and to resist loss of impregnant at elevated temperatures. Results of tests on these and other charcoals are given in Table 13.5.

During the laboratory ignition tests, some of the iodized charcoals were observed to be releasing iodine vapor as the temperature was being raised. In some cases the iodine vapors could be detected visually when the temperature was 150 to 200°C . In a laboratory test in which a sample of MSA 85851 was held in the temperature range 275 to 300°C (with air flowing through it), about 23% of the iodine was swept out in 1 hr and 39% in 3 hr (see "Application of Iodized Charcoals to Air Cleaning Systems," this chapter, for additional information).

Analytical Description of Charcoal Ignition Temperature

Charcoal ignition temperature is descriptively defined as the temperature above which oxidation

is self-sustaining. Experimentally, it is observed by slowly raising the temperature of a sample and noting the temperature at which an abrupt increase in heating rate occurs.

An equation has been developed³⁷ which relates ignition temperature to the parameters of first-order importance, namely, the charcoal activity (including the effects of promoters, inhibitors, and surface area), the oxygen activity (air velocity, oxygen concentration), the stoichiometry of the rate-determining step of the mechanism, and the activation energy of the oxidation reaction.

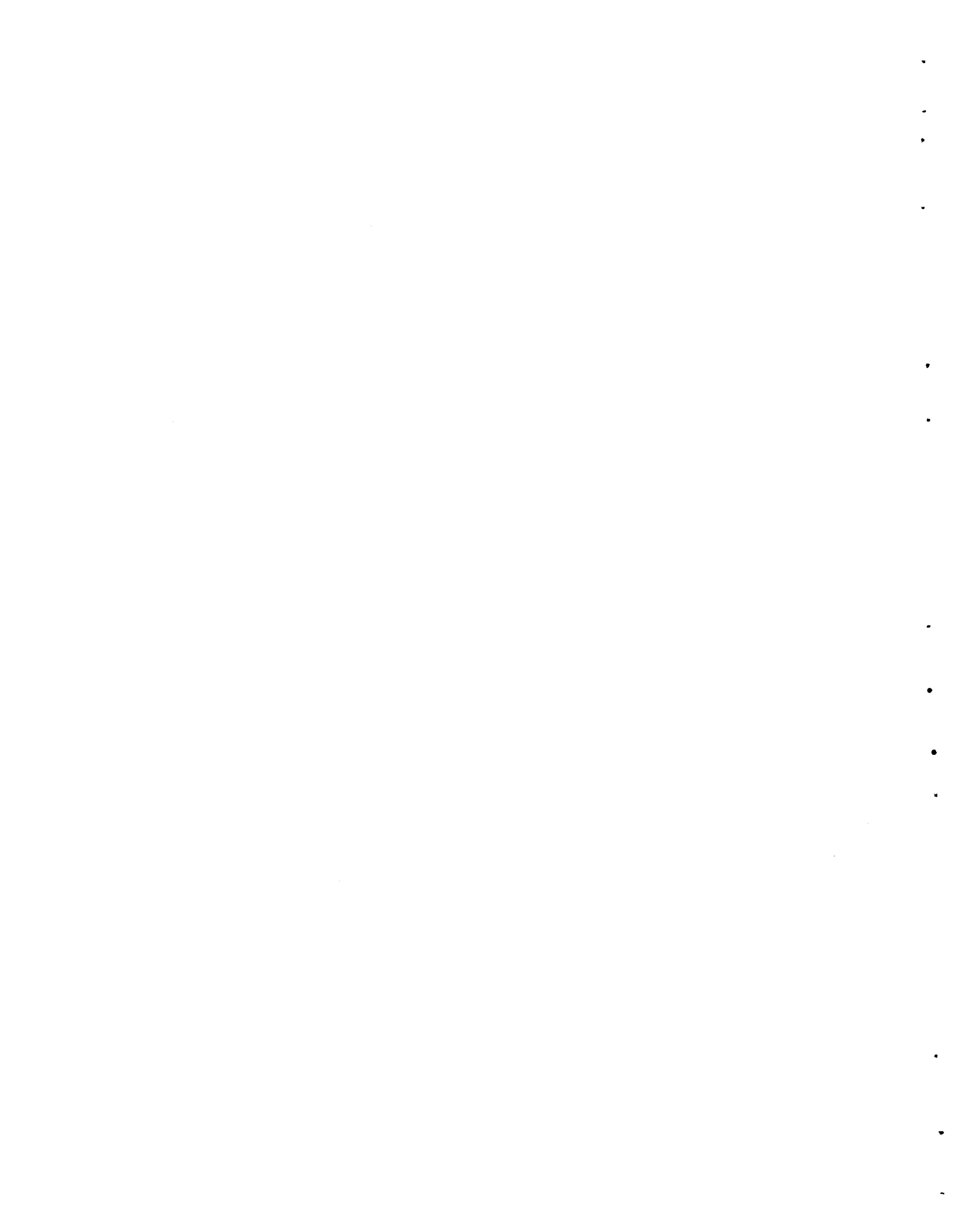
Briefly, the derivation depends on the following steps: (1) The ignition temperature is defined as the temperature at which the slope of the temperature-time plot is the average of the slopes before and after ignition. (2) A heat balance in the charcoal sample is derived; one term in the heat balance is the rate of oxidation. (3) The rate of oxidation after ignition is limited by the oxygen available; from this and step 1, an expression is written for the oxidation rate at ignition. (4) A second rate expression is derived from the Arrhenius equation. (5) Combination of the two expressions for the rate at ignition gives the working equation. The applicability of the equation has been demonstrated with experimental data.

³⁷R. J. Davis, *The Significance of Charcoal Ignition Temperatures*, ORNL-4129 (July 1967).



Part V

Other ORNL Programs

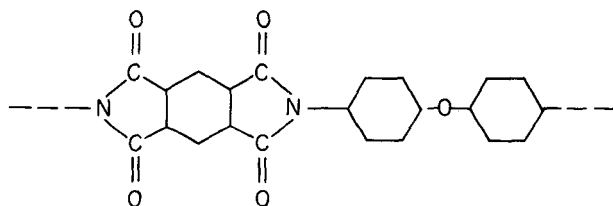


14. Effects of Radiation on Organic Materials

EFFECT OF RADIATION ON POLYMERS

W. W. Parkinson W. K. Kirkland

The complex polymers derived from the pyromellitimides are useful in high temperature applications because of their long-term stability at temperatures as high as 270°C in air. These polymers are also reported to be highly resistant to radiation, probably because of the relatively high fraction of aromatic rings in the molecular structure. A common use of these materials is as electrical insulation in thin sheet form. In this form, materials are most susceptible to oxidation when irradiated in air. On the other hand, some oxygen-containing polymers, for example, polymethyl methacrylate, are not very sensitive to the presence of oxygen during irradiation.¹ To investigate the possibility of accelerated degradation of the polyimides in air, commercial film stock derived from the polyimide of bis-aminophenyl ether and pyromellitic acid has been irradiated in air and in vacuum. The significant mechanical properties – tensile strength and elongation at break – were measured since the insolubility and infusibility of the polymer make determination of molecular weights impractical.



diated in air and in vacuum. The significant mechanical properties – tensile strength and elongation at break – were measured since the insolubility and infusibility of the polymer make determination of molecular weights impractical.

¹P. Alexander and D. J. Toms, *Radiation Res.* 9, 509 (1958).

The specimens were $\frac{1}{2} \times 4$ in. strips, 0.002 in. thick, with a 2-in. gage length for tensile testing. For irradiations in air, the specimens were exposed to ^{60}Co gamma radiation at an average dose rate of 1.8×10^6 rads/hr at 22°C in a current of air. Specimens irradiated in vacuum were exposed at a similar dose rate, 1.6×10^6 rads/hr, except for the group subjected to the highest dose. This group was irradiated at 6.5×10^6 rads/hr to shorten the exposure time. (The radiation effects in vacuum would not be expected to depend on dose rate but only on total dose.) The samples for irradiation in vacuum were outgassed by heating to 140°C for at least 12 hr while maintaining the pressure at 10^{-5} torr or lower. The specimens were cooled and sealed off in their glass capsules at about 5×10^{-6} torr.

After irradiation, the tensile properties were measured by standard procedures. The tensile strengths and elongations at break are shown in Fig. 14.1 for both the specimens irradiated in air and in vacuum. In this thin sheet stock there is an appreciable effect of atmosphere during irradiation. For a reduction of the tensile strength to 90% of the original, an order of magnitude greater dose is required if the samples are in vacuum during irradiation. The ductility or elongation at break is more sensitive than tensile strength, but the effect of air during irradiation is similar. A 50% reduction in this property requires 1.2×10^{10} rads in vacuum but only 2.9×10^9 rads in air.

Because the initial mechanical properties of this polymer are relatively high it will still be useful at about the maximum doses of the respective curves. At 10^{10} rads in air, 0.002-in. film has 12,000 psi tensile strength and 3.3% elongation at break, values superior to the original properties of most rigid polymers. An inert atmosphere or a thicker cross section would give greater durability.

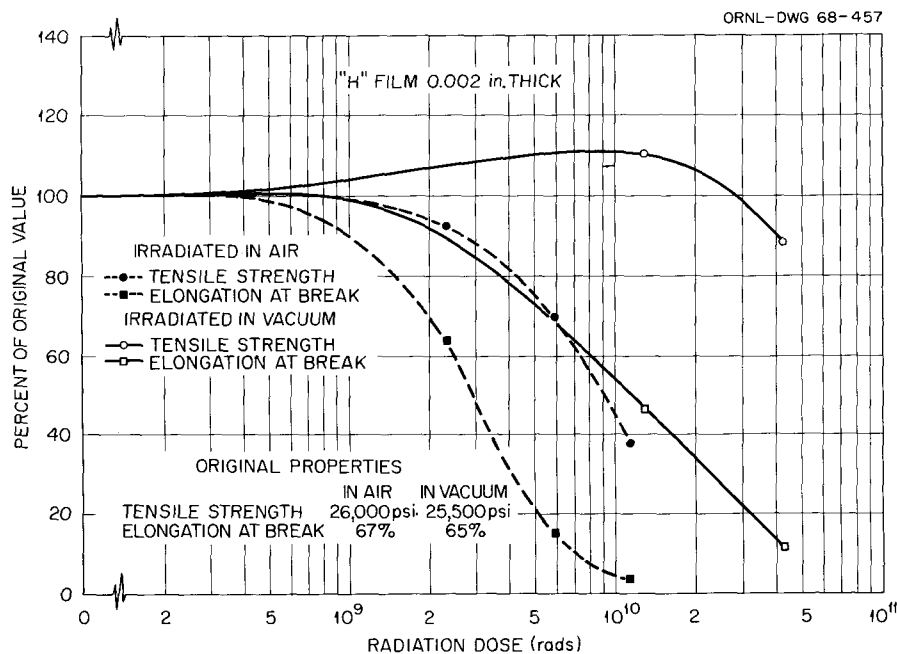


Fig. 14.1. The Effect of Radiation on the Tensile Properties of Polyimide Film (Du Pont H Film).

RADIATION-INDUCED REACTIONS OF HYDROCARBONS

R. M. Keyser W. K. Kirkland

The previous report² dealt with a preliminary characterization of products resulting from gamma irradiation of solutions of naphthalene in *n*-hexane. These solutions constitute a model system for studying radiation-induced hydrogenation and alkylation reactions of coal in a chemonuclear process. The preliminary characterization involved separation of radiolysis products by gas chromatography and collection by trapping from the effluent. The ultraviolet spectra of a number of these products exhibited characteristics similar to the uv spectrum of methylnaphthalene, suggesting that the unknowns were monosubstituted alkylnaphthalenes. These predictions have been confirmed, and this report deals with the detailed structure assignments of ten of these products using mass, nuclear magnetic resonance (n.m.r.), and infrared spectrometry.

Both the 70- and 20-ev mass spectra of the isolated products were obtained,³ the 20-ev spectra being used to confirm the assignment of the parent ion peak in the 70-ev spectra. The spectra showed

characteristics expected of monosubstituted alkylnaphthalenes. Molecular weights of the unknowns were obtained from the *m/e* value of the respective parent peaks. Subtraction of the molecular weight of the naphthyl group thus gave the sizes of the alkyl substituents. Ethyl, propyl, butyl, and hexyl groups were identified in this manner, accounting for ten unknowns: ethylnaphthalene, two isomeric propylnaphthalenes, a butylnaphthalene, and six isomeric hexylnaphthalenes.

The mass spectra of the propylnaphthalenes required structure assignments of *n*-propylnaphthalene and isopropylnaphthalene, while that of the butyl compound required a *sec*-butylnaphthalene structure. Fragmentation peaks corresponding to loss of methyl, ethyl, etc., from the parent molecule were evident in the mass spectra of the hexyl compounds, but it was not possible to utilize these to obtain an unambiguous assignment of the structures of the hexyl substituents. Toward this end, therefore, n.m.r. spectra were obtained.⁴

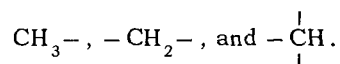
The n.m.r. spectra of the six hexylnaphthalene isomers exhibited varying degrees of absorption in the spectral regions corresponding to aliphatic and aromatic protons. A small amount of olefinic proton absorption was also evident. Peaks in the aliphatic

²R. M. Keyser *et al.*, *Reactor Chem. Div. Ann. Progr. Rept.* Dec. 31, 1966, ORNL-4076, p. 127.

³W. T. Rainey, Jr., Analytical Chemistry Division.

⁴J. R. Lund, Analytical Chemistry Division.

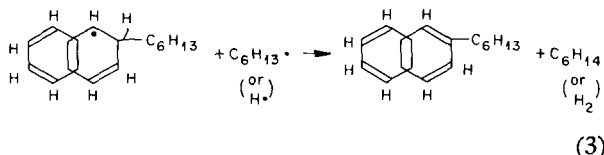
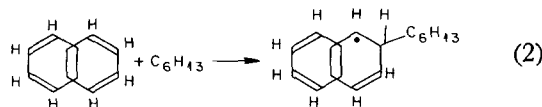
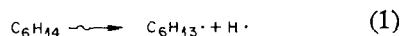
region were assigned to protons of the following types:



The major portion of the absorption in the aromatic proton region was characteristic of monosubstituted naphthalenes, as expected.

The areas under the absorption peaks in the aliphatic proton region were consistent with the following assignments for the structures of the hexyl substituents: *n*-hexyl, 2-hexyl, and 3-hexyl. Each of these hexyl isomers could be found at either the α or β position on the naphthalene ring, thereby accounting for six isomeric hexylnaphthalenes. The position of substitution on the ring was also confirmed from infrared spectra in the 650–900 cm^{-1} region. Hence, the six isomeric hexylnaphthalenes are identified as α - and β -(*n*-hexyl)naphthalene, α - and β -(2-hexyl)naphthalene, and α - and β -(3-hexyl)naphthalene.

We propose the following mechanism to explain the formation of the hexylnaphthalenes:



The reaction scheme for α substitution is entirely analogous. The formation of the other alkyl naphthalenes is the same, but with reaction (1) involving a C–C bond rupture rather than a C–H.

ADDITION REACTIONS OF FURAN DERIVATIVES

C. D. Bopp J. J. Myron W. W. Parkinson

The radiation-induced addition of saturated furan derivatives to olefinic compounds has been studied as a possibility for utilizing radioisotopes in chem-

ical synthesis.⁵ Solutions of cyclohexene in tetrahydrofuran in various concentrations have been irradiated with gamma radiation at 20 to 300°C.

The principal liquid products were a codimer, 2-(cyclohexen-1-yl)tetrahydrofuran; a diether, α, α' -di(tetrahydrofuryl); an olefin dimer, 3,3'-dicyclohexenyl; and higher-boiling products (HBP). The G values of all but the HBP were determined by gas chromatography, as was the cyclohexene consumption. The HBP was determined as the weight of the residue remaining after the other products were separated by low-pressure distillation. Elemental analysis of the HBP indicated that the ratio of tetrahydrofuran to cyclohexene incorporated in the formation of these products averaged about 3/1. The use of this figure gives approximate agreement between the disappearance of cyclohexene and its incorporation in the products listed in Table 14.1.

The position of the double bond in the codimer was deduced from its nuclear magnetic resonance spectrum.⁶ The identification of this compound was confirmed by molecular weight, elemental analysis, infrared spectroscopy, and gas chromatography. Similar methods were used to identify the diether, but only the gas chromatographic retention time was used to identify the diolefin.

The average molecular weight of the HBP was about 240. Separation of the HBP was obtained through thin-layer chromatography, and the isolated fractions were examined by infrared spectroscopy. It was established that about seven compounds were present, each ranging from 5 to 25% of the total. One of the compounds was a hydrocarbon (probably a cyclohexene trimer); the others contained one or more ether groups. The absence of hydroxy and carbonyl groups in any of the compounds suggests that the tetrahydrofuran rings remained intact in these reactions.

The absence of a saturated codimeric product (Table 14.1) is evidence that the tetrahydrofuryl radical does not add to the unexcited cyclohexene molecule. Although the addition of α -ether radicals to halo-olefins and terminal olefins is well known, the nucleophilic character of the ether radical retards its addition to more electron-rich olefins.⁷

⁵C. D. Bopp *et al.*, *Reactor Chem. Div. Ann. Progr. Rept. Dec. 31, 1966*, ORNL-4076, p. 129.

⁶Determined by J. R. Lund, Analytical Chemistry Division.

⁷I. Rosenthal and D. Elad, *Tetrahedron* **28**, 3193 (1967).

Table 14.1. Products from Tetrahydrofuran-Cyclohexene System

Temperature of Irradiation (°C)	Composition, Ether/Olefin (mole ratio)	Yields (molecules/100 ev)				
		Consumption of Cyclohexene	Codimer	Diether	Diolefin	High-Boiling Products ^a
20	10/1	3.0	1.1	0.3	0.3	5
20	1/1	<i>b</i>	1.3	0.3	0.7	<i>b</i>
300	2/1	<i>b</i>	8	0.0	4	<i>b</i>

^aIn terms of the total number of molecules of cyclohexene and tetrahydrofuran which were incorporated in these products.

^bNot determined.

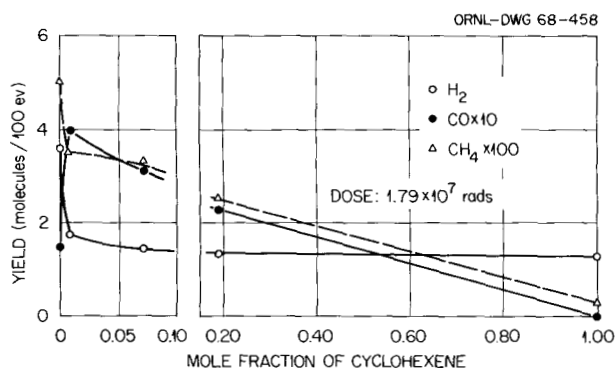


Fig. 14.2. Gas Yields in THF Solutions of Cyclohexene.

The *unsaturated* codimer may be formed by either of two schemes:

1. addition of an ether radical to an excited olefin molecule with ejection of a hydrogen atom, or
2. addition of an ether radical to an olefin cation with the transfer of a proton to the substrate.

In order to explain the high yield of codimer at 300° through scheme 2, it is necessary to assume a short chain reaction, since ion yields are generally low. Very high yields are not to be expected of either scheme. With scheme 2 the chain length is short because of termination by recombination of ions, while in scheme 1 the radiation yield of excited molecules is limiting. The yield of HBP was found to be independent of dose. This is possible if the combination of three or more molecules is initiated by a single ion or excited molecule, or if the HBP is produced within a track or spur.

To complete the study of radiation products from the tetrahydrofuran-cyclohexene system, the gaseous products have been analyzed as a function of dose and concentration. The yields (*G* values) of hydrogen and total gas were reduced 20 and 10%, respectively, by a tenfold increase in dose. The dependence of gas yields, H₂, CH₄, and CO, on concentration is shown in Fig. 14.2 at a dose of 1.79×10^7 rads. Apparently, 0.01 mole fraction of the olefin is effective in reacting with scavengeable precursors of hydrogen from THF. On the other hand, a low concentration of cyclohexene markedly increased the fragmentation of the THF ring to produce CO.

DEVELOPMENT OF RADIATION-RESISTANT INSULATORS

M. J. Kelly W. W. Parkinson
E. J. Kennedy⁸ B. J. Sturm
C. D. Bopp

The Office of Civil Defense, the U.S. Army Electronics Command, and ORNL, in a cooperative program, are developing improved insulating materials for use in electrostatic dosimeters.⁹ This requires investigation of the electrical and chemical properties of insulating materials before, during, and after irradiation, concurrent with literature studies to develop a theoretical basis

⁸Instrumentation and Controls Division.

⁹M. J. Kelly *et al.*, *Annual Summary Report on the Development of Radiation-Resistant Insulators*, ORNL-TM-2077 (in preparation).

(specific to structure and additives) in order to synthesize better materials.

The dielectric medium of the ranging capacitor is the limiting use for these insulators. An ultimate resistivity of 2×10^{20} ohm-cm is required, and the "dielectric soaking" effects must be both small and rapid. After irradiation there must be no long-term aftereffects, observable as a decrease in resistivity or persistent internal polarization, of such magnitude as to preclude recharging and re-usage of the dosimeter after some arbitrary recovery time.

Literature studies identified over 20 prospective materials for testing. These plastics, as well as several copolymers with unreported resistivities, were acquired either as bulk material or commercial films. Electrical measurements prior to irradiation on thin films with sputtered aluminum electrodes eliminated most of these materials from further consideration.

Polyphenylene oxide, polyethylene, poly-*p*-xylylene, polymethylpentene, polystyrene, and various copolymers of styrene appeared satisfactory when tested both in vacuum and dry air. The presently used dosimeter insulating material, a copolymer of styrene and α -methylstyrene, did not differ significantly in preirradiation results from pure polystyrene. Polyethylene terephthalate, while not completely acceptable in air, was included for the detailed investigations now proceeding.

The postirradiation properties of these materials were determined by irradiating the film specimens uniformly in a ^{60}Co source at ~ 300 r/sec for 6 sec. Four minutes later, potential was applied to the electrodes (in vacuum), and current was recorded vs time. Conductivities were substantially higher after irradiation, and the decay of the dielectric charging current was markedly different.

Pure polyphenylene oxide, polyethylene, polymethylpentene, polystyrene, and various copolymers of styrene have postirradiation properties unsatisfactory for dosimeter use. Various ultraviolet stabilizers and antioxidants were added to polystyrene samples without effect or with a decrease in resistivity beyond tolerable limits. Only one additive has shown promise, tris(2-chloroethyl)phosphite. This additive radically improved the radiation recovery time in one sample but also caused several other samples to become grossly conductive prior to irradiation. This additive also improved postirradiation recovery in a single sample of polyphenylene oxide. The variations in performance of this additive are unresolved and are under further study.

The present dosimeter plastic exhibits much better recovery properties than the materials above. Since it is similar in molecular structure to several of these, it is assumed that some minor constituent is copolymerized into the polymer during the emulsion polymerization process used in its manufacture. Detailed recipe ingredients are not available from the manufacturer, and efforts to discover the "additive" have not reached fruition.

Poly-*p*-xylylene and polyethylene terephthalate have recovery properties similar to the dosimeter material. Both of these plastics are characterized by phenyl groups in the polymer chain. The recovery time for polyethylene terephthalate appears to be a function of total dose rather than dose rate. Dose and dose-rate effects will be studied for other materials.

All of the irradiated plastics appear to recover their preirradiation properties if allowed sufficient time. The recovery seems to follow a fixed rate law for each material, taking months in some cases, and is not a simple process.

15. Support for Other ORNL Programs

STUDY OF UNCLAD-METAL-FUELED FAST BREEDER

J. E. Savolainen E. L. Compere

Economic seawater desalination by distillation requires an abundant supply of heat at a moderate temperature. An evaluation¹ has shown that a liquid-sodium-cooled fast breeder reactor using unclad fuel and blanket elements has promise in satisfying this requirement provided, among other things, that direct contact of the unclad fuel by the sodium coolant is acceptable.

In the 3500-Mw (thermal) process heat reactor, one of several versions considered, the coolant enters the core at 170°C and leaves at 350°C. The fuel material, Th-15% U-7% Pu, is a two-phase alloy and has excellent radiation stability, even at its maximum temperature of 600°C, because of the face-centered cubic lattice symmetry of the bulk thorium phase.

Since the depleted uranium blanket is not subjected to extensive burnup, an alloy similar to the British "adjusted uranium" (U, 400-1200 ppm Al, 600 ppm C, and 300 ppm Fe) is adequate.

Evaluations of compatibility problems and methods of controlling them have been made, based on thermodynamic and chemical data of the ingredients of the proposed reactor system components and on reported behavior of other sodium-cooled reactor systems and experimental sodium loops. From a chemical viewpoint the major components of the proposed reactor system, listed in order of their affinity toward oxygen, are the Th-15% U-7% Pu fuel alloy, the uranium metal blanket, the liquid sodium coolant, the austenitic stainless steel structure, and the helium cover gas. The two main

problems concerning reactor chemistry are corrosion of the fuel and blanket metal and the behavior of the fission products in the coolant and cover gas.

The sodium coolant is a vehicle for most of the contaminants which may enter the system from the environment or which occur initially as structural impurities. The principal contaminants are carbon, hydrogen, and oxygen in various combinations and probably nitrogen. Of these, oxygen predominates as a potential corrosive agent for the fuel and blanket metal. Control of corrosion of these metals demands removal and exclusion of oxygen from the system. This would be done initially in a preliminary operation by preconditioning with liquid sodium at a sufficiently high temperature to promote the diffusion of the labile impurities from the stainless steel structure into the sodium, from which the oxygen would be removed by gettering methods.

The design and operation of the reactor system would, of course, be such as to reduce the influx of contaminants, but small amounts of oxygen and other contaminants can be accommodated by absorption on the surfaces of the uranium metal blanket elements. At low oxygen concentrations, uranium metal removes oxygen from liquid metal coolants by forming an oxide scale which adheres to the surface of the metal and does not erode. The Dounreay Fast Reactor is reported to operate successfully in this manner with a 10-fps sodium flow past a U-7% Mo fuel alloy.

The oxide scale behavior on the fuel alloy needs experimental confirmation. Successful demonstration of the oxide scale integrity would be expected because of the favorable Pilling and Bedworth critical density ratio, particularly for thorium, although some adjustments in fuel alloy composition may be desired to increase oxide scale integrity. The oxygen impurity in sodium will also react

¹R. P. Hammond *et al.*, *High Gain Breeders for Desalting or Power Using Unclad Metal Fuels*, ORNL-4202, to be published.

with thorium metal, but the reaction rate decreases rapidly as the oxide scale increases in thickness.

In the absence of cladding, 0.1 to 0.2% of the fission products will be transported into the coolant primarily by fission recoil, rather than by subsequent diffusion, because of the moderate operating temperature. The behavior of the fission products in the coolant is expected to follow that observed in other sodium-cooled reactors in which fission product release incidents have occurred. The behavior closely follows that deduced from chemical and thermodynamic properties. The retention of the halogen fission products by alkali metal coolants in all the incidents is of specific interest in hazards evaluation.

Krypton and xenon fission products have been observed to find their way almost immediately into the reactor cover gas. In the proposed reactor the helium cover gas would be processed by passing it through the sodium dump tanks to allow for decay. The residual xenon and krypton fission products, nitrogen contaminant, and other heavy gases then would be removed in chilled charcoal traps before recirculating back into the reactor. The sodium dump tanks would also contain any gas release caused by an unexpected fuel meltdown.

Some vapor phase transport of cesium activity from liquid sodium has been observed when it can condense out onto cold surfaces and accumulate. This is not expected to be significant in the proposed system.

Fission products which form oxides more stable than sodium, such as barium, strontium, and lanthanum, tend to be removed by deposition from the coolant usually onto the colder surfaces of the container. Some which remain in the metallic state, such as cesium and antimony, tend to remain dissolved in the liquid sodium.

Under normal operating conditions and for some days after shutdown, the calculated radioactivity in the coolant will be predominantly that induced in the sodium by neutron irradiation rather than that of the fission products. Trapping methods could be used to remove fission products from the coolant.

CHEMICAL SUPPORT FOR THE CONTROLLED THERMONUCLEAR RESEARCH PROGRAM

Burnout V Gas Analysis

D. M. Richardson

Recent experiments in the controlled thermonuclear research program performed in an extensively modified calutron apparatus (the Burnout series) made it desirable to apply mass spectrometric techniques to the analysis of the residual gases present in, but outside the limits of, the arc and electromagnetic field.

We connected a sampling probe to a midplane part of the Burnout V liner. The sampling probe was metal gasketed and electrically heated; it was 3.75 m long and had an estimated pumping speed for air of 2 liters/sec. A Veeco model RGA-3 gas analyzer was mounted on a specially designed vacuum system and attached to the probe so that samples of the gas taken from the edge of the liner could be brought out and analyzed. The spectrometer and ion gage were also metal gasketed and electrically heated and were mounted at equivalent positions of the auxiliary pumping system. The estimated speed at the ion gage was 210 liters/sec for air. Trapping with liquid nitrogen was not used because of the uncertainties caused by slow sorption and desorption of some of the deuterocarbon compounds.

During the Burnout experiments an arc is formed between carbon electrodes, and a small stream of H_2 or D_2 gas is fed into the arc. Depending on various experimental conditions, the arc may be intense and of small diameter (mode I), or it may become diffuse and expand to fill the magnetic-field container (mode II). The pressures outside the plasma region were 3×10^{-4} to 10^{-2} torr.

The principal finding from the gas analyses was that gas sampled during the operation of the device contained low-molecular-weight compounds of carbon and deuterium in amounts up to 5%. The light-hydrogen impurity increased from about 1.5% to as much as 3% as a result of operation (with a

single hot graphite cathode and with graphite liners in the magnetic mirror orifices). The changes in the physics experiments did not permit us to determine the relationship between the sampled gas composition and the physics parameters (such as the production rate of energetic protons). Nevertheless, the feasibility of this gas analytical approach was clearly demonstrated.

Mass spectra obtained during mode II operation (presumed maximum turbulent heating) are graphed in Fig. 15.1. The spectra are corrected for residual

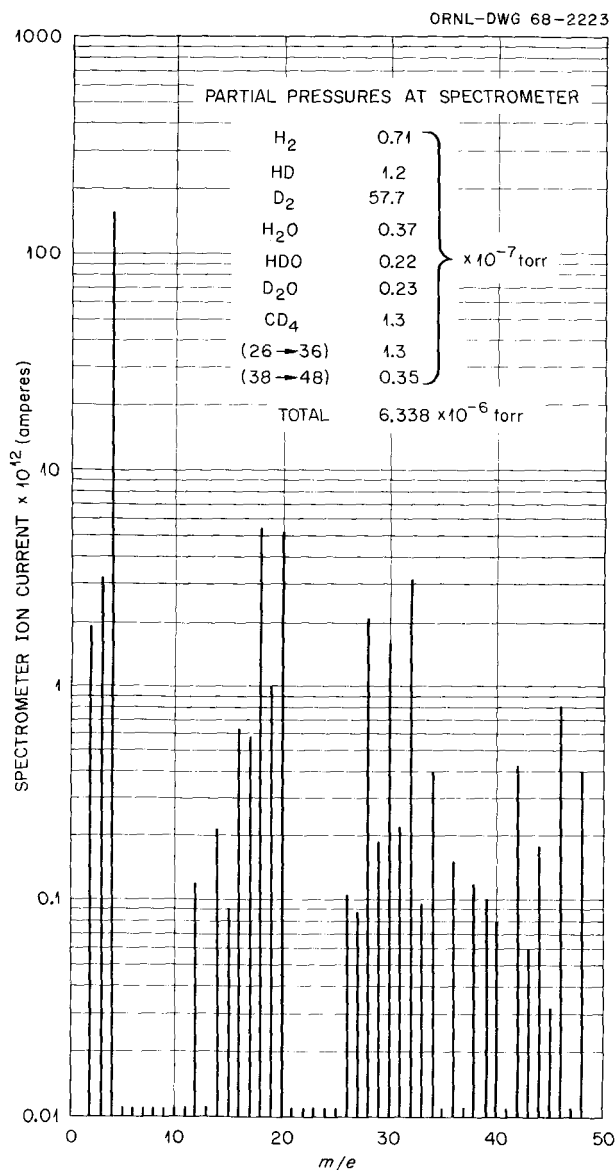


Fig. 15.1. Mass Spectra At Gas Analyzer During Mode II Operation.

Table 15.1. Estimated Pressures (torrs) at Burnout V Liner During Operation

	× 10 ⁻⁴	
H ₂	0.075	(1.12%)
HD	0.126	(1.88%)
D ₂	6.121	(91.13%)
H ₂ O	0.039	(0.58%)
HDO	0.023	(0.34%)
D ₂ O	0.025	(0.37%)
CD ₄	0.136	(2.02%)
(m/e 26 → 36) ^a	0.135	(2.01%)
(m/e 38 → 48) ^b	0.037	(0.55%)
Total	6.717	

^aSpectra indicate C₂D₂, C₂D₄, C₂D₆.

^bSpectra indicate C₃D_x.

gas background at the spectrometer and normalized in accordance with the transmission characteristics of the RGA-3.² By comparison of these peak heights with standard patterns,³ a reasonable identification of gas species was possible, and the fraction of the total spectrometer ion current due to each species was calculated. Since the energies of the ionizing electrons of the ion gage and the spectrometer were nominally identical, it was assumed that the fraction of total ion current due to each species was the same in the ion gage. These fractions of ion gage current were multiplied by appropriate gage factors to obtain the "true" partial pressures at the spectrometer tabulated in Fig. 15.1.

The partial pressures of neutral gas at the inlet to the probe, at normal temperature, were calculated for each gas species according to the estimated speeds of the system. The results are shown in Table 15.1.

²Thermonuclear Div. Semiann. Progr. Rept. Oct. 31, 1966, ORNL-4063, pp. 128-29.

³Mass Spectral Data Sheets, American Petroleum Institute, Research Project 44.

Publications

JOURNAL ARTICLES

AUTHOR(S)	TITLE	PUBLICATION
Adams, R. E., and R. D. Ackley	Ninth AEC Air-Cleaning Conference	<i>Nucl. Safety</i> 8(3), 238 (1967)
Barton, C. J.	The Hazard of Dispersed Plutonium Particles	<i>Nucl. Safety</i> 7(4), 468 (1966)
Bien, P. B.	Corresponding States of Aqueous Salt Solutions	<i>J. Phys. Chem.</i> 71, 2731 (1967)
Blakely, J. P., and L. G. Overholser	Deposition of Carbon on ATJ Graphite from Gas Mixtures	<i>Carbon</i> 5, 87 (1967)
Bohlmann, E. G., <i>et al.</i>	The Catastrophic Corrosion Behavior of Titanium in Chemical Processes	<i>Mater. Protect.</i> 6(10), 22 (1967)
Bopp, C. D., and W. W. Parkinson	Radiation-Induced Codimerization of Ether-Unsaturate Mixtures	<i>Nucl. Sci. Abstr.</i> 21, 12443 (1967)
Brunton, G. D.	The Crystal Structure of Li_4UF_8	<i>J. Inorg. Nucl. Chem.</i> 29, 1631 (1967)
Carroll, R. M., R. B. Perez, and O. Sisman	The Mixing of a Trace Gas in Flowing Helium	<i>Trans. Am. Nucl. Soc.</i> 10(2), 657 (1967)
Carroll, R. M.	Fission-Gas Behavior in Fuel Materials	<i>Nucl. Safety</i> 8(4), 345 (1967)
Compere, E. L., and J. E. Savolainen	The Chemistry of Hydrogen in Liquid Alkali Metal Mixtures Useful as Nuclear Reactor Coolants. I. Sodium Potassium Eutectic	<i>Nucl. Sci. Eng.</i> 28, 325 (1967)
Davis, R. J.	Oxide Growth and Capacitance on Pre-Irradiated Zircaloy-2 and Zirconium	<i>J. Electrochem. Soc.</i> 114(2), 124 (1967)
	The Significance of Charcoal Ignition Temperatures	<i>Trans. Am. Nucl. Soc.</i> 10(2), 511 (1967)
de Bruin, H. J., G. M. Watson, C. M. Blood, and D. Roman	Cation Self-Diffusion in Fast-Neutron-Irradiated Beryllium Oxide	<i>Phil. Mag.</i> 16, 427 (1967)
Evans, R. B., III, R. B. Perez, and J. L. Rutherford	Recoil of Fission Products in Homogeneous Carbon Structures	<i>J. Appl. Phys.</i> 38(8), 3127 (1967)
Field, P. E., and J. H. Shaffer	The Solubilities of Hydrogen Fluoride and Deuterium Fluoride in Molten Fluorides	<i>J. Phys. Chem.</i> 71, 3218 (1967)
Friedman, H. A.	High Temperature Centrifuge for Phase Equilibrium Studies	<i>J. Sci. Instr.</i> 44, 454 (1967)

AUTHOR(S)	TITLE	PUBLICATION
Hammond, R. P., T. D. Anderson, C. C. Burwell, R. P. Wichner, D. B. Lloyd, J. E. Savolainen, J. G. Delene, and R. S. Carlsmith	The Use of Unclad-Metal Fuel in High Gain Breeders for Desalting or Power	<i>Trans. Am. Nucl. Soc.</i> 10(2), 644 (1967)
Keilholtz, G. W.	Air-Cleaning Systems as Engineered Safeguards in Nuclear Reactor Containment	<i>Nucl. Safety</i> 8(4), 360 (1967)
	Removal of Radioactive Noble Gases from Off-Gas Streams	<i>Nucl. Safety</i> 8(2), 155 (1967)
Keilholtz, G. W., and R. E. Moore	Irradiation Damage to High-Density Aluminum Oxide Exposed to Fast-Neutron Doses up to 5×10^{21} neutrons/cm ²	<i>Nucl. Appl.</i> 3, 687 (1967)
	Irradiation Damage to High-Density Aluminum Oxide Exposed to Fast Neutron Doses up to 5×10^{21} neutrons/cm ²	<i>Trans. Am. Nucl. Soc.</i> 10(1), 117 (1967)
Kirsliis, S. S., F. F. Blankenship, and W. R. Grimes	Fission Product Behavior in Molten Salt Reactors	<i>Trans. Am. Nucl. Soc.</i> 10(1), 155 (1967)
Lorenz, R. A., and G. W. Parker	Fission Product Release from Water Reactor Transient Accidents Simulated in TREAT	<i>Trans. Am. Nucl. Soc.</i> 10(1), 340 (1967)
Marshall, W. L.	Aqueous Systems at High Temperature. XX. The Dissociation Constant and Thermodynamic Functions for Magnesium Sulfate to 200°	<i>J. Phys. Chem.</i> 71, 3584 (1967)
Marshall, W. L., and A. S. Quist	A Representation of Isothermal Ion-Ion-Pair-Solvent Equilibria Independent of Changes in Dielectric Constant	<i>Proc. Natl. Acad. Sci. U.S.</i> 58, 901 (1967)
Mason, E. A., R. B. Evans III, and A. P. Malinauskas	Flow and Diffusion of Gases in Porous Media	<i>J. Chem. Phys.</i> 46(8), 3199 (1967)
Mesmer, R. E., and C. F. Baes, Jr.	The Hydrolysis of Beryllium(II) in 1 Molal NaCl	<i>Inorg. Chem.</i> 6, 1951 (1967)
Morgan, M. T., E. L. Long, Jr., and D. M. Hewett III	Fuel Migration into Coatings of Pyrolytic Carbon Coated UO ₂ and UC ₂ Particles as a Result of Irradiation and Heat Treatment	<i>Trans. Am. Nucl. Soc.</i> 10(1), 97 (1967)
Morgan, M. T., and O. Sisman	Fission Product Release During Postirradiation Annealing of Pyrolytic Carbon Coated Fuel Particles	<i>Trans. Am. Nucl. Soc.</i> 10(1), 98 (1967)
Parker, G. W., and H. Buchholz	Low-Pressure Cascade Impactor as a Tool for the Study of Size Distribution of Fission Product Aerosols	<i>Trans. Am. Nucl. Soc.</i> 10(1), 338 (1967)
Reagan, P. E., R. L. Beatty, and E. L. Long, Jr.	Performance of Pyrolytic Carbon Coated Uranium Oxide Particles During Irradiation at High Temperatures	<i>Nucl. Sci. Eng.</i> 28, 34 (1967)
Roberts, B. F.	A Procedure for Estimating Pore Volume and Area Distributions from Sorption Isotherms	<i>J. Colloid Interface Sci.</i> 23, 266 (1967)
Romberger, K. A., C. F. Baes, Jr., and H. H. Stone	Phase Equilibrium Studies in the UO ₂ -ZrO ₂ System	<i>J. Inorg. Nucl. Chem.</i> 29, 1619 (1967)

AUTHOR(s)	TITLE	PUBLICATION
Soldano, B. A., and W. T. Ward	Uptake of Methyl Iodide from Wind-Tunnel Gases by a Suspended Drop of Water	<i>Trans. Am. Nucl. Soc.</i> 10(2), 720 (1967)
Thoma, R. E., W. R. Grimes, and F. F. Blankenship	Chemical Behavior in the Molten Salt Reactor Experiment	<i>Trans. Am. Nucl. Soc.</i> 10(1), 155 (1967)
Watson, G. M., R. B. Perez, and M. H. Fontana	Effects of Containment System Size on Fission Product Behavior	<i>Trans. Am. Nucl. Soc.</i> 10(1), 339 (1967)
Yeatts, L. B., and W. L. Marshall	Aqueous Systems at High Temperature. XVIII. Activity Coefficient Behavior of Calcium Hydroxide in Aqueous Sodium Nitrate to the Critical Temperature of Water	<i>J. Phys. Chem.</i> 71, 2641 (1967)

REPORTS ISSUED

AUTHOR(S)	TITLE	REPORT NUMBER
Ackley, R. D., and R. E. Adams	Removal of Radioactive Methyl Iodide from Steam-Air Systems (Test Series II)	ORNL-4180 (October 1967)
Adams, R. E., and R. D. Ackley	Removal of Elemental Radioiodine from Flowing Humid Air by Iodized Charcoals	ORNL-TM-2040 (November 1967)
Adams, R. E., R. L. Bennett, and W. E. Browning, Jr.	Characterization of Volatile Forms of Iodine at High Relative Humidity by Composite Diffusion Tubes	ORNL-3985 (August 1966)*
Adams, R. E., J. S. Gill, W. D. Yuille, L. F. Parsly, and C. E. Guthrie	Filtration of Particulate Aerosols Under Reactor Accident Conditions	ORNL-TM-1707 (December 1966)*
Adams, R. E., R. D. Ackley, and W. E. Browning, Jr.	Removal of Radioactive Methyl Iodide from Steam-Air Systems	ORNL-4040 (January 1967)
Barton, C. J., and H. H. Stone	Removal of Protactinium from Molten Fluoride Breeder Blanket Mixtures	ORNL-TM-1543 (June 1966)*
	Reduction of Iron Dissolved in Molten LiF-ThF ₄	ORNL-TM-2036 (November 1967)
Blood, C. M., and L. G. Overholser	Compatibility of Pyrolytic-Carbon Coated Fuel Particles with Water Vapor	ORNL-4014 (November 1966)*
Brandon, C. A., D. R. Cuneo, G. B. Engle, and E. L. Long, Jr.	An Irradiation Experiment to Study the Compatibility of BeO with Graphite at 1500°C. Part II. Operation and Postirradiation Evaluation	ORNL-TM-1799 (October 1967)
Clark, W. E., D. N. Hess, P. D. Neumann, L. Rice, and J. L. English	Laboratory Development of Processes for Fixation of High Level Radioactive Wastes in Glassy Solids. (4) Corrosion Studies on Candidate Materials of Construction	ORNL-3816 (August 1967)

*Inadvertently left off 1966 list.

AUTHOR(S)	TITLE	REPORT NUMBER
Coobs, J. H., and O. Sisman	Coated Particle Fuels Development at ORNL for Period May 15, 1966 to Jan. 15, 1967	ORNL-TM-1772 (March 1967)
	Coated Particle Fuels Development at ORNL for Period Jan. 15, 1967 to Oct. 15, 1967	ORNL-TM-2061 (December 1967)
Davis, R. J.	Mechanisms of Sorption of Molecular Iodine	ORNL-4126 (August 1967)
	The Significance of Charcoal Ignition Temperatures	ORNL-4129 (July 1967)
Gadiyar, H. S.	Electrochemical Measurements on Crystal Bar Zirconium in Oxygenated 0.05 M K_2SO_4	ORNL-TM-1834 (April 1967)
	Electrochemical Measurements on Iodide Bar Titanium at Elevated Temperatures	ORNL-TM-1882 (June 1967)
Gadiyar, H. S., A. L. Bacarella, and A. L. Sutton	Electrochemical Measurements on Niobium at Elevated Temperatures	ORNL-TM-1883 (June 1967)
Grimes, W. R.	Chemical Research and Development for Molten Salt Breeder Reactors	ORNL-TM-1853 (June 1967)
Keilholtz, G. W.	Chemical Safety	ORNL-TM-1884 (June 1967)
Kelly, M. J.	An Analytical Approach to Waterlogging Failure	ORNL-3867 (December 1966)
Kelly, M. J., B. J. Sturm, and W. W. Parkinson	Annual Summary Report on the Development of Radiation-Resistant Insulators	ORNL-TM-2077 (December 1967)
Jenks, G. H., and J. C. Griess	Water Chemistry in Pressurized and Boiling Water Power Reactors	ORNL-4173 (November 1967)
Malinauskas, A. P., J. L. Rutherford, and R. B. Evans III	Gas Transport in MSRE Moderator Graphite. I. Review of Theory and Counterdiffusion Experiments	ORNL-4148 (September 1967)
Miller, C. E., Jr.	The Light Bulb Model of Fission Product Release from Reactor Fuels	ORNL-4060 (April 1967)
Neumann, P. D.	Some Prospects for Chemicals Recovery from Large Desalination Plant Brine Effluent	ORNL-TM-1885 (September 1967)
Parker, G. W., G. E. Creek, C. J. Barton, W. J. Martin, and R. A. Lorenz	Out-of-Pile Studies of Fission-Product Release from Overheated Reactor Fuels at ORNL, 1955-1965	ORNL-3981 (July 1967)
Parkinson, W. W., and W. K. Kirkland	The Effect of Air on the Radiation Induced Degradation of Poly Tetra Fluoro Ethylene (Teflon)	ORNL-TM-1757 (February 1967)
Reagan, P. E.	Fission-Gas Release and Irradiation Damage to AVR Pyrolytic-Carbon Coated Thorium-Uranium Carbide Particles	ORNL-4053 (January 1967)
Reed, S. A. (contributor)	Conceptual Design Study of a 250 Million Gallons per Day Multistage Flash Distillation Plant	ORNL-3912 (February 1966)*
Savage, H. C., E. L. Compere, J. M. Baker, and E. G. Bohlmann	Operation of Molten-Salt Convection Loops in the ORR	ORNL-TM-1960 (December 1967)
Shields, R. P., and C. E. Miller, Jr.	The Effect of Fission Products on Charcoal Ignition (In-Pile Experiment)	ORNL-TM-1739 (January 1967)

AUTHOR(S)	TITLE	REPORT NUMBER
Silverman, M. D., J. Truitt, W. E. Browning, Jr., and L. F. Franzen	Characterization of Radioactive Particulate Aerosols by the Fibrous Filter Analyzer	ORNL-4047 (March 1967)
Toth, L. M.	Containers for Molten Fluoride Spectroscopy	ORNL-TM-2047 (November 1967)
Watson, G. M., R. B. Perez, and M. H. Fontana	Effects of Containment System Size on Fission Product Behavior	ORNL-4033 (January 1967)
Weaver, C. F., and H. A. Friedman	A Literature Survey of the Fluorides and Oxy- fluorides of Molybdenum	ORNL-TM-1976 (October 1967)

BOOKS

AUTHOR(S)	TITLE OF ARTICLE	BOOK TITLE
Parkinson, W. W., and W. C. Sears	The Effects of Radiation on the Olefinic Groups in Polybutadiene	pp. 57-70 in <i>Irradiation of Polymers</i> , N. Platzner, Chmn., Advances in Chemistry Series, Am. Chem. Soc., Washington, D.C., 1967
Thoma, R. E.	Determination of Phase Diagrams	Chap. 20 in <i>Handbook of X-Rays</i> , ed. by Emmett F. Koelble, McGraw-Hill, 1967
Thoma, R. E., R. G. Ross, and C. F. Weaver	Production of Lithium Fluoride Crystals with Selected Isotopic Ratios of Lithium	p. 124 in <i>Crystal Growth: Proceedings of an Inter- national Conference on Crystal Growth, Boston, June 1966</i> , ed. by H. Steffen Peiser

PATENTS

AUTHOR	TITLE	PATENT NUMBER
de Bruin, H. J	Method for Bonding Beryllium Oxide to Graphite	U.S. Pat. 3,300,852, Jan. 31, 1967
Kelly, M. J.	Distillation Method for Reprocessing Molten Salt Reactor Fuels	U.S. Pat. 3,310,500, March 21, 1967
Thoma, R. E.	Fast Reactor Fuel	U.S. Pat. 3,287,278, Nov. 22, 1966

Papers Presented at Scientific and Technical Meetings

AUTHOR(s)	TITLE	PLACE PRESENTED
Braunstein, J.	Molten Salt Research	University of Maine, Chemistry Seminar, March 26, 1967
	Thermodynamics of Electrolyte Solutions with Water as a Solute	University of Tennessee, Chemistry Seminar, Apr. 20, 1967
	Electrolyte Solutions with Water as a Solute	Polytechnic Institute of Brooklyn, Chemistry Colloquium, Oct. 20, 1967
	On Relations Between Deviations from Ideality and Association in Binary Mixtures	American Chemical Society, Atlanta, Ga., Nov. 1-3, 1967
Burns, J. H., ¹ A. C. Tennissen, and G. D. Brunton	The Crystal Structure of Alpha Lithium Aluminum Fluoride	American Crystallographic Association, Atlanta, Ga., Jan. 25-27, 1967
Cantor, S.	Temperature Dependence of Heat Capacity (at Constant Volume) and of Isothermal Compressibility in Molten Salts	American Chemical Society, Miami Beach, Fla., Apr. 9-14, 1967
	Thermodynamic Properties of Molten Salts	4th Summer State-of-the-Art Symposium, Division of Industrial and Engineering Chemistry, American Chemical Society, Washington, D.C., June 1967
Carroll, R. M., R. B. Perez, O. Sisman, and G. M. Watson	Utilization of the Oak Ridge Research Reactor to Study the Mechanism of Fission-Gas Release from Reactor Fuels	International Conference on Research Reactor Utilization and Reactor Mathematics, Mexico City, Mexico, May 2-4, 1967
Carroll, R. M., R. B. Perez, and O. Sisman	The Mixing of a Trace Gas in Flowing Helium	American Nuclear Society, Chicago, Ill., Nov. 5-9, 1967
Coobs, J. H., ² and O. Sisman	Coated-Particle Fuels Development at Oak Ridge National Laboratory for Period May 15, 1966 to Jan. 15, 1967	12th AEC Coated-Particle Working Group Meeting, Nevada Test Site, Mercury, Nev., Mar. 14-15, 1967
Cuneo, D. R., E. L. Long, Jr., J. A. Conlin, C. A. Brandon, and G. B. Engle	Compatibility of Graphite Under Irradiation with (1) (U,Th)O ₂ at 1650°C and (2) BeO at 1500°C	American Chemical Society, Miami Beach, Fla., Apr. 9-14, 1967

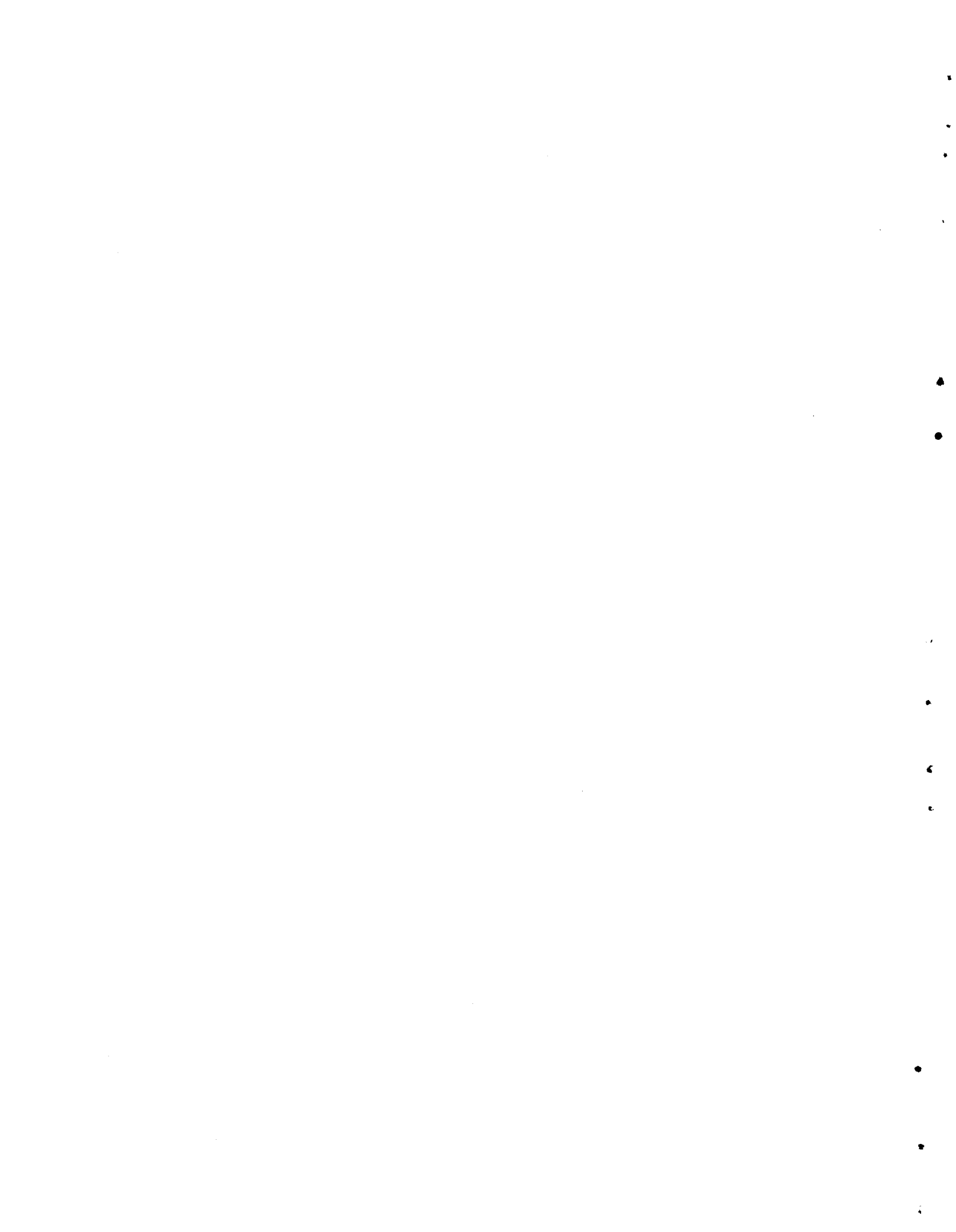
¹Chemistry Division.

²Metals and Ceramics Division.

AUTHOR(S)	TITLE	PLACE PRESENTED
Davis, R. J.	The Significance of Charcoal Ignition Temperatures	American Nuclear Society, Chicago, Ill., Nov. 5-9, 1967
Grimes, W. R.	Behavior of Fluoride Mixtures in the Molten Salt Reactor Experiment	Electrochemical Society Symposium on Fused Salt Reactions, Toronto, Canada, Feb. 17, 1967
Holmes, H. F., E. L. Fuller, Jr., and C. H. Secoy	Adsorption of Water and Nitrogen on Porous and Non-Porous Thorium Oxide	American Chemical Society, Miami, Fla., Apr. 9-14, 1967
Fuller, E. L., Jr., H. F. Holmes, J. E. Stuckey, and C. H. Secoy	Heats of Immersion of Thorium Oxide in Water at 25°C	American Chemical Society, Miami Beach, Fla., Apr. 9-14, 1967
Keilholtz, G. W., and R. E. Moore	Irradiation Damage to High-Density Aluminum Oxide Exposed to Fast Neutron Doses up to 5×10^{21} neutrons/cm ²	American Nuclear Society, San Diego, Calif., June 11-15, 1967
Kirslis, S. S., F. F. Blankenship, and W. R. Grimes	Fission Product Behavior in Molten Salt Reactors	American Nuclear Society, San Diego, Calif., June 11-15, 1967
Lorenz, R. A., and G. W. Parker	Fission Product Release from Water Reactor Transient Accidents Simulated in TREAT	American Nuclear Society, San Diego, Calif., June 11-15, 1967
Malinauskas, A. P.	Thermal Transpiration	ORAU Traveling Lecture Program, Tennessee Polytechnic Institute, Nov. 10, 1967
	ORNL HTGR Oriented Nuclear Safety Program-Chemical Research	ACRS Reactor Safety Meeting, Washington, D.C., May 16, 1967
Marshall, W. L.	Dissociation Constant of Magnesium Sulfate to 200°C and Its Application to Saline Water Behavior	American Chemical Society, Miami Beach, Fla., Apr. 9-14, 1967
Marshall, W. L., and A. S. Quist	A New Concept of Ion-Pair Formation in Aqueous and Non-Aqueous Solutions	ORAU Traveling Lecture Program, Purdue University, Oct. 19, 1967
		ORAU Traveling Lecture Program, Yale University, Nov. 3, 1967
		ORAU Traveling Lecture Program, Princeton University, Nov. 2, 1967
		ORAU Traveling Lecture Program, University of Tennessee, Nov. 16, 1967
Mesmer, R. E., and C. F. Baes, Jr.	The Hydrolysis of Beryllium(II) in 1 m (Na)Cl	American Chemical Society, Chicago, Ill., Sept. 10-15, 1967

AUTHOR(S)	TITLE	PLACE PRESENTED
Miller, C. E., Jr.	The Light Bulb Model of Fission Product Release	American Chemical Society, Miami Beach, Fla., Apr. 9- 14, 1967
Morgan, M. T., E. L. Long, Jr., and D. M. Hewett III	Fuel Migration into Coatings of Pyrolytic Carbon Coated UO_2 and UC_2 Particles as a Result of Irradiation and Heat Treatment	American Nuclear Society, San Diego, Calif. June 11- 15, 1967
Morgan, M. T., and O. Sisman	Fission Product Release During Postirradiation Annealing of Pyrolytic Carbon Coated Fuel Particles	American Nuclear Society, San Diego, Calif. June 11- 15, 1967
Parker, G. W.	Nuclear Safety	Faculty and Student Seminar, Argonne National Labora- tory, Aug. 22, 1967
Parker, G. W., and H. Buchholz	Low-Pressure Cascade Impactor as a Tool for the Study of Size Distribution of Fission Product Aerosols	American Nuclear Society, San Diego, Calif., June 11- 15, 1967
Parkinson, W. W.	A Multicurie Cobalt-60 Irradiation Facility	Health Physics Training Lecture, Oak Ridge Asso- ciated Universities, Apr. 17, 1967
	The Effects of Radiation on Plastics and Rubber	U.S. Naval Reserve Lecture, Oak Ridge, Tenn., Oct. 25, 1967
Perez, R. B., G. M. Watson, and R. M. Carroll	Mathematical Analysis of Fission-Gas Release Using Flux and Temperature Oscillations	International Conference on Research Reactor Utiliza- tion and Reactor Mathe- matics, Mexico City, Mexico, May 2-4, 1967
Posey, F. A., and E. G. Bohlmann	Pitting of Titanium Alloys in Saline Waters	2d European Symposium on Fresh Water from the Sea, Athens, Greece, May 12, 1967
Shoup, C. S., Jr., and C. H. Secoy	Infrared Spectra of the Thorium Oxide-Water Vapor Interface	American Chemical Society, Miami Beach, Fla., Apr. 9-14, 1967
Sisman, O., J. G. Morgan, and P. E. Reagan	Evaluation of the Properties of Coated Fuel Particles by In-Pile Experiments	International Conference on Research Reactor Utiliza- tion and Reactor Mathematics, Mexico City, Mexico, May 2- 4, 1967
Soldano, B. A., And W. T. Ward	Uptake of Methyl Iodide from Wind Tunnel Gases by a Suspended Drop of Water	American Nuclear Society, Chicago, Ill., Nov. 5-9, 1967
Thoma, R. E., W. R. Grimes, and F. F. Blankenship	Chemical Behavior in the Molten Salt Reactor Experiment	American Nuclear Society, San Diego, Calif., June 11- 15, 1967

AUTHOR(S)	TITLE	PLACE PRESENTED
Watson, G. M., R. B. Perez, and M. H. Fontana	Effects of Containment System Size on Fission Product Behavior	American Nuclear Society, San Diego, Calif., June 11- 15, 1967
Yeatts, L. B., and W. L. Marshall	Dissociation Constant of Calcium Sulfate to 350°C Obtained from Solubility Behavior in Mixed Electrolytes	American Chemical Society, Miami Beach, Fla., Apr. 9- 14, 1967



INTERNAL DISTRIBUTION

1. Biology Library
- 2-4. Central Research Library
5. Laboratory Shift Supervisor
- 6-7. ORNL Y-12 Technical Library
(Document Reference Section)
- 8-58. Laboratory Records Department
59. Laboratory Records, ORNL R.C.
60. C. E. Larson
61. A. M. Weinberg
62. H. G. MacPherson
- 63-67. G. E. Boyd
68. F. R. Bruce
69. F. L. Culler
70. W. H. Jordan
71. A. H. Snell
72. G. Young
73. A. F. Rupp
74. M. Bender
75. A. L. Boch
76. R. B. Briggs
77. W. B. Cottrell
78. A. P. Fraas
79. K. A. Kraus
80. J. A. Lane
81. A. J. Miller
82. M. W. Rosenthal
83. D. B. Trauger
84. G. D. Whitman
85. S. E. Beall
86. D. S. Billington
87. D. E. Ferguson
88. J. H. Frye, Jr.
89. M. T. Kelley
90. E. H. Taylor
91. E. S. Bettis
92. M. A. Bredig
93. L. T. Corbin
94. J. E. Cunningham
95. J. H. Crawford
96. P. N. Haubenreich
97. P. R. Kasten
98. M. A. Kastenbaum
99. E. M. King
100. R. N. Lyon
- 101-102. R. B. Parker
103. M. J. Skinner
104. J. C. White
105. G. C. Williams
- 106-116. W. R. Grimes
117. E. G. Bohlmann
118. H. F. McDuffie
119. G. M. Watson
120. F. F. Blankenship
121. R. D. Ackley
122. R. E. Adams
123. A. L. Bacarella
124. C. F. Baes
125. J. E. Baker
126. J. M. Baker
127. C. E. Bamberger
128. C. J. Barton
129. C. D. Baumann
130. R. L. Bennett
131. P. B. Bien
132. C. M. Blood
133. C. D. Bopp
134. J. Braunstein
135. W. E. Browning, Jr.
136. G. D. Brunton
137. S. Cantor
138. R. M. Carroll
139. Zell Combs
140. E. L. Compere
141. G. E. Creek
142. D. R. Cuneo
143. R. J. Davis
144. F. A. Doss
145. L. A. Dunn
146. J. L. English
147. R. B. Evans, III
148. L. L. Fairchild
149. H. F. Feurenstein
150. M. H. Fontana
151. S. H. Fried
152. H. A. Friedman
153. E. L. Fuller, Jr.
154. R. B. Gammage
155. J. S. Gill
156. L. O. Gilpatrick
157. J. C. Griess, Jr.

158. G. M. Hebert
159. D. N. Hess
160. B. F. Hitch
161. H. F. Holmes
162. G. H. Jenks
163. G. W. Keilholtz
164. M. J. Kelly
165. R. M. Keyser
166. S. S. Kirslis
167. R. A. Lorenz
168. A. P. Malinauskas
169. W. L. Marshall, Jr.
170. W. J. Martin
171. T. H. Mauney
172. R. E. Mesmer
173. R. E. Moore
174. J. G. Morgan
175. M. T. Morgan
176. D. M. Moulton
177. J. J. Myron
178. P. D. Neumann
179. M. F. Osborne
180. L. G. Overholser
181. G. W. Parker
182. W. W. Parkinson, Jr.
183. A. S. Quist
184. P. E. Reagan
185. J. D. Redman
186. S. A. Reed
187. D. M. Richardson
188. G. D. Robbins
189. B. F. Roberts
190. H. E. Robertson
191. K. A. Romberger
192. H. C. Savage
193. J. E. Savolainen
194. D. R. Sears
195. J. H. Shaffer
196. R. P. Shields
197. A. J. Shor
198. M. D. Silverman
199. O. Sisman
200. Ruth Slusher
201. B. A. Soldano
202. H. H. Stone
203. R. A. Strehlow
204. B. J. Sturm
205. D. A. Sundberg
206. F. H. Sweeton
207. R. E. Thoma, Jr.
208. L. M. Toth
209. J. Truitt
210. W. T. Ward
211. G. C. Warlick
212. C. F. Weaver
213. J. F. Winesette
214. L. B. Yeatts
215. Leo Brewer (consultant)
216. J. W. Cobble (consultant)
217. R. W. Dayton (consultant)
218. P. H. Emmett (consultant)
219. H. S. Frank (consultant)
220. N. Hackerman (consultant)
221. D. G. Hill (consultant)
222. H. Insley (consultant)
223. E. V. Jones (consultant)
224. T. N. McVay (consultant)
225. G. Mamantov (consultant)
226. J. L. Margrave (consultant)
227. E. A. Mason (consultant)
228. R. F. Newton (consultant)
229. R. B. Perez (consultant)
230. J. E. Ricci (consultant)
231. Howard Reiss (consultant)
232. G. Scatchard (consultant)
233. D. A. Shirley (consultant)
234. H. Steinfink (consultant)
235. R. C. Vogel (consultant)
236. T. F. Young (consultant)

EXTERNAL DISTRIBUTION

237. D. F. Bunch, Health Physics Branch, AEC, Washington
238. Paul E. Field, Dpt. of Chemistry, Virginia Polytechnic Institute
239. Reactor Div., AEC, ORO
240. Asst. General Manager for Research and Development, AEC, Washington
241. Division of Research, AEC, Washington
242. Division of Isotopes Development, Washington
243. Asst. General Manager for Reactors, AEC, Washington

- 244. Laboratory and University Division, AEC, ORO
- 245. Division of Reactor Development and Technology, AEC, Washington
- 246. Space Nuclear Propulsion Office, AEC, Washington
- 247. J. A. Swartout, 270 Park Ave., New York, N.Y.
- 248. Milton Shaw, AEC, Washington
- 249. W. W. Grigorieff, Assistant to the Executive Director, Oak Ridge Associated Universities
- 250-502. Given distribution as shown in TID-4500 under Chemistry category (25 copies - CFSTI)